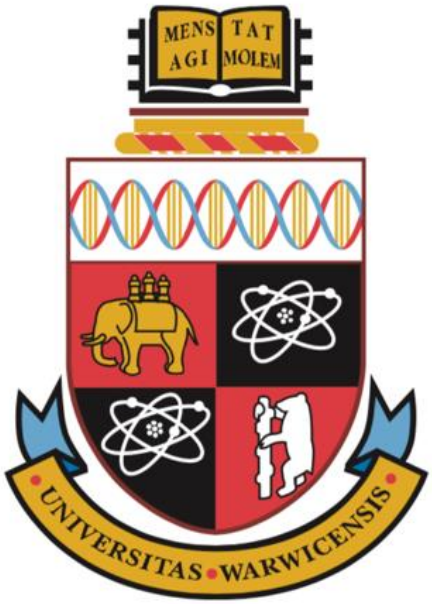

An interaction between mTOR and Myc in cell size control

By

Luis Steven Servín González

A thesis submitted for the degree of Doctor of Philosophy

University of Warwick, School of Life Sciences

January, 2021

Table of Contents

Acknowledgments ..... ***I***

Declarations ..... ***II***

Abstract ..... ***III***

Abbreviations ..... ***IV***

Chapter 1: Introduction ***1***

1.1 Cell Size **1**

1.2 Cell Size Regulation **2**

1.2 Drugs for Cell Size Discovery **3**

1.2.1 Rapamycin 3

1.2.2 LY294002 4

1.2.3 AZD5363 5

1.2.4 Actinomycin D 6

1.2.4 SB203580 7

1.3 Measuring the Cell Size **7**

1.3.1 Moxi Z 7

1.3.2 Flow cytometry 8

1.4 Staining the Nucleic Acid of the Cells **10**

1.4.1 Hoechst 33342 10

1.4.2 Pyronin Y to stain the dsRNA 11

1.4 The physiological effects of cell size and its dysregulation **12**

1.5 Noise in Gene Expression **14**

1.6 Cell size variability as a Cause of Extrinsic Noise **15**

1.7 Cells used in this study **16**

1.7.1 HEK293 16

1.7.2 HeLa 17

1.7.3 U2OS 17

Chapter 2: Materials and Methods ***19***

2.1 Materials **19**

2.1.1 Bacterial Strains 19

2.1.2 Human Cell Lines 19

2.1.3 Specific Kits 19

2.1.4 Culture Media 20

2.1.5 Drugs 20

2.1.6 Nucleic Acid Stains 20

2.1.7 Antibodies 20

2.1.8 silencing RNAs (siRNAs) 21

2.1.9 Plasmids 21

2.1.10 Western Blot 22
2.2 Methods 22
2.2.1 Bacterial Growth and Storage 22
2.2.2 Bacterial Transformation 22
2.2.3 Plasmid Extraction 22
2.2.4 Transfection 23
2.2.5 Mammalian Cell Culture 23
2.2.6 Pharmacological Treatments 24
2.2.7 Flow Cytometry 25
2.2.8 Staining Nucleic Acids 26
2.2.9 SUnSET 27
2.2.10 Western Bot 27
2.2.11 RNA Extraction 28
2.2.12 RNA sequencing & sequencing analysis 28
Chapter 3: Chemical manipulation of a size regulating pathway in mammalian cell lines and its effects. 31
3.1 Introduction 31
3.1.1 The PI3K/AKT/mTOR Pathway Regulates Cell Growth 31
3.2 Results 35
3.2.1 Inhibition of PI3K and AKT reduces Mammalian Cell Size. 35
3.2.2 Inhibition of PI3K by LY294002 changes the cell cycle distribution and cell size independently of mammalian cell lines 37
3.2.3 The Macrolide Rapamycin affects mammalian cell lines' size 41
3.2.4 Rapamycin affects the cell cycle distribution 45
3.2.5 Rapamycin reduces the size of the cells independently of the cell cycle distribution. 46
3.2.6 siRNA knockdown of mTOR's effector 49
3.2.7 RNAseq analysis of HeLa cells exposed to Rapamycin. 50
3.3 Discussion 57
Chapter 4: Overexpression of Myc and its effects on cellular size 63
4.1 Introduction 63
4.1.1 Myc as a Transcription Amplifier 65
4.1.2. The MycER system 68
4.1.4. Using SUnSET to analyse translation 70
4.2 Results 72
4.2.1 C-Myc Plasmid reduced cell size 72
4.2.2 Myc-GFP expressing cells are still smaller than controls 73
4.2.3 Myc Plasmid is only expressed in G1 cells 73
4.2.4 MycER is expressed in U2OS cells 75
4.2.5 MycER overexpression increases cell size in U2OS cells 76
4.2.6 Myc's overexpression rescues cell size from Serum Starvation 77
4.2.7 Myc overexpression rescues cells from the effects of Rapamycin. 79
4.2.8 Cell cycle is impacted by Rapamycin, Myc overexpression or both. 81
4.2.9 G1 phase an G2/M phase cell size changes upon Myc overexpression, Rapamycin exposure or both 82
4.2.10 MycER induced cells increased ribosomal RNA 83
4.2.11 Myc overexpression increases protein content 86
4.2.12 RNAseq analysis of U2OS cells. 89
4.4 Discussion 110
Chapter 5: 120
Chapter 6: Inhibiting ribosomal synthesis impacts the Rapamycin resistance effect of Myc activation. 120
5.1 Introduction 120

5.1.1 Ribosomal biosynthesis drives cell size 120
5.1.2 Cell size and p38 MAPK signalling 122
5.2 Results 123
5.3 Discussion 128
Chapter 7: Conclusions. 134
References 137

Table of figures

Figure 1.1 Rapamycin Molecule. 4
Figure 1.2 The PI3K inhibitor LY294002. 5
Figure 1.3 AZD5363 structure. 6
Figure 1.4 How light scattering gives information of the cell's biology.. 9
Figure 1.5 Hoechst 33342. 11
Figure 1.6 Pyronin Y. 12
Figure 2.1 pMyc-GFP plasmid. 21
Figure 3.1 The PI3K/AKT/mTOR signaling pathway. 34
Figure 3.2 The PI3K and AKT inhibitors reduce the size of HEK293 cells. 35
Figure 3.3 Incubation with the PI3K and AKT inhibitors reduces HeLa cell size. 36
Figure 3.4 Mammalian cell size is reduced by high concentration of LY294002. 38
Figure 3.5 The Cell Cycle distribution of Mammalian cells change with exposure to LY294002. 39
Figure 3.6 LY294002 treated cells are overall smaller. 40
Figure 3.7 HeLa cells exposed to 30 µM LY294002 treated cells are overall smaller. 41
Figure 3.8 Rapamycin reduces the volume and diameter of HEK293 cells. 42
Figure 3.9 Rapamycin reduces the diameter and volume of HeLa cells. 43
Figure 3.10 Rapamycin reduces the size of mammalian cells measured by flow cytometry. 44
Figure 3.11 Cell Size measurements by flow cytometry correlate with diameter measurements taken by Moxi Z. 45
Figure 3.12 Cell Cycle Distribution changes in Cells treated with Rapamycin. 46

Figure 3.13 Rapamycin treated HEK293 cells are overall smaller. 47
Figure 3.14 Asynchronous HeLa cells exposed to 1 μM of Rapamycin cells are overall smaller. 48
Figure 3.15 HEK293 cells size is reduced when transfected with siRNAs aimed at PI3K/AKT/mTOR Pathway. 49
Figure 3.16 Quality check plots generated from the GSE130006 dataset. 51
Figure 3.17 Heatmap of the differentially expressed genes of HeLa cells exposed to Rapamycin...... 52
Figure 3.18 Volcano plot showing differentially expressed genes in the Rapamycin dataset...... 53
Figure 3.19 XY Scatter plot of HeLa cell RNAseq data..... 54
Figure 3.20 Top Gene Ontology terms from Rapamycin treated cells are related to Translation. 56
Figure 3.21 Gene Ontology Term enrichment by g:Profiler from Rapamycin treated HeLa cells point to Translation. 57
Figure 4.1 Myc releases RNA Pol II from Pausing. 64
Figure 4.2 Representation of increased binding frequencies with increasing Myc concentrations. 66
Figure 4.3 Schematic model for the stepwise recruitment of Myc-Max on chromatin..... 67
Figure 4.4 Chimeric MycER architecture...... 69
Figure 4.5 MycER Mechanism...... 70
Figure 4.6 SUnSET Mechanism...... 71
Figure 4.7 Myc-GFP is accumulated in the cell nuclei. 72
Figure 4.8 PCDNA3-MYC-GFP expressing cells are smaller. 73
Figure 4.9 Myc is expressed mainly in G1 cells. 74
Figure 4.10 G1 cells comparison. 74
Figure 4.11 Myc-ER Western blot...... 76
Figure 4.12 MYC overexpressing cells are larger...... 76
Figure 4.13 MycER cells increase their cell size. 78
Figure 4.14 Myc overexpression rescues cells from Serum Starvation cell size reduction...... 78
Figure 4.15 Myc overexpression rescues cells from Rapamycin effects. 80
Figure 4.16 U2OS cells measured by Moxi.. 80

Figure 4.17 Cell Cycle distribution changes with Rapamycin and 4-OHT treatments. 81
Figure 4.18 U2OS MycER G1 and G2/M size changes. 83
Figure 4.19 Pyronin Stains dsRNA. 84
Figure 4.20 Myc Overexpression increases rRNA content. 85
Figure 4.21 SUnSET timepoints. 87
Figure 4.22 Protein translation increases with Myc forced expression. 88
Figure 4.23 Quality check plots generated from the U2OS RNAseq. 89
Figure 4.24 PCA plot from U2OS samples. 90
Figure 4.25 Heatmap of the most significant differentially expressed genes. .. 91
Figure 4.26 Volcano plot showing differentially expressed genes in the different U2OS dataset. 92
Figure 4.27 XY Scatter plot of U2OS samples. 95
Figure 4.28 Top 20 BP Gene Ontology term enrichment of control U2OS cells vs Rapamycin. 96
Figure 4.29 Top 20 Biological Process Gene Ontology term enrichment of U2OS cells exposed to Rapamycin. 97
Figure 4.30 Top 10 Biological Process Gene Ontology term enrichment of U2OS cells exposed to RapaMycin by Enrichr. 98
Figure 4.31 Venn Diagram of DE genes. 98
Figure 4.32 Top 20 GO terms from downregulated genes from both HeLa and U2OS cells. 99
Figure 4.33 Venn diagram of upregulated DE genes from HeLa and U2OS cells exposed to Rapamycin. 100
Figure 4.34 Top 20 GO terms from upregulated DE genes between HeLa and U2OS cells. 101
Figure 4.35 Top 20 BP Gene Ontology term enrichment of U2OS cells incubated with 4-OHT. 102
Figure 4.36 Top 20 Biological Process Gene Ontology term enrichment of U2OS cells induced with 4-OHT. 103
Figure 4.37 Top 9 Biological Process Gene Ontology term enrichment of U2OS cells exposed to 4-OHT by Enrichr. 103
Figure 4.38 Top 20 BP Gene Ontology term enrichment of Myc overexpressing U2OS cells exposed to RapaMycin. 105

Figure 4.39 Top 20 Biological Process Gene Ontology term enrichment of Myc overexpressing U2OS cells exposed to Rapamycin. 106
Figure 4.40 Top 10 Biological Process Gene Ontology term enrichment of Myc overexpressing U2OS cells exposed to Rapamycin by Enrichr. 107
Figure 4.41 Heatmaps of DEG's associated with different GO Terms from Ribosomal Biogenesis. 108
Figure 4.42 Top 20 Biological Process Gene Ontology Terms. 109
Figure 4.43 Top 20 Biological Component terms from DE Downregulated Genes. 110
Figure 5.1 Myc Overexpression inhibitor resistance is abolished by combination of Rapamycin with a RNA Pol I inhibitor. 124
Figure 5.2 Ribosomal RNA signal was reduced by a RNA Pol I inhibitor. MycER 125
Figure 5.3 Incubation with a p38 MAPK inhibitor reduces cell size. 126
Figure 5.4 Incubation with a p38 MAPK inhibitor reduced ribosomal RNA signal. 127
Figure 5.5 The mTOR pathway – Rapamycin relationship. 133
Figure 5.6 Myc induced-ribosome biogenesis drives cell size regulation. 133

Index of Tables

T**able 2.1 Kits.** 19
Table 2.2 Drugs. 24
Table 3.1 Top 20 Downregulated Differentially Expressed Genes in Rapamycin-treated HeLa cells. 54
Table 3.2 Top 20 Upregulated Differentially Expressed Genes in Rapamycin-treated HeLa cells. 55
Table 4.1 Top 20 Upregulated Genes. 93
Table 4.2 Top 20 Downregulated Genes. 94

Acknowledgments

I want to thank all the people involved directly or indirectly in this journey:

- To my parents and my brother, without them I wouldn't be here, your support and love have always guided me in every adventure. EDC
- To Dr. Daniel Hebenstreit for accepting me as part of your group, guiding me and helping me learn through these difficult times. It has been one wild journey and I wouldn't have made it without your help.
- To my Servin and Gonzalez family, always with me even when I was in another part of the world.
- To my girlfriend Elena, who has been the emotional support during these challenging times.
- To the present and past members of the Hebenstreit lab, Mark, Massimo, Michael, Philip, Jie, Francesca, Juntai, Shuo, David, and specially Nathan, Maria and Matt for being great colleagues and greater friends.
- To Dr. Sarah Bennet for always helping me with issues in Flow Cytometry, access to the M029 lab and above all being a great colleague.
- To CONACyT for sponsoring my PhD and allowing me to pursue my dream of becoming a Doctor.
- To my best friends Aldo and Ricardo, who were always on the other line of the phone even when the time zones weren't ideal.
- To Dr. Jesus Adrian Lopez for supporting me all this time and helping me chase my dream to become a scientist.
- To Helena, you were there in the beginning and helped me so many times.
- To Dr. Yañez, you always believed in me and helped me survive so I could live for this moment. Rest in Peace.

Declarations

I hereby declare that this thesis entitled ‘An interaction between mTOR and Myc in cell size control’ is an original work and has not been submitted for a degree or diploma or other qualification at any university.

RNA sequencing libraries were prepared by Novogene Europe from total RNA extracted in our laboratory.

Abstract

Regulation of cell size is controlled by multiple biochemical pathways, such as the mammalian target of rapamycin (mTOR) signalling pathway and the transcription factor Myc. The loss of tightly regulated control of cell size is known to be associated with multiple diseases such as cancer. Understanding how key molecular components in such pathways is necessary to elucidate the mechanisms behind cell size control. Since pathways consist of large networks of interacting molecules, changes in the expression of such molecules may have a large impact on the signalling cascade output, therefore investigating the impact of how the growth-regulating signalling cascade is affected by hampering expression of effectors involved in the pathway is of great interest. This thesis shows that chemical and siRNA downregulation of central pathway effectors of the mTOR pathway reduces cell size and volume, which also change the cell cycle distribution. Furthermore, RNAseq analysis from a dataset similar to our experiments showed that differentially expressed genes from cells exposed to rapamycin seem to be involved in ribosomal biogenesis and metabolism.

We observed that over-expression of Myc lead to notable increases in cell size and volume which were linked to higher levels of protein and rRNA content. RNAseq analysis of this cells showed that differentially expressed genes seemed to be involved in different cellular mechanisms related to cell size. Remarkably, Myc over expressing cells that were exposed to the mTOR inhibitor Rapamycin had a size like non-treated cells but with higher content of protein and rRNA. Sequencing analysis from these cells revealed many down-regulated genes involved in cell metabolism, translation, and other cellular process. A combination of Rapamycin and the rRNA synthesis inhibitor, Actinomycin D reduced the size and rRNA content of the Myc overexpressing cells, suggesting that ribosome biogenesis could be the mechanism behind the size control. To identify an alternative effector involved in cell size and ribosome biogenesis, we show that incubation of cells with a p38 MAPK inhibitor further reduces cell size and rRNA content, suggesting a possible interaction between the PI3K/AKT/mTOR pathway, with the p38 MAPK pathway and Myc.

Abbreviations

4EBP1/2/3: eIF4E-binding proteins 1, 2, 3
4-OHT: 4-hydroxytamoxifen
5'TOP: 5'-terminal oligopyrimidine tract
5'UTR: 5'-untranslated region
ACACA: acetyl-CoA carboxylase
AD5: adenovirus type 5
ATP: adenosine triphosphate
AU: Arbitrary Units
bHLHZ: basic-helix-loop-helix leucine zipper
CCND1: cyclin D1
CDK: Cyclin-dependent kinase
CK2: casein kinase 2
CSZ: Cell Sensing Zone
DEG: Differentially expressed genes
DEPTOR: DEP domain-contaning mTOR-interacting protein
DMEM: Dulbecco's Modified Eagle Medium
DMSO: Dimethyl Sulfoxide
DNA-PK: DNA-dependent protein kinase
dsRNA: double-stranded RNA
ECL: Enhanced chemiluminescent
EDTA: Ethylenediaminetetraacetic acid
eEF2: eukaryotic elongation factor 2
eIF: eukaryotic initiation factor
ER: oestrogen receptor
ESCC: esophageal squamous cell carcinoma
FASN: fatty acid synthetase
FBS: Fetal Bovine Serum
FCS: Fetal Calf Serum
FKBP12: 12-kDa FK506-binding protein
FOXO: Forkhead box O

FRB: FKP12-Rapamycin binding
FSC: Forward-scattered signal
GAP: GTPase-activating protein
GFP: Green fluorescent protein
GO: Gene Ontology
GSK: Glycogen synthase kinase
HBD: hormone-binding domain
Hsp90: Heat shock protein 90
IGF: Insulin Growth Factor
IMS: Industrial Methylated Spirit
JNK: c-Jun N-terminal kinase
LPS: Lipopolysaccharide
MAPK: mitogen-activated protein kinase
MDM2: mouse double minute 2 homolog
MKKs: MAPK kinases
MNK: MAPK-interacting Kinase
mRNA: messenger RNA
mTOR: mammalian target of Rapamycin
mTORC1/2: mammalian TOR complex 1/2
NMD: nonsense mediated decay
MAPK: mitogen-activated protein kinase
p70S6K: 70-kDa ribosomal protein S6 kinase
PABP: poly(A)-tail-binding protein
pAKT: phosphorylated activated AKT
PBS: Phosphate Buffered Saline
PCA: Principal Component Analysis
Pdcd4: programmed cell death 4
PDK1: 3-phsphoinositide-dependent kinase 1
PI3K: phosphoinositide 3-kinase
PIP2: phosphatidylinositol-4,5-P2
PIP3: phosphatidylinositol-3,4,5-P3
PKB: protein kinase B, also known as AKT
PMTs: Photomultiplier tubes
RNA Pol I/II/III: RNA Polymerase I/II/III

PRAS40: Proline-rich Akt substrate 40kDa
PRTE: pyrimidine-rich translational element
PTC: premature termination codons
PTEN: Phosphatase and tensin homolog
PY: Pyronin Y
RAPTOR: regulatory associated protein of TOR
Rheb: Ras-homolog enriched in brain
RIPA: Radioimmunoprecipitation assay buffer
RP: Ribosomal protein
RPS6K: ribosomal protein S6 kinase
rRNA: ribosomal RNA
S6K: S6 Kinase
SCD: stearoyl-CoA
SDS: Sodium Dodecyl Sulfate
siRNA: Small interfering RNA
SL1/TIF-1B: Selectivity factor 1
SRP: Signal recognition particle
SSC: Side-scattered light
SUnSET: Surface Sensing of Translation
SV40: Simian Vacuolating virus 40
TAD: transcriptional activation domain
TFIIIA/B/C: Transcription factor III A/B/C
TLR: Toll-Like-Receptor
TNF: Tumour Necrosis Factor
TNFR: Tumour Necrosis Factor Receptor
TORC1: Target of Rapamycin Complex 1
TRFC: transferrin receptor
TRRAP: Transformation/Transcription Domain Associated Protein
TSC1/2: tuberous sclerosis complex 2
UBF: upstream binding factor
UPR: unfolded protein response
UV: Ultra Violet

Chapter 1: Introduction

1.1 Cell Size

The question ‘does size matter?’ is one that has occupied researchers and humanity for a long time, and we can appreciate its importance when we see how living organisms can be found in many sizes and shapes. Take animals for example; there are gigantic 30-meter blue whales and tiny 0.5 mm tardigrades. Adult animals result from multiple rounds of cell proliferation, growth and remodelling that takes place during development, and its overall size depends on the number and size of its cells (Lloyd, 2013). The average size of any animal cell is ~10-20 μm in diameter; this small size allows for a large surface area to volume ratio which permits efficient transport of materials in and out of the cell. If cells were too large, the transportation would be inefficient and incapable of sustaining the metabolic needs of the cell. For this reason, large animals consist of more cells rather than bigger cells (Conlon and Raff, 1999). In multicellular organisms, growth, proliferation, and survival are differentially regulated in multiple tissues (Alberts, 1998). A mammalian cell cultured *in vitro* surrounded by nutrients will not enter the cell cycle or add mass in the absence of a mitogens or growth factors, respectively (Rathmell et al., 2000).

The human body is made of around 30 trillion cells, all with different functions and sizes (Bianconi et al., 2013). Size can be related to function, for example, in metabolically active organs like the liver, cells are larger in size than in more static tissues (Schmidt and Schibler, 1995). The size of a cell can change under certain circumstances; B cells shrink at a particular stage of maturation, only to expand in the following stage, and then become small again in the next (Cancro, 2004). Chondrocytes increase their volume by 10 to 20 fold during hypertrophic bone growth (Cooper et al., 2013).

1.2 Cell Size Regulation

Cell growth is understood as mass accumulations that results in increased cell size. Cells can accumulate water (which complies 70% of the cell's weight), ions, small molecules and other complex macromolecules (composed mainly of four basic building blocks: amino acids, carbohydrates, nucleotides and lipids). Proteins make up for 18% of total mammalian cell weight.

The regulation of protein synthesis is therefore an important step in increase of cell size. Proteins are synthesized in the cytoplasm by the ribosome. An ordinary eukaryotic cell has millions of ribosomes capable of adding amino acids to a polypeptide. In this cell, protein synthesis begins by associating the messenger RNA (mRNA) to the ribosomes, which is controlled by regulatory factors known as "initiating factors". When the cell is stimulated by external cues, growth factors, which are small peptides that bind receptors on the extracellular surface of cells and activate intracellular signalling pathways, activate the initiation factors.

Protein synthesis is a very energetically costly project for the cell and for this reason the cells have mechanisms for integrating and controlling both nutrient and protein synthesis pathways.

The growth-signalling network is an ancient mechanism that is evolutionarily conserved in eukaryotic cells. It is centrally regulated by the kinase protein target of Rapamycin (TOR), which in yeast, is regulated solely by nutrient availability in the surrounding environment, most importantly amino acids, followed by secondary signals from glucose metabolism.

In unicellular organisms such as yeast, cell growth and proliferation are mostly controlled by the extracellular nutritional environment, which allows a direct coupling of resources to cell generation (Lloyd, 2013).
In multicellular organisms, however, growth proliferation, and survival need to be differentially regulated in multiple tissues, so additional levels of control are required (Alberts, 1998). A mammalian cell sitting in a culture dish surrounded by nutrients will not enter the cell cycle or add mass in the absence of a mitogen or growth factor,

respectively (Rathmell et al., 2000). In proliferating animal cells, growth and cell cycle progression are independent processes, each governed by extracellular cues. According to this view, size itself is not actively controlled, but merely results from the independent control of the rates of cell growth and cell division (Conlon et al., 2001, Conlon and Raff, 2003)

1.2 Drugs for Cell Size Discovery

To understand the function of the pathways that govern the cell size regulation, multiple drugs have been developed with the aim to downregulate key components of these pathways.

1.2.1 Rapamycin

In 1964 a Canadian expedition to the South Pacific Island of Rapa Nui (known as Easter Island) collected soil samples to identify novel antimicrobial agents. From these samples, *Streptomyces hygroscopicus* produced a novel antimicrobial agent with antifungal, immunosuppressive, and antitumor properties. Rapamycin (also known as sirolimus and later marketed under the trade name Rapamune by Pfizer) is a macrocyclic lactone (Figure 1.1) (Sehgal et al., 1975)**.**

Rapamycin was later found to be effective as an immunosuppressant with anti-proliferative properties in humans (Heitman et al., 1991, Sehgal, 2003). Rapamycin binds to mTOR and prevents the phosphorylation of its downstream substrates p70 ribosomal protein S6 kinase (RPS6K) and eukaryotic translation initiation factor 4E-binding protein 1 (4EBP1). Rapamycin associates with its intracellular receptor, FK 506-bining protein of 12 kDa (FKBP12), and the resulting complex interacts with the FKP12-Rapamycin binding (FRB) domain located in the C-terminus of mTOR (Dowling et al., 2010b, Li et al., 2014).

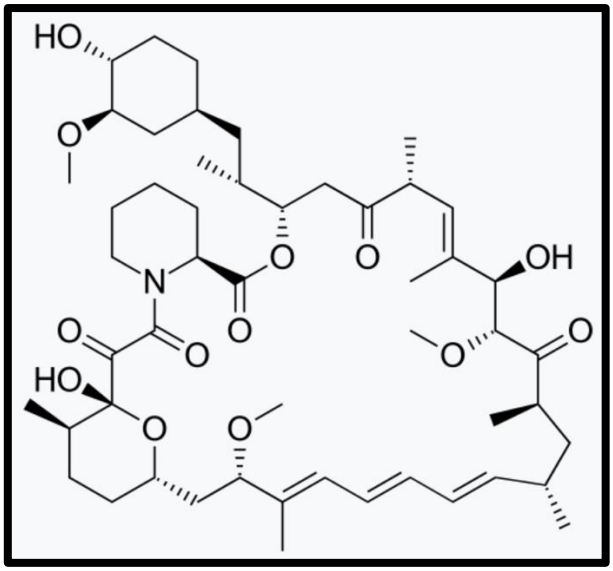

Figure 1.1 Rapamycin Molecule. Sirolimus or Rapamycin is a molecule originally found to be secreted by *Streptomyces hygroscopicus* as an antifungal compound and later found to be capable of hampering mTOR's kinase activity. Image obtained from the Selleckchem catalogue.

1.2.2 LY294002

LY294002 has been identified as a pan-class PI3K inhibitor by competing ATP binding sites to inhibit the catalytic subunit of PI3K (Ihle and Powis, 2010). The perturbation of the PI3K/AKT axis has been shown in different malignancies, giving it an importance as a possible target for therapy. The compound 2-(4-morpholinyl)-8-phenylchrome (2-morpholino-8-phenyl4H-1-benzopyran-4-one, also known as LY294002 (figure n), was found to be a selective inhibitor of PI3K with a 2.7 fold greater potency than the bioflavonoid quercetin (Vlahos et al., 1994).

LY294002 (Figure 1.2) has been identified as a pan-class PI3K inhibitor by competing with ATP binding sites to inhibit the catalytic subunit of PI3K (Ihle and Powis, 2010). PI3Ks (phosphatidylinositol 3-kinases) are lipid kinases responsible for the phosphorylation of phosphatidylinositol on the D3 position of their inositol ring.

These enzymes have a critical role in the life, death, growth proliferation, metabolism and diverse cell functions (Engelman et al., 2006). The PI3K is made up of 14 enzymes

that are divided into four classes, I to IV, of which the class I PI3Ks are the most studied (Vanhaesebroeck and Waterfield, 1999). In order to hamper PI3K's activity, the compound 2-(4-morpholinyl)-8-phenylchrome (2-morpholino-8-phenyl4H-1-benzopyran-4-one, also known as LY294002 was utilized, as it has been found to be a selective inhibitor of PI3K with a 2.7 fold greater potency than the bioflavonoid quercetin (Vlahos et al., 1994).

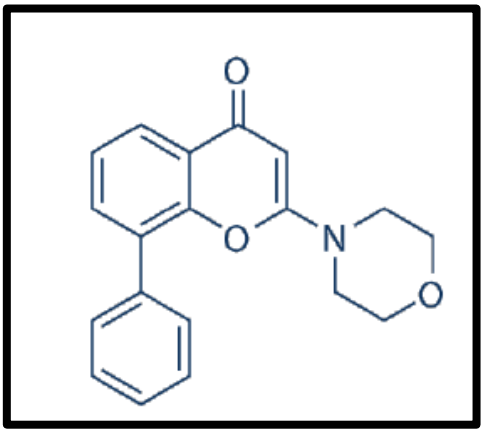

Figure 1.2 The PI3K inhibitor LY294002. The PI3K inhibitor competes for ATP binding sites to inhibit the catalytic subunit of PI3K. Image obtained from the Selleckchem catalogue.

1.2.3 AZD5363

AKT is one of the frequently deregulated proteins in cancer, a key node in the mTOR signalling network, with multiple substrates that mediate processes as diverse as cell proliferation, resistance to apoptosis, and glucose and fatty acid metabolism (Wendel et al., 2004). AZD5363 is a potent pan-AKT kinase inhibitor developed by Astra Zeneca with pharmacodynamic properties consistent with the mechanism of action of an AKT inhibitor in vivo. In isolated enzyme assays, AZD5363 inhibited all 3 isoforms of AKT, and its activity in cells was determined by its ability to inhibit the phosphorylation of its substrates PRAS40 and GSK3β, S6 and 4EBP1.

Protein kinase B (PKB, also known as AKT) is a key node in the signalling network, with multiple substrates that mediate processes as diverse as cell proliferation, resistance to apoptosis, and glucose and fatty acid metabolism (Wendel et al., 2004).

To block AKT's activity, the inhibitor AZD5363 was used; AZD5363 is a potent pan-AKT kinase inhibitor (Figure 1.3), developed by Astra Zeneca with pharmacodynamic properties consistent with the mechanism of action of an AKT inhibitor in vivo.

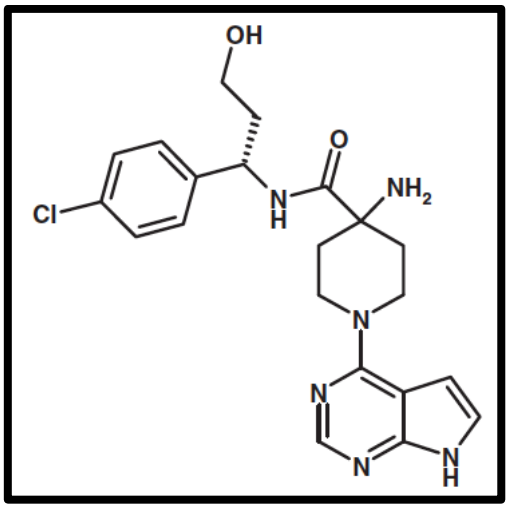

Figure 1.3 AZD5363 structure. AZD5363, [(S)-4-amino-N-[1-(4-chlorophenyl)-3-hydroxypropyl]-1-(7H-pyrrolo[2,3-d]pyrimidin-4-yl)piperidine-4-carboxamide also known as Capivasertib. Image obtained from the Selleckchem catalogue.

In isolated enzyme assays, AZD5363 inhibited all 3 isoforms of AKT, and its activity in cells was determined by its ability to inhibit the phosphorylation of its substrates PRAS40 and GSK3β, S6 and 4EBP1.

1.2.4 Actinomycin D

Actinomycin D (Act D) is a polypeptide antibiotic isolated from the genus *Streptomyces.* Act D is also one of the oldest chemotherapy drugs, commonly used to treat different types of cancer (Bensaude, 2011, Cortes et al., 2016, Lu et al., 2015). Act D binds to DNA, preferentially intercalating into GC rich sequences and stabilising topoisomerase-I DNA covalent complexes that prevent RNA polymerase progression. (Perry and Kelley, 1970). It is widely used as a transcription inhibitor. RNA polymerase I, which is catalysing ribosomal RNA transcription, is most sensitive to lower concentrations of Act D (IC 50, 0.05 μg/mL); followed by RNAP II a (0.5 μg/mL) and a less sensitive RNAP III (about 5 μg/mL). Low concentrations of Act D block

transcription of RNA polymerase I and induce nucleolar stress by interfering with ribosome biogenesis (Chen and Jiang, 2004, Liu et al., 2016b).

1.2.4 SB203580

P38α is an interesting pharmaceutical target because of its important role in inflammatory diseases such as psoriasis, arthritis or chronic obstructive pulmonary disease. SB203580 was the first p38 mitogen-activated protein kinase (MAPK) inhibitor to be identified that binds competitively at the ATP-binding pocket (Zhang et al., 2007, Kumar et al., 2003, Cuenda et al., 1995, Wrobleski and Doweyko, 2005). It has been widely used to assess the role of p38 MAPK in a wide array of biological systems, including its antiproliferative activity (Lali et al., 2000), the p38 MAPK pathway's influence on inflammation (Gao et al., 2019), and epithelial-to-mesenchymal transition (Yan et al., 2016).

1.3 Measuring the Cell Size

To understand more adequately the process behind cell size regulation, and the physical changes in the cells driven by these processes, we must rely on multiple approcheas and technologies:

1.3.1 Moxi Z

Moxi Z is an automated cell counter that uses the Coulter Principle (Graham, 2013) to count and measure the size of different types of cells. Electric current is passed through a small hole (Cell Sensing Zone) in a thin-film membrane. Cells flow through the CSZ causing momentary increases in measured voltage that are directly proportional to cell or particle volume. Thousands of cells are measured during a single

test and the size of each cell is plotted and saved in histogram format. Total volumetric counts are determined by precisely measuring the volume of fluid being analysed.
In order to analyse cells in the Moxi Z, these must first be resuspended, and from this, 75 µl of the sample are carefully added to the Moxi Z cassette, followed by waiting for the machine to detect the sample and fit a curve.

1.3.2 Flow cytometry

Flow cytometry is a technology that measures physical characteristics of biological or nonbiological single particles as they flow in a fluid stream through a beam of light.
A flow cytometer is made up of three main systems: fluidics, optics and electronics.
The purpose of the fluidics system is to transport particles in a fluid stream to the laser beam for interrogation.

Light scattering occurs when a particle deflects incident laser light. The extent to which this occurs depends on the physical properties of the particle, to be precise, its size and internal complexity. Forward-scattered light (FSC) is proportional to cell-surface area or size (Figure 1.4). FSC is a measurement of mostly diffracted light and is detected just off the axis of the incident laser beam in the forward direction by a photodiode. Side-scattered light (SSC) is affected by cell granularity or internal complexity. SSC is a measurement of mostly refracted and reflected light that occurs at any interface within the cell where there is a change in refractive index. SSC is collected at approximately 90 degrees to the laser beam by a collection lens and then redirected by a beam splitter to the appropriate detector.

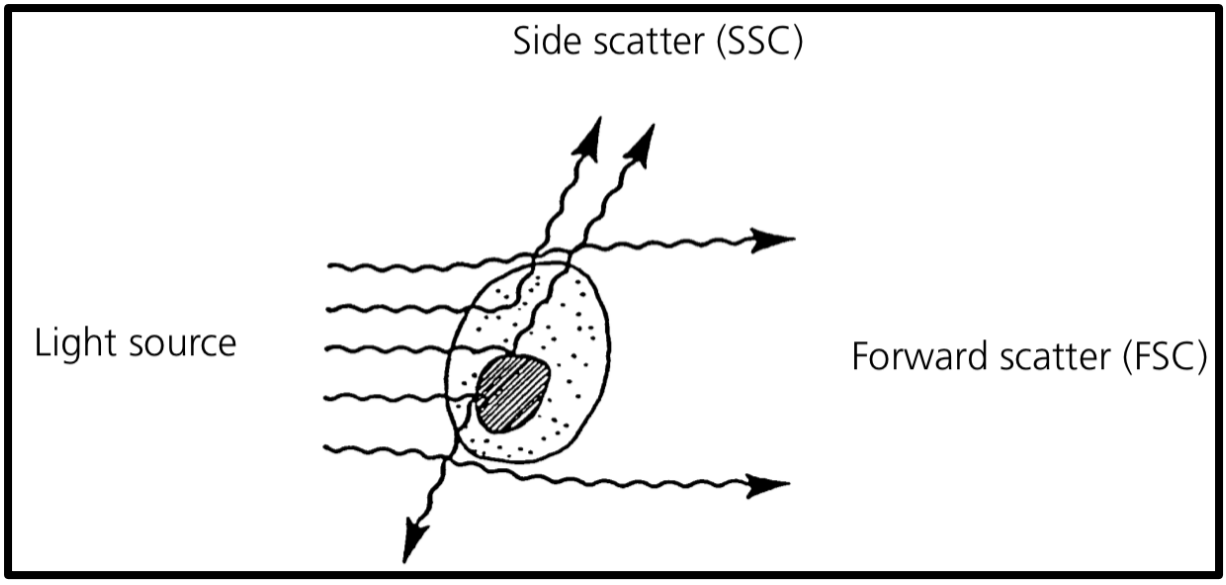

Figure 1.4 How light scattering gives information of the cell's biology. When light is deflected in a side scattered fashion (SSC) information on the granularity of the cell can be obtain. The forward scattered light gives us a proxy measurement for cell size.

The optical system consists of excitation optics and collection optics. Once a cell or particle passes through the laser light, emitted SSC and fluorescence signals are diverted to the photomultiplier tubes (PMTs), and a photodiode collects the FSC signals. PMTs detect fluorescence signals, which are often weak. The specificity of a detector for a particular fluorescent dye is optimized by placing a filter in front of the PMT, which allows only a narrow range of wavelengths to reach the detector. This spectral band of light is close to the emission peak of the fluorescent dye. Such filters are called bandpass (BP) filters.

Light signals are generated as particles pass through the laser beam in a fluid stream. These signals are converted to electronic signals by photodetectors and then assigned a channel number on a data plot. The photodiode is less sensitive to light signals than the PMTs and thus is used to detect the stronger FSC signal. PMTs are used to detect the weaker signals generated by SSC and fluorescence.

Data can be analysed using a gate, which is a numerical or graphical boundary that can be used to define the characteristics of particles to include for further analysis.
For every signal (electromagnetic pulse) which passes into a detector, there are three characteristics which can be recorded: Height, width, and area.

In order to remove spurious doublets that can be detrimental to analyses, a forward scatter height (FSC-H) vs forward scatter area (FSC-A) gate is drawn. Doublets will have double the area and width values of single cells whilst the height is roughly the same. Therefore, disproportions between height, width and area can be used to identify doublets (Shapiro, 1981, Shapiro, 2003, Wersto et al., 2001, Watson, 2004)

1.4 Staining the Nucleic Acid of the Cells

1.4.1 Hoechst 33342

The assessment of cell cycle distribution of cells is important for studying different things such as growth differentiation, senescence, apoptosis, and even understanding disease. During cell cycle progression, proliferating cells sequentially undergo a transition from G1 to S to G2 to M phases for synthesis of DNA (Malumbres and Barbacid, 2009). A simple approach to analyse cell cycle status is to measure cellular DNA content at a single time point. This reveals a snapshot of cell cycle status among three distinct groups (G0/G1, S, and G2/M (Darzynkiewicz and Huang, 2004).

The most widely used chemical that fluorescently label DNA is the Hoechst 33342 dye, which comprises a group of benzamide dyes consisting of Hoechst 33342, 33258 and 34580 that were designed by the German company Hoechst AG back in 1970.

These dyes are excited by UV light (~360 nm) of xenon or mercury-arc lamps or UV lasers and emit a broad spectrum of blue light with a maximum excitation in the 460 nm region. These dyes bind to the minor groove of the DNA molecule, preferentially to adenine-thymine (A-T) regions (Mazzini and Danova, 2017, Pjura et al., 1987).
Hoechst 33342 (Figure 1.5) is used for specifically staining the nuclei of living or fixed cells and tissues, which helps to sort cells based on their DNA content (Darzynkiewicz et al., 2017, Kim and Sederstrom, 2015).

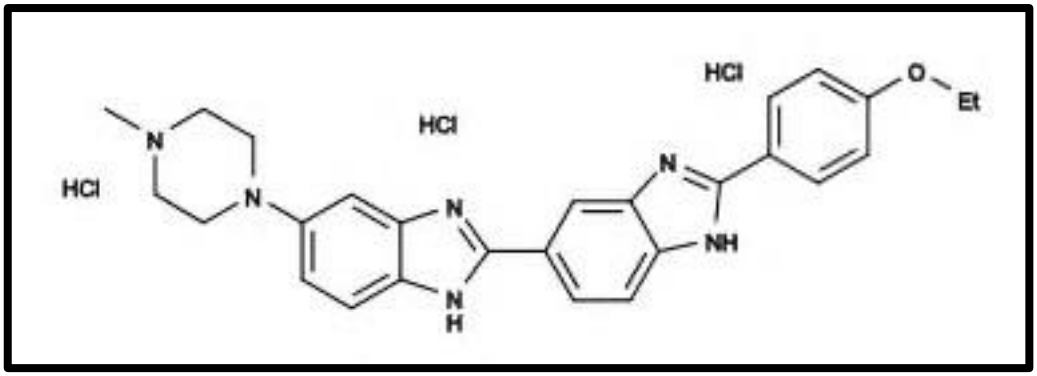

Figure 1.5 Hoechst 33342. The structure of the Hoechst 33342 (2'-[4-ethoxyphenyl]-5-[4-methyl-1-piperazinyl]-2,5'-bi-1H-benzimidazole trihydrochloride trihydrate) molecule. Image taken from abcam catalogue.

The assessment of cell cycle distribution of cells is important for studying different things such as growth differentiation, senescence, apoptosis, and even understanding disease. During cell cycle progression, proliferating cells sequentially undergo a transition from G1 to S to G2 to M phases for synthesis of DNA (Malumbres and Barbacid, 2009). A simple approach to analyse cell cycle status is to measure cellular DNA content at a single time point. This reveals a snapshot of cell cycle status among three distinct groups (G0/G1, S, and G2/M (Darzynkiewicz and Huang, 2004).

The most widely used chemical that fluorescently label DNA is the Hoechst 33342 dye, which comprises a group of benzamide dyes consisting of Hoechst 33342, 33258 and 34580 that were designed by the German company Hoechst AG back in 1970.

1.4.2 Pyronin Y to stain the dsRNA

Pyronin Y (PY) (Figure 1.6) was proposed to bind to nucleic acids after it was observed that treatment with ribonuclease removed its staining (Kurnick, 1955b, Kurnick, 1955a). It is a cationic environment-sensitive probe used to label endogenous double-stranded RNA (dsRNA) including mRNA, tRNA and ribosomal RNA (rRNA). Taking advantage of the fact that PY exhibits fluorescence, the dye has been adapted as an RNA stain in both fluorescent microscopy and flow cytometry (Kapuscinski and Darzynkiewicz, 1987). Pyronin alone can stain both DNA and RNA. However, in the

presence of a DNA dye such as Hoechst 33342 it can specifically stain RNA (Shapiro, 1981, Darzynkiewicz et al., 1987, Andrews et al., 2013).

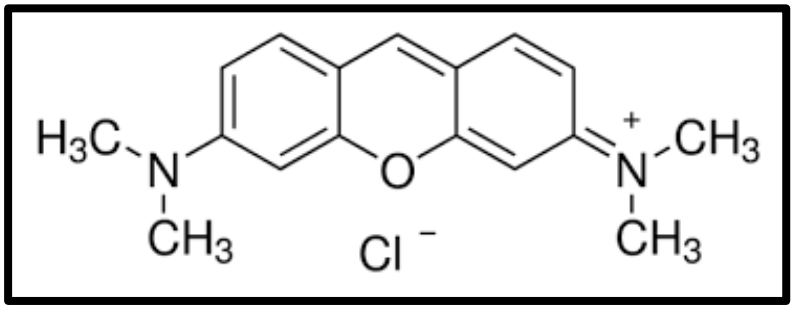

Figure 1.6 Pyronin Y. The chemical structure of Pyronin Y. Image taken from the sigma Aldrich catalogue**.**

Recently, the Pyronin Y/Hoechst 33342 combination has been used to detect G0 phase cells, as these have a lower level of RNA compared to active cells that are in G1, S, G2 or M phases. (Kim and Sederstrom, 2015). By combining RNA and DNA quantitation it is possible to discriminate between cell populations with the same DNA content and to assess their translational activity, cell proliferation and differentiation status (El-Naggar, 2004). Pyronin Y was also used to show that mTORC1 activation in B cells enhances Ribosome biogenesis (Ersching et al., 2017).

1.4 The physiological effects of cell size and its dysregulation

As discussed before, cells need to regulate their growth, and this may be linked to their function. Kidney epithelial cells for example, modulate their size in response to rates of fluid flow in the nephron ducts, sensed by mechanical shear on the primary cilium (Boehlke et al., 2010). Lymphocytes rapidly grow larger after exposure to cytokines or Toll-Like-Receptor (TLR) stimulation (Abbas et al., 2018) and pancreatic beta cells increase their size by over 25% during pregnancy, in response to increased insulin demand (Dhawan et al., 2007). It was found that the rate of insulin production of individual rat beta cells is more strongly correlated with cell size than with metabolic

activity (Giordano et al., 1993). Cells probably have an “adequate size” in which they are the most efficient. A deviation of this size would break the homeostasis of the cells’ actions. For example, beta cells from mice that lack S6K1 are smaller and secrete less insulin per cell when compared to normal beta cells. This could be due to a reduction in membrane surface available, leading to hypoinsulinemia. On the other hand, treating wild-type beta cells with Rapamycin, neither changed beta cell size, nor affected insulin secretion. This could indicate that reduced insulin secretion might result from a size defect rather than the absence of S6K1(Pende et al., 2000, Fabian et al., 1993). Furthermore, mice expressing constitutively active protein kinase AKT1 have larger beta cells than wild type mice and an increased rate of insulin secretion (Bernal-Mizrachi et al., 2001).

Clear differences in gene expression between large and small adipocytes suggest that cell size influences adipocyte biology (Farnier et al., 2002). Cellular enlargement by increasing cell surface area and modifying interactions between the cell and its extracellular matrix activates the β1-integrin/ERK signalling pathway that modulates several transcription factors (Farnier et al., 2003). Large adipocytes display a marked increase in the activity of fatty acid synthase and lipoprotein lipase. These changes are further manifested in the altered metabolic activity of large adipocytes and found that large adipocytes have higher rates of lipid synthesis (Smith, 1971, Smith and Jacobsson, 1973). However, the increased metabolic efficiency of large adipocytes comes at a price. Larger cells are less sensitive to the stimulating effects of insulin on glucose uptake, the oxidation of glucose to CO2 (Salans et al., 1968) and the uptake of triglyceride fatty acids (Nestel et al., 1969). The balance between metabolic capacity that scales positively with adipocyte size and insulin sensitivity that scales negatively with size implies an optimal adipocytes size. Supporting this idea, increased adipocyte size, rather than total body fat, is associated with insulin resistance in obesity and is a risk factor for development of type II diabetes mellitus (Guilherme et al., 2008).

Changes in cell size have also been linked to transcriptional and metabolic changes in other cell types, including hepatocytes and erythrocytes (Gregory, 2002, Miettinen et al., 2014)

While cancer is a disease of deregulated proliferation, in clinical histology it is the size of cancer cells that renders their appearance distinct from the surrounding tissue (Kufe et al., 2003). Malignant tumour cells are both larger and more variable in size than normal cells. Pleomorphism, the increased variability in cell size and shape, is a histological characteristic of many malignant lesions (Majno and Joris, 2004).

The loss of cell size regularity in cancer cells also occurs when cell lines of normal and neoplastic origin are grown in matching culture conditions, indicating that the increased size variability in cancer is cell-autonomous and not a product of the tumour microenvironment. When epidermoid carcinoma cell lines were classified based on cell size variability, only the highly heterogeneous lines initiated tumours upon hetero-transplantation into mice (Caspersson et al., 1963). These experiments raise the question of whether aberrant regulation of cell size has a role in tumorigenesis, although increased cell size variability may also be a mere correlate of tumour biology (perhaps the result of aneuploidy), and further experiments are warranted to resolve this question.

1.5 Noise in Gene Expression

Despite careful design and computer simulation, building a gene circuit in vivo may still be challenging due to transcriptional noise or stochastic fluctuations in cellular processes.

The term “noise” in gene expression is used to refer to the measured level of variation in gene expression among cells, regardless of source, within a supposedly identical population (Dennis Tu, 2006).

A cell increases its size and content to split into two daughter cells but, even though they are both clonal copies, it is impossible for them to receive the exact amount of the original content and if they did receive exactly one copy of a particular transcription factor, each will perform a Brownian random walk through its cellular volume before finding its target promoter and activating gene expression, rendering it statistically

impossible for both genes to become activated at the same time, further amplifying the phenotypic difference between the two daughter cells (Munsky et al., 2012). One of the first encounters of noise within a synthetic gene circuit was the one experienced by the “repressilator”; a synthetic network of repressors that was capable of producing oscillations in gene expression. The authors found that the oscillations were subject to fluctuations in their period and magnitude and conjectured that stochastic effects in gene expression were causing loss of coordination amongst cells (Elowitz and Leibler, 2000). Stochastic noise has been divided in two kinds, *intrinsic noise* which mainly involves the stochasticity of biochemical interactions relevant for gene expression, and *extrinsic noise* which arises from fluctuations of the environment, as well as cell size, its shape and cell cycle stage (Elowitz et al., 2002, Entrevan, 2013).

1.6 Cell size variability as a Cause of Extrinsic Noise

To design more predictable and stable synthetic genetic circuits, we need to understand the different sources of biological noise. Extrinsic noise is one of the main sources of gene stochasticity, therefore our goal is to analyse one of the possible causes of extrinsic noise, cell size variability. Little attention has been paid to the biological origins of extrinsic variability (Volfson et al., 2006). It has been noted that one of the main sources of extrinsic noise is cell volume (Raj and van Oudenaarden, 2008). Isolation of a yeast cell population by homogenous size showed that total noise was reduce by around 25% (Raser and O'Shea, 2004).

Even in an isogenic population, every cell is unique and larger cells need to produce and maintain more components than small cells. As the half-lives of transcripts and proteins are limited, there is a constant need to replace these molecules, and the demand for such replacement scales with cell size (Marguerat and Bahler, 2012). Mammalian cells exhibit large variability in cell volume, and they must compensate for differences in DNA concentration in order to maintain constant concentration of gene expression. Individual cells globally control transcription to compensate for variability in the ratio of DNA to cellular content. These compensatory mechanisms help to

maintain the concentration of mRNA in the cell, which is presumably useful from the perspective of the cell because the rates of most chemical reactions in the cell depend on concentrations rather than absolute number (Padovan-Merhar et al., 2015). As mentioned before, biochemical reaction rates depend on the concentration of reactants and enzymes. Thus, proper cellular concentrations must be maintained despite volume variations (Padovan-Merhar et al., 2015). The number of biomolecules in a cell is linked to its size, therefore, changes in overall molecule numbers associated with an imbalance in the production or degradations in size changes could affect concentrations of regulators that ultimately will affect global dynamics of biochemical networks involved in the cellular fate (Shahrezaei and Swain, 2008).

1.7 Cells used in this study

1.7.1 HEK293

The human embryonic 293 cell line was stablished in 1973 by Alex van der Eb's laboratory in the Netherlands (Shaw et al., 2002) by exposing primary embryonic kidney cell culture of an aborted embryo to the mechanically sheared DNA of adenovirus type 5 (AD5) (Graham et al., 1977). The 293-cell line and its derivates have been the most frequently used cells after HeLa in cell biology studies and after CHO in biotechnology, sometimes incorrectly supposed as a non-tumorigenic or even a "normal" human cell line. It has been hypothesized that 293 cells originated from the embryonic adrenal precursor structure (adrenal medulla), which closely associated with the kidney during development and of the neural crest ectodermal origin (Lin et al., 2014). The 293T cell line contains the SV40 large T-antigen, which allows the episomal replication of transfected plasmids containing the SV40 origin of replication. The HEK293FT is a fast growing variant of the HEK293T variant, designed for lentiviral production (Stepanenko and Dmitrenko, 2015).HEK293 cells are fed with 10% FBS-containing DMEM with 1% Penicillin-Streptomycin.

1.7.2 HeLa

The first cell line to be grown continuously in a laboratory was the HeLa cell line (Masters, 2002). The cell line was established by George Grey from cervical cancer originated in an African American patient named Henrietta Lacks (and hence the name HeLa). To this day, most of our knowledge of cellular and biochemical processes comes from this cell line (Schepers, 1992). The cell line keeps being used because of its stable genome after years of cultivation (Macville et al., 1999). HeLa cells have from 76 to 80 chromosomes (Heng, 2013). HeLa cells grow very rapidly even compared to other cancer cells, with a doubling time of around 24 hours. This unlimited replication capacity is because of HeLa cells' high telomerase activity (Sfeir and de Lange, 2012).

1.7.3 U2OS

Normal epithelial cells show a limited capacity to grow and proliferate in culture conditions and for this reason Pontén & Saksela established the 2T cell line, obtained from a 15-year-old patient's osteosarcoma derived from an amputated leg in 1964 (Ponten and Saksela, 1967). This resulted in the U2OS cells which are one of the first ever cell lines created and of the most used in research (Niforou et al., 2008). This cell line has showed chromosomal instability (Bayani et al., 2003). Contrary to other more aggressive osteosarcoma cell lines, U2OS cells have functional p53 and Rb tumour suppressor genes and, perhaps for this reason, have the lowest level of chromosomal numerical variation (Wesierska-Gadek and Schmid, 2005, Zhu, 2005, Isfort et al., 1995).

1.8 A quick overview of this thesis

In this thesis we will dissect the involvement of multiple biological pathways involved in mammalian cell growth control by inhibiting the action of multiple regulators of the mTOR pathway. We will analyse the sequencing data belonging to cells with downregulated mTOR pathway to elucidate which genes are affected by this

treatment. We will also discuss the effects of the overexpression of the transcription factor Myc on mammalian cell growth and a combination of this with the downregulation of the mTOR pathway. RNA sequencing data from these cells will be analysed to further dissect the genes differentialy expressed and their functions. Our goal is to understand the pathways involved in the control of mammalian cell size regulation.

Chapter 2: Materials and Methods

2.1 Materials

2.1.1 Bacterial Strains

Escherichia coli DHα5 strains used to clone the Myc plasmid were purchased from ThermoFisher Scientific (Massachusets, USA).

2.1.2 Human Cell Lines

HEK293 cells were provided by Dr Daniel Hebenstreit (School of Life Sciences, University of Warwick). HeLa cells were provided by Dr Keith Leppard (School of Life Science, University of Warwick). MycER U2OS cells were kindly provided by Dr Stefano Campaner (Instituto Italiano di Tecnologia*)*.

2.1.3 Specific Kits

T**able 2.1 Kits.** Different Kits used in the thesis.

Method/Aim	**Kit Name**	**Manufacturer**
RNA Extraction	RNeasy® Micro Kit (50)	Qiagen
Plasmid Extraction	QIAprep® Spin Miniprep Kit (50)	Qiagen
Transfection Reagent	jetPRIME	Polyplus Transfection

2.1.4 Culture Media

Dulbelcco's Modified Eagle's Medium (DMEM), Luria-Bertani (LB) broth (LB), Penicilin-streptomycin, Phosphate-Buffered Saline (PBS) and trypsin were provided by the School of Life Science's Media Preparation Room. Tetracycline-free Foetal Bovine Serum (FBS) was purchased from Labtech International Ltd. East Sussex, UK.

2.1.5 Drugs

Rapamycin Ready Made Solution in DMSO, Actinomycin D Ready Made solution in DMSO, Puromycin dihydrochloride Ready Made Solution and 4-Hydroxytamoxifen Ready Made Solution in Ethanol were purchased from Sigma-Aldrich (Merck). LY294002 and SB203580 were purchased from Cell Signal Technology. AZD5363 was purchased from Selleckchem.

2.1.6 Nucleic Acid Stains

Hoechst 33342 (20mM solution in water) was purchased from Stratech. Pyronin Y (1 g) was purchased from Sigma (Merck).

2.1.7 Antibodies

Monoclonal anti-c-Myc antibody 9E10 produced in Mouse and Anti-Puromycin, clone 12D10, Alexa Fluor® 647 Conjugated Antibody were purchased from Sigma (Merck). GAPDH Monoclonal antibody produced in Mouse was purchased from Proteintech®. Goat anti-mouse IgG-HRP sc-2031 was purchased from Santa Cruz Biotechnology.

2.1.8 silencing RNAs (siRNAs)

SignalSilence® Control siRNA Unconjugated (C-) #6568, SignalSilence® Akt siRNA I #6211 and SignalSilence® p70/85 S6 Kinase siRNA I #6566 were purchased from Cell Signaling Technology®.

2.1.9 Plasmids

pMyc was purchased from Addgene (Addgene plasmid # 42142; http://n2t.net/addgene: 42142; RRID: Addgene_42142).

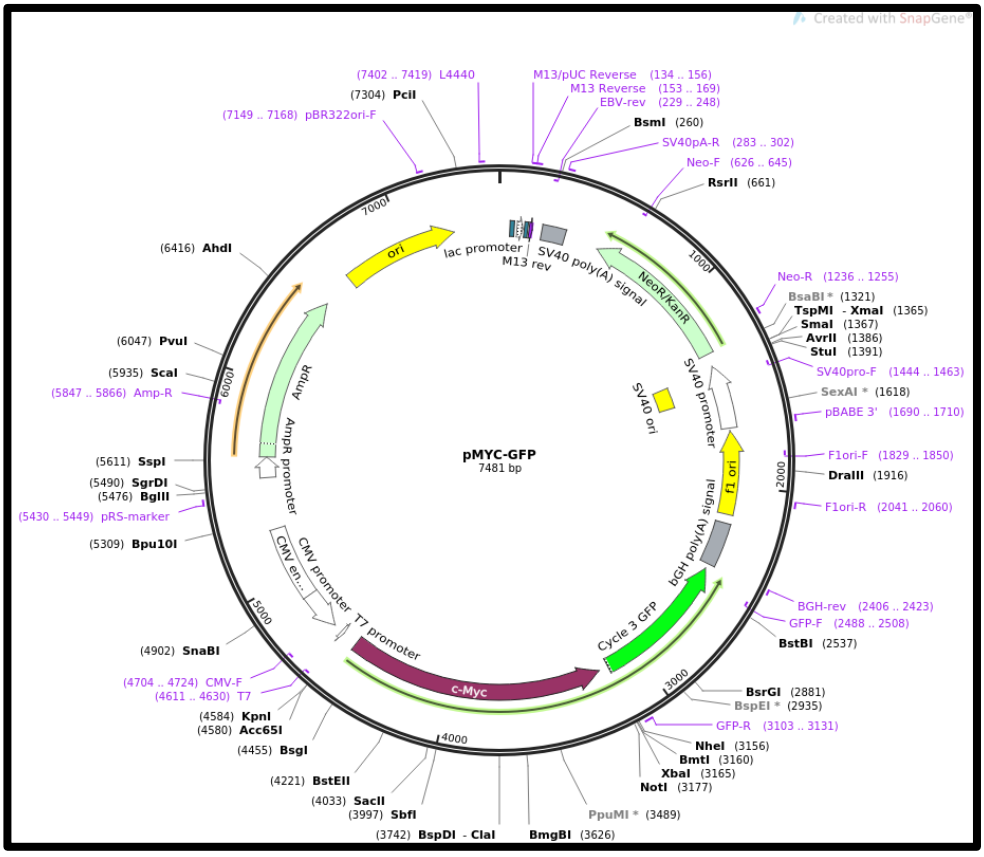

Figure 2.1 pMyc-GFP plasmid. The full length of c-Myc protein coding DNA fragment was inserted in the 5' end of GFP under the control of the cytomegalovirus (CMV) promoter. Image taken from (Addgene plasmid # 42142; http://n2t.net/addgene:42142 ; RRID:Addgene_42142)

2.1.10 Western Blot

XT Tricine 20X Running buffer and Nitrocellulose Membrane 0.45 µm were purchased from Bio Rad. Pre-cast RunBlue SDS Gel 4-12% were purchased from Expedeon (now part of abcam). Pierce™ ECL Western Blotting Substrate (for detection of HRP), Pierce™ RIPA buffer, and Halt™ phosphatase inhibitor cocktail (100X) were purchased from Thermo Scientific.

2.2 Methods

2.2.1 Bacterial Growth and Storage

E. coli strains were grown on either liquid or solid LB media produced and provided by the School of Life Science's Media Preparation Room, at 37ºC.

2.2.2 Bacterial Transformation

Bacterial strains, microtubes and 200-250 ng of DNA (per transformation) are placed on ice. 50 µL of competent cells are added to the DNA and are mixed by pipetting gently (avoiding vortex). The mixture is then placed on ice for 30 minutes. Afterwards, the mixture is heat shocked at 42 ºC for 40 seconds. Then, 950 µL of LB media at room temperature is added to the mixture and placed in an incubator at 37 ºC shaking at 250 revolutions per minute (rpm) for 1 hour. Afterwards, 50 µL to 100 µL of cells are spread in LB agar plates with selective antibiotics and incubated overnight for further analysis.

2.2.3 Plasmid Extraction

Plasmid extraction was performed using a QIAprep® Spin Miniprep Kit (50) by QIAgen following the manufacturer instructions.

2.2.4 Transfection

Transfection of both siRNAs and Plasmid was performed using the jetPRIME transfection reagent from the Polyplus company. 100,000 cells are seeded in 6 well dishes in a total of 2 mL complete growth medium. The next day, a final concentration of 50 nM siRNA, or 4 µg of plasmid are mixed with 200 µl of jetPRIME buffer in a sterile microtube, the mixture is vortexed for 15 seconds and then 4µl of jetPRIME regent is added. The mixture is vortexed for 5 seconds and then incubated for 10 minutes at room temperature. After the incubation, the mixture is added to each well and cells are brought back to the incubator for further analysis.

2.2.5 Mammalian Cell Culture

To start (or restart) a cell culture, cells are removed from the liquid nitrogen storage and placed into dry ice (or the container of liquid nitrogen), this is to keep them cool whilst transferring them to the cell culture room. Then cells are rapidly thawed by placing them in a 37^{o}C water bath (ideally with gentle agitation) for 1-2 minutes. The vial must be wiped with 70 % Ethanol or IMS to decontaminate, the vial contents are slowly transferred into 10ml of Growth Medium into a sterile falcon tube (15 or 50ml), the cells are then centrifuged at 500 x g for 5 minutes. The supernatant is removed, the cell pellet is resuspended in the desired volume of pre-warmed growth medium at 37 ^{o}C and this is finally transferred into a flask or plate for culture.

Once cells have reached confluency, they must be passed to another flask or plate. The media is removed from the flask where cells are cultured, and cells are rinsed with PBS to wash away the remnants of anti-trypsin protein. Cells are incubated in trypsin-EDTA for 5 minutes at 37 ^{o}C (mechanical stress can be applied to help cells detach) and then quenched with growth medium. Cells are transferred to a falcon tube and centrifuged at 500 x g for 5 minutes, followed by removal of the medium. Then the pellet is resuspended in fresh growth medium and seeded at the desired concentration in a flask or dish.

2.2.6 Pharmacological Treatments

The pharmacological treatments follow a similar strategy, with the main variation being the type of drug and/or their concentration. The drugs and concentrations were selected based on other research using the same drugs in concentrations with similar ranges (Choi et al., 2016, Liao et al., 2019) (Table 2.2).

Table 2.2 Drugs. Table of different drugs and concentrations used in the thesis.

Drug	**Concentration**
Rapamycin	1 μM, 5 μM, 10 μM and 20 μM
LY294002	5 μM, 10 μM and 20 μM
AZD5363	5 μM, 10 μM and 20 μM
4-Hydroxytamoxifen	1 μM
Actinomycin D	100 ng/mL
SB203580	15 μM

In a six-well plate, 100,000 cells are seeded per well in 10% FBS-containing DMEM, then the drug to be utilized is added to the experimental wells along with the equivalent volumes of DMSO/Ethanol as a vehicle control. Cells are then incubated for 24 hours at 37^{o}C in 5% CO_2 to let Rapamycin affect the cells. After 24 hours, the growth medium is removed, and the cells are rinsed with PBS to wash away Rapamycin. Cells are then incubated with trypsin-EDTA for 5 min at 37^{o}. After the five minutes, trypsin is quenched with complete growth medium, and the cells are resuspended and deposited into 1.5ml microtubes which are then pelleted at 500 x g for 5 minutes. The media is removed, and the pellet is washed in room temperature PBS three times and then resuspended in PBS-4% FBS and then analysed by flow cytometry or Moxi Z.

2.2.7 Flow Cytometry

Flow cytometry analysis was recorded on a BD LSRFortessa Cell Analyser flow cytometer. Cell size was collected using the FSC channel, DNA content was captured by illuminating the Hoechst 33342 dye using a 20 mW UV355 laser, signal was collected through 355 nm long-pass and 450/50 nm band-pass filters. Green fluorescent protein signal (GFP) was captured by using a 50 mW, Blue 488 nm laser collecting through a 488 nm long-pass and 530/30 nm band-pass filters. Pyronin Y was recorded using a 50 mW Yellow-Green 561 nm laser, collecting data through a 561 long-pass and a 710/50 band-pass filters. The signal from the anti-puromycin antibody was collected using a 40 mW Red 640 nm laser colleting through a 640 long-pass and a 670/30 short-bandpass filters. All the data is recorded with the area, width and height option.

The data was analysed using the software FlowJo 8.7.

In order to remove spurious doublets that can be detrimental to analyses, a forward scatter height (FSC-H) vs forward scatter area (FSC-A) gate is drawn. Doublets will have double the area and width values of single cells whilst the height is roughly the same. Therefore, disproportions between height, width and area can be used to identify doublets.

Once the doublets have been eliminated, gates for the appropriate channel can be drawn to extract the mean values of fluorescence for each desired channel.
Graphical representations of the fluorescence values can be plotted using the histograms option.

A Watson Pragmatic cell cycle analysis was performed using the FlowJo software to identify the Cell Cycle distribution. To perform this analysis the data from samples

stained with Hoechst 33342 dye was recorded using the 355 nm long-pass and 450/50 nm band-pass filters and in linear scale.

2.2.8 Staining Nucleic Acids

Cells in complete growth medium are incubated with 10 µg/mL Hoechst 33342 dye for 15 minutes at 37 ^{o}C, (anything longer than 20 minutes will prove to be toxic to the cells). If cell cycle is to be analysed, washed in PBS, and incubated with trypsin for 5 minutes at 37 ^{o}C, and then the reaction is quenched with complete DMEM. Cells are resuspended and then centrifuged at 500 x g. The pellet of cells is subsequently washed in PBS and centrifuged at 500 x g, then cells are prepared for flow cytometry.

If cells are to be stained with Pyronin Y, the cells are firstly stained with Hoechst 33342 for 15 minutes, washed in PBS and then incubated with 4 µg/mL of Pyronin Y dye for 45 minutes at 37 ^{o}C in complete growth medium. Afterwards, cells are incubated with trypsin-EDTA for 5 min at 37^{o}C. After five minutes trypsin is quenched with complete growth medium and the cells are resuspended and transferred into 1.5ml microtubes, which are then pelleted at 500 x g for 5 minutes. The media is removed, and the pellet is resuspended in PBS-4% FBS and then analysed with flow cytometry

To detect Pyronin Y's capacity to bind to RNA, growth medium is removed, cells are washed in PBS, incubated for with trypsin-EDTA for 5 min at 37^{o}C, then trypsin is quenched with complete growth medium, cells are transferred into microtubes, they are pelleted and resuspended in PBS. After this, cells are pelleted and resuspended in 4% PFA-PBS for 20 minutes at room temperature, washed and incubated for 1 hour at 37 ^{o}C with RNase A. After the time has passed, cells are pelleted, resuspend in PBS and taken to flow cytometry.

Hoechst 33342 dye is excited at 350 nm and its emission can be recorded between 440 and 480 nm. Pyronin Y optimal excitation is at 550 nm and its optimal emission is around 575 nm.

2.2.9 SUnSET

100,000 cells are seeded in 6 well dishes in a total of 2 mL complete growth medium. On the day of the experiment, negative control cells are incubated for 30 minutes with 100 µg cycloheximide then, cells are incubated for 10 minutes with puromycin (Puromycin Pulse) afterwards, cells are incubated in trypsin for 5 minutes at 37 ºC, washed with PBS and then re-seeded in a six-well dish with 5% FBS,1% Penicillin-streptomycin DMEM for 30 minutes (Chase). After 30 minutes, the cells are resuspended with either DMEM or ice-cold PBS and collected, then washed in PBS-4% FBS and incubated with 50 µl PBS-4% FBS + 2 µl 12D10 Anti-Puromycin Antibody for 1 hour in ice covered from light. After one hour, cells are resuspended and washed in PBS-4% FBS twice and finally surface proteins and antibodies are fixed with PBS-2% Paraformaldehyde (PFA) and stored at 4 ºC protected from light until analysis.

2.2.10 Western Blot

Cells are previously grown in a 6-well plate, growth medium is removed, and cells are washed twice with ice-cold PBS. Then, 130 µl of ice-cold Pierce™ RIPA buffer is added to the cells, along with 1.6 µl of Halt™ phosphatase inhibitor cocktail (100X). Cells are then lysed and transferred to a 1.5 mL microtube, which is then centrifuged at 14,000g for 15 minutes. After that, the supernatant is collected. The protein content is quantified using the Pierce™ BCA Protein Assay Kit by measuring absorbance at 562 nm on an Infinite® M Nano TECAN plate reader.

The lysate is mixed with Leammli buffer and boiled at 100ºC for 5 minutes to denature the protein. A total of 30 µg of protein were loaded on a precast 4-12% RunBlue™ Tricine SDS gel along with 2 µl of molecular weight ladder, and then run for 1-2 hours at 100 V. After that, the gel is transferred onto a nitrocellulose membrane by semi-wet transfer for 15 minutes at 15 V in a Trans-Blot SD Semi-Dry Transfer cell from Bio Rad. The membrane is then blocked in 5% fat-free milk-PBS-Tween for 1 hour at room temperature. Afterwards, the membrane is incubated in 1:1000 primary antibody overnight at 4 ºC. As a control GAPDH Monoclonal antibody produced in Mouse was

used, and Monoclonal anti-c-Myc antibody 9E10 produced in Mouse to detect Myc. The next day, the membrane is washed 3 times with PBS-Tween and then incubated with 1:10,000 Goat anti-mouse IgG-HRP sc-2031secondary antibody, at room temperature. Once the incubation has ended, the membrane is washed in PBS-Tween for 5 minutes in agitation, 3 times. Next, the membrane is incubated in a 1:1 solution A and B buffers from the Pierce™ ECL Western Blotting Substrate and taken to the ImageQuant LAS 4000 to analyse for chemiluminescence.

2.2.11 RNA Extraction

RNA extraction was performed using the RNeasy® Micro Kit (50) by QIAGEN and following the manufacturer's instructions.

2.2.12 RNA sequencing & sequencing analysis

For RNA sequencing analysis in Chapter 4, 20 µl of RNA (20ng/µl) from MycER U2OS cells were sent to the Novogene Europe Company (United Kingdom) for library preparation and sequencing. Sequencing was performed on a NovaSeq 6000 system.

For Chapter 3, the dataset from Gene Expression Omnibus: GSE130006 (Liao et al., 2019) was used for analysis. It consists from high-throughput RNA-sequencing were performed on HeLa cells treated with DMSO (as control) and 1 µM Rapamycin. The sequencing generated more than 30 million reads for each sample.

All raw fastq files were downloaded from the Novogene server (Chapter 4) or from the Gene Expression Omnibus (Chapter 3). Quality assessment was performed using FastQC (https://www.bioinformatics.babraham.ac.uk/projects/fastqc/). Trimming of adapter sequences was carried out using the function trim_galore (`trim_galore --fastqc --paired A$i\_1.fq.gz A$i\_2.fq.gz`).

The paired-end RNAseq files were aligned to the reference genome (*H. sapiens*, GRCh38) using Hisat2 alignment program:
(hisat2 -x /<Directory>/<reference genome>/ -1 A$i_1_val_1.fq.gz -2 A$i_2_val_2.fq.gz -S A$i.sam --thread 20) and generating SAM files as a result.

SAM files generated by Hisat2 where then converted to BAM files, sorted and indexed using these three samtools commands: (samtools view -S -b A$i.sam > A$i.bam) (samtools sort A1.bam A1.sorted) (samtools index A1.sorted.bam) generating indexed SAM files which were used to create Gene counts.

Then Gene counts were generated using LiBiNorm software
(LiBiNorm count -z -r pos -i gene_name -s no A$i.sorted.bam ~/<directory>/2_aligned/Homo_sapiens.GRCh38.77.gtf > A$i.txt)

An input .txt file, made up from the metadata information, was created to identify the samples and their treatment for the analysis.

The DESeq function in RStudio (Version 1.3.1093) takes the raw counts produced in LiBiNorm and performs a default analysis where estimation of size factors and estimation of dispersion were determined to extract the differentially expressed genes (DEGs). Wald test was used for differential expression analysis, and we used adjusted p-value (padj) <0.05 as a threshold.

Volcano plots were drawn by using the *Enhanced Volcano* package in R. The volcano plot is constructed by plotting the negative log of the p-value on the y-axis (usually base 10). This results in data points with low p-values (highly significant) appearing toward the top of the plot. The x-axis is the log of the fold change between the two conditions. The cut-off thresholds were defined by adjusted p-value (padj) <0.05 and a log2Fold change cut-off of 2 in datasets form chapter 4 and a log2Fold change cut-off of 1 in dataset from chapter 3.

Scatter X-Y plots were produced using R package. It plots the log2 of the replicate average of two of the treatments against each other. Genes where the adjusted p-value is less than 0.05 are marked in red.

Gene Ontology analysis was performed using datasets containing either a mix of both upregulated and downregulated differentially expressed genes unless specified otherwise.

GO analysis was performed using the `topGo` package on the genes that were found to be differentially expressed between conditions to determine which GO terms arranged by biological process are associated with them. Using the `Genetable` function a summary table with the results of the analysis was generated which was then plotted using `ggplot2` in a bubble plot.

Other platforms were also used to perform Gene Ontology term analysis:

g:Profiler: (https://biit.cs.ut.ee/gprofiler/gost)

GOrilla: (http://cbl-gorilla.cs.technion.ac.il)

Enrirchr: (https://maayanlab.cloud/Enrichr/)

Chapter 3: Chemical manipulation of a size regulating pathway in mammalian cell lines and its effects.

3.1 Introduction

3.1.1 The PI3K/AKT/mTOR Pathway Regulates Cell Growth

Cell growth (mass accumulation) and proliferation (cell division) are separated (yet very close) processes that require specific mitogens or growth factors in order to either add mass or trigger cell cycle (Conlon et al., 2001).

The best-characterized regulatory pathway that controls cell growth is the IGF/PI3K/AKT/mTORC1 pathway. This evolutionarily conserved pathway has been shown to be a major regulator of cell growth and thus a key determinant of cell size; moreover, artificial activation of this pathway can promote additional growth. Insulin Growth Factor (IGF) is a classic example of a limiting growth factor that acts both systematically and at local tissue levels. Overexpression during development results in larger animals, mainly due to increases in cell size, and overexpression in the adult can result in cell hypertrophy. Binding of IGF to its receptor activates multiple signalling pathways, but key to regulating cell growth is the activation of the PI3K/AKT/mTORC1 axis with mTORC1, a central mediator of the signal from the growth factor to biogenic pathways. In addition, mTORC1 integrates inputs from at least four other major cues

that can affect cell growth – stress, energy status, oxygen, and amino acid levels- and thus acts as a signalling node at which energetic and stress signals can modulate growth factor signals (Laplante and Sabatini, 2012).

The mTOR pathway controls cell growth in response to energy, nutrients, growth factors and other environmental cues (Lloyd, 2013). Central to the pathway is the mTOR protein, which belongs to the phosphoinositide 3-kinase (PI3K) related protein kinase family. mTOR assembles into two complexes with distinct inputs and downstream effects, mTOR complex 1 (mTORC1) and mTOR complex 2 (mTORC2). mTORC1 regulates cell growth by promoting ribosome biogenesis and autophagy, its activation requires nutrients and amino acids, whilst mTORC2 responds primarily to growth factors, promoting cell cycle entry, cell survival, actin cytoskeleton polarization and anabolic output (Yang et al., 2013). In mammalian cells, protein synthesis and cell growth are regulated by mTOR pathway and it has been observed that serum starvation leads to decrease in p70S6K and 4EBP1 phosphorylation, key downstream regulators of mTOR pathways, which is consistent with mTOR downregulation (Pirkmajer and Chibalin, 2011) (Foster and Fingar, 2010).

Signalling to induce rpS6 phosphorylation by growth factors starts by activation of the respective receptor tyrosine kinase. This in turn leads to activation of class I phosphatidylinositol-3kinase (PI3K); PI3K converts the lipid phosphatidylinositol-4,5-P2 (PIP2) into phosphatidylinositol-3,4,5-P3 (PIP3), in a reaction that can be reversed by the PIP3 phosphatase PTEN (phosphatase and tensin homolog detected from chromosome 10) (Leslie and Downes, 2002). PIP3 recruits both 3-phsphoinositide-dependent kinase 1 (PDK1) and AKT (also known as protein kinase B (PKB)) to the plasma membrane (Brazil and Hemmings, 2001, Rameh and Cantley, 1999), and PDK1 phosphorylates and activates AKT, which in turn phosphorylates tuberous sclerosis complex 2 (TSC2) at multiple sites (Inoki et al., 2002). This phosphorylation blocks the ability of TSC2, while residing within the TSC1-TSC2 tumour suppressor dimer, to act as a GTPase-activating protein (GAP) for Rheb (Ras-homolog enriched in brain), thereby allowing Rheb-GTP to accumulate and operate as an activator of the Rapamycin-sensitive mammalian TOR complex 1 (mTORC1) (Avruch et al., 2006). The latter is consisting of target of Rapamycin (TOR), RAPTOR (regulatory associated protein of TOR), LST8 and PRAS40 (Proline-rich AKT substrate 40kDa).

AKT can also activate mTORC1 independently of TSC1-TSC2 by phosphorylating PRAS40, thereby relieving the PRAS40-mediated inhibition of mTORC1.

Active mTORC1 phosphorylates two translational regulators, S6 Kinases (S6K) and eukaryotic initiation factor 4E (eIF4E)-binding protein (4EBP1, 2 and 3). Activation of S6Ks requires phosphorylation by PDK1 in a reaction that does not need binding of PDK1 to PIP3. Finally, activated S6K phosphorylates rpS6, as well as many other substrates (Figure 3.1). mTORC1 phosphorylates the S6Ks 1&2, contributing to their activation. S6Ks in turn phosphorylates several proteins linked to mRNA translation, including ribosomal protein S6, eEF2 (eukaryotic elongation factor 2) kinase, eIF4B (eukaryotic initiation factor 4B) and Pdcd4 (programmed cell death 4). S6K-mediated phosphorylation of eEF2 kinase inhibits its activity, which promotes translation elongation.

eIF4B and Pdcd4 are positive and negative regulators of the RNA helicase eIF4A (Shahbazian et al., 2006). eIF4A helps to unravel secondary structure in the 5'-untranslated regions (5'UTRs) of mRNAs. Such secondary structure inhibits efficient translation and occurs in a number of mRNAs that encode key regulators of cellular functions. eIF4A is recruited to the 5'-end of the mRNA through its interaction with the scaffold protein eIF4G. In turn, eIF4G is brought to the mRNA through its interaction with eIF4E, the protein that binds the 5'-terminal 7-methylguanosine "cap" structure (Proud, 2009).

The association of eIF4G with eIF4E is regulated through another substrate of mTORC1, the 4EBPs (eIF4E-binding proteins) that, when bound to eIF4E, prevent eIF4E's association with eIF4G (since eIF4G occupies overlapping sites in eIF4E). Phosphorylation by mTORC1 disrupts binding of 4EBP1 to the eIF4E, allowing the latter protein to bind to eIF4G. Once eIF4E is bound to the 5'end of the mRNA, this allows the recruitment of eIF4A and other partners for eIF4G, such as PABP [poly(A)-tail-binding protein]. The complex of eIF4E, eIF4G and eIF4A is often termed "eIF4". Recent results have demonstrated that 4EBPs are involved in the control of cell proliferation by mTORC1, probably because they affect (impair) the translation of proteins required for cell cycle progression (Dowling et al., 2010a).

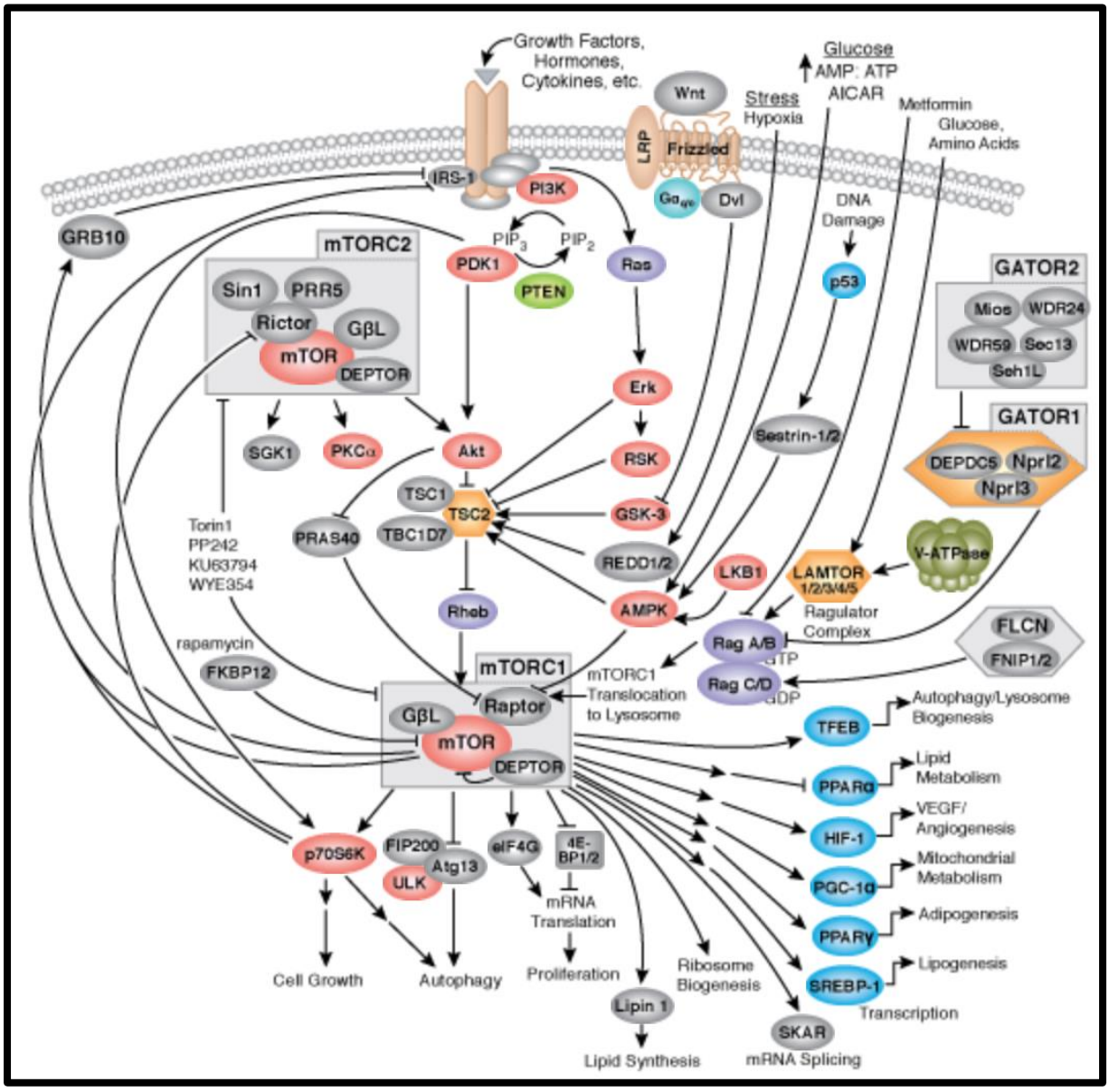

Figure 3.1 The PI3K/AKT/mTOR signaling pathway. The mTOR pathway plays a major role in many pathways involved in multiple cell fates, including cell growth, proliferation, translation, cell cycle progression, apoptosis, and others. Image obtained from Cell Technology.

3.2 Results

3.2.1 Inhibition of PI3K and AKT reduces Mammalian Cell Size.

As mentioned before, the PI3K/AKT/mTOR pathway is central to cell size control. In order to manipulate mammalian cell size, it was decided to chemically impair two central components of this pathway; PI3K and AKT, both up-regulators of the central protein mTOR (Lloyd, 2013).

Asynchronous HEK293 cells were incubated with increasing concentrations of both AZD5363 and LY294002 for 24 hours in complete growth media, afterwards the cells were resuspended, washed, and analysed using flow cytometry for cell size using the parameter forward scatter area (FSCA) which is a measure of relative cell size.
HEK293 cells exposed to 5 μM, 10 μM and 30 μM of both LY294002 and AZD5363 showed a notable reduction of cell size according to FSCA measurements with no apparent difference between the concentration when compared to non-treated controls (Figure 3.2).

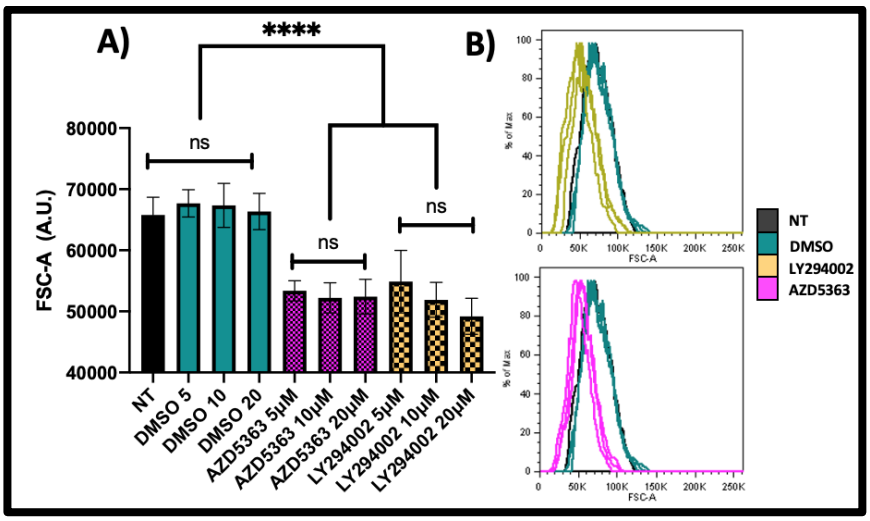

Figure 3.2 The PI3K and AKT inhibitors reduce the size of HEK293 cells. HEK293 cells were exposed to rising concentrations of LY294002 and AZD5363 inhibitors. A) Bar plots of

HEK293 cells exposed to increasing concentrations of AZD5363 and LY294002 and then analysed with flow cytometry. B) Representative histograms generated in Flow Jo of LY294002 and AZD5363 treatments compared to controls. Arbitrary Units (A.U.). Data shown are mean values ± standard deviations (N = 3 independent biological replicates). Statistical significance was assessed by ANOVA with Tukey's test, Asterisks represent the p-value: * p < 0.05, ** p < 0.01, *** p < 0.001, **** p < 0.0001.

To see if the effect observed before was not exclusive to HEK293 cells, we exposed HeLa cells to 5 µM, 10 µM and 30 µM of LY294002 and AZD5363 inhibitors separately for 24 hours and then they were analysed with flow cytometry and the changes in cell size were as well visualized by means of the FSCA. HeLa cells exposed to both inhibitors showed a reduction of cell size when compared to non-treated cells. The greater effect was observed in cells exposed to LY294002 followed by AZD5363 exposure (Figure 3.3).

HEK293 cells showed a slightly larger cell reduction than HeLa cells.

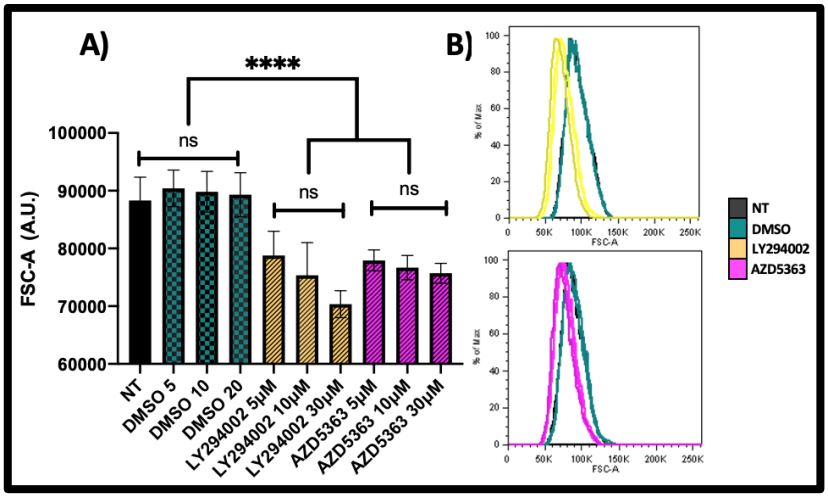

Figure 3.3 Incubation with the PI3K and AKT inhibitors reduces HeLa cell size. HeLa cells were exposed to increasing concentrations of LY294002 and AZD5363 inhibitors. A) Bar plots of HEK293 cells exposed to increasing concentrations of AZD5363 and LY294002 and then analysed with flow cytometry. B) Representative histograms generated in Flow Jo of LY294002 and AZD5363 treatments compared to controls. Arbitrary Units (A.U.). Data shown are mean values ± standard deviations (N = 3 independent biological replicates). Statistical

significance was assessed by ANOVA with Tukey's test, Asterisks represent the p-value: * p < 0.05, ** p < 0.01, *** p < 0.001, ****p < 0.0001.

These results show that chemically blocking the activity of both P3IK and AKT caused cell size reduction in both HEK293 and HeLa cells. This reduction could be due to different reasons, including changes in the cell cycle distribution of the cell population. Unfortunately, when the last measurements were taken, the cells were not stained for a cell cycle analysis and the AKT inhibitor was not available anymore; for this reason, we focused the next assays on the LY294002 inhibitor.

3.2.2 Inhibition of PI3K by LY294002 changes the cell cycle distribution and cell size independently of mammalian cell lines.

In order to understand the mechanisms underlying the effects of LY294002 on cell size, both HeLa and HEK293 cells were incubated with 30 μM of the PI3K inhibitor for 24 hours at 37 C, then stained with 10 μM of the DNA stain Hoechst 33342 for 10 minutes and washed with PBS and resuspended to be analysed by flow cytometer, using the FSCA as a cell size indicator and the UV355 channel to detect the Cell Cycle distribution.

Both HEK293 (Figure 3.4 A) and HeLa (Figure 3.4 B) cells exposed to 30 μM were smaller than non-treated cells as expected.

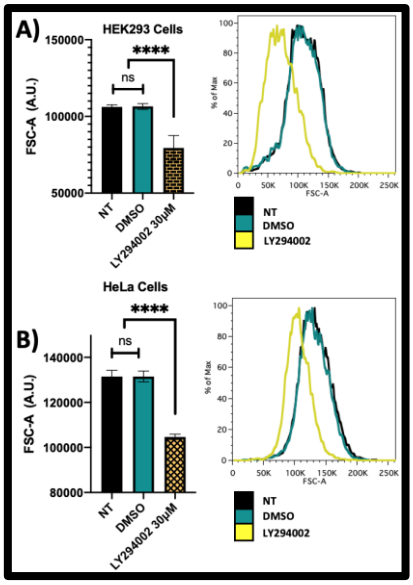

Figure 3.4 Mammalian cell size is reduced by high concentration of LY294002. A) Bar plots of HEK293 cells were exposed to 30 µM of LY294002 and then analysed with flow cytometry, representative histograms of cytometry size data. B) Bar plots representing size changes in HeLa cells after exposure to LY294002, representative histograms of the effects on cell size analysed by flow cytometry. Arbitrary Units (A.U.). Data shown are mean values ± standard deviations (N = 3 independent biological replicates). Statistical significance was assessed by ANOVA with Tukey's test, Asterisks represent the p-value: * $p < 0.05$, ** $p < 0.01$, *** $p < 0.001$, ****$p < 0.0001$.

As the PI3K/AKT/mTOR pathway is intimately related to cell cycle, it was important to analyse the effects of this inhibitor on the distribution of the cells in their cell cycle stages.

The PI3K inhibitor LY294002 showed a significative increase in the proportion of cells in G1; in asynchronous non-treated and control HEK293 around 48% of the population is in G1, whereas this population increases 55% and we can see a reduction of around 5% of the population of cells in S phase after treatment, compared to the controls (Figure 3.5 A). HeLa cells seemed the most susceptible to the effects of LY294002 on cell cycle changes. On asynchronous non-treated and control cells, the population of these in G1 is around 45% whereas in the treated cells it rises to an average of 66%, with a reduction of cells in S phase from 31% in control cells to 15% for LY294002-treated cells and another 5% reduction in G2 phase cells (Figure 3.5 B).

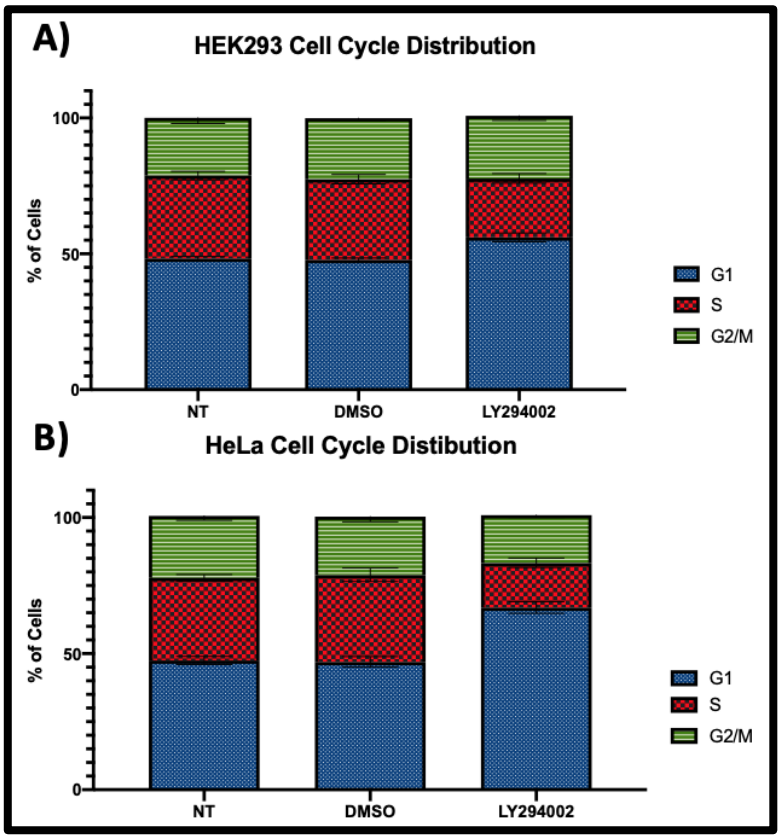

Figure 3.5 The Cell Cycle distribution of Mammalian cells change with exposure to LY294002. Cell cycle distribution of A) HEK293 or B) HeLa cells exposed to 30 μM LY294002 for 24 hours. Blue colour represents G1 phase, Red represents S phase and Green represents G2/M phase. Cell cycle distribution was obtained by Watson Pragmatic cell cycle analysis in Flow Jo.

As mentioned before, exposure of asynchronous HEK293 cells to LY294002 increased the population of G1 cells. To verify that this wasn't the reason why treated cells were smaller, by using Hoechst 33342 we were able to measure the G1 and G2 cell population's size by FSCA. We observed that G1 treated cells were overall smaller than non-treated (Figure 3.6 A), the same applied to G2 cells (3.6 B).

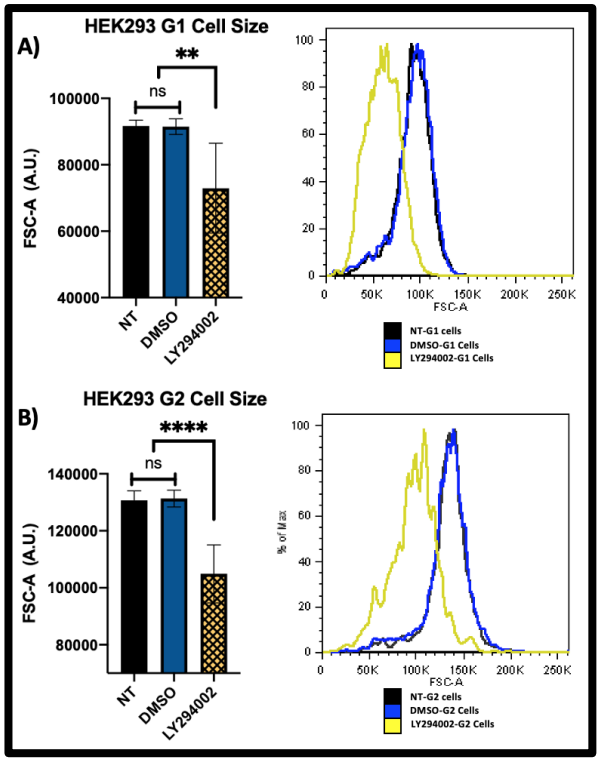

Figure 3.6 LY294002 treated cells are overall smaller. A) HEK293 G1 cells exposed to 30 μM of LY294002 are smaller than controls. B) HEK293 G2 cells from an asynchronous population exposed to 30μM of LY294002 are smaller compared to controls. Arbitrary Units (A.U.). Data shown are mean values ± standard deviations (N = 3 independent biological replicates). Statistical significance was assessed by ANOVA with Tukey's test, Asterisks represent the p-value: * $p < 0.05$, ** $p < 0.01$, *** $p < 0.001$, ****$p < 0.0001$.

HeLa cells also showed a shift in their cell cycle distribution, with G1 having more cells. They were also analysed using flow cytometry to determine the G1 and G2 cell size by FSCA. We observed that G1 treated cells were overall smaller than non-treated (Figure 3.7 A), the same applied to G2 cells (3.7 B).

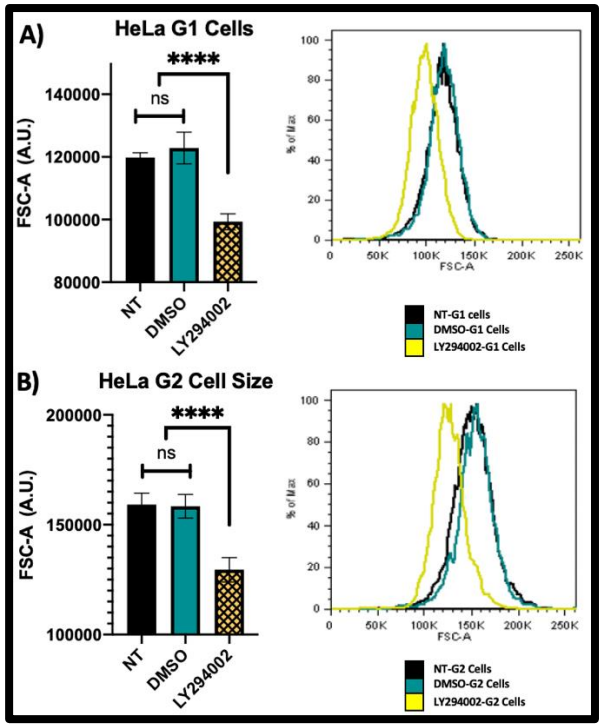

Figure 3.7 HeLa cells exposed to 30 μM LY294002 treated cells are overall smaller. A) HeLa G1 cells exposed to 30 μM of LY294002 are smaller than controls. B) HeLa G2 cells from an asynchronous population exposed to 30 μM of LY294002 are smaller compared to controls. Arbitrary Units (A.U.). Data shown are mean values ± standard deviations (N = 3 independent biological replicates). Statistical significance was assessed by ANOVA with Tukey's test, Asterisks represent the p-value: * $p < 0.05$, ** $p < 0.01$, *** $p < 0.001$, ****$p < 0.0001$.

This shows that inhibiting PI3K has strong effects on the mechanisms controlling the cell size by altering the cell cycle distribution of these cells and shrinking all the cells, no matter in which stage of the cell cycle they were.

3.2.3 The Macrolide Rapamycin affects mammalian cell lines' size

We can see that manipulation of the PI3K/AKT/mTOR pathway results in changes in the cell size and the cell cycle. In order to understand the mechanisms underlying this

and the control of cell size variability, it was decided to interfere with the central node of the size-regulating pathway, mTOR.

To be more precise with the effects of the chemical inhibition of mTOR on cell size, the cells' diameters (µm) and volumes (pL) were assessed by using the Moxi Z automated cell counter.

HEK293 cells were exposed to increasing concentrations of a 100 nM, 500 nM and 1 µM of Rapamycin for 24 hours and then analysed through the Moxi Z cell counter, where it was observed that the diameter of the cells exposed to Rapamycin was reduced by 10% compared with non-treated or control cells (Figure 3.8A), whilst the volume reduced approximately 28% on treated cells (Figure 3.8B).

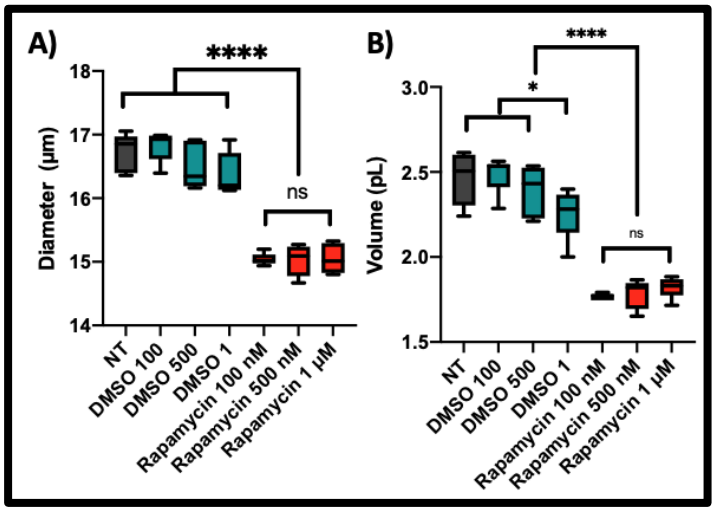

Figure 3.8 Rapamycin reduces the volume and diameter of HEK293 cells. HEK293 cells exposed to varying concentrations of Rapamycin were measured by Moxi Z. A) Cell diameter shows smaller cells when exposed to Rapamycin not necessarily in a concentration manner. B) Cell volume of cells exposed to Rapamycin is reduced. Statistical significance was assessed by ANOVA with Tukey's test, ns = non-significant, * $p < 0.05$, ** $p < 0.01$, *** $p < 0.001$, ****$p < 0.0001$. Data shown are mean values ± standard deviations (N = 3 independent biological replicates). Box and whiskers plots calculated in GraphPad Prim, selecting the Min to Max option, the line in the middle of the box is the median.

HeLa cells were also exposed to increasing concentrations of Rapamycin for 24 hours and analysed in the Moxi Z coulter counter. After exposure to Rapamycin the diameter

reduced approximately 7% comparing to the non-treated and control cells (Figure 3.9A). The volume on the other hand showed a reduction of around 21% on Rapamycin-treated cells compared to non-treated cells (Figure 3.9B).

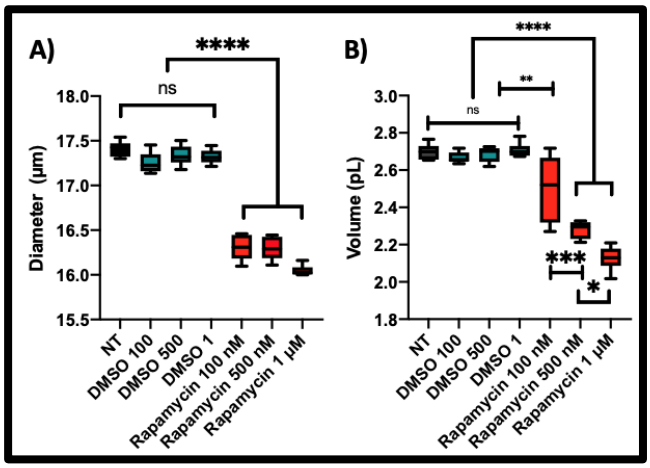

Figure 3.9 Rapamycin reduces the diameter and volume of HeLa cells. HeLa cells exposed to increasing concentrations of Rapamycin were measured by Moxi Z. A) Diameter is reduced when cells are exposed to Rapamycin in a concentration dependent manner. B) Volume of cells exposed to Rapamycin is reduced not in a concentration dependent manner. Statistical significance was assessed by ANOVA with Tukey's test, ns = non-significant, * $p < 0.05$, ** $p < 0.01$, *** $p < 0.001$, ****$p < 0.0001$. Data shown are mean values ± standard deviations (N = 3 independent biological replicates). Box and whiskers plots calculated in GraphPad Prism, selecting the Min to Max option, the line in the middle of the box is the median.

The cells were taken to the flow cytometer to analyse their size and cell cycle distribution by means of the forward scatter area and UV channel respectively, to compare size changes with those obtained by Moxi Z and see if there was a positive correlation. At the same time, this would allow us to gate specific cell cycle stages and obtain the size changes in those cells.

Although both cell types showed an overall reduction of cell size, HEK293 cells were slightly more affected (Figure 3.10A) than HeLa cells (Figure 3.10B) when compared to non-treated cells.

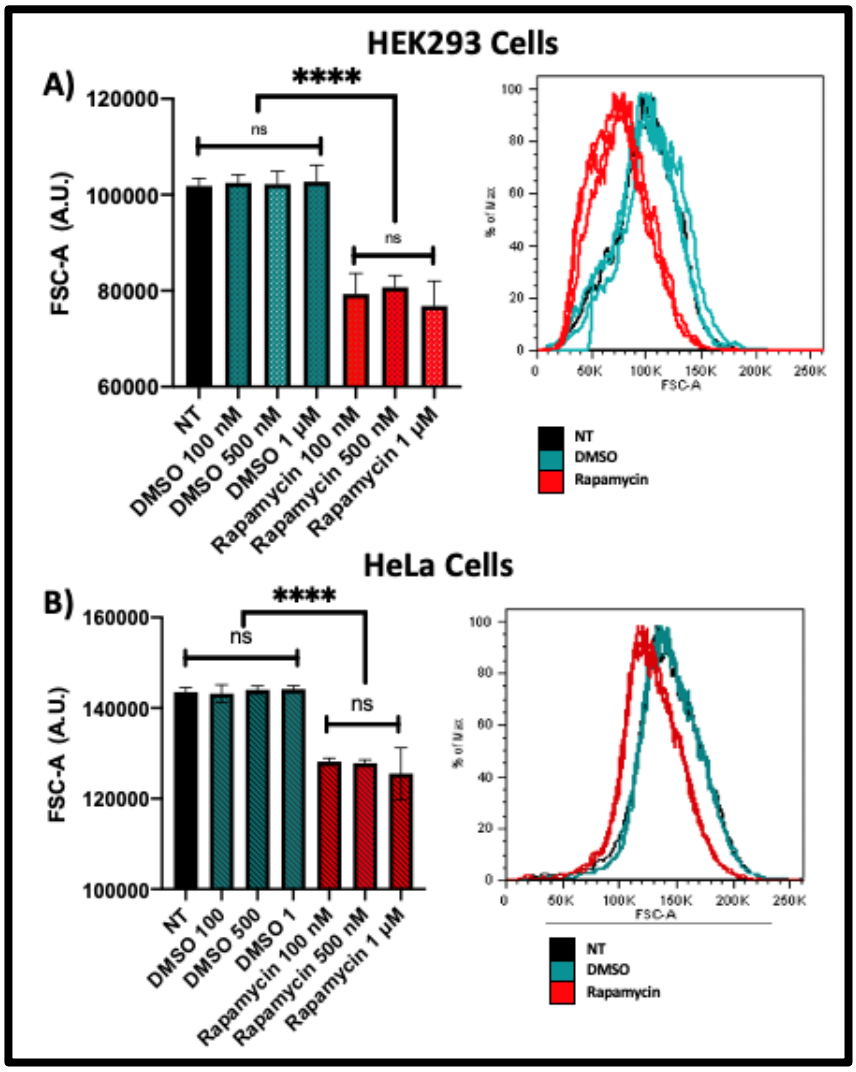

Figure 3.10 Rapamycin reduces the size of mammalian cells measured by flow cytometry. Two mammalian cell lines were exposed to increasing concentrations (100 nM, 500 nM and 1 µM) of Rapamycin and then analysed with flow cytometry. A) Bar plots and representative histograms displaying size changes in HEK293 cells after exposure to Rapamycin. B) Bar plots and representative histograms indicating size changes in HeLa cells after Rapamycin incubation. Arbitrary Units (A.U.). Data shown are mean values ± standard deviations (N = 3 independent biological replicates). Statistical significance was assessed by ANOVA with Tukey's test, Asterisks represent the p-value: * $p < 0.05$, ** $p < 0.01$, *** $p < 0.001$, ****$p < 0.0001$.

To assure that FSCA is indeed a proxy for cell size, a correlation between both cell lines' diameters and FSCA values were plotted, where, indeed, the forward scatter channel has a positive correlation with the measurements of diameter by the Moxi Z counter (Figure 3.11 A&B).

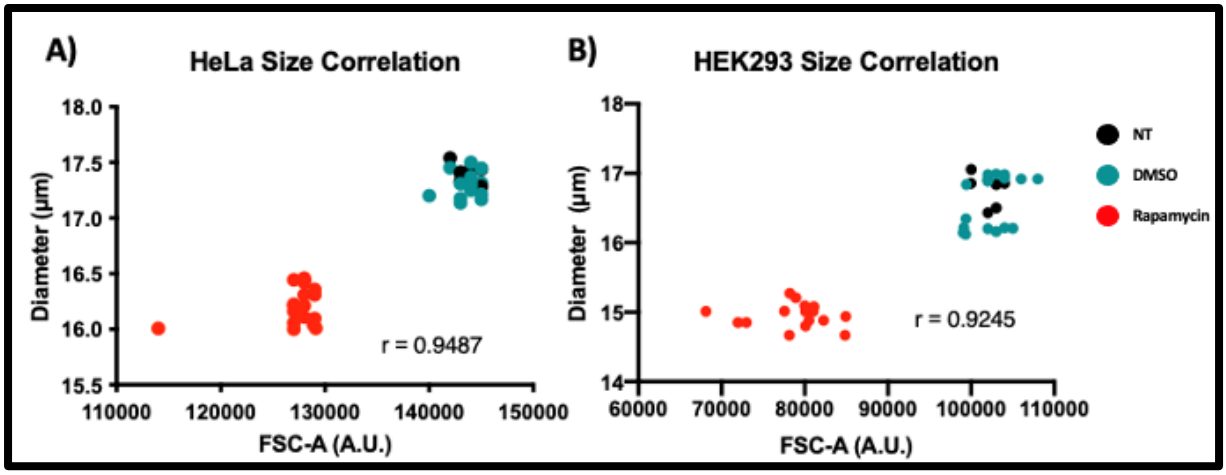

Figure 3.11 Cell Size measurements by flow cytometry correlate with diameter measurements taken by Moxi Z. Correlation between Diameter and FSCA. A) HeLa cells show a correlation between both values, with r = 0.9487. B) HEK293 cells show a correlation between both values with r = 0.9245.

3.2.4 Rapamycin affects the cell cycle distribution

Since cell cycle is intimately related to mTOR, it was of importance to analyse the impact of Rapamycin treatment on both HEK293 and HeLa cells.

HEK293 cells exposed to Rapamycin showed a slight accumulation of cells in G1, from an average of 47% in non-treated and control cells, to 55% in Rapamycin-treated cells. The cells accumulated in G1 probably are derived from the 5% reduction of the population of cells in S phase in non-treated cells compared to Rapamycin-treated cells (Figure 3.12A). HeLa cells showed an increment as well in the population of cells in G1, changing from a 44% of the non-treated and control cells in G1, to 52% of cells exposed to Rapamycin. In contrast to HEK293 cells, the shift in cell cycle distribution seemed to come from G2 cells, where in non-treated cells the population is 25%

whereas in Rapamycin treated cells the population of cells in G2 phase is only 15% (Figure 3.12B).

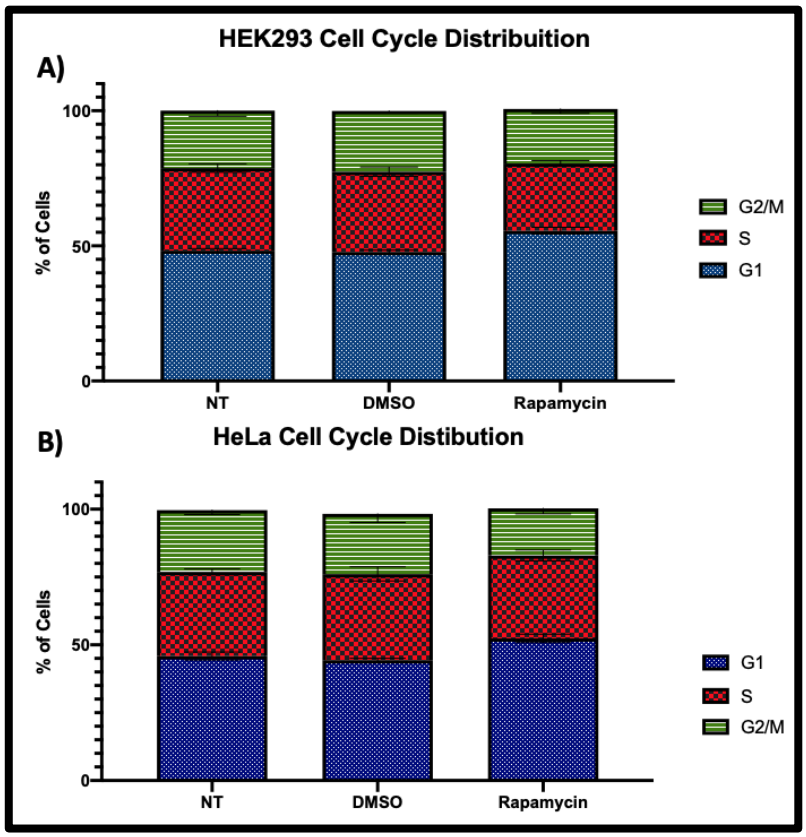

Figure 3.12 Cell Cycle Distribution changes in Cells treated with Rapamycin. Cell cycle distribution of A) HEK293 or B) HeLa cells exposed to 1 μM Rapamycin for 24 hours. Blue colour represents G1 phase, Red represents S phase and Green represents G2/M phase. Cell cycle distribution was obtained by Watson Pragmatic cell cycle analysis in Flow Jo. Data shown are mean values ± standard deviations (N = 3 independent biological replicates).

3.2.5 Rapamycin reduces the size of the cells independently of the cell cycle distribution.

To further understand the effects of Rapamycin on HEK293 and HeLa cells upon cell size, it was necessary to corroborate if Rapamycin's size reduction was because of the increment of the number of cells in G1 or if it was indeed an effect upon the cells

in all stages of the cell cycle. Both cell types were stained with the DNA stain Hoechst 33342 and then the cells belonging to G1 and G2 phases were gated, and their size was extracted.

As expected HEK293 cells in both G1 and G2 affected by Rapamycin were smaller than non-treated a cell (Figure 3.13).

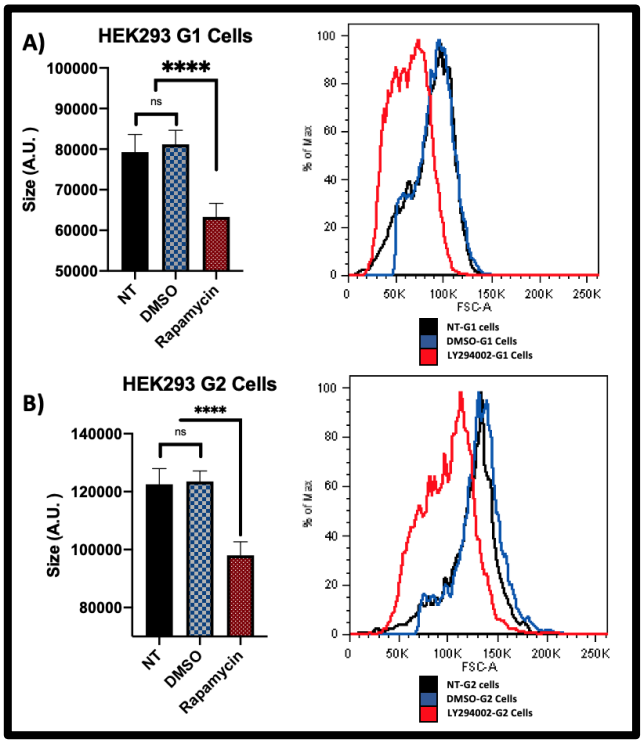

Figure 3.13 Rapamycin treated HEK293 cells are overall smaller. HEK293 cells treated for 24 hours with 1 μM Rapamycin were analysed by flow cytometry using the UV355 channel to gate them by their cell cycle distribution. A) Bar plot and representative histogram from FSCA channel data of G1 Size HeLa cells from both control and Rapamycin treated groups, Rapamycin G2 cells are smaller than controls. B) Bar plot and representative histogram from FSCA channel data of G2 HeLa cells gated from both control and Rapamycin treated samples. Arbitrary Units (A.U.). Data shown are mean values ± standard deviations (N = 3 independent biological replicates). Statistical significance was assessed by ANOVA with Tukey's test, Asterisks represent the p-value: * $p < 0.05$, ** $p < 0.01$, *** $p < 0.001$, ****$p < 0.0001$.

The G1 and G2 populations from HeLa cells exposed to Rapamycin were also smaller when compared to the non-treated cells (Figure 3.14).

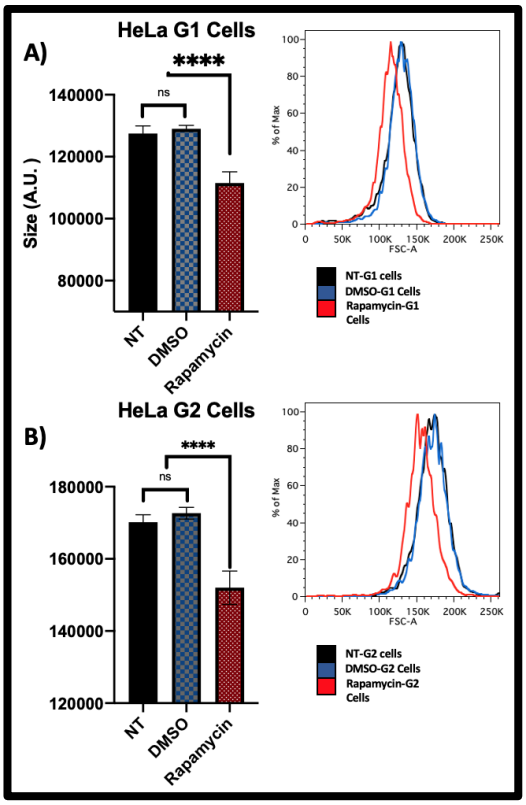

Figure 3.14 Asynchronous HeLa cells exposed to 1 μM of Rapamycin cells are overall smaller. HeLa cells treated for 24 hours with 1 μM Rapamycin were analysed by flow cytometry using the UV355 channel to gate them by their cell cycle distribution. A) Bar plot and representative histogram from FSCA channel data of G1 HeLa cells from both control and Rapamycin treated groups, Rapamycin G2 cells are smaller than controls. B) Bar plot and representative histogram from FSCA channel data of G2 HeLa cells gated from both control and Rapamycin treated samples Arbitrary Units (A.U.). Data shown are mean values ± standard deviations (N = 3 independent biological replicates). Statistical significance was assessed by ANOVA with Tukey's test, Asterisks represent the p-value: * $p < 0.05$, ** $p < 0.01$, *** $p < 0.001$, ****$p < 0.0001$.

3.2.6 siRNA knockdown of mTOR's effector

Given the fact that chemically inhibiting the upstream regulators of the PI3K/AKT/mTOR pathway produced smaller cells, it was considered to interfere with AKT and a downstream effector of the pathway, the mTOR effector S6K, by using siRNA technology. Since HEK293 are known to be easier to transfect, these cells were selected for the procedure. HEK293 cells were transfected with anti S6K and anti AKT siRNA independently to explore their effects on cell size. Both siRNAs reduced the cell size with anti-S6K having a slightly stronger effect than anti AKT (Figure 3.15).

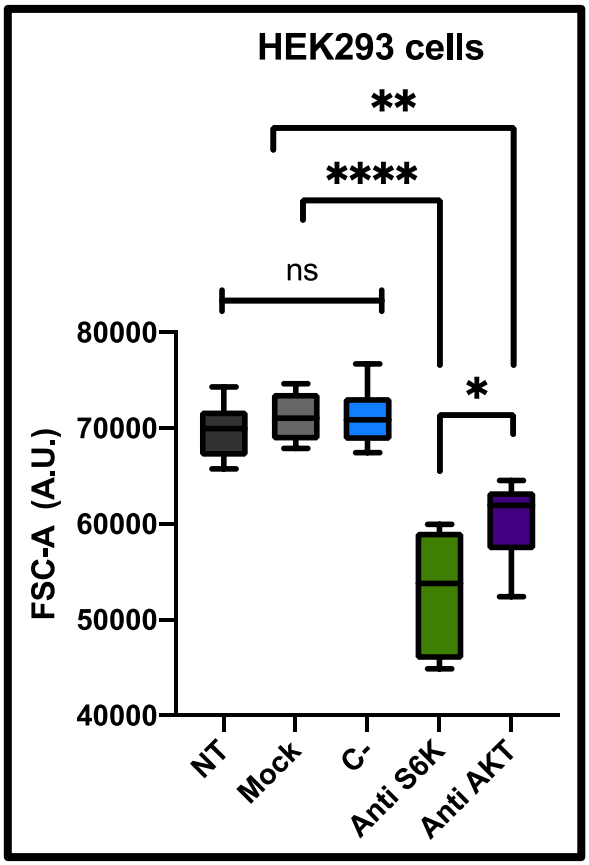

Figure 3.15 HEK293 cells size is reduced when transfected with siRNAs aimed at PI3K/AKT/mTOR Pathway. Boxplot representing the results from HEK293 cells transfected with siRNAs against S6K protein, AKT and Negative control (C-). Arbitrary Units (A.U.). C- is a negative control consisting of a siRNA that does not lead to the specific degradation of any cellular message. Statistical significance was assessed by ANOVA with Tukey's test, * $p < 0.05$, ** $p < 0.01$, *** $p < 0.001$, ****$p < 0.0001$. Data shown are mean values ± standard

deviations (N = 3 independent biological replicates). Box and whiskers plots calculated in GraphPad Prim, selecting the Min to Max option, the line in the middle of the box is the median.

Blocking effectors of the mTOR pathway using siRNAs further confirms what has been observed before with chemical inhibitors; interruption of the PI3K/AKT/mTOR pathway will result in cell size reduction.

3.2.7 RNAseq analysis of HeLa cells exposed to Rapamycin.

In order to further understand the possible mechanisms and gene regulation involved in Rapamycin's effect upon cell size, we analysed data from mRNA profiles of HeLa cells treated with DMSO and Rapamycin generated by RNA sequencing using Illumina technology. A general RNAseq pipeline was followed using a dataset from Gene Expression Omnibus: GSE130006 (Liao et al., 2019).

3.2.7.1 Quality Analysis of the Data

Scatterplots of counts from the different samples' replicates were plotted as a quality control. We observed that replicates closely correlate with each other (Figure 3.16A). A Principal Component Analysis (PCA) plot was generated primarily for quality control purposes. We can observe replicates clustering closer and variability between the different conditions (Figure 3.16B).

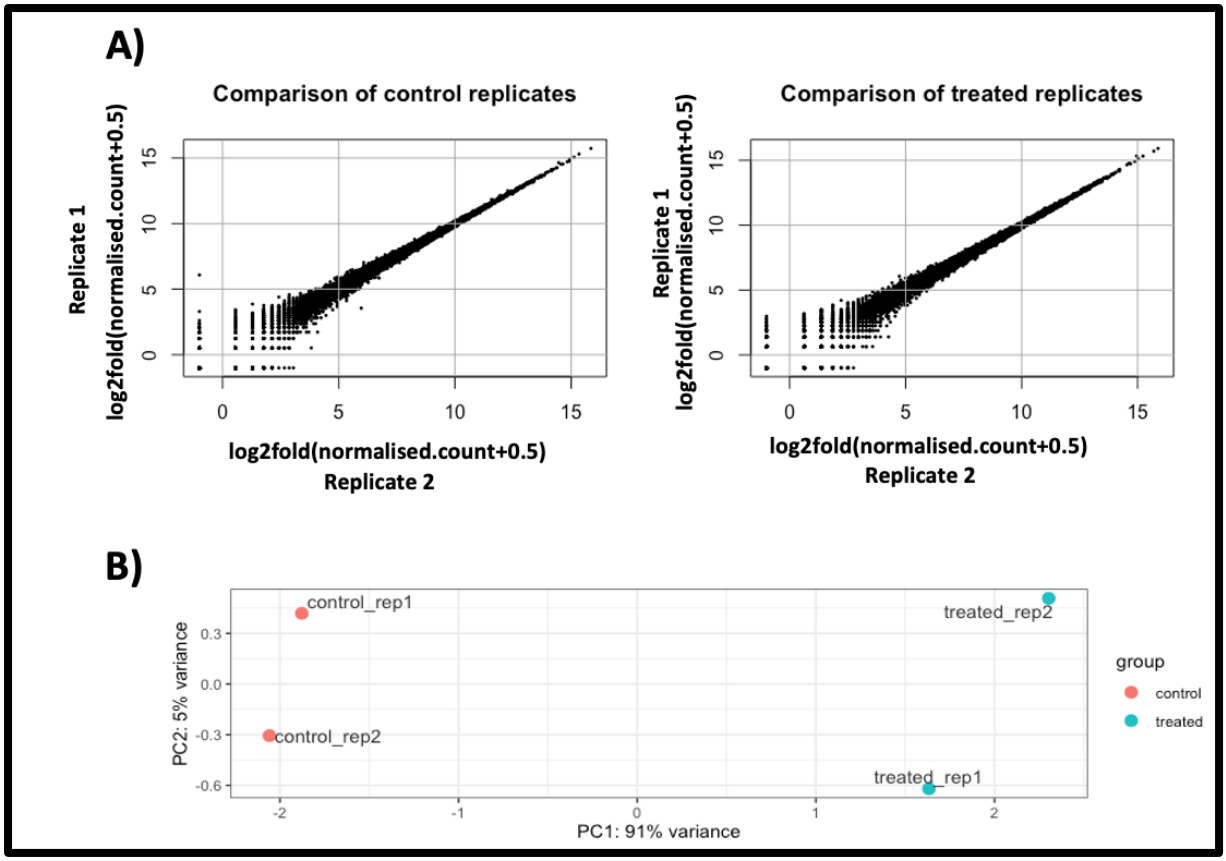

Figure 3.16 Quality check plots generated from the GSE130006 dataset. A) replicates seem to correlate relatively well between each other. B) PCA of the dataset

Clustering and visualization can be useful in data quality assessment and quality control, for this reason a heatmap of all the differentially expressed genes (those that meet a p(adjusted) value of < 0.05) is shown (Figure 3.17). The heatmap displays changes in gene expression between samples, with each row representing a gene and each column a sample. Red colour represents upregulated genes, blue represents downregulated genes and yellow represents unchanged expression.

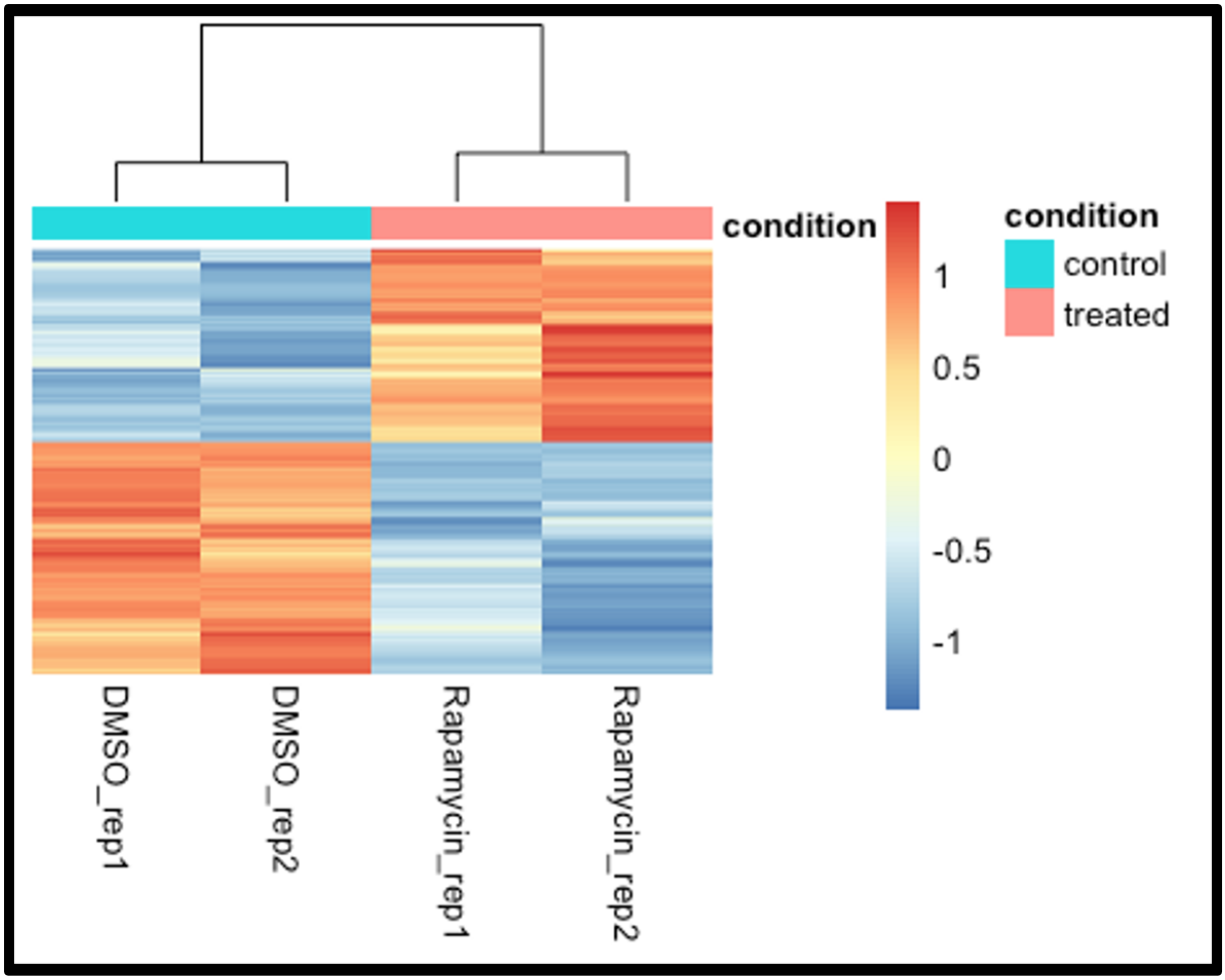

Figure 3.17 Heatmap of the differentially expressed genes of HeLa cells exposed to Rapamycin. Heatmap differentially expressed genes among the 4 samples of the analysis. The data is from regularized log (rlog) transformation. Red = upregulated, Blue = downregulated and Yellow = no change.

3.2.7.2 Extraction of Differentially Expressed Genes

Differentially expressed genes between the different conditions were visualised in a volcano plot with a log2Fold cut-off of 1 and a p-value (padj) <0.05 as a threshold, showing differentially expressed genes. It is noticeable that there do not seem to be many differentially expressed genes (Figure 3.18).

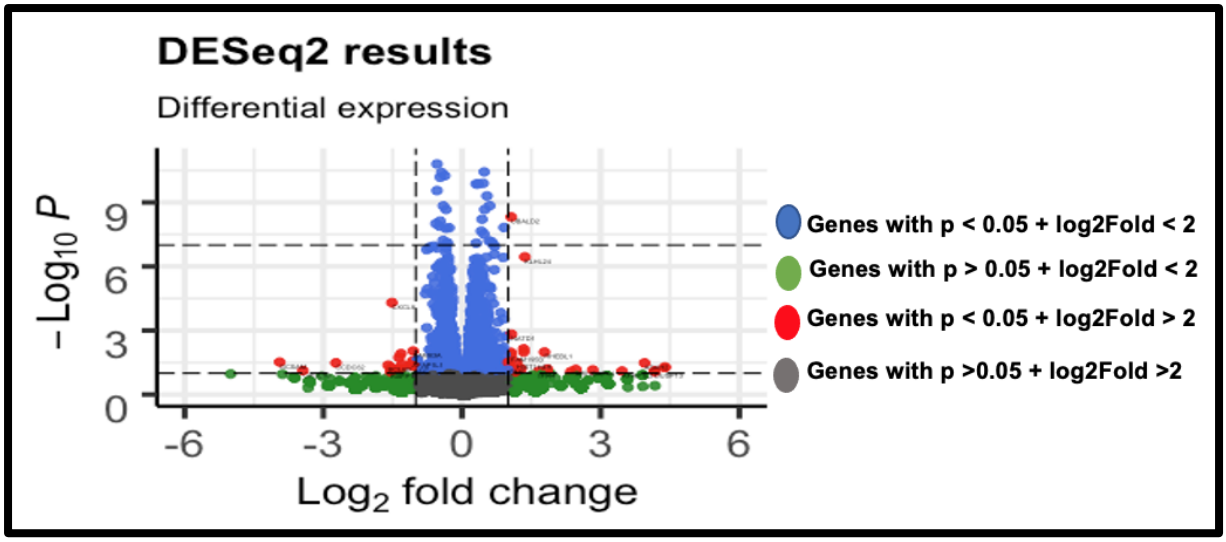

Figure 3.18 Volcano plot showing differentially expressed genes in the Rapamycin dataset. Volcano plot generated using the *Enhanced Volcano* package in R, showing the highly significant data points with the lowest P-values in blue, large magnitude fold-changes in green and those genes with both characteristics in red.

Scatter (XY) plots of condition comparisons were also generated (Figure 3.19), this figure shows the differentially expressed genes between control (DMSO) samples and treated (Rapamycin) samples coloured in red. 462 genes were found to be differentially expressed. The top 20 downregulated DE genes are presented (Table 3.1) as well as the Top 20 upregulated DE genes (Table 3.2).

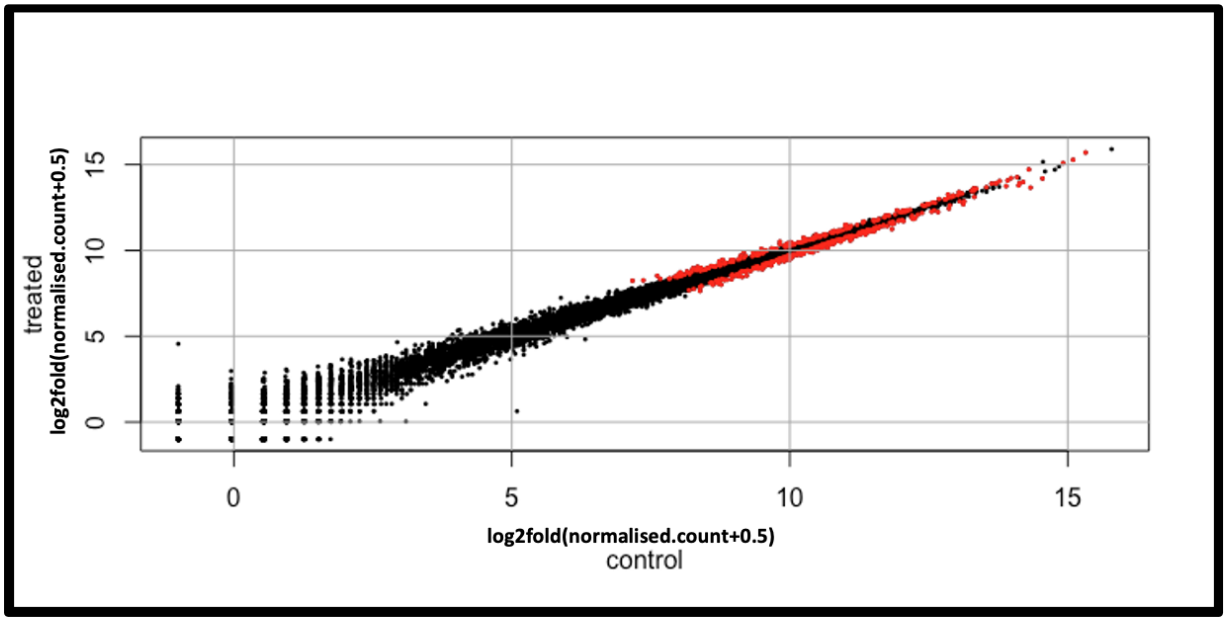

Figure 3.19 XY Scatter plot of HeLa cell RNAseq data. Scatter plot of treated (Rapamycin) vs control (DMSO) differentially expressed genes (shown in red).

Table 3.1 Top 20 Downregulated Differentially Expressed Genes in Rapamycin-treated HeLa cells. The 20 most downegulated differentially expressed genes from HeLa cells exposed to Rapamycin compared to control cells are shown in the table, arranged by their lower p-adjusted value.

genes	log2FoldChange	padj
HSPA8	-0.67195898	9.08E-33
DDX21	-0.59669261	5.20E-13
NCL	-0.425664311	9.82E-13
HSPD1	-0.429362277	2.28E-12
HSP90AA1	-0.354399428	2.36E-12
CCT5	-0.426234281	2.64E-12
HSP90AB1	-0.328487704	4.32E-10
KPNB1	-0.398781476	7.15E-10
DNAJA1	-0.51659948	3.39E-09
HSPH1	-0.539254246	6.08E-09
CCT2	-0.440085104	1.37E-08
CCT6A	-0.373786519	1.80E-08
NOLC1	-0.469078591	2.04E-08
NOP2	-0.540085589	7.09E-08
STIP1	-0.403549909	3.31E-07
TARS	-0.344621375	4.54E-07
BRIX1	-0.473113052	1.43E-06
CHORDC1	-0.563693916	1.84E-06
DKC1	-0.485526049	2.31E-06
EIF4A1	-0.277626781	2.63E-06

Table 3.2 Top 20 Upregulated Differentially Expressed Genes in Rapamycin-treated HeLa cells. The 20 most expressed differentially expressed genes from HeLa cells exposed to Rapamycin compared to control cells are shown in the table, arranged by their lower p-adjusted value.

genes	log2FoldChange	padj
EEF1A1	0.382825933	9.37E-17
ULK1	0.687905563	7.45E-13
EEF2	0.415461857	9.82E-13
RPL13A	0.415309173	7.92E-12
PLEC	0.410052938	9.88E-11
MT2A	0.742376368	1.27E-10
WISP2	0.481796447	1.34E-08
CTSD	0.457926327	3.67E-08
RPL3	0.354397421	3.67E-08
TM4SF1	0.307297943	3.67E-08
TXNIP	0.540718024	1.21E-07
HBP1	0.600089213	3.31E-07
H1FX	0.492873041	4.54E-07
UBALD2	1.066172352	9.85E-07
NDRG1	0.434185565	1.22E-06
ABTB1	0.90853739	2.62E-06
GABARAPL1	0.418535015	3.57E-06
NBR1	0.475299831	4.70E-06
ALDH3B1	0.583076323	9.36E-06
PBXIP1	0.638203864	1.02E-05

3.2.7.3 GO Analysis

GO analysis was performed using the `topGo` package on a dataset of genes that were found to be differentially expressed between conditions, comprising of both upregulated and downregulated genes to determine which GO terms arranged by biological process are associated with the effects of the Rapamycin treatment on HeLa cells. The top 20 Go terms enriched by the DEG's were plotted (Figure 3.20).

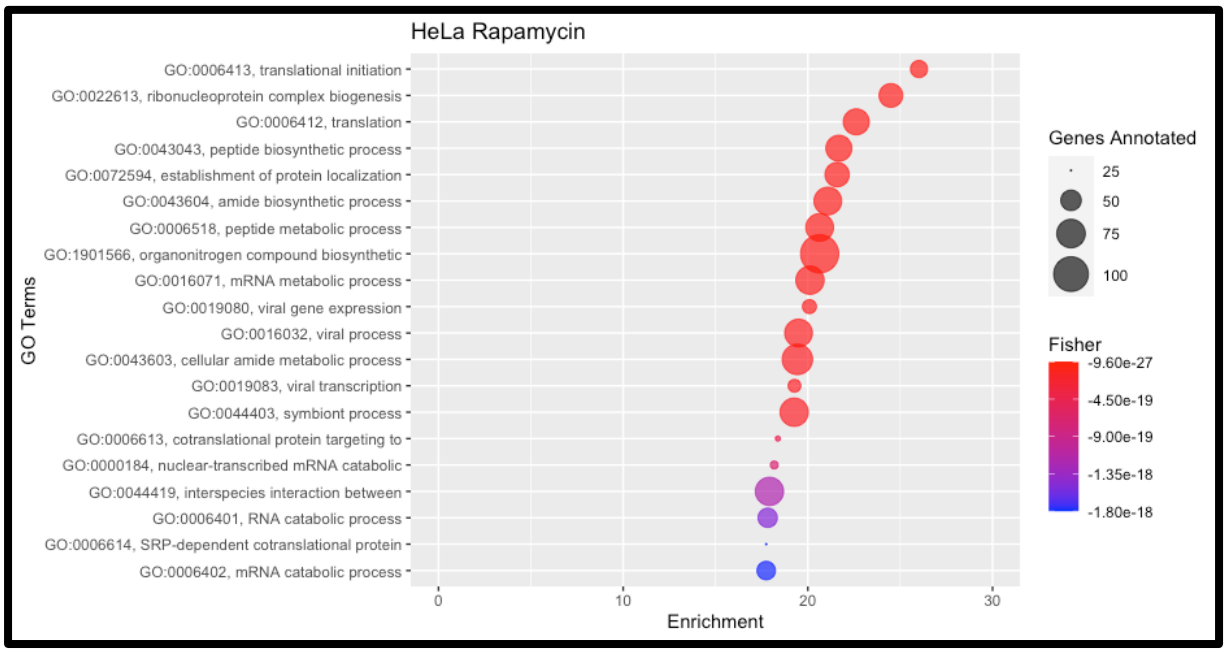

Figure 3.20 Top Gene Ontology terms from Rapamycin treated cells are related to Translation. List of Gene Ontology terms enrichment of HeLa cells exposed to Rapamycin. Graph produced by Top20 GO terms obtained using TopGO and then plotted with ggplot2, bubble size represents the genes annotated and coloration represents enrichment.

The top 4 most enriched Gene Ontology terms enriched of HeLa cells exposed to Rapamycin are GO:0006413 Translational initiation, GO:0022613 Ribonucleoprotein complex biogenesis, GO: 0006412 translation and GO:0043043 peptide biosynthetic process. All of these terms are related to each other by the process of translation and therefore mass accumulation. This plot showing the top Gene Ontology terms based on differentially expressed genes allows us to visualize the possible mechanisms behind the observed effects after Rapamycin treatment.

A similar result was observed when an enrichment analysis was performed using the g:Profiler server and the g:GOst tool (Reimand et al., 2016)(Figure 3.21).

ID	Source	Term ID	Term Name	p_{adj} (query_1)
1	GO:BP	GO:0006413	translational initiation	1.266×10^{-24}
2	GO:BP	GO:0022613	ribonucleoprotein complex biogenesis	1.204×10^{-22}
3	GO:BP	GO:0072594	establishment of protein localization to organelle	5.996×10^{-20}
4	GO:BP	GO:0016071	mRNA metabolic process	1.784×10^{-19}
5	GO:BP	GO:0006412	translation	8.291×10^{-18}
6	GO:BP	GO:0043043	peptide biosynthetic process	4.548×10^{-17}
7	GO:BP	GO:0043604	amide biosynthetic process	1.018×10^{-16}
8	GO:BP	GO:0006613	cotranslational protein targeting to membrane	1.065×10^{-16}
9	GO:BP	GO:0000184	nuclear-transcribed mRNA catabolic process, ...	1.394×10^{-16}
10	GO:BP	GO:0042254	ribosome biogenesis	3.676×10^{-16}

Figure 3.21 Gene Ontology Term enrichment by g:Profiler from Rapamycin treated HeLa cells point to Translation. List of the most enriched Gene Ontology terms from HeLa cells exposed to Rapamycin. The most enriched term is GO:0006413 Translational initiation, the rest of the terms are related to protein synthesis. Graph produced by g:Profiler (https://biit.cs.ut.ee/gprofiler/gost).

3.3 Discussion

The PI3K/AKT/mTOR pathway is a highly conserved evolutionary mechanism to regulate multiple important cell functions, such as cell size, cell cycle and metabolism. We have used two different inhibitors of this regulatory pathway; LY294002 and AZD5363 to assess the effects of chemically impairing it. The PI3K inhibitor LY294002 has been used in therapies for many maladies related to inflammation, such as Tourette syndrome, where its administration hinders the PI3K/AKT mediated neuroinflammation pathway (Hongyan et al., 2017). It has also been observed to prevent the development of myocardial injury induced in autoimmune myocarditis (Liu et al., 2016a). LY294002 has also been explored as a cancer treatment in combination with oxaliplatin where it showed promising results inhibiting proliferation of gastric cancer (Liu et al., 2011) and on its own was capable to inhibit proliferation of esophageal squamous cell carcinoma (ESCC) cells (Hou et al., 2018).

The AKT protein kinase transduces signals from growth factors to downstream targets, phosphorylating many effectors, including MDM2 (mouse double minute 2 homolog), GSK3, FOXO, p27 and TSC2, leading to cell growth, survival and proliferation

(Hennessy et al., 2005) (Yudushkin, 2019) (Noorolyai et al., 2019). This AKT activation increases cancer cell survival and resistance to apoptosis induced by drugs (Choi et al., 2014). AZD5363 is an oral small-molecule, new generation drug that potentially inhibits all three isoforms of the protein kinase B (AKT) proteins: AKT1, AKT2 and AKT3 (Davies et al., 2012) (Addie et al., 2013) (Maynard et al., 2013) (Sommer et al., 2013) and has been tested as an anticancer drug in models for various tumours, such as breast cancer, prostate cancer, and leukaemia (Ribas et al., 2015) (Lamoureux et al., 2013) (Lamoureux and Zoubeidi, 2013) (Meja et al., 2014).

We observed that both LY294002 and AZD5363 caused a general impact on cellular growth regulation, as cells showed a reduction of their cell size when analysed by flow cytometry without an apparent significance between the concentrations used.

Interestingly, Choi et al observed that in AZD5363-treated cells, the levels of phosphorylated activated AKT (pAKT) increased. Since pAKT positively correlates with cancer growth and survival, the authors co-treated LY294002 with AZD5363 to reduce the levels of pAKT (Choi et al., 2016) and demonstrated that the effectivity of these drugs on the pathway were reinforced when used in combination.

Our work showed that HeLa and HEK293 cells treated with 30 μM LY294002 not only had their overall size reduced, but they also accumulated in G1, something that was seen as well by Xing et al, where the authors noted that the proportion of G1 gastric cancer cells treated with LY294002 went from 48% at 0 hours of treatment to 75% after 24 hours (Xing et al., 2008). Given the fact that both PI3K and AKT are upstream regulators of mTOR, a known cell size regulator, it is no surprise that these chemicals were able to cause the cell shrinkage, however, it is important to notice that there is evidence showing that LY294002 might not be as specific as expected, as it was shown to inhibit not only PI3K but also mTOR and the DNA-dependent protein kinase (DNA-PK) (Brunn et al., 1996), as well as other protein kinases, such as CK2 (casein kinase 2) and Pim-1. Furthermore, other PI3K-independent effects directly attributed to LY294002 have been reported, for example inhibition of Ca2+ signalling, NF-kB (Gharbi et al., 2007).

As LY294002 seems to have a broader effect on several proteins, it was considered to approach the outcome of Rapamycin treatment on both HEK293 and HeLa cell lines, as Rapamycin seems to only target the mTOR protein.

To properly determine the efficacy of the Rapamycin treatments, western blots showing the expression of phospho-4EBP and phospho-S6K should be performed. These western blots would consist of the protein extracts from both Rapamycin treated and non-treated cells. The signal from p-4EBP and p-S6K would be non-present in Rapamycin treated samples, whereas control samples would have shown a signal. A similar procedure should be performed to determine the effects of the siRNA treatments in this case, antibodies against S6K and AKT proteins would suffice to show the effectiveness of the siRNA transfection.

This time, cell size was also analysed using a Moxi Z cell counter, which can measure both the average diameter and volume of cells. HeLa and HEK293 cells showed a reduction of their diameter and volume after being exposed to 1 μM Rapamycin for 24 hours, and the effect seemed slightly higher in HEK293 cells than in HeLa cells. Interestingly, the Human Protein Atlas shows a higher RNA expression of mTOR in HeLa cells, compared to HEK293 cells (https://www.proteinatlas.org/ENSG00000198793-MTOR/cell#rna), however, more experimental work would be needed to prove this. Nonetheless, the overall size of both cell types was also shown to be reduced by flow cytometry, a result like that of Fingar et al., where the authors engineered a rat.1a-derived cell line (RT16.15) to overexpress p16, which made the cells accumulate in G1 and keep gaining mass. Exposure of these cells to both Rapamycin and LY294002 showed a reduction of their cell size. The same applied to asynchronous U2OS that were exposed for 72 hours to both chemicals and showed a reduced cell size by means of flow cytometry (Fingar et al., 2002). Interestingly, they also observed that overexpression of both eIF4E and S6K1 showed a 5% size increase compared to their controls, prompting the idea that both mTORC1 effectors were responsible for the effects on cell size.

mTORC1 relays nutrient, energy and growth signals to drive cell growth through promotion of anabolic process such as protein synthesis (Tee, 2018), regulating protein translation through an array of translation factors that include 4EBP1 and S6K1 (Schalm et al., 2003)**.** S6K has been implicated as an important regulator of cell and body size, for this reason we used siRNA directed to this protein in HEK293 cells which showed a reduction of 20% of their size. The result observed in HEK293 cells is similar to what has been observed in S6K1 -/- mice, which have a reduced size in all of their organs (Shima et al., 1998), and smaller pancreatic β cells (Pende et al., 2000, Ohanna et al., 2005). One of the known multiple substrates of S6K is rpS6 phosphorylation, which has been observed to be directly involved in the control of cell size. Thus, a wide variety of cell types derived from $rpS6^{p-/-}$ mice are significantly smaller than their wild type counterparts. Another effector of S6K1 linked to cell size is SKAR, a specific binding partner of S6K1, but not S6K2, which is a nuclear protein with homology to the Aly/REF family of RNA binding proteins and which has been proposed to couple transcription with pre-mRNA splicing and mRNA export. When SKAR was downregulated by RNAi, cell size reduction was observed by flow cytometry (Richardson et al., 2004). It is expected then that interfering with upstream regulators of the PI3K/AKT/mTOR pathway would result in the impairment of its effectors and this in turn would result in loss of mass accumulation and cell size reduction.

This aligns well with results obtained from the RNAseq analysis performed on Rapamycin treated HeLa cells, where the most enriched Gene Ontology terms pointed towards alterations in the translation initiation process, translation, and ribosome biogenesis. As mentioned before, an effector of mTOR is the protein 4EBP1, which acts as a negative regulator of cap-dependant protein translation by binding to eIF4E and thus preventing the translation of mRNAs involved in cell growth (Beretta et al., 1996). mTORC1, however, phosphorylates 4EBP1, allowing the binding of the eIF4G to eIF4E which then permits translation initiation. As part of the eIF4F complex, eIF4A has RNA helicase activity that unwinds the secondary structure within the 5'-untranslated region (5'UTR) of the mRNA to help the efficacy of ribosome scanning to the start codon. Via mTORC1, S6K1 further enhances the RNA helicase activity of eIF4A by phosphorylating eIF4B on Ser4222 (Raught et al., 2004). The length and degree of secondary structure within the 5'-UTR contributes to the dependency of

these mRNAs on mTORC1 and the availability of eIF4F (Siddiqui and Sonenberg, 2015). Examples of mRNAs involved in cell growth that are highly dependent on eIF4F include the MYC proto-oncogene, bHLH transcription factor (MYC) and cyclin D1 (CCND1) (Graff et al., 2007), genes known to mediate cell size and proliferation.

We can find several eukaryotic initiation factors to be amongst the genes differentially expressed when HeLa cells are exposed to Rapamycin, therefore it is logical to relate the effects observed in cell size to the alteration of these intermediates of protein translation being altered through the drug treatment.

In addition to controlling the activity of the translational machinery, the cells' capacity to accumulate mass is also regulated by the number of ribosomes they have (Tee, 2018). Regulation of ribosome biogenesis by mTORC1 ensures a rapid growth and it does so by promoting the activities of the RNA polymerases that make ribosomal RNA (polymerase I and III) and by stimulating the translation of mRNAs for ribosomal proteins (Mayer et al., 2004). These mRNAs contain a 5'-terminal oligopyrimidine tract (5'-TOP) (Terada et al., 1994, Jefferies et al., 1997) that impairs their translation under basal conditions, this impairment being overcome when the mTORC1 pathway is activated. 5'TOP mRNAs are sensitive to Rapamycin and are found to be dependent on S6K1. Over 75% of the proteins involved in ribosomal biogenesis are estimated to be controlled by S6K1 (Chauvin et al., 2014). In a recent study, high resolution ribosomal profiling identified 144 mRNAs that were sensitive to mTORC1 inhibitors. Only 68% of these mRNAs possessed putative 5'-TOP tracts, while 63% contained a newly discovered cis-regulatory pyrimidine-rich translational element (PRTE). Rather than being dependent on S6K1, PRTE mRNAs were found to be highly sensitive to 4EBP1. Many of the mTORC1-sensitive target genes uncovered by Hsieh et al were ribosomal proteins (Hsieh et al., 2012) which highlights the critical involvement of mTORC1 in the generation of new ribosomes. Loss of just the 4EBP family of translational repressors is sufficient to render TOP and TOP-like mRNA translation resistant to the mTOR inhibitor Torin 1. Loss of this interaction diminishes the capacity of eIF4E to bind TOP and TOP-like mRNAs much more than other mRNAs, explaining why mTOR inhibition selectively supresses their translation (Thoreen et al., 2012). This would explain why ribosome biogenesis and overall translation are the Gene Ontology terms affected by Rapamycin treatment. Ablation of these pathways will

have a profound negative effect on cell size, leading to cell shrinking upon reduction of the mass accumulation mechanisms.

In addition, Rapamycin blocks cell proliferation by preventing progression into S-phase (Huo et al., 2011), which would explain the accumulation of cells in G1.

As it has been stated, the measurement of cell diameter and volume by Moxi Z has shown that cell size is diminished when these are exposed to the mTOR pathway inhibitors. However as mentioned before, Rapamycin is known to prevent progression into S-phase, ultimately accumulating cells in G1. To make sure that the size changes that we were observing weren't because of this G1 "arrest", we analysed the cell cycle distribution of the cell by flow cytometry, then by gating the G1 and G2 population of the inhibitor-exposed cells and control cells, comparing the sizes of both populations. We saw that Rapamycin exposed G1 and G2 cells were overall smaller than untreated control cells, showing that even if there were accumulations in the G1 population of cells (which are smaller than G2 cells) these G1 cells exposed to the inhibitor were smaller than non-exposed G1 cells, thereby demonstrating that by blocking the mTOR pathway, cells were getting smaller in a mass-related way and not only by changes in the cell cycle.

At the end we have demonstrated the influence of the PI3K/AKT/mTOR in the regulation of cell size, by ablating multiple important nodes that regulate the cell's growth. Furthermore, we analysed gene expression in HeLa cells exposed to Rapamycin, which demonstrated how translation and ribosomal biogenesis was affected by blocking mTOR and subsequentially reducing mass accumulation. This ultimately shows how important the mTOR pathway is in the regulation of the mammalian cell growth by regulating ribosome biogenesis, translational components and multiple metabolic processes. This explains why this pathway is so often observed to be dysregulated in multiple diseases, whether it is up or downregulated.

We have observed that disrupting the PI3K/AKT/mTOR pathway produces smaller cells. In order to understand how to control cell size, it was decided to manipulate a different regulator of cell size, the Myc transcription factor.

Chapter 4: Overexpression of Myc and its effects on cellular size

4.1 Introduction

Another major regulator of biogenic pathways is the transcription factor Myc, which has been associated with increased cell growth and metabolic reprogramming required for the latter.

During 1960-1970, four avian retroviruses capable of causing tumours in chicken were isolated. When analysed, they possessed a common genetic element that, when deleted, the transformation capabilities of the virus were crippled. This oncogene was named *v-Myc*, for myelocytomatosis, and was shown to have a cellular homolog in uninfected vertebrae cells denoted *c-Myc* (cellular Myc) (Conacci-Sorrell et al., 2014). The *c-Myc* gene is the prototype for a family of proteins that are conserved in metazoans (Hartl et al., 2010) and in similar form and function in premetazoan organisms (Young et al., 2011). In mammalian cells, Myc proteins come from three different gene family members- *c-Myc, N-myc and L-myc*- which function similarly but have different patterns of expression, especially in different types of cancer; c-Myc is expressed broadly in blood-borne and solid tumours, N-myc is frequently overexpressed in solid cancers of neural origin, such as neuroblastoma and glioma, and L-myc is found in small cell lung carcinoma (Nesbit et al., 1998).

Myc contains several highly conserved regions amongst its three paralogs: An N-terminal transactivation domain (TAD), a C-terminal region of 100 amino acid carboxy-terminal region comprising the basic-helix-loop-helix leucine zipper (bHLHZ) domain, and a DNA-binding domain(Carabet et al., 2018).

Members of this bHLHZ domain form homo- and heterodimers with themselves and with other members of the family. Myc usually binds to Max through the bHLHZ motif which is required for DNA-protein interactions (Adhikary and Eilers, 2005). The Myc/Max heterodimer recruits a chromatin modifying complex (TRRAP, CGN5, TIP60 and TIP48) and activates transcription by binding to the conserved E-box DNA sequence (CACGTG) located in the transcriptional regulatory region of target genes (Figure 4.1) (Pelengaris et al., 2002). When the Myc/Max heterodimer binds to a proximal gene promoter sequence, it releases transcriptionally paused RNA polymerases and catalyses transcriptional elongation (Rahl et al., 2010).

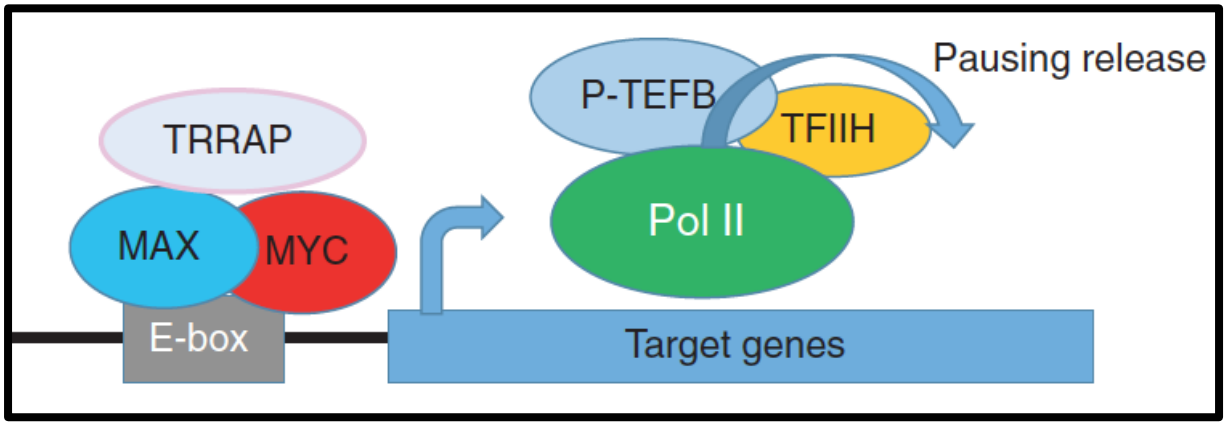

Figure 4.1 Myc releases RNA Pol II from Pausing. Myc associates with its partner Max, binds to E-boxes and forms a heterodimer which then recruits the chromatin modifying complex, subsequently releasing the RNA Pol II from pausing.

Myc is estimated to be involved in 20% of all human cancers as well as to influence up to 15% of all genes. Myc target genes are involved in different intermediary steps of metabolism from glycolysis and glutaminolysis to nucleotide and lipid synthesis. (Dang et al., 2006). One of its functions is its ability to promote cell proliferation and inhibit cell differentiation (Gandarillas and Watt, 1997). In order to promote entrance to S-phase of the cell cycle, Myc can regulate the expression of cyclins D1 and D2, CDK4 and cyclin B1 (Fernandez et al., 2003, Li et al., 2003). This increased proliferation would require an increment in protein synthesis, which has been observed in c-Myc overexpressing cells when compared to knockout cells (Mateyak et al., 1997).

Smaller keratinocytes can be observed in mice in which Myc has been knocked out in the epidermis (Zanet et al., 2005). In addition, in Myc -/- mice, there are significantly lower number of granulocytes, B and T lymphocytes, but an increased number of megakaryocytic progenitors in bone and spleens. However, the latter cells seem to be smaller in size and lower in ploidy than normal control mice (Guo et al., 2009).

Myc is normally not expressed in the adult heart, however its expression is rapidly upregulated in response to hypertrophic stimuli. Artificial overexpression of Myc in myocytes produced changes in size, protein synthesis and cell cycle re-entry (Xiao et al., 2001). Amongst the overexpressed genes associated to c-Myc expression are several ribosomal RNAs and ribosome biogenesis proteins (Schlosser et al., 2003).

4.1.1 Myc as a Transcription Amplifier

In normal cells, Myc proteins appear to integrate environmental signals in order to modulate many processes, including proliferation, growth, apoptosis, metabolism, and differentiation. Myc proteins are nuclear proteins and, as such, may have several functions; however, there is consensus in the field that one major activity is to regulate transcription (Wolf et al., 2015). In the last decade, growing interest in dissecting the mechanism by which Myc is able to transform cells and direct gene expression in their healthy counterparts has led groups to propose a new hypothesis that involves a general amplification of transcription by supraphysiological levels of Myc expression. In 2003, Li et al. showed that DNA binding of Myc correlated with transcription activity throughout the genome, and this led them to propose a system in which Myc plays a general role in the regulation of global gene expression in Burkitt lymphoma cells (Li et al., 2003). Almost ten years later, Lin et al. used the human P493-6 Burkitt's lymphoma cell line to investigate the effects of increased levels of Myc on its genome wide occupancy and on gene expression. The results showed that Myc generally occupies the core promoter of actively transcribed genes, as evidenced by co/occupancy with RNA Pol II, as similarly observed by Li et al. Not only promoters, but enhancers associated with active genes become occupied by Myc in cells with elevated levels of the factor, and a 1.5 fold increase in total RNA levels was observed (Lin et al., 2012). In that same year, Nie et al. observed that, after B cell activation with LPS, a Myc early response expression caused a redistribution of RNA pol II from

promoters into gene bodies, suggesting that Myc is a universal amplifier of transcription that releases RNA pol II from pausing, with around 40 – 50% of the Myc B cell target genes overlapping with those from Lin et al., 2013. They proposed that a sustained Myc overexpression in cancer would leave cells in a state of chronic overdrive through all cellular networks (Nie et al., 2012). These experiments have resulted in the proposal of a system in which, at physiological levels, Myc binds mainly to active promoters pre-marked by H3K4me3 and RNA pol II, and, when overexpressed, the level of Myc that is bound to promoters increases, with more promoters being occupied and Myc starting to bind to larger numbers of distal sites. At highest levels, Myc can be crosslinked at almost all active promoters and enhancers in the genome in a phenomenon deemed “Invasion” (Figure 4.2). During invasion, binding is less selective and includes E-box variants that have lower affinity for Myc-Max and, in extreme cases, other sequences, suggesting the union can be less specific.

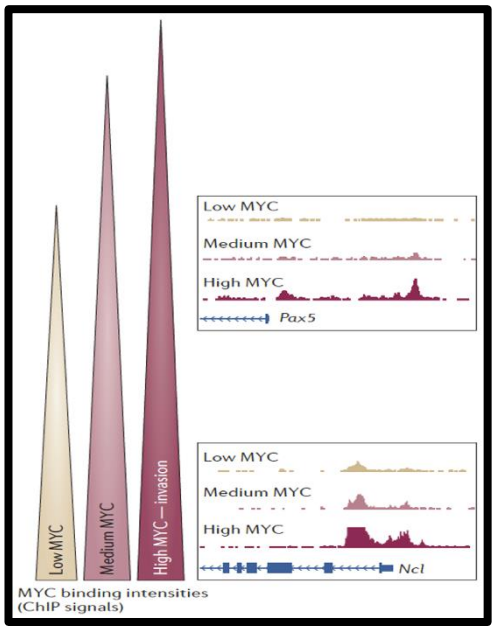

Figure 4.2 Representation of increased binding frequencies with increasing Myc concentrations. Examples of Myc ChIP-seq tracks for a high-affinity Myc binding site (nucleolin (*Ncl*)) and a low-affinity Myc binding site (paired box 5 (*Pax5*)) are show. Image obtained from (Sabo et al 2014).

The structures of DNA-bound Myc-Max show that basic residues mediate contacts not only with specific DNA bases but also with its backbone, allowing for significant non-

sequence specific binding. Mechanism-wise, initial interactions with open chromatin domains (both promoters or enhancers) are facilitated by interactions with chromatin-associated proteins by sequence-independent engagement of the Myc-Max dimer on the double helix and local scanning of the DNA sequence, leading to stabilization on medium-to-high affinity binding sites (E-boxes or variants). Myc overexpression increases binding probability, leading to enhanced crosslinking at all open regulatory elements (invasion), yet preserves the relative binding hierarchy between high and low affinity sites (Figure 4.3) (Kress et al., 2015, Wolf et al., 2015).

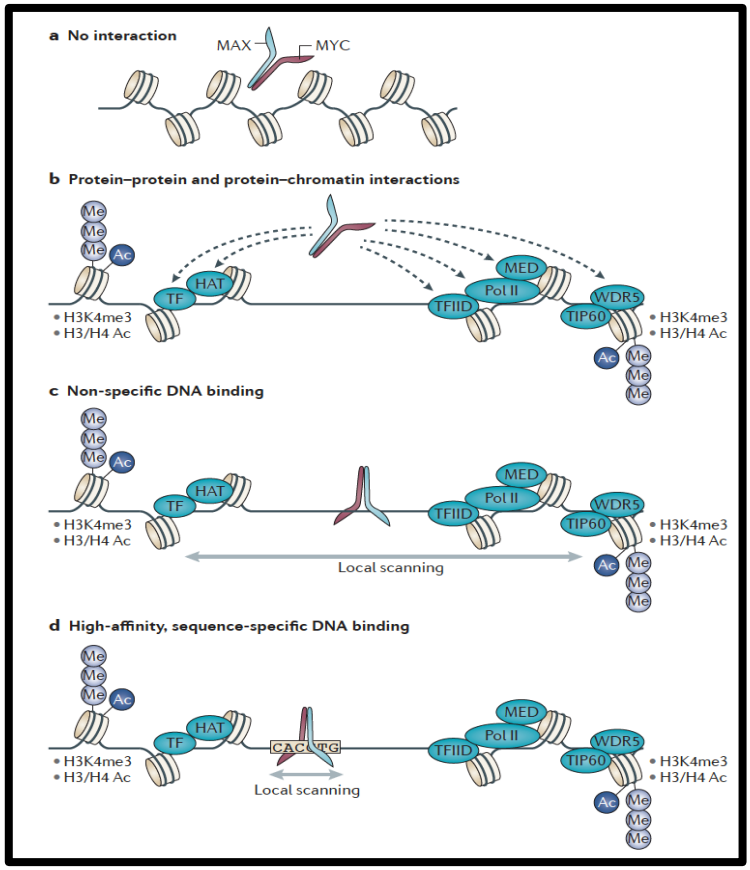

Figure 4.3 Schematic model for the stepwise recruitment of Myc-Max on chromatin. A) E-boxes in a closed chromatin context are inaccessible to Myc/Max B) Protein-protein interaction, C) non-sequence specific protein-DNA interactions, allowing D) a local scanning of the DNA sequence and stabilization on consensus binding motifs if present. Image taken from (Kress et al., 2015)

Sabò et al observed promoter invasion by Myc in a mouse model that progressively develops B cell lymphoma. They proposed that whether associated with RNA amplification, Myc drove the differential expression of distinct subsets of target genes.

Hence, although having the potential to interact with all active regulatory elements in the genome, Myc does not directly act as a global transcriptional amplifier. Instead, Myc activates and represses transcription of discrete gene sets, leading to changes in cellular state that can in turn feedback on global RNA production and turnover (Sabo et al., 2014). RNA amplification is most consistently interpretable as a late, indirect consequence of Myc activation, mediated by a selective, yet complex set of target genes (Tesi et al., 2019).

Whether Myc acts as a universal transcriptional amplifier or not, the evidence does point at a general increase in RNA production in the cells in which Myc has been upregulated, which consequently leads to changes in metabolism, cell growth and cell cycle, ultimately leading to a deviation from homeostasis.

4.1.2. The MycER system

Inducible systems which fused hormone-binding domain (HBD) of steroid receptors to intracellular proteins have been used before to control the activity of different proteins (Figure 4.4). In the absence of hormone, the HBD maintains the heterologous proteins in an inactive state due to HBD-fusion proteins bound to polypeptides, including Hsp90. Once treating the cells with a ligand, this repression is reversed (Figure 4.5) (Picard, 1993). The HBD of the human oestrogen receptor (ER) has been widely used because of the lower price of its ligand and the fact that many cells naturally lack this receptor. However, this HBD has significant practical drawbacks as a switch; most *in vitro* experimental systems use media containing phenol red, a weak agonist of ER, and serum which usually contains oestrogen (Danielian et al., 1993). To overcome these problems, Littlewood et al used the mutant murine oestrogen receptor G525R. This mutant no longer binds E2, but remains responsive to activation by the synthetic steroid 4-hydroxytamoxifen (4-OHT). Littlewood et al., fused the human c-Myc protein to the mutant HBD of the murine ER which showed a 1000-fold lower affinity to oestrogen than the wild type, whilst maintaining its affinity to 4-OHT (Littlewood et al., 1995).

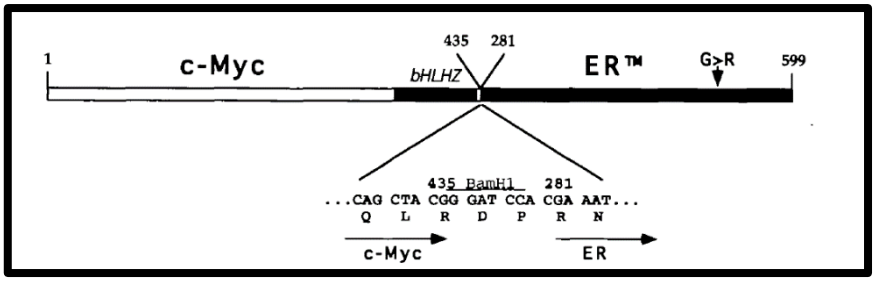

Figure 4.4 Chimeric MycER architecture. The mutant hormone domain of the murine oestrogen receptor (amino acids 281-599 containing a single amino acid change from glycine to arginine at position 525) was fused at the C-terminus of the human c-Myc protein (amino acids 1-435) to form c-MycER. This fusion replaces the C-terminal four amino acids of c-Myc immediately adjacent to the bHLHZ with two amino acids (DP) generated by the insertion of a *Bam*HI site to facilitate fusion with ER. Image taken from (Littlewood et al., 1995).

The MycER system has proven useful to study different c-Myc gene targets (Eilers et al., 1989). It has been used to show that Myc requires a specific threshold to induce proliferation (Murphy et al., 2008). Gandarillas et al. demonstrated that, in human keratinocytes, c-Myc did not stimulate apoptosis or proliferation but differentiation of the cells by using MycER (Gandarillas and Watt, 1997). By overexpressing MycER in Rat1 cells for prolonged periods, it was shown that c-Myc caused irreversible chromosomal aberrations in these cells (Fukasawa et al., 1997). The MycER system has also been used on U2SO cells to show that Myc disrupts the circadian clock and metabolism in cancer cells (Stine et al., 2015) as well as to prove that the cohesion complex is dispensable for Myc-dependent transcription but essential to prevent Myc-induced replicative stress (Rohban et al., 2017).

The MycER system used here was expressed in U2OS cells (kindly donated by Dr. Stefano Campaner from the *Instituto Italiano di Tecnologia*). These cells were produced by transducing U2OS cells with a pBabe-puro retrovirus encoding a puromycin resistant gene for selection and the MycER chimeric construct expressed under the control of the retroviral 5' LTR (Rohban et al., 2017, Gandarillas and Watt, 1997, Littlewood et al., 1995).

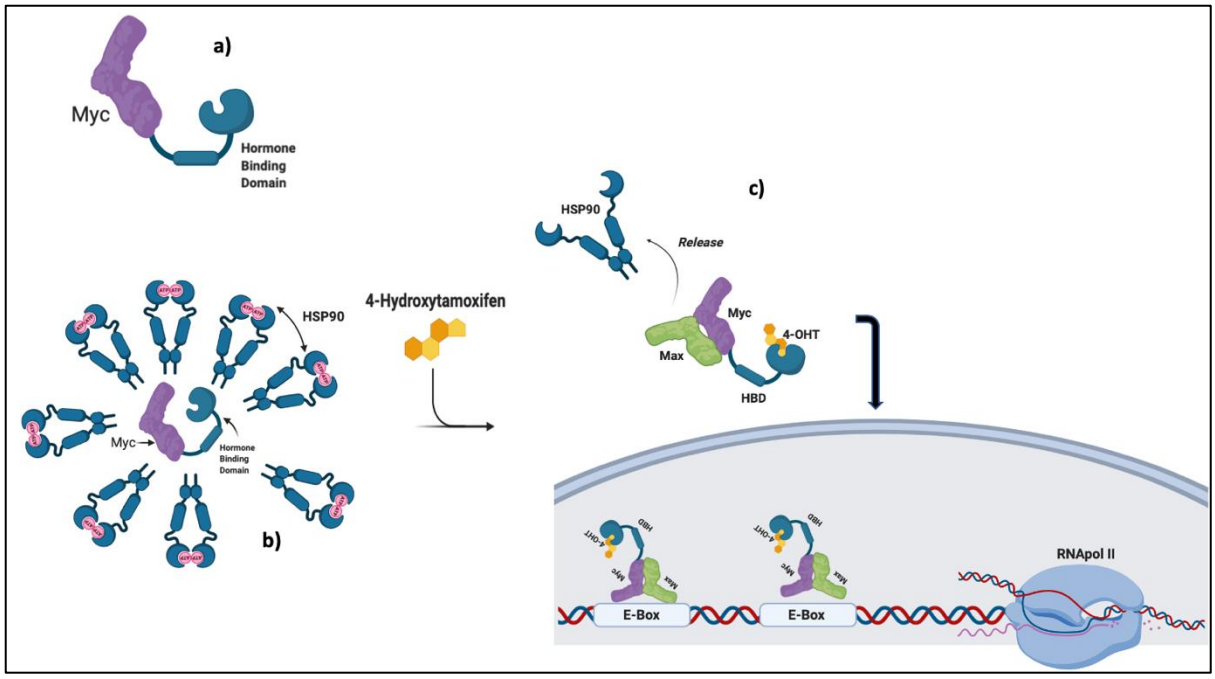

Figure 4.5 MycER Mechanism. A) MycER is a hormone binding domain fused to c-Myc, B) it is synthesized in cells but remains inactive, bound to hsp90, C) unless 4-hydroxytamoxifen is given to cells, which activates the transcription factor.

4.1.4. Using SUnSET to analyse translation

Traditionally, translation has been analysed utilising radioactively labelled amino acids which requires specialized laboratory protocols and procedures to deal with radioactive samples. In 2009 Schmidt et al designed a technique to monitor and quantify global protein synthesis, utilizing puromycin in a technique known as Surface Sensing of Translation (SUnSET). Puromycin is a structural analogue of aminoacyl-transfer RNA (aminoacyl-tRNA; specifically, tyrosyl-tRNA) and, as such, it can be incorporated into elongating peptides chains via the formation of a peptide bond. However, whereas aminoacyl-tRNAs contain a hydrolysable ester bond between their tRNA ribose moiety and the attached amino acid molecule, puromycin has a non-hydrolysable amide bond in the equivalent position. Thus, the binding of puromycin to a growing peptide chain prevents a new peptide bond from being formed with the next aminoacyl-tRNA. Therefore, puromycin binding results in the termination of peptide elongation, and leads to the release of the truncated puromycin bound peptide from the ribosome. When used in minimal amounts, puromycin incorporation in newly

synthesized protein directly reflects the rate of mRNA translation *in vitro* (Figure 4.6). Schmidt et al used monoclonal 12D10 antibodies that detect puromycin to directly monitor translation; using standard immunochemical methods and flow cytometry, they compared puromycin detection to classical radioactive methionine and cysteine labelling which showed comparable results(Schmidt et al., 2009). SUnSET has been used to measure *in vivo* relative rates of protein synthesis in skeletal muscle and other tissues (Goodman and Hornberger, 2013). Using an ex vivo approach, Deliu et al labelled newly synthesized peptides in *Drosophila* larvae with puromycin and used SUnSET to detect changes in protein synthesis induced by the TORC1 pathway and the transcription factor dMyc (Deliu et al., 2017). Applying the SUnSET assay, Ravi et al measured the cardiac protein synthesis in mice of different ages and successfully tracked the increase of synthesis during the different stages of a model for pathological hypertrophy (Ravi et al., 2018). SUnSET was also used to determine the presence of fully functional ribosomes and their general location in the presynaptic compartment of mice (Scarnati et al., 2018).

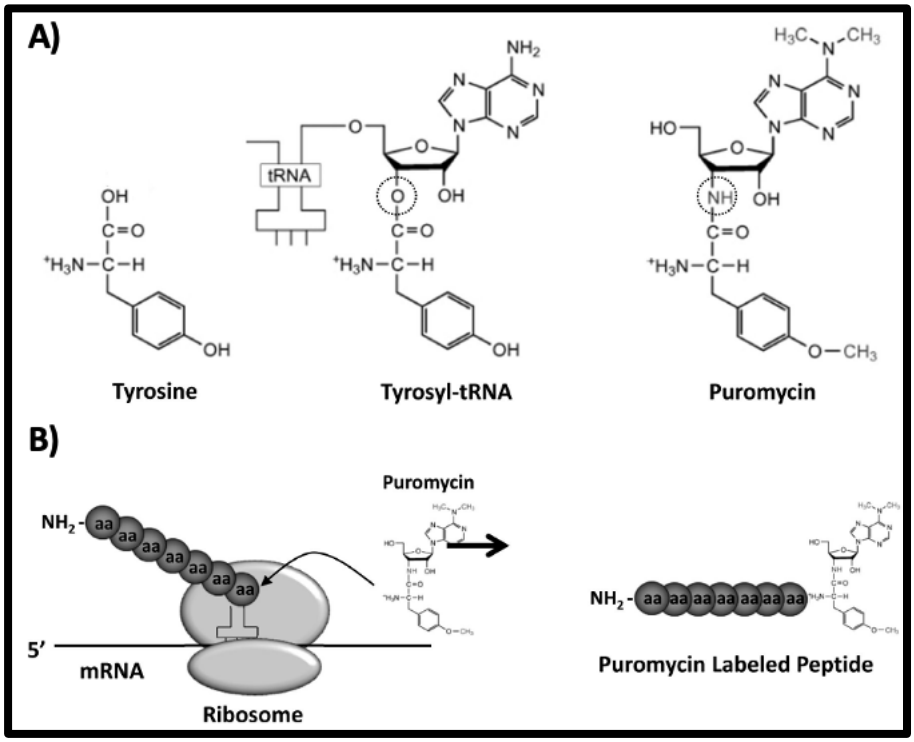

Figure 4.6 SUnSET Mechanism. A) Puromycin's structure is like that of tyrosyl-tRNA B) Incorporation of puromycin into the nascent peptide. Image taken from (Goodman and Hornberger, 2013)

SUnSET has not only been used in animal cells. In order to understand if proteasome inhibition in plants supresses protein synthesis, Hoewyk treated Arabidopsis plants with cycloheximide and measured the levels of newly synthesized proteins in root and shoot tissue (Van Hoewyk, 2016).

4.2 Results

4.2.1 C-Myc Plasmid reduced cell size

To further dissect the pathways involved in cell size regulation it was decided to increase the expression of the Myc protein. The first attempt to overexpress Myc was through transfecting the PCDNA3-MYC-GFP into HeLa cells.

24 hours after transfection, cells were visualized on a fluorescent microscope to verify the expression of Myc, which, as expected, was observed to be expressed in the cell nucleus (Figure 4.7).

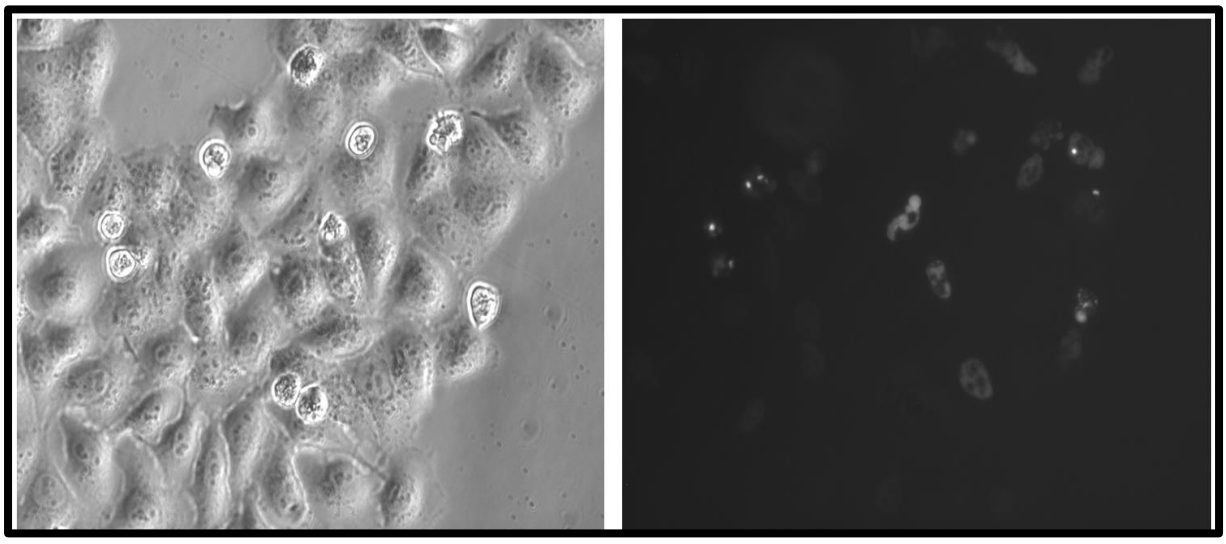

Figure 4.7 Myc-GFP is accumulated in the cell nuclei. Fluorescent signal of c-Myc GFP was observed inside the nuclei of HeLa cells.

4.2.2 Myc-GFP expressing cells are still smaller than controls

HeLa cells that expressed Myc were identified by the GFP signal. These cells, paradoxically, seemed slightly smaller than those that were not transfected (Figure 4.8A). The expression of Myc could be detected as early as 4 hours (Figure 4.8B), and cells seemed to be smaller even then already.

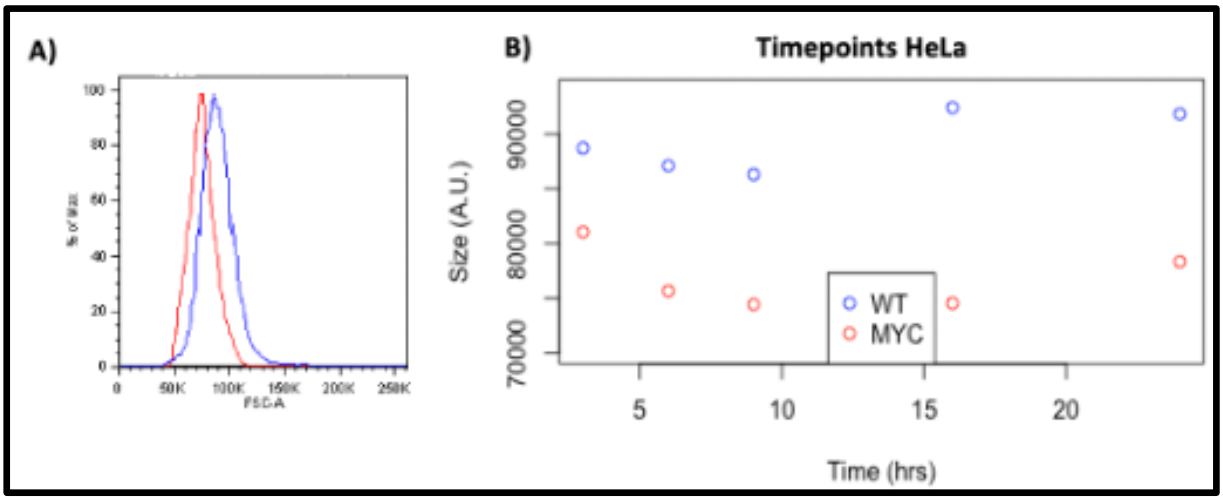

Figure 4.8 PCDNA3-MYC-GFP expressing cells are smaller. Transfected HeLa cells are smaller than controls. A) Representative histogram from HeLa cells transfected and non-transfected with GFP-Myc. B) Measurements from HeLa cells expressing Myc or not at different timepoints. Myc-expressing cells (in red) are smaller than non-expressing cells (blue). Data shown are mean values ± standard deviations (N = 3 independent biological replicates).

4.2.3 Myc Plasmid is only expressed in G1 cells

When analysing the expression of Myc with regards of the cell cycle distribution, it was found that Myc was only being expressed in G1 cells (Figure 4.9).

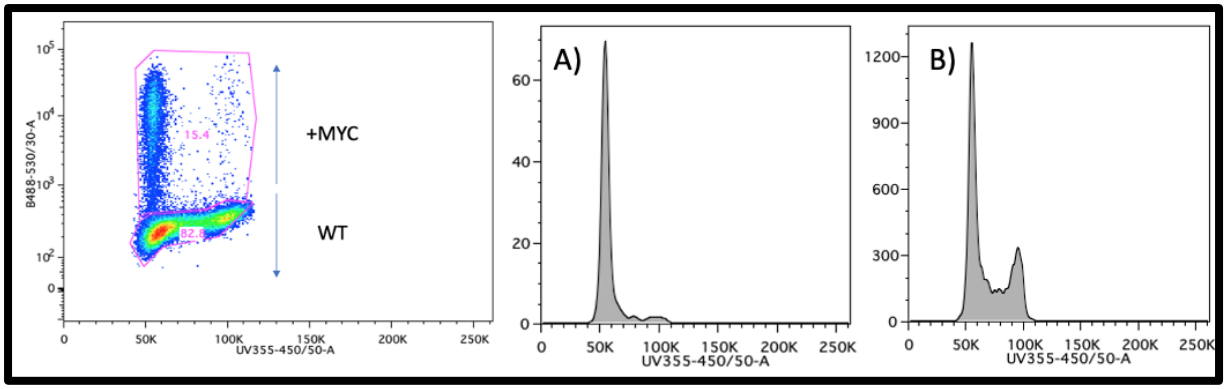

Figure 4.9 Myc is expressed mainly in G1 cells. The expression of Myc could only be detected in G1 cells. A) histogram of Myc-GFP expressing cells shows them distributed mostly in G1 phase, B) Histogram of normal HeLa cell cycle distribution. Data shown are mean values ± standard deviations (N = 3 independent biological replicates).

Since Myc is only being expressed in G1 cells and these cells tend to be inherently smaller than cells in G2, the size of G1 cells expressing Myc (Myc +) was compared with that from G1 cells non-transfected (Myc -). This revealed that G1 cells expressing the Myc-GFP plasmid were still smaller than G1 cells from the non-transfected population (Figure 4.10).

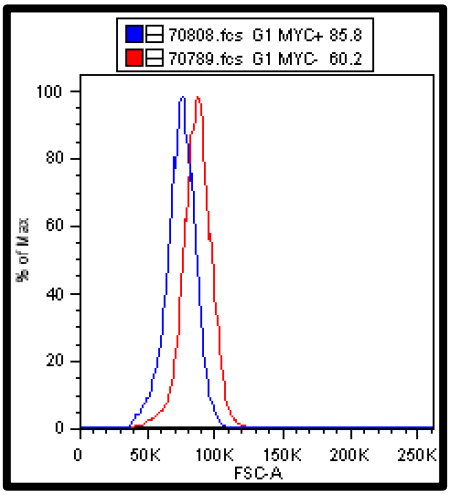

Figure 4.10 G1 cells comparison. Comparison of G1 cells of both Myc+ and Myc – HeLa cell line. Data shown are mean values ± standard deviations (N = 3 independent biological replicates).

The expression of this plasmid proved to be difficult, and the results were unconvincing considering the theorical Myc capacity to increase cell mass. For this reason, it was decided to change the system for Myc expression.

4.2.4 MycER is expressed in U2OS cells

To have a more homogenous expression of Myc in mammalian cells, it was decided to use the MycER system. This system consists of a hormone binding domain (HBD) of a steroid receptor which is fused to the protein of interest. Littlewood et al used the mutant murine oestrogen receptor G525R, which no longer binds oestrogen, yet remains responsive to activation by the synthetic steroid 4-hydroxytamoxifen (4-OHT) (Littlewood et al., 1995). Once the cells are exposed to 4-OHT they activate the already synthetised Myc.

A western blot was performed on U2OS MycER cells exposed to 4-OHT for 24 hours, as well as on Raji cells as these are derived from Burkitt's lymphoma, known to express high levels of Myc **(**Nishikura et al., 1985).

MycER was identified at ~97kDa and normal Myc was shown at around ~50kDa, as expected, MycER was only identified in U2OS cells, and not in Raji cells (Figure 4.11)

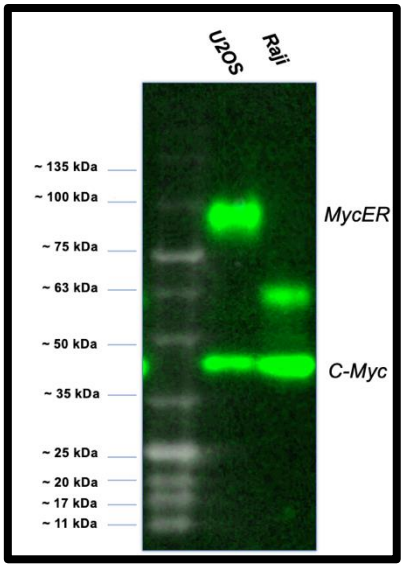

Figure 4.11 Myc-ER Western blot. A band at ~97kDa can be observed in U2OS cells, confirming the presence of the MycER construct. Another band at ~50kDa is observed in both U2OS and Raji cell lines, and corresponds to Myc.

4.2.5 MycER overexpression increases cell size in U2OS cells

The MycER U2OS cell line was exposed to 1 µM of 4-OHT for 24 hours in order to overexpress Myc, then they were analysed by both flow cytometry and Moxi Z coulter counter in order to analyse its effects on cell size.

It was observed that cells exposed to 4-OHT and analysed by flow cytometry increased their size compared to control cells (Figure 4.12 A), and when measured in the Moxi Z cell counter, cells with activated Myc showed a diameter 7% larger (Figure 4.9 B) and 22% more volume (Figure 4.12 C) than control cells.

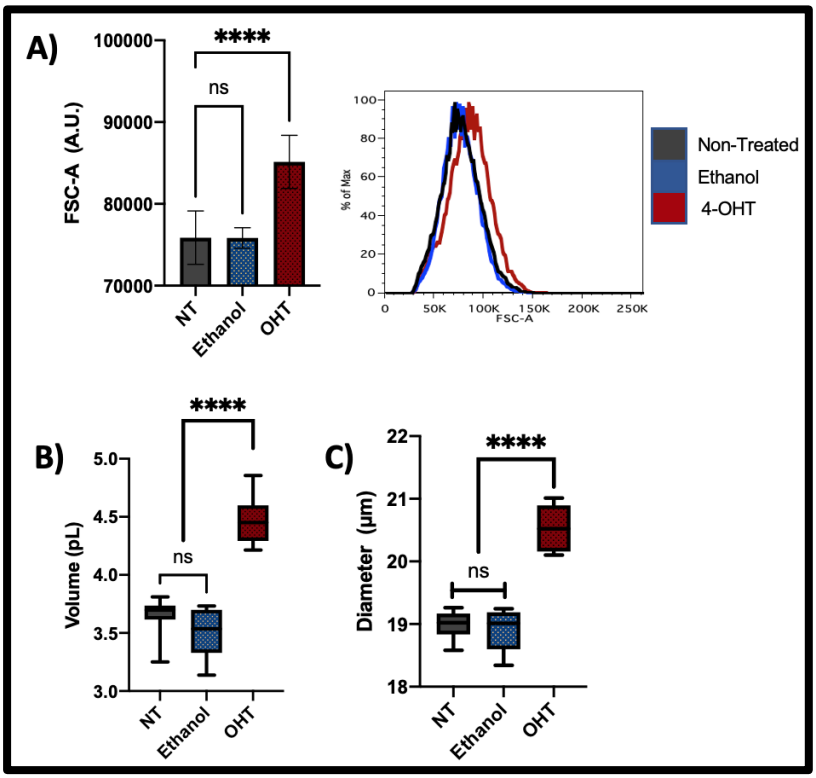

Figure 4.12 MYC overexpressing cells are larger. MycER U2OS cells incubated with 1 µM 4-OHT for 24 hours. A) Bar plots from cells analysed by flow cytometry and histograms representative of the data. B) Boxplots of values representing volume data from U2OS cells

treated with 4-OHT measured by Moxi Z. C) Boxplots of values representing diameter data from U2OS cells treated with 4-OHT measured by Moxi Z. Arbitrary Units (A.U.). Data shown are mean values ± standard deviations (N = 3 independent biological replicates). Statistical significance was assessed by ANOVA with Tukey's test, Asterisks represent the p-value: * p < 0.05, ** p < 0.01, *** p < 0.001, ****p < 0.0001. Box and whiskers plots calculated in GraphPad Prim, selecting the Min to Max option, the line in the middle of the box is the median.

4.2.6 Myc's overexpression rescues cell size from Serum Starvation

Since U2OS cells forced to overexpress Myc showed an increment in cell size, it was decided to test Myc's overexpression effect upon cells that have been serum starved. Cells were incubated with 1 μM of 4-OHT and were either seeded with DMEM containing 10% FBS or with just DMEM without FBS for 24 hours and then analysed through both flow cytometry and Moxi Z cell counter. As expected, serum starved cells showed a cell size reduction, whereas those given 4-OHT and incubated complete media were larger than control cells. However, cells that were both serum-starved and 4-OHT incubated were able to maintain the same size as control cells (Figure 4.13).

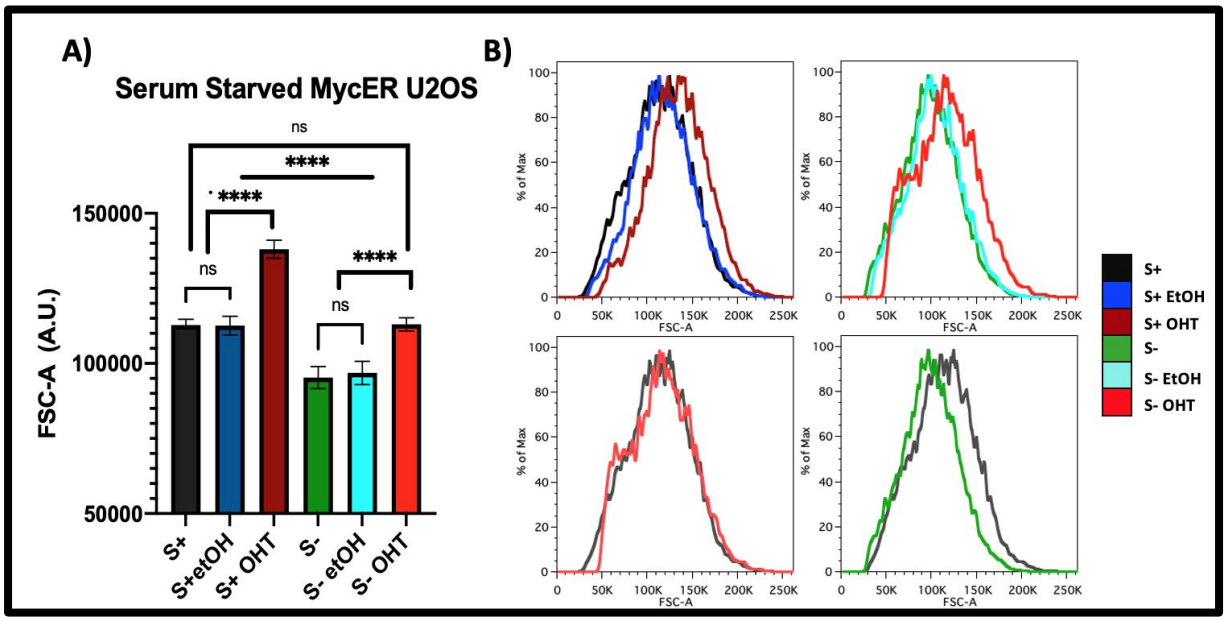

Figure 4.13 MycER cells increase their cell size. A) Bar plots representing MycER U2OS cells either serum starved or fed analysed by flow cytometry. B) Representative histograms from data generated by flow cytometry. Serum fed (S+), Serum Starved (S-), Serum fed and Ethanol control (S+ EtOH), Serum Starved and Ethanol control (S- EtOH), Serum starved cells incubated with 4-OHT (S-OHT) and Serum fed cells incubated with 4-OHT (S+ 4-OHT). Arbitrary Units (A.U.). Data shown are mean values ± standard deviations (N = 3 independent biological replicates). Statistical significance was assessed by ANOVA with Tukey's test, Asterisks represent the p-value: * $p < 0.05$, ** $p < 0.01$, *** $p < 0.001$, ****$p < 0.0001$.

When measured by Moxi Z cell counter, serum starved U2OS cells showed a reduction of ~7% of their diameter (figure 4.14 A) and 30% of their volume (Figure 4.14 B), whilst cells both starved and incubated with 4-OHT resisted the effects of serum starvation and maintained a similar diameter and volume to that of control cells (Figure 4.14 A & B).

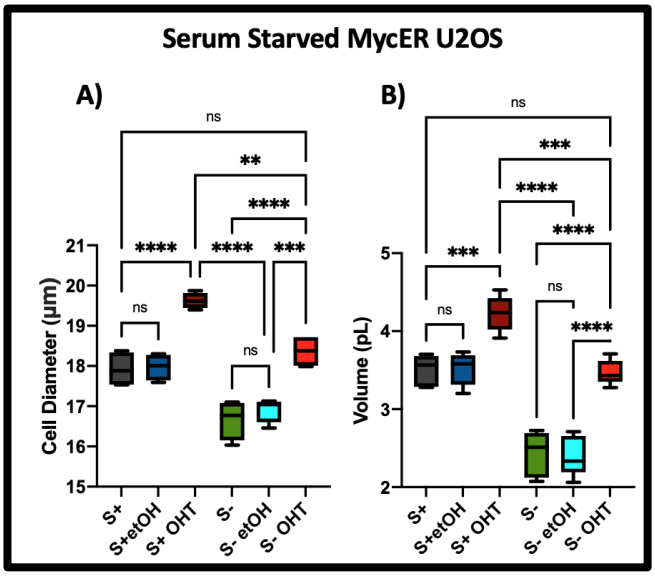

Figure 4.14 Myc overexpression rescues cells from Serum Starvation cell size reduction. Boxplot representing data from MycER U2OS cells serum starved or fed analysed by Moxi Z. A) Serum starved cells' diameter was reduced, whilst Myc overexpressing serum starved cells kept their diameter similar to serum fed controls. B) Serum starved cells drastically reduced their cell volume compared to cells incubated with FBS, whilst Myc overexpressing starved cells kept a similar volume to that of the serum fed cells. Statistical

significance was assessed by ANOVA with Tukey's test, ns = non-significant, * $p < 0.05$, ** $p < 0.01$, *** $p < 0.001$, ****$p < 0.0001$. Data shown are mean values ± standard deviations (N = 3 independent biological replicates). Box and whiskers plots calculated in GraphPad Prim, selecting the Min to Max option, the line in the middle of the box is the median.

4.2.7 Myc overexpression rescues cells from the effects of Rapamycin.

Myc has been shown to be involved in the control of cell growth in multiple models, by targeting multiple size-related mechanisms and pathways. For this reason, Myc overexpression effects were tested in cells where downregulation of the mTOR pathway was induced by chemical inhibition.

MycER U2OS cells were incubated for 24 hours with 1μM 4-OHT to induce an accumulation and activation of Myc and then exposed to 1μM Rapamycin. The effects on cell size were analysed by both flow cytometry and Moxi Z cell counter.

As expected, U2OS cells exposed to Rapamycin had a cell size reduction of around 20% compared to control cells (Figure 4.15 A & B). Surprisingly, cells both exposed to Rapamycin and 4-OHT resisted the shrinking effects of the drug, maintaining a similar size to non-treated controls (Figure 4.15 A & C).

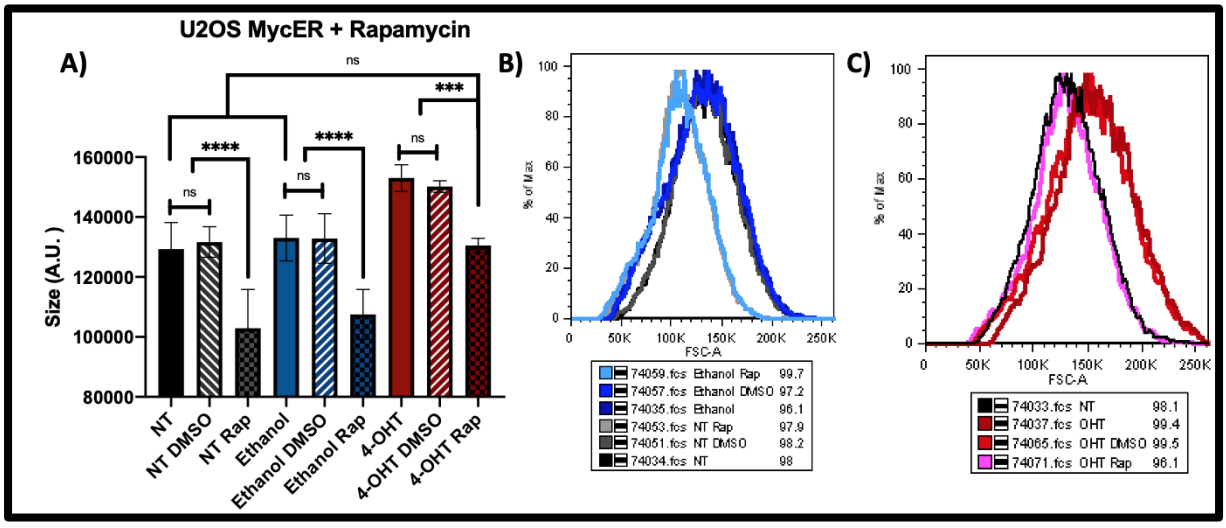

Figure 4.15 Myc overexpression rescues cells from Rapamycin effects. MycER U2OS cells incubated with 4-OHT were analysed by flow cytometry. A) Bar plot shows the effects of treatments with Rapamycin, OHT or both. B) Representative histograms of cells exposed Rapamycin show shows U2OS cells exposed are smaller than controls. C) Representative histograms of cells exposed to 4-OHT are larger than controls and cells exposed to both Rapamycin and 4-OHT are similar to controls. Arbitrary Units (A.U.). Data shown are mean values ± standard deviations (N = 3 independent biological replicates). Statistical significance was assessed by ANOVA with Tukey's test, Asterisks represent the p-value: * $p < 0.05$, ** $p < 0.01$, *** $p < 0.001$, ****$p < 0.0001$.

A similar effect can be observed when cells' diameter and volume are measured with the Moxi Z cell counter; MycER U2OS cells only exposed to Rapamycin show a decrement of around 10% of their diameter (Figure 4.16 A) and 30% of their volume (Figure 4.16 B). On the other hand, cells exposed to Rapamycin that were at the same time incubated with 4-OHT had a diameter (Figure 4.16 A) and volume (Figure 4.16 B) similar to the control cells.

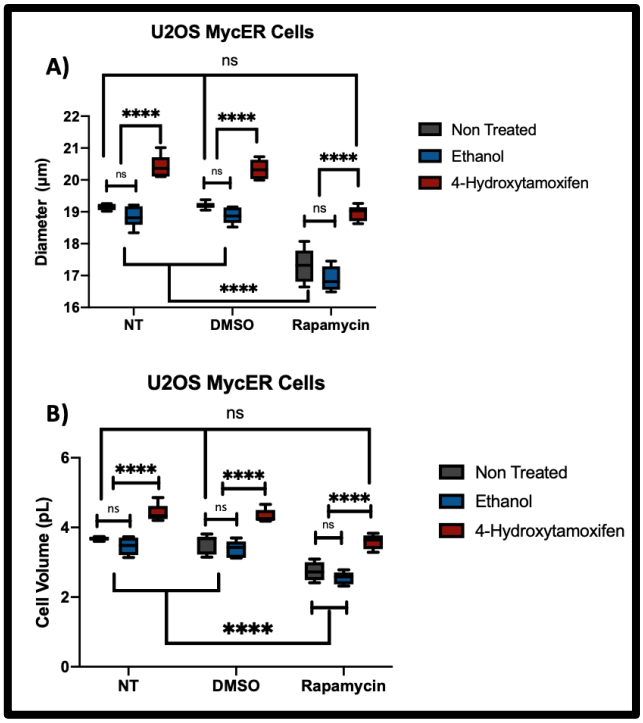

Figure 4.16 U2OS cells measured by Moxi. MycER U2OS cells induced by 4-OHT and exposed to Rapamycin were measured by Moxi Z. A) Cell volume shows bigger cells when exposed to 4-OHT and smaller when exposed to Rapamycin. B) Cell diameter of cells exposed

to 4-OHT and Rapamycin. Statistical significance was assessed by ANOVA with Tukey's test, ns = non-significant, * p < 0.05, ** p < 0.01, *** p < 0.001, ****p < 0.0001. Data shown are mean values ± standard deviations (N = 3 independent biological replicates). Box and whiskers plots calculated in GraphPad Prim, selecting the Min to Max option, the line in the middle of the box is the median.

4.2.8 Cell cycle is impacted by Rapamycin, Myc overexpression or both.

Cell size is tightly related to cell cycle; therefore, the next step was to analyse the cell cycle distribution of MycER cells exposed to Rapamycin and 4-OHT (Figure 4.17).

Asynchronous U2OS cells were exposed to both Rapamycin and 4-OHT as mentioned before, then they were stained using Hoechst 33342 dye to analyse their cell cycle distribution by flow cytometry using the UV355 channel.

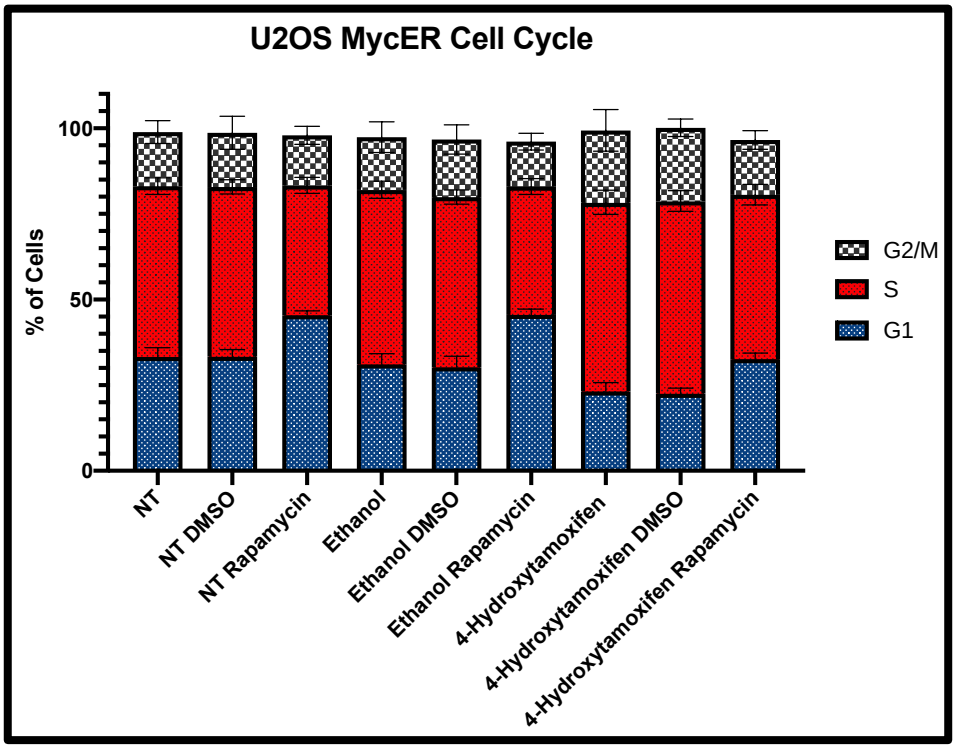

Figure 4.17 Cell Cycle distribution changes with Rapamycin and 4-OHT treatments. Cell cycle distribution of cells exposed to Rapamycin, 4-OHT or both. Rapamycin treated cells increased their proportion of cells in G1, whilst those treated with 4-OHT had a reduced

proportion of G1 cells. Those treated with both chemicals showed a similar cell cycle distribution to control cells. Cell cycle distribution was obtained by Watson Pragmatic cell cycle analysis in Flow Jo. Data shown are mean values ± standard deviations (N = 3 independent biological replicates).

U2OS cells that were exposed to Rapamycin, showed an increment of the percentage of cells in G1, from 33% in control cells to 45% in treated cells, exposure to Rapamycin changed the proportion of cells in S phase from ~49% in control cells, to ~37% in treated cells. G2 proportions of cells had a lesser impact with only 1% reduction from cells exposed to Rapamycin compared to the controls.

MycER activation with 4-OHT produced a reduction of the proportion of cells in G1, from 33% in control cells to 22% in 4-OHT exposed cells. Induced overexpression of Myc produced an increment of cells in S phase from 49% in control cells to 55% 4-OHT induced cells. The proportion of cells exposed to 4-OHT increased to ~21% from 15% of control cells.

On the other hand, U2OS cells exposed to both Rapamycin and 4-OHT showed an almost identical cell cycle distribution in all cell cycle phases when compared to control cells.

4.2.9 G1 phase an G2/M phase cell size changes upon Myc overexpression, Rapamycin exposure or both.

Given the fact that Myc overexpression and Rapamycin incubation produced changes in the cell cycle distribution, we had to exclude the possibility that the effects on cell size are because of the overall shifts in the cell cycle distribution. Both G1 and G2/M cells were gated using the UV355 channel, and information of their cell size was extracted using the FSCA channel (Figure 4.18).

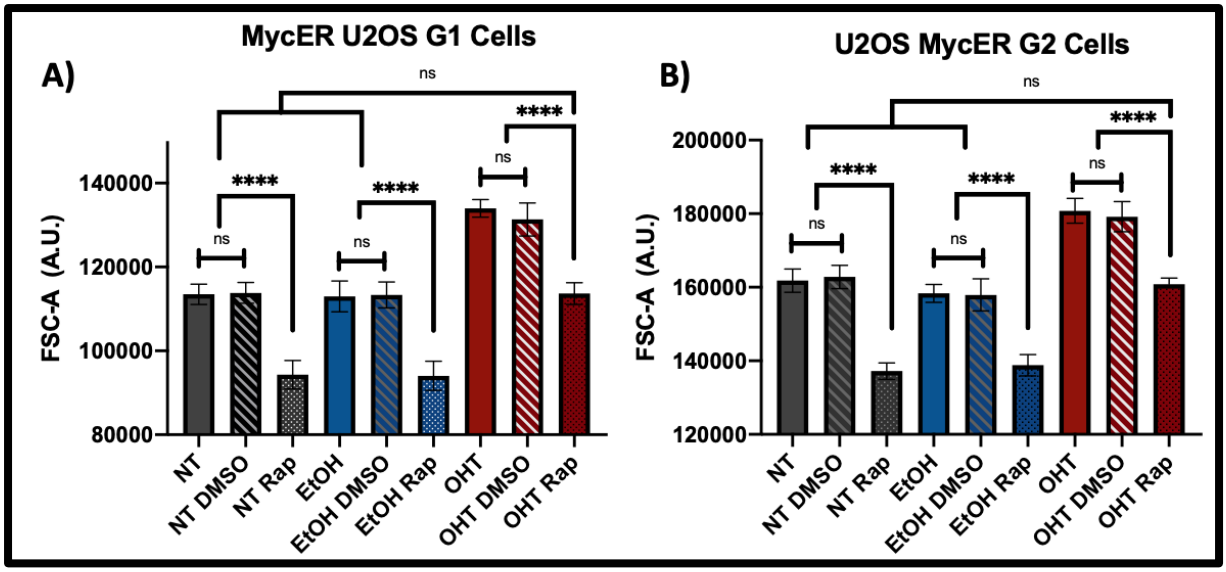

Figure 4.18 U2OS MycER G1 and G2/M size changes. U2OS MycER cells were exposed to Rapamycin, 4-OHT or both, then gated in G1 and G2/M phases and their size was extracted. A) Bar plots from G1 cells exposed to Rapamycin, 4-OHT or both. Rapamycin only produced smaller cells whereas 4-OHT inductions produced larger cells. Cells exposed to both 4-OHT and Rapamycin showed a similar size to control cells. B) Bar plots from G2 cells exposed to Rapamycin, 4-OHT or both. Rapamycin only produced smaller cells whereas 4-OHT inductions produced larger cells. Cells exposed to both 4-OHT and Rapamycin showed a similar size to control cells. Arbitrary Units (A.U.). Data shown are mean values ± standard deviations (N = 3 independent biological replicates). Statistical significance was assessed by ANOVA with Tukey's test, Asterisks represent the p-value: * $p < 0.05$, ** $p < 0.01$, *** $p < 0.001$, ****$p < 0.0001$.

Even though both Rapamycin exposure and Myc overexpression caused changes in the cell cycle distribution, the effects observed on cell size were not due to these changes and more likely due to growth effects on cells. We can observe that both G1 and G2 cells from Rapamycin treatments were smaller than control cells whereas those incubated with 4-OHT to induce Myc overexpression were overall larger than controls and Rapamycin treated cells. On the other hand, G1 and G2 cells that had a forced Myc overexpression and then were incubated with Rapamycin showed a similar size to that of the controls.

4.2.10 MycER induced cells increased ribosomal RNA

As observed before, Myc acts as a regulator of cell growth. One of the ways Myc can control cell size is by increasing the cell's biomass, which includes increasing the synthesis of ribosomes and proteins, amongst other macromolecules.

In order to measure ribosomal RNA content of the cells by flow cytometry, cells were stained with Pyronin Y (Kapuscinski and Darzynkiewicz, 1987).

To prove that Pyronin Y signal came from RNA, cells were incubated with RNase A and analysed by flow cytometry (Figure 4.19).

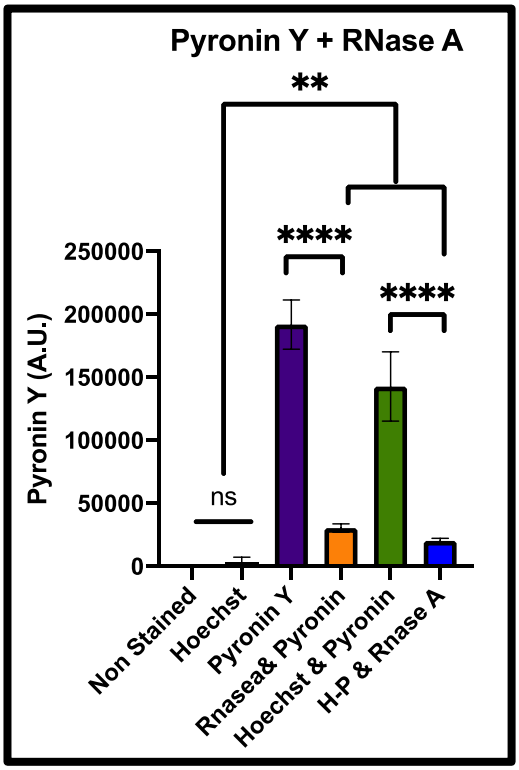

Figure 4.19 Pyronin Stains dsRNA. U2OS MycER cells were stained with Hoechst 33342 (H), Pyronin Y (P) or both, as well as incubated with RNase A, then stained with Pyronin Y. Signal is higher in Pyronin Y-only stained cells and lowers when co-incubated with Hoechst 33342 dye. Arbitrary Units (A.U.). Data shown are mean values ± standard deviations (N = 3 independent biological replicates). Statistical significance was assessed by ANOVA with Tukey's test, Asterisks represent the p-value: * $p < 0.05$, ** $p < 0.01$, *** $p < 0.001$, ****$p < 0.0001$.

Non-stained cells and Hoechst 33342-stained cells showed an insignificant background signal, cells stained with Pyronin Y showed a greater signal, and those stained with both Hoechst 33342 stain and Pyronin Y showed a lower signal than Pyronin Y only. This could be because of Pyronin Y's capacity to bind to both DNA and dsRNA, this way, Hoechst 33342 stain would bind to DNA before Pyronin Y and reduce the signal detected**.**

In order to measure the effects on rRNA synthesis after exposure of U2OS cells to Rapamycin, 4-OHT incubation or both, cells were stained with Pyronin Y after treatments and analysed by flow cytometry as previously described (Figure 4.20).

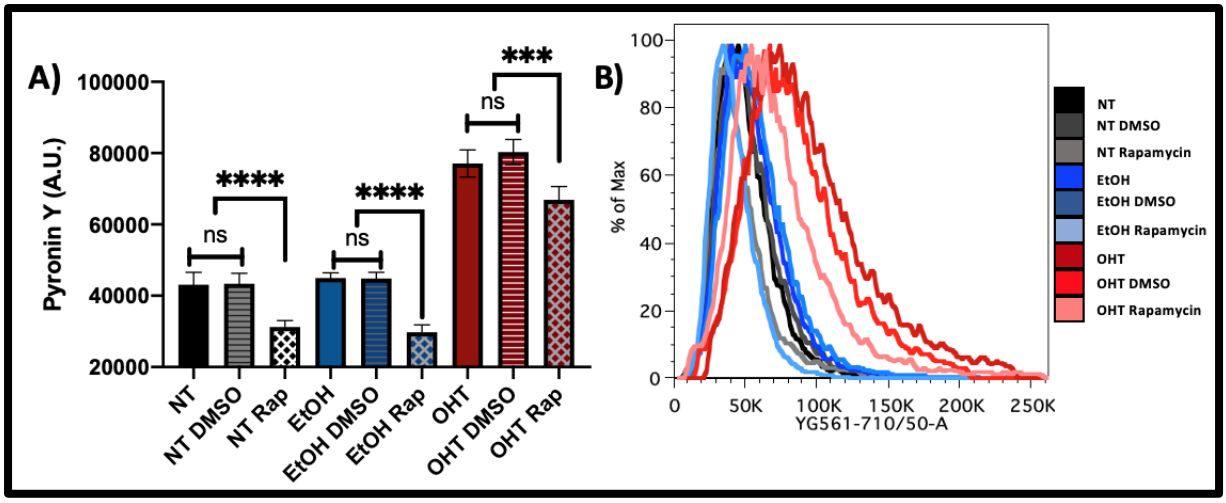

Figure 4.20 Myc Overexpression increases rRNA content. MycER U2OS cells exposed to Rapamycin and 4-OHT show different levels of Pyronin Y signal determined by flow cytometry. A) Bar plots from U2OS cells exposed to Rapamycin, 4-OHT or both. Rapamycin reduced Pyronin Y signal whilst Myc overexpression increased it. B) Representative histogram from flow cytometry data of treatments. Arbitrary Units (A.U.). Data shown are mean values ± standard deviations (N = 3 independent biological replicates). Statistical significance was assessed by ANOVA with Tukey's test, Asterisks represent the p-value: * $p < 0.05$, ** $p < 0.01$, *** $p < 0.001$, ****$p < 0.0001$.

U2OS cells that were only exposed to Rapamycin showed a reduction of the Pyronin Y signal when compared to control cells, on the other hand U2OS cells that were

incubated with 4-OHT and therefore had an overexpression of Myc showed a higher signal. Interestingly, cells exposed to both Rapamycin and 4-OHT have a higher signal of Pyronin Y as well. This could highlight a possible way by which Myc overexpressing cells resist the size reducing effects of Rapamycin, by having a greater number of ribosomes that are already translating proteins even when mTOR's function has been abrogated in the presence of Rapamycin.

4.2.11 Myc overexpression increases protein content

We observed that U2OS cells treated with Rapamycin, induced with 4-OHT or both, reduced, increased, or maintained their Pyronin Y signal respectively. For this reason, it was decided to observe the effects of these on protein content. To measure total protein content by flow cytometry, the Surface Sensing of Translation (SUnSET) technique was performed on U2OS MycER cells. Broadly, SUnSET requires cells to be given a pulse of Puromycin, a structural analogue of tRNA, which is incorporated into elongating peptide chains, some of which are transported to the cell membrane. Then, by using a fluorescent conjugated anti-puromycin antibody, the translation rate can be visualized by flow cytometry.

U2OS cells were incubated with puromycin and exposed to different chase times in order to determine the best incubation time (Figure 4.21) to obtain an adequate signal, similar to Schmidt et al (Schmidt et al., 2009).

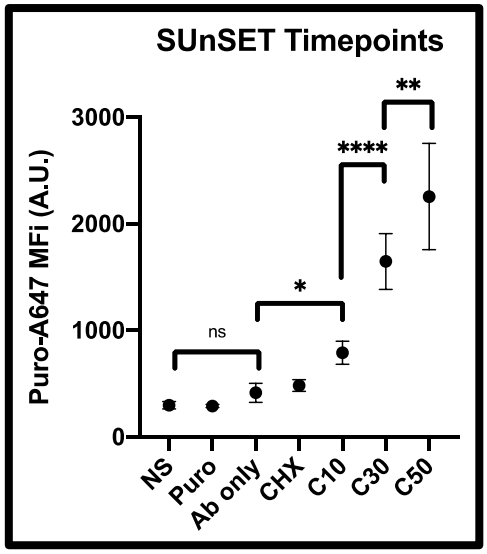

Figure 4.21 SUnSET timepoints. MycER U2OS cells were given a 10-minute pulse and chased for different time points. Background fluorescence was also observed in puromycin or antibody only treated cells. The cells were then analysed by flow cytometry. Non-stained (NS), Puromycin (Puro), Antibody only (Ab only), Cycloheximide (CHX), 10 minute chase (C10), 30 minute chase (C30) and 50 minutes chase (C50) MFI = Mean fluorescent intensity. Arbitrary Units (A.U.). Data shown are mean values ± standard deviations (N = 3 independent biological replicates). Statistical significance was assessed by ANOVA with Tukey's test, Asterisks represent the p-value: * $p < 0.05$, ** $p < 0.01$, *** $p < 0.001$, ****$p < 0.0001$.

U2OS cells were then exposed to Rapamycin, incubated with 4-OHT to induce Myc's overexpression or a combination of both and then fed puromycin and chased for 30 minutes (Figure 4.22).

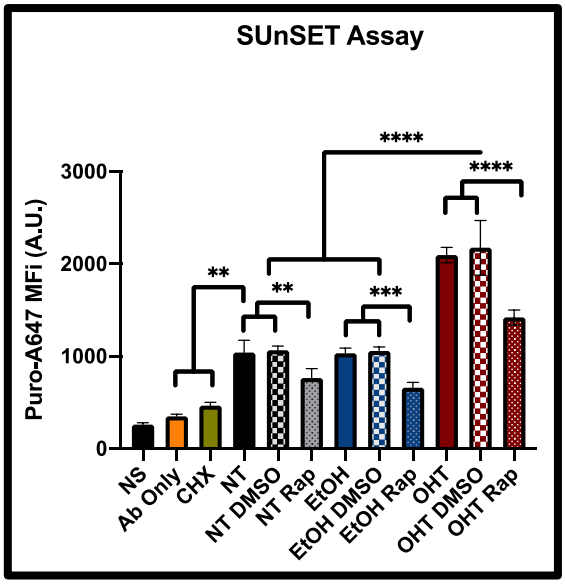

Figure 4.22 Protein translation increases with Myc forced expression. MycER U2OS cells exposed to Rapamycin and 4-OHT show different levels of anti-puromycin signal determined by flow cytometry. Bar plots from U2OS cells exposed to Rapamycin, 4-OHT or both. Rapamycin reduced anti-puromycin antibody signal whilst Myc overexpression increased it. Arbitrary Units (A.U.). Data shown are mean values ± standard deviations (N = 3 independent biological replicates). Statistical significance was assessed by ANOVA with Tukey's test, Asterisks represent the p-value: * $p < 0.05$, ** $p < 0.01$, *** $p < 0.001$, ****$p < 0.0001$.

U2OS cells exposed to Rapamycin showed a reduction of the puromycin signal when compared to the control cells, whilst those that were activated Myc overexpression had a two-fold increase of the puromycin signal. Interestingly, like what was observed in the Pyrionin Y signal. U2OS cells that were both exposed to Rapamycin and incubated with 4-OHT showed an anti-puromycin signal slightly larger than that of control cells.

Overall, we can observe that Myc over expressing cells are larger and have a higher rRNA and protein content. The opposite can be observed in Rapamycin treatments, with smaller cells that have less rRNA and protein content. Notably, when cells overexpressing Myc were incubated with the mTOR inhibitor, their size remained like non-treated cells, and the rRNA and protein content was slightly higher than non-treated cells.

4.2.12 RNAseq analysis of U2OS cells.

To identify the possible mechanisms regulating the changes in size observed before, we decided to evaluate gene expression on the U2OS cells. We proceeded to extract total RNA from U2OS control cells, Rapamycin exposed U2OS cells and 4-OHT induced U2OS cells and sent the total RNA to Novogene Europe for library preparation and sequencing using the NovaSeq 6000 system.

4.2.12.1 Quality Analysis of the Data

We made scatterplots of counts from the different samples replicates as a quality control and observed that replicates closely correlate with each other (Figure 4.23).

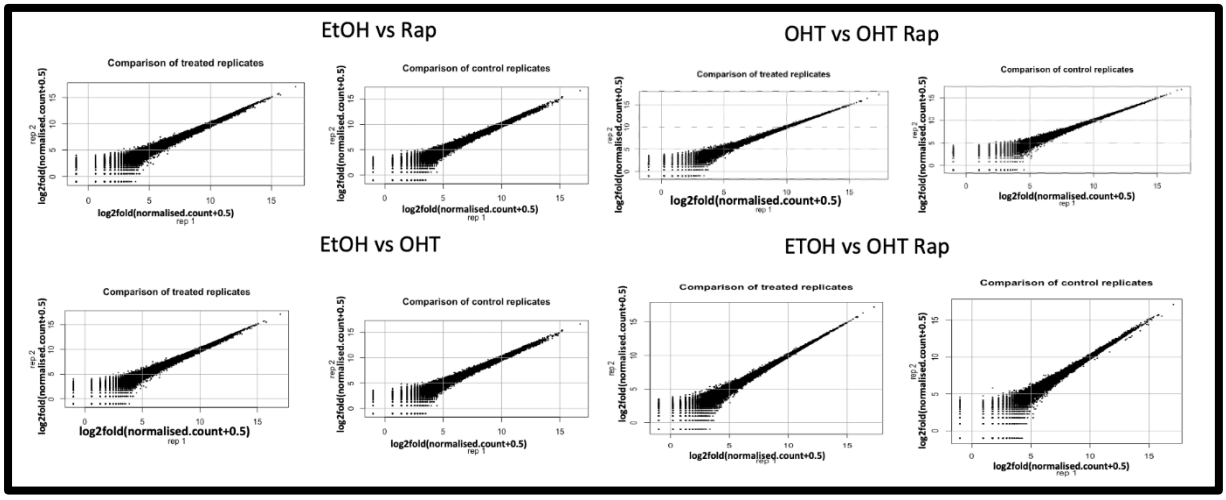

Figure 4.23 Quality check plots generated from the U2OS RNAseq. Replicates seem to correlate relatively well between each other in all samples. A) Replicate scatter plots of EtOH vs Rap dataset, B) Replicate scatter plot of EtOH vs OHT, C) Replicate scatterplot of OHT vs OHT_Rap dataset and D) Replicate scatter plot of EtOH vs OHT_Rap dataset.

A principal component analysis (PCA) was generated for quality control purposes. We can observe that Rapamycin + OHT is very different from the other samples and the replicates are very similar. The total variance in the data is captured by PC1 and PC2 (Figure 4.24)

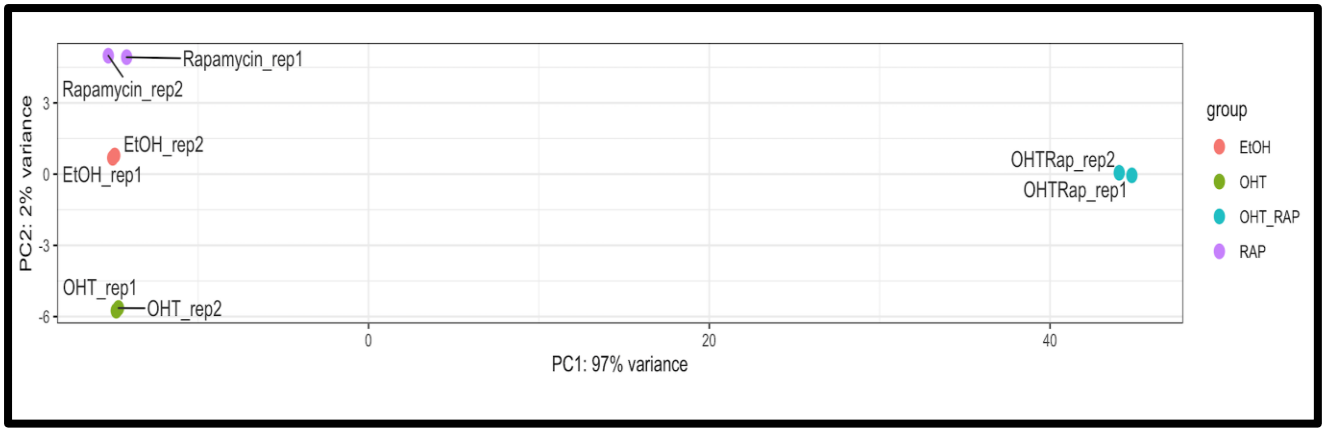

Figure 4.24 PCA plot from U2OS samples. 3 samples (Rapamycin, EtOH and 4-OHT cells express less variability. 4-OHT + Rapamycin samples present the highest variability amongst the samples.

Heatmaps from the three samples showing the DE genes were drawn for quality purposes (Figure 4.25). We can observe the changes in the signature of gene expression amongst samples depending on the treatments that they were exposed to. The colour coding is as follows; Red = upregulated genes, Blue = downregulated genes and Yellow = No change in gene expression.

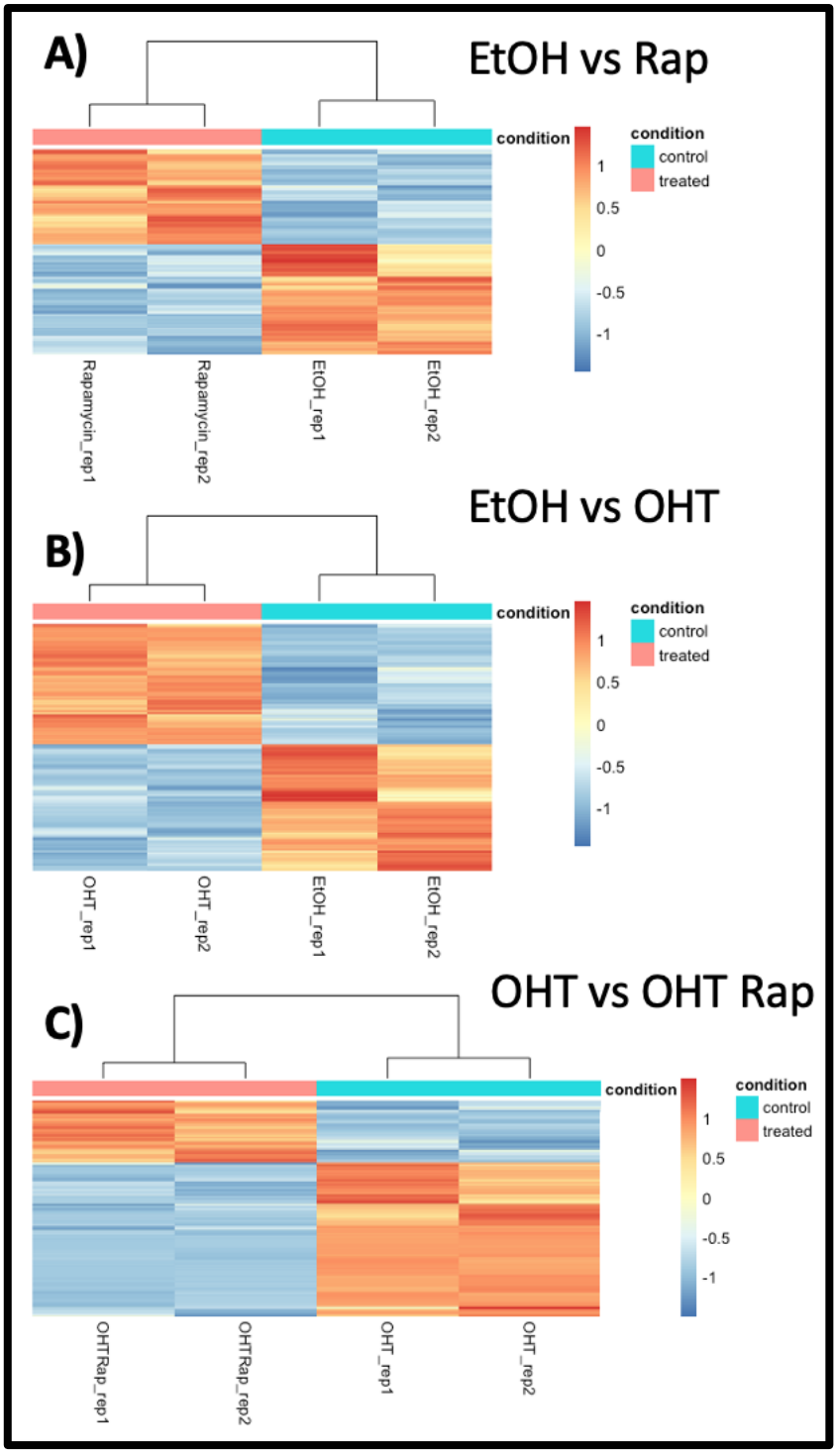

Figure 4.25 Heatmap of the most significant differentially expressed genes. Heatmap of the most highly expressed genes among the 4 datasets of the analysis. The data has been subjected to regularized log (rlog) transformation. A) EtOH vs Rapamycin, B) EtOH vs OHT and C) OHT vs OHT Rap. Red = upregulated, Blue = downregulated and Yellow = No change.

4.2.12.2 Differentially Expressed Genes and Volcano Plot

A volcano plot was drawn using the `Enhanced Volcano` package in R, showing differentially expressed genes from different datasets. Red dots in the volcano plot represent genes that have a p-value (padj) <0.05 and surpass the log2fold 2 cut-off as a threshold. Rapamycin exposed cells show both upregulated and downregulated genes (Figure 4.26 A), 4-OHT cells show more upregulated genes than downregulated Figure 4.26 B), and Myc overexpressing cells show a larger number of genes to be downregulated (Figure 4.26 C).

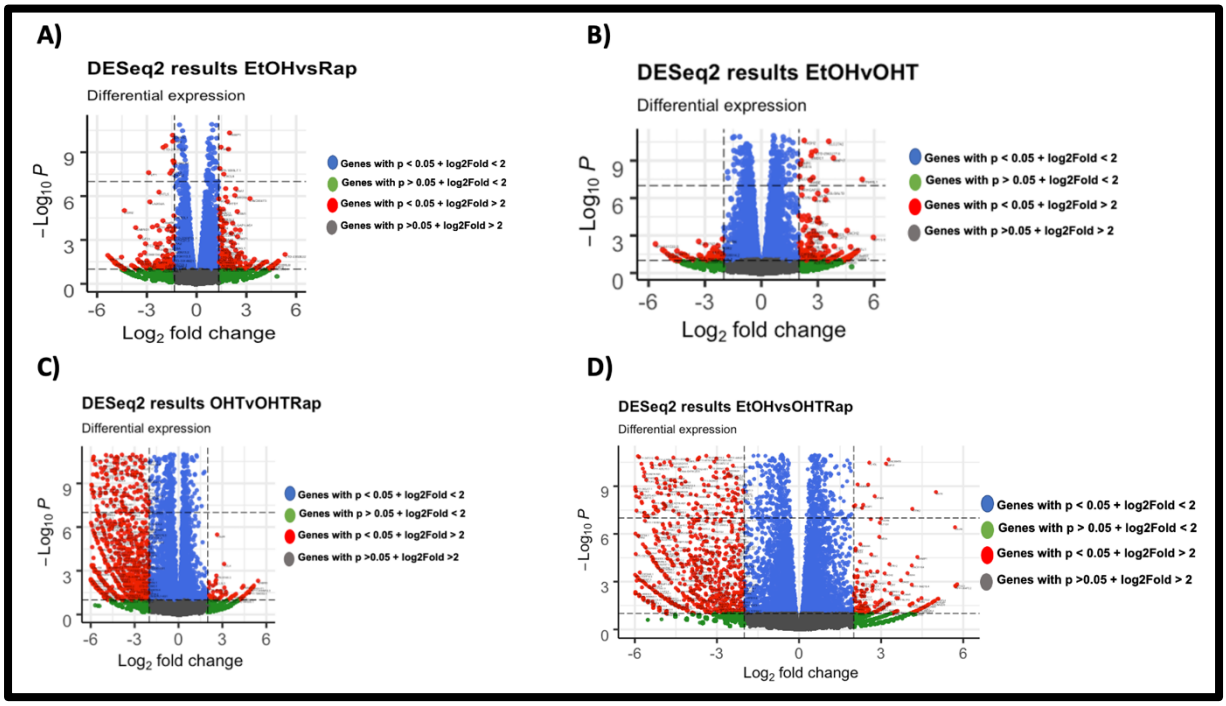

Figure 4.26 Volcano plot showing differentially expressed genes in the different U2OS dataset. Volcano plot generated using the *Enhanced Volcano* package in R, showing the highly significant data points with the lowest P-values in blue, large magnitude fold-changes in green and those genes with both characteristics in red. A) Volcano plot representing EtOH vs Rap dataset, B) Volcano plot representing EtOH vs OHT dataset, C) Volcano plot representing the OHT vs OHT_Rap dataset, and d) Volcano plot showing the DE genes in the EtOH vs OHT_Rap dataset.

The top 20 upregulated (Table 4.1) and downregulated (Table 4.2) differentially expressed genes from the different samples were shown.

Table 4.1 Top 20 Upregulated Genes. Tables showing the top 20 upregulated genes from sequencing samples. Genes are arranged by p-value (padj) <0.05.

Top 20 Upregulated Genes

EtOH vs Rap

Genes	log2FoldChange	padj
CTGF	1.5124521	1.13E-61
UBALD2	2.27020213	5.25E-56
MT2A	1.26485896	1.47E-43
PIM1	1.81264709	1.50E-36
LTBP2	1.35882961	7.04E-30
EMP1	1.33157134	1.24E-28
ITGB5	1.06949853	6.57E-25
CCNG2	2.03259624	2.85E-24
PDCD4	1.96760443	1.24E-23
LBH	1.52964907	4.12E-23
NBR1	1.19048645	7.98E-19
APOBEC3B	1.22373488	2.17E-17
RP11-69I8.3	1.38457809	1.53E-16
KLHL24	2.75428891	1.07E-15
GRN	1.03273419	5.56E-15
NEDD9	1.51829647	9.17E-15
H6PD	1.61390061	6.74E-14
HDAC5	1.1885985	4.07E-13
ADCK3	1.19944366	4.43E-13

EtOH vs OHT

Genes	log2FoldChange	padj
ADCYAP1R1	5.10338682	1.31E-69
CR2	4.69258487	1.42E-53
SPHK1	2.11988721	7.74E-43
CAMKV	3.83853424	5.20E-37
CA12	2.18144701	1.82E-36
CXCL14	2.97019194	7.13E-35
ABCA3	2.61152184	1.17E-34
PDE1B	3.50940591	2.13E-34
RGS16	2.45032767	1.62E-30
PDZRN3	2.58905086	4.19E-29
TXNIP	2.280246	1.78E-26
NIPAL4	2.96361798	1.93E-26
G0S2	2.89323803	1.88E-23
DHCR7	1.26359229	3.85E-23
SH2B2	2.39618298	5.07E-23
ANKH	1.4410381	8.71E-23
IGSF9	1.88358699	2.96E-22
CCND2	1.28594201	3.35E-22
DUSP2	1.70855983	1.80E-21

EtOH vs OHT

Genes	log2FoldChange	padj
MT2A	1.32158549	1.12E-77
LTBP2	1.11872535	3.97E-53
CTGF	1.09801294	1.63E-47
EMP1	1.46225545	1.53E-42
ITGB5	1.12685411	1.97E-41
UBALD2	1.88698624	3.65E-36
MTURN	1.02912654	8.71E-25
NBR1	1.13339053	1.96E-24
AL353644.3	2.3654014	1.26E-23
LBH	1.60437163	2.73E-21
SMAD6	1.14586605	1.31E-20
PIM1	1.532241	1.84E-19
PDCD4	1.52745116	2.55E-18
HDAC5	1.01859154	5.86E-18
ADCK3	1.03578103	3.68E-16
NR4A2	2.04580576	1.66E-15
H6PD	1.31170918	6.62E-15
MAFF	1.08863525	7.35E-14
EGR1	1.09678683	1.71E-13

Table 4.2 Top 20 Downregulated Genes. Tables showing the top 20 downregulated genes from sequencing samples. Genes are arranged by p-value (padj) <0.05.

Top 20 Downregulated Genes

EtOH vs Rap

Genes	log2FoldChange	padj
DDIT4	-2.9012356	2.94E-26
PHGDH	-1.0663497	9.95E-20
SLC7A11	-1.2990905	2.01E-19
CHAC1	-3.3349374	2.15E-19
CCND2	-1.1813284	8.33E-19
PSAT1	-1.266028	4.61E-17
MAP1A	-1.2082379	6.42E-16
RP11-442H21.2	-2.612856	1.23E-14
WFDC21P	-2.5579127	1.54E-14
PDLIM1	-1.5019629	2.74E-13
CRABP2	-1.3928556	5.13E-12
PSPH	-1.2999649	1.30E-11
VEGFA	-1.02143	1.60E-11
COL8A1	-1.1602348	1.28E-10
DDR2	-1.2683017	2.10E-10
IFRD1	-1.035916	3.64E-10
SESN2	-1.0580669	1.82E-09
CTD-2319I12.2	-2.0884931	1.93E-09
FAM46B	-1.259163	3.55E-09

EtOH vs OHT

Genes	log2FoldChange	padj
LGALS1	-1.7803459	1.82E-79
MT2A	-1.2958745	2.39E-36
FLJ22447	-1.6298526	1.45E-34
ANXA2	-1.0077753	4.06E-34
CAV1	-1.3945565	9.02E-33
MT1E	-1.2218106	2.32E-31
ARHGAP29	-1.1694065	1.20E-26
AXL	-1.0689375	1.77E-26
TUBB3	-1.1901785	5.25E-24
TENM2	-1.286949	4.08E-23
KRT17	-1.1250093	1.12E-22
MYEOV	-1.0495414	3.08E-21
AHNAK2	-1.8264389	3.18E-20
CCDC80	-1.5965442	7.23E-20
SDC1	-1.1883478	3.03E-15
AOX1	-1.0762209	3.99E-15
SNAPC1	-1.3333312	9.03E-15
TGM2	-1.3332194	2.60E-14
TCF19	-1.1200454	1.16E-13

OHT vs OHT Rap

Genes	log2FoldChange	padj
DNASE1	-3.5826111	4.40E-303
TYMS	-2.2943131	2.82E-301
EEF1D	-2.2504014	1.98E-290
RP11-363E6.3	-5.9527293	9.33E-287
ATP1A1-AS1	-6.6837259	1.19E-284
RPL30	-2.598916	1.92E-269
RP11-661A12.8	-7.0575216	1.98E-263
MXD3	-3.1865858	2.66E-263
MMACHC	-3.0356664	4.17E-263
SNORA72	-7.8821967	4.66E-259
VIM	-1.6496369	9.68E-250
RUSC1-AS1	-5.0890528	2.17E-245
XX-FW83563B9.5	-9.4450906	5.01E-230
UBB	-2.1121424	1.71E-228
GDF9	-6.6431819	5.95E-225
CTD-2292P10.4	-5.1237818	2.47E-219
RP11-159D12.6	-4.7609231	7.10E-213
PPIB	-2.1397086	2.45E-210
FTH1	-1.6194045	3.96E-203

Scatter (XY) plots of condition comparisons were generated to show the differentially expressed genes (in red) of the different datasets (Figure 4.27). Figure 4.27C shows the differentially expressed genes between Myc overexpressing U2OS cells and Myc overexpressing cells exposed to Rapamycin. A total of 5404 genes were found to be differentially expressed with most of them downregulated. This could be caused by a feedback mechanism involving downregulation of genes driven by Myc in combination with the downregulatory effects of Rapamycin.

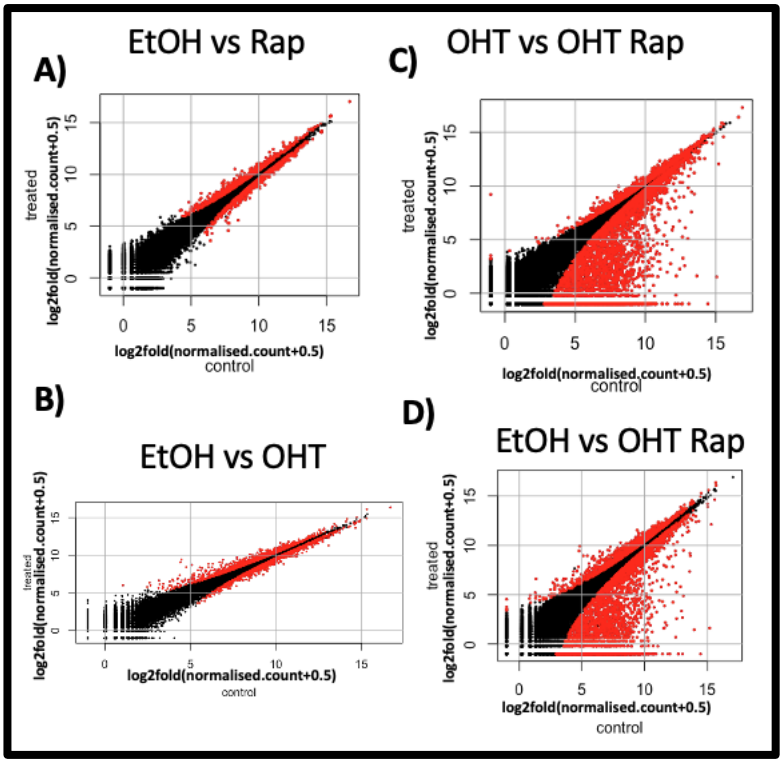

Figure 4.27 XY Scatter plot of U2OS samples. A) Scatter plot of the EtOH vs Rap dataset highlighting 1468 differentially expressed genes in red, B) Scatter plot of the EtOH vs OHT dataset, highlighting 2243 differentially expressed genes in red, C) Scatter plot representing the 4-OHT vs 4-OHT +Rap data set highlighting 5404 differentially expressed genes in red, and D) Scatter plot representing the EtOH vs 4-OHT + Rap data set highlighting 4927 DE genes in red.

4.2.12.3 Gene Ontology Analysis of MycER U2OS Cells

A Gene Ontology tool analysis critically depends on using the most-up to date GO annotations. Hence, we used several tools to perform our GO analysis. The softwares used were: `topGo` package in R, the g:Profiler server; (https://biit.cs.ut.ee/gprofiler/gost), and the Enrichr software (https://maayanlab.cloud/Enrichr/).

The GO enrichment analysis was performed in the different samples, starting with U2OS cells exposed to Rapamycin, using `topGo` (Figure 4.28).

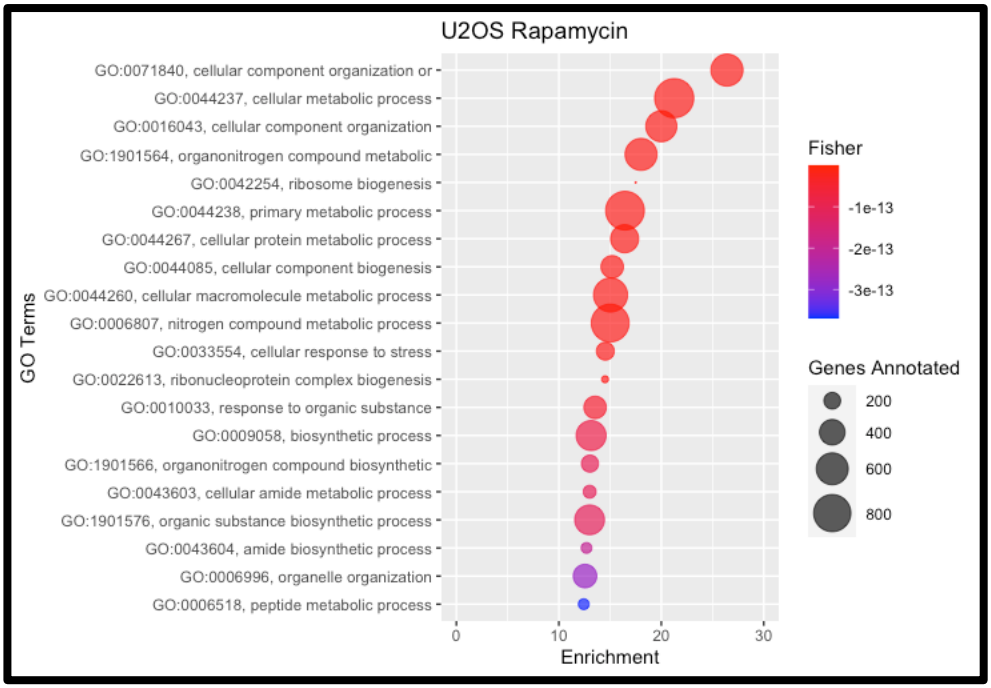

Figure 4.28 Top 20 BP Gene Ontology term enrichment of control U2OS cells vs Rapamycin. List of Gene Ontology terms enrichment of U2OS cells exposed to Rapamycin show terms related to Metabolism and Cell Growth. Graph produced by Top20 GO terms obtained using TopGO and then plotted with ggplot2, bubble size represents the numbers of genes annotated and coloration represents enrichment.

The top 5 most enriched Gene Ontology terms from U2OS cells exposed to Rapamycin are GO:0071840 Cellular component organization or biogenesis, GO:0044237 Cellular metabolic process, GO: 0016043 Cellular component organization, GO:1901564 Organonitrogen compound metabolic process and GO:0042254 Ribosome biogenesis. These terms seemed to be related to metabolic processes involved in mass accumulation.

The list of differentially expressed genes from Rapamycin exposed U2OS cells were also submitted in the g:Profiler server, using the g:GOst enrichment tool (Figure 4.29) which showed results similar to those observed using topGO.

ID	Source	Term ID	Term Name	p_{adj} (query_1)
1	GO:BP	GO:0071840	cellular component organization or biogenesis	6.239×10^{-19}
2	GO:BP	GO:0044237	cellular metabolic process	2.263×10^{-18}
3	GO:BP	GO:0042254	ribosome biogenesis	4.398×10^{-16}
4	GO:BP	GO:0022613	ribonucleoprotein complex biogenesis	4.666×10^{-15}
5	GO:BP	GO:0008152	metabolic process	6.254×10^{-15}
6	GO:BP	GO:0071704	organic substance metabolic process	7.684×10^{-15}
7	GO:BP	GO:0044238	primary metabolic process	1.010×10^{-14}
8	GO:BP	GO:0006807	nitrogen compound metabolic process	7.691×10^{-14}
9	GO:BP	GO:0016043	cellular component organization	6.950×10^{-13}
10	GO:BP	GO:0044085	cellular component biogenesis	1.396×10^{-11}
11	GO:BP	GO:0034641	cellular nitrogen compound metabolic process	7.461×10^{-11}
12	GO:BP	GO:0006364	rRNA processing	1.959×10^{-10}
13	GO:BP	GO:0043604	amide biosynthetic process	2.860×10^{-10}
14	GO:BP	GO:0033554	cellular response to stress	2.727×10^{-10}
15	GO:BP	GO:0043603	cellular amide metabolic process	3.764×10^{-10}
16	GO:BP	GO:0043170	macromolecule metabolic process	4.864×10^{-10}
17	GO:BP	GO:0044267	cellular protein metabolic process	5.997×10^{-10}
18	GO:BP	GO:0043043	peptide biosynthetic process	6.851×10^{-10}
19	GO:BP	GO:0016072	rRNA metabolic process	1.149×10^{-9}
20	GO:BP	GO:0042273	ribosomal large subunit biogenesis	1.195×10^{-9}

Figure 4.29 Top 20 Biological Process Gene Ontology term enrichment of U2OS cells exposed to Rapamycin. Differentially expressed genes from Rapamycin treated U2OS cells were submitted to Gene Ontology analysis in the g:Profiler platform, where it showed different terms associated with metabolic processes and ribosome biogenesis to be the most enriched terms.

Gene Ontology enrichment analysis performed by Enrichr shows a similar result to that observed on HeLa cells exposed to Rapamycin where translation and ribosome-related process where the most significant enriched terms, again associating with protein synthesis (Figure 4.30). This result could vary from the others because Enrichr constantly updates the gene-set libraries used (Kuleshov et al., 2016).

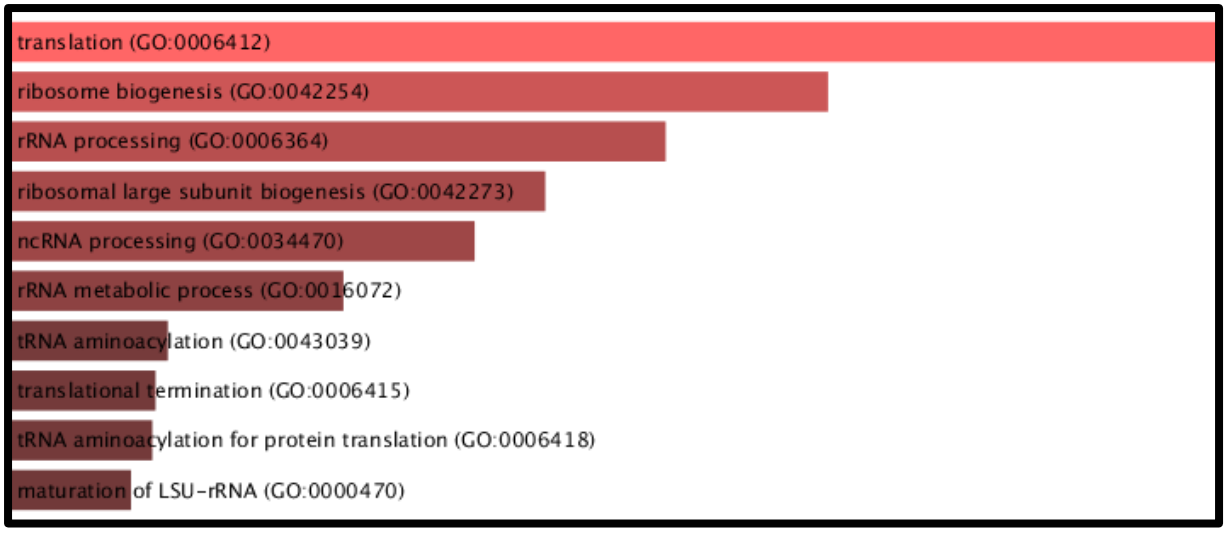

Figure 4.30 Top 10 Biological Process Gene Ontology term enrichment of U2OS cells exposed to RapaMycin by Enrichr. Differentially expressed genes from Rapamycin treated U2OS cells were submitted to Gene Ontology analysis in the Enrichr platform, where it showed Translation to be the most significant term enriched.

Datasets of downregulated DE genes from both HeLa and U2OS cells treated with Rapamycin were used to generate a Venn diagram (http://genevenn.sourceforge.net) showing that amongst both datasets there were 110 genes in common (Figure 4.31).

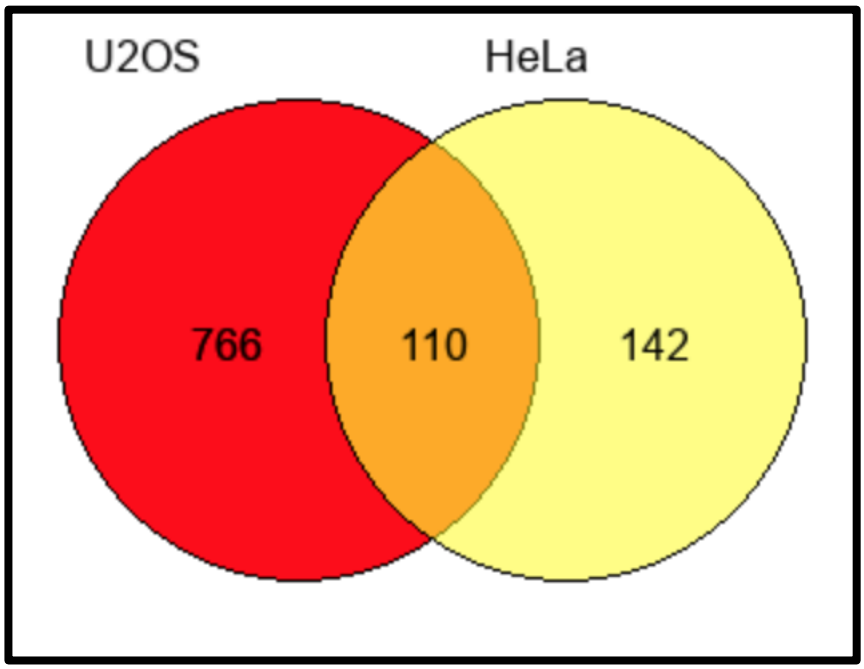

Figure 4.31 Venn Diagram of DE genes. Venn diagram showing the number of DE genes in datasets from both U2OS and HeLa cells.

These genes were used to perform a GO term analysis using gProfiler. We show the top 20 GO terms from the downregulated genes in common between HeLa and U2OS cells exposed to Rapamycin (Figure 4.32). Amongst the list of GO terms associated with the list of downregulated genes, we can observe Ribosome biogenesis and ribonucleoprotein complex biogenesis.

ID	Source	Term ID	Term Name	p_{adj} (query_1)
1	GO:BP	GO:1904816	positive regulation of protein localization to chr...	4.112×10^{-15}
2	GO:BP	GO:0022613	ribonucleoprotein complex biogenesis	9.865×10^{-15}
3	GO:BP	GO:1904814	regulation of protein localization to chromoso...	2.853×10^{-14}
4	GO:BP	GO:1904851	positive regulation of establishment of protein l...	5.142×10^{-14}
5	GO:BP	GO:1904869	regulation of protein localization to Cajal body	1.877×10^{-13}
6	GO:BP	GO:0070203	regulation of establishment of protein localizati...	1.877×10^{-13}
7	GO:BP	GO:1904871	positive regulation of protein localization to Caj...	1.877×10^{-13}
8	GO:BP	GO:0042254	ribosome biogenesis	2.083×10^{-13}
9	GO:BP	GO:1904867	protein localization to Cajal body	5.606×10^{-13}
10	GO:BP	GO:1903405	protein localization to nuclear body	5.606×10^{-13}
11	GO:BP	GO:0070202	regulation of establishment of protein localizati...	5.606×10^{-13}
12	GO:BP	GO:0006457	protein folding	8.146×10^{-13}
13	GO:BP	GO:1990173	protein localization to nucleoplasm	3.370×10^{-12}
14	GO:BP	GO:1904874	positive regulation of telomerase RNA localizat...	7.189×10^{-12}
15	GO:BP	GO:0070200	establishment of protein localization to telomere	1.431×10^{-11}
16	GO:BP	GO:1904872	regulation of telomerase RNA localization to C...	4.823×10^{-11}
17	GO:BP	GO:0070198	protein localization to chromosome, telomeric r...	7.618×10^{-11}
18	GO:BP	GO:0090672	telomerase RNA localization	8.292×10^{-11}
19	GO:BP	GO:0090670	RNA localization to Cajal body	8.292×10^{-11}
20	GO:BP	GO:0090685	RNA localization to nucleus	8.292×10^{-11}

Figure 4.32 Top 20 GO terms from downregulated genes from both HeLa and U2OS cells. A list of 110 shared downregulated DE genes from datasets of HeLa and U2OS cells exposed to Rapamycin was used to produce GO terms that associated these gene. Ribosome biogenesis figures amongst the GO terms.

Datasets containing the DE upregulated genes from both HeLa and U2OS cells exposed to Rapamycin were used to generate a Venn diagram of the shared upregulated genes between both cell types, showing 98 shared genes between cells (Figure 4.33).

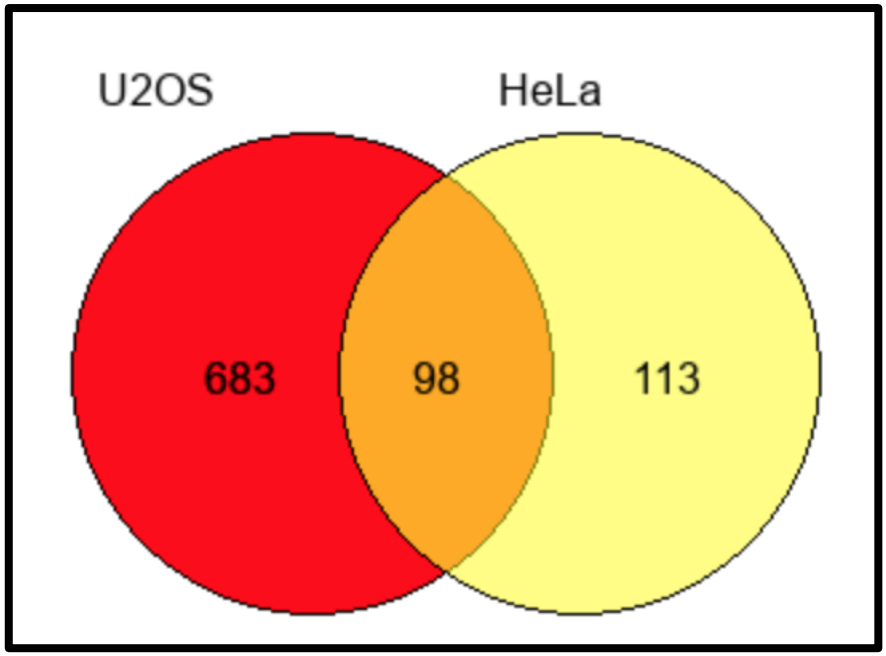

Figure 4.33 Venn diagram of upregulated DE genes from HeLa and U2OS cells exposed to Rapamycin. A Venn diagram showing 98 DE upregulated genes shared between datasets from U2OS and HeLa cells exposed to Rapamycin

The 98 genes shared between both datasets were used in gProfiler to generate a GO term list with the top 20 GO terms associated to the upregulated genes based on biological processes (Figure 4.34). Amongst the GO terms from upregulated genes, we can find some related to autophagy and mitochondrion disassembly.

ID	Source	Term ID	Term Name	p_{adj} (query_1)
1	GO:BP	GO:0002181	cytoplasmic translation	1.023×10^{-12}
2	GO:BP	GO:0070972	protein localization to endoplasmic reticulum	1.704×10^{-11}
3	GO:BP	GO:0006614	SRP-dependent cotranslational protein targeti...	7.385×10^{-11}
4	GO:BP	GO:0006413	translational initiation	1.050×10^{-10}
5	GO:BP	GO:0006613	cotranslational protein targeting to membrane	1.560×10^{-10}
6	GO:BP	GO:0045047	protein targeting to ER	4.398×10^{-10}
7	GO:BP	GO:0072599	establishment of protein localization to endopl...	6.771×10^{-10}
8	GO:BP	GO:0000184	nuclear-transcribed mRNA catabolic process, ...	1.531×10^{-9}
9	GO:BP	GO:0006605	protein targeting	1.524×10^{-8}
10	GO:BP	GO:0006612	protein targeting to membrane	9.232×10^{-8}
11	GO:BP	GO:0000956	nuclear-transcribed mRNA catabolic process	1.050×10^{-6}
12	GO:BP	GO:0006412	translation	2.550×10^{-6}
13	GO:BP	GO:0043043	peptide biosynthetic process	4.787×10^{-6}
14	GO:BP	GO:0006518	peptide metabolic process	1.792×10^{-5}
15	GO:BP	GO:0051668	localization within membrane	5.667×10^{-5}
16	GO:BP	GO:0043604	amide biosynthetic process	6.657×10^{-5}
17	GO:BP	GO:0072657	protein localization to membrane	7.371×10^{-5}
18	GO:BP	GO:0000422	autophagy of mitochondrion	1.900×10^{-4}
19	GO:BP	GO:0061726	mitochondrion disassembly	1.900×10^{-4}
20	GO:BP	GO:0044804	autophagy of nucleus	1.417×10^{-3}

Figure 4.34 Top 20 GO terms from upregulated DE genes between HeLa and U2OS cells. Different Gene Ontology terms from upregulated DE genes from HeLa and U2OS cells datasets. Several terms belong to autophagy because of Rapamycin treatment.

Next, DE genes from U2OS cells with activated Myc from incubation with 4-OHT, were submitted to Gene Ontology analysis in multiple platforms to observe which significant mechanisms could drive the effects observed.

Gene Ontology analysis was performed on MycER U2OS cells induced by 4-OHT, using `topGo` package in R, and the Top 20 GO terms were plotted using ggplot2 (Figure 4.35).

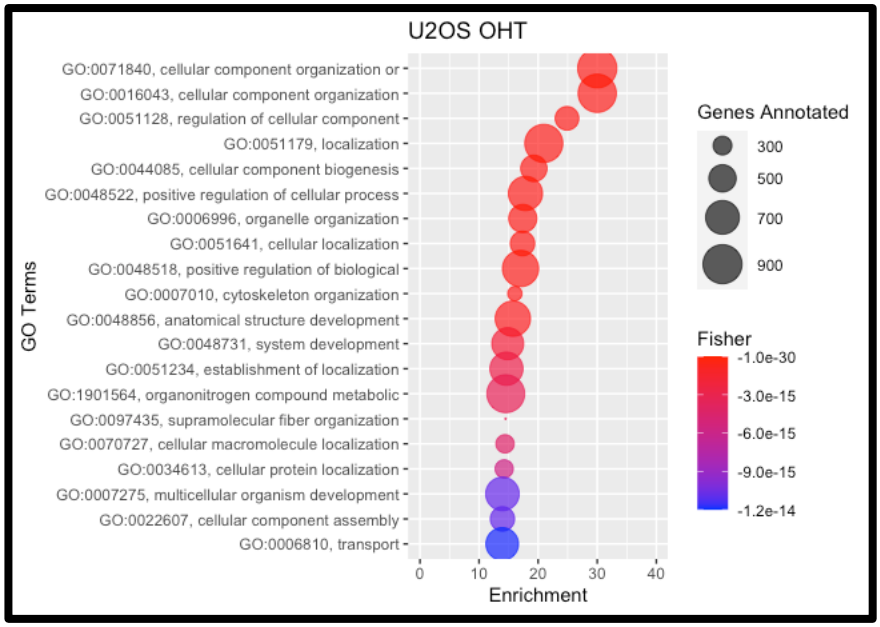

Figure 4.35 Top 20 BP Gene Ontology term enrichment of U2OS cells incubated with 4-OHT. List of Gene Ontology terms enrichment of U2OS cells exposed to 4-OHT show terms related to Cellular component biosynthesis. Graph produced by the top 20 GO terms obtained using TopGO and then plotted with ggplot2. Bubble size represents the number of genes annotated and coloration represents enrichment.

The top 5 most enriched Gene Ontology terms enriched of U2OS cells induced with 4-OHT are GO:0071840 Cellular component organization or biogenesis, GO:00160043 Cellular component organization, GO: 0051128 Regulation of cellular component, GO:0051179 Localization and GO:0044085 Cellular component biogenesis.

All the terms are related to the synthesis and accumulation of biological components of the cell. Next, we used the list of DE expressed genes from 4-OHT induced cells and performed Gene Ontology term enrichment using the g:GOst tool in the g:Profiler server (Figure 4.36).

ID	Source	Term ID	Term Name	p_{adj} (query_1)
1	GO:BP	GO:0071840	cellular component organization or biogenesis	3.694×10^{-30}
2	GO:BP	GO:0016043	cellular component organization	7.184×10^{-27}
3	GO:BP	GO:0051128	regulation of cellular component organization	3.554×10^{-24}
4	GO:BP	GO:0048522	positive regulation of cellular process	2.280×10^{-15}
5	GO:BP	GO:0051179	localization	1.636×10^{-14}
6	GO:BP	GO:0051641	cellular localization	2.248×10^{-14}
7	GO:BP	GO:0044085	cellular component biogenesis	1.755×10^{-13}
8	GO:BP	GO:0097435	supramolecular fiber organization	5.063×10^{-12}
9	GO:BP	GO:0048518	positive regulation of biological process	6.853×10^{-12}
10	GO:BP	GO:0007010	cytoskeleton organization	1.591×10^{-11}
11	GO:BP	GO:0048856	anatomical structure development	4.680×10^{-11}
12	GO:BP	GO:0009653	anatomical structure morphogenesis	4.738×10^{-11}
13	GO:BP	GO:0006996	organelle organization	7.490×10^{-11}
14	GO:BP	GO:0048731	system development	1.420×10^{-10}
15	GO:BP	GO:0030036	actin cytoskeleton organization	2.640×10^{-10}
16	GO:BP	GO:0007275	multicellular organism development	6.293×10^{-10}
17	GO:BP	GO:0033043	regulation of organelle organization	1.102×10^{-9}
18	GO:BP	GO:0030198	extracellular matrix organization	1.264×10^{-9}
19	GO:BP	GO:0000902	cell morphogenesis	7.867×10^{-9}
20	GO:BP	GO:0044087	regulation of cellular component biogenesis	7.590×10^{-9}

Figure 4.36 Top 20 Biological Process Gene Ontology term enrichment of U2OS cells induced with 4-OHT. Differentially expressed genes from 4-OHT induced U2OS cells were submitted to Gene Ontology analysis in the g:Profiler platform, where it showed Biological Process terms associated with ‘cellular component’ biosynthesis.

The results observed in g:Profiler were similar to those obtained using TopGO, with ‘cellular component’ biosynthesis being the most enriched term.

GO enrichment was also performed using the Enrichr software where we can observe different terms involved in cell growth, metabolism and rRNA processing (Figure 4.37)

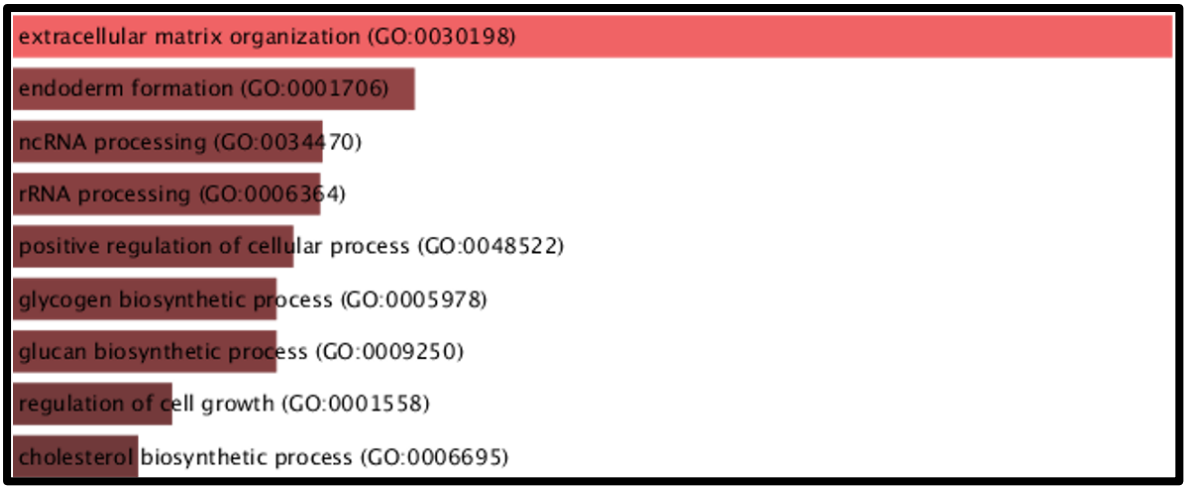

Figure 4.37 Top 9 Biological Process Gene Ontology term enrichment of U2OS cells exposed to 4-OHT by Enrichr. Differentially expressed genes from 4-OHT induced U2OS cells were submitted to Gene Ontology analysis in the Enrichr platform, where it showed

enriched terms to be associated with different cellular components biosynthesis, including regulation of cell growth.

Again, we used the GOrilla tool to perform enrichment analysis from the 4-OHT induced cells' DE genes. The most enriched terms were similar to those observed in Enricher, topGO and g:Profiler.

The results coming from different platforms show that upon Myc overexpression, the U2OS cells' differentially expressed genes were found to be related to Gene Ontology terms associated with processes that result in synthesis of constituent macromolecules, and biogenesis of cellular components.

Observing these results from the different platforms, we can infer that the differentially expressed genes in response to Myc overexpression are indeed involved in mechanisms that regulate growth, by increasing the synthesis of macromolecules and different cellular components that ultimately could possibly explain the increment of cell size observed in U2OS cells induced by 4-OHT.

An interesting effect was observed when Myc overexpressing U2OS cells were exposed to Rapamycin, where the cells maintained a similar size to that of non-treated and control cells. To elucidate the possible mechanisms underlying this effect, we analysed the DE genes from these cells in different Gene Ontology enrichment platforms.

Gene Ontology analysis was performed on DE genes from Myc overexpressing cells exposed to Rapamycin using `TopGo` package in R, and the Top 20 GO terms were plotted using ggplot2 (Figure 4.38).

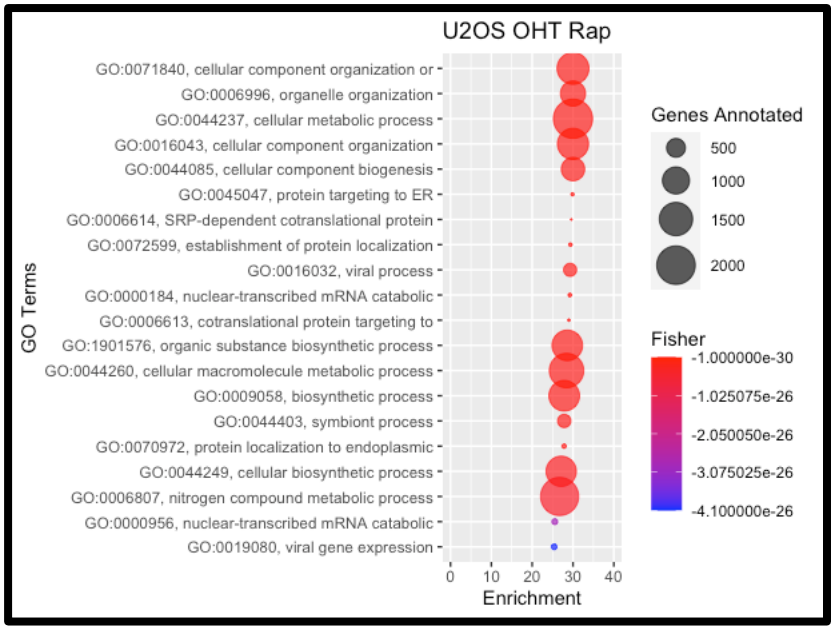

Figure 4.38 Top 20 BP Gene Ontology term enrichment of Myc overexpressing U2OS cells exposed to RapaMycin. List of Gene Ontology terms enrichment of Myc overexpressing U2OS cells exposed to RapaMycin show terms related to Cellular component biosynthesis. Graph produced by the top 20 GO terms obtained using `TopGO` and then plotted with ggplot2. The bubble size represents the number of genes annotated and coloration represents enrichment.

The top 5 most enriched GO terms generated by TopGo were GO:0071840 cellular component organization or biogenesis, GO:0006996 organelle organization, GO:0044237 cellular metabolic process, GO:0016043 cellular component organization and GO:0044085 cellular component biogenesis. All these terms are related to those observed in U2OS cells overexpressing Myc.

Again, GO terms were obtained using the g:Profiler server (Figure 4.39).

ID	Source	Term ID	Term Name	p_{adj} (query_1)
1	GO:BP	GO:0044237	cellular metabolic process	1.677×10^{-35}
2	GO:BP	GO:0071840	cellular component organization or biogenesis	1.205×10^{-31}
3	GO:BP	GO:0006807	nitrogen compound metabolic process	8.005×10^{-28}
4	GO:BP	GO:0034641	cellular nitrogen compound metabolic process	1.290×10^{-27}
5	GO:BP	GO:0006614	SRP-dependent cotranslational protein targeti...	3.971×10^{-27}
6	GO:BP	GO:0000184	nuclear-transcribed mRNA catabolic process, ...	8.128×10^{-27}
7	GO:BP	GO:0045047	protein targeting to ER	1.158×10^{-26}
8	GO:BP	GO:0006996	organelle organization	1.570×10^{-26}
9	GO:BP	GO:0072599	establishment of protein localization to endopl...	3.563×10^{-26}
10	GO:BP	GO:0006613	cotranslational protein targeting to membrane	4.071×10^{-26}
11	GO:BP	GO:0044238	primary metabolic process	1.436×10^{-25}
12	GO:BP	GO:0044085	cellular component biogenesis	5.675×10^{-25}
13	GO:BP	GO:0016043	cellular component organization	7.106×10^{-25}
14	GO:BP	GO:0008152	metabolic process	7.429×10^{-25}
15	GO:BP	GO:0046483	heterocycle metabolic process	1.441×10^{-24}
16	GO:BP	GO:0006139	nucleobase-containing compound metabolic p...	1.591×10^{-24}
17	GO:BP	GO:0070972	protein localization to endoplasmic reticulum	1.921×10^{-24}
18	GO:BP	GO:1901360	organic cyclic compound metabolic process	5.027×10^{-24}
19	GO:BP	GO:0006725	cellular aromatic compound metabolic process	1.447×10^{-23}
20	GO:BP	GO:0006413	translational initiation	9.329×10^{-23}

Figure 4.39 Top 20 Biological Process Gene Ontology term enrichment of Myc overexpressing U2OS cells exposed to Rapamycin. Differentially expressed genes from Rapamycin treated U2OS cells overexpressing Myc were submitted to Gene Ontology analyasis in the g:Profiler platform, where it showed cellular metabolic processes the most enriched term.

The results produced by g:Profiler listed ‘cellular metabolic process’ as the most enriched term, followed by ‘component biogenesis’ and other metabolic processes, similar to that observed in Myc overexpressing cells. However, it also shows terms involving processes in the ER, such as GO:0006614 SRP-dependent co-translational protein targeting to membrane and GO:0045047 protein targeting to ER.

When the differentially expressed genes from the Myc overexpressing cells exposed to Rapamycin were submitted to the Enrichr software, we observed similar results (Figure 4.40).

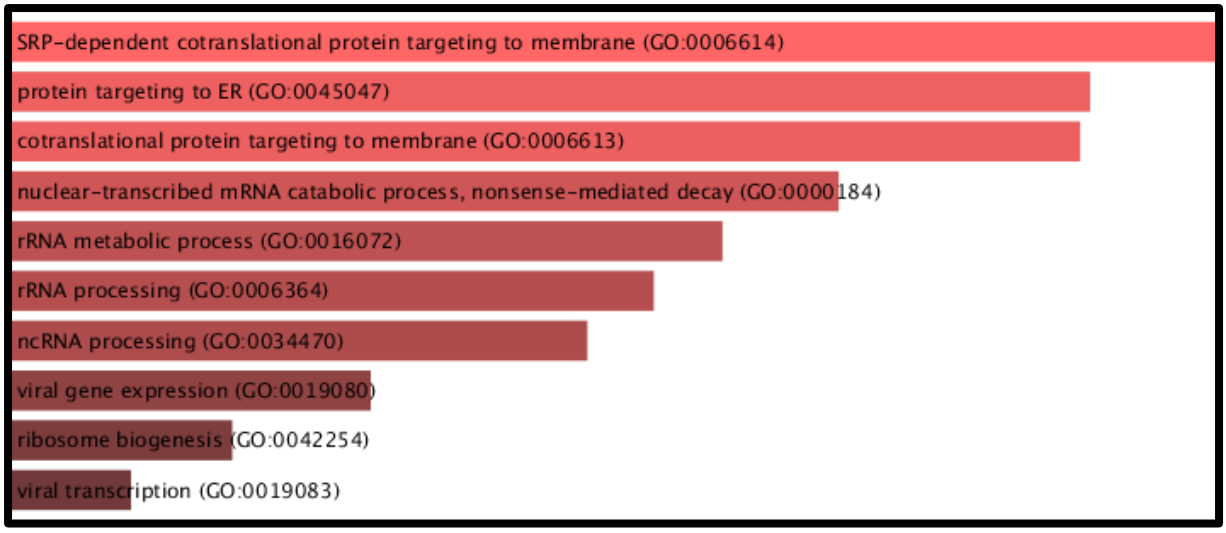

Figure 4.40 Top 10 Biological Process Gene Ontology term enrichment of Myc overexpressing U2OS cells exposed to Rapamycin by Enrichr. Differentially expressed genes from Rapamycin treated U2OS Myc-overexpressing cells were submitted to Gene Ontology analysis in the Enrichr platform, where it showed SRP-dependent co-translational protein targeting to membrane to be the most significant term enriched, followed by protein targeting to ER.

An interesting observation is that by plotting a heatmap representing the ribosomal protein genes, we can observe that Myc overexpressing cells that were exposed to Rapamycin seem to have slightly more transcripts from RP than the former without Rapamycin; on the other hand, we can observe that mitochondrial ribosomal proteins are more expressed in the latter (Figure 4.41).

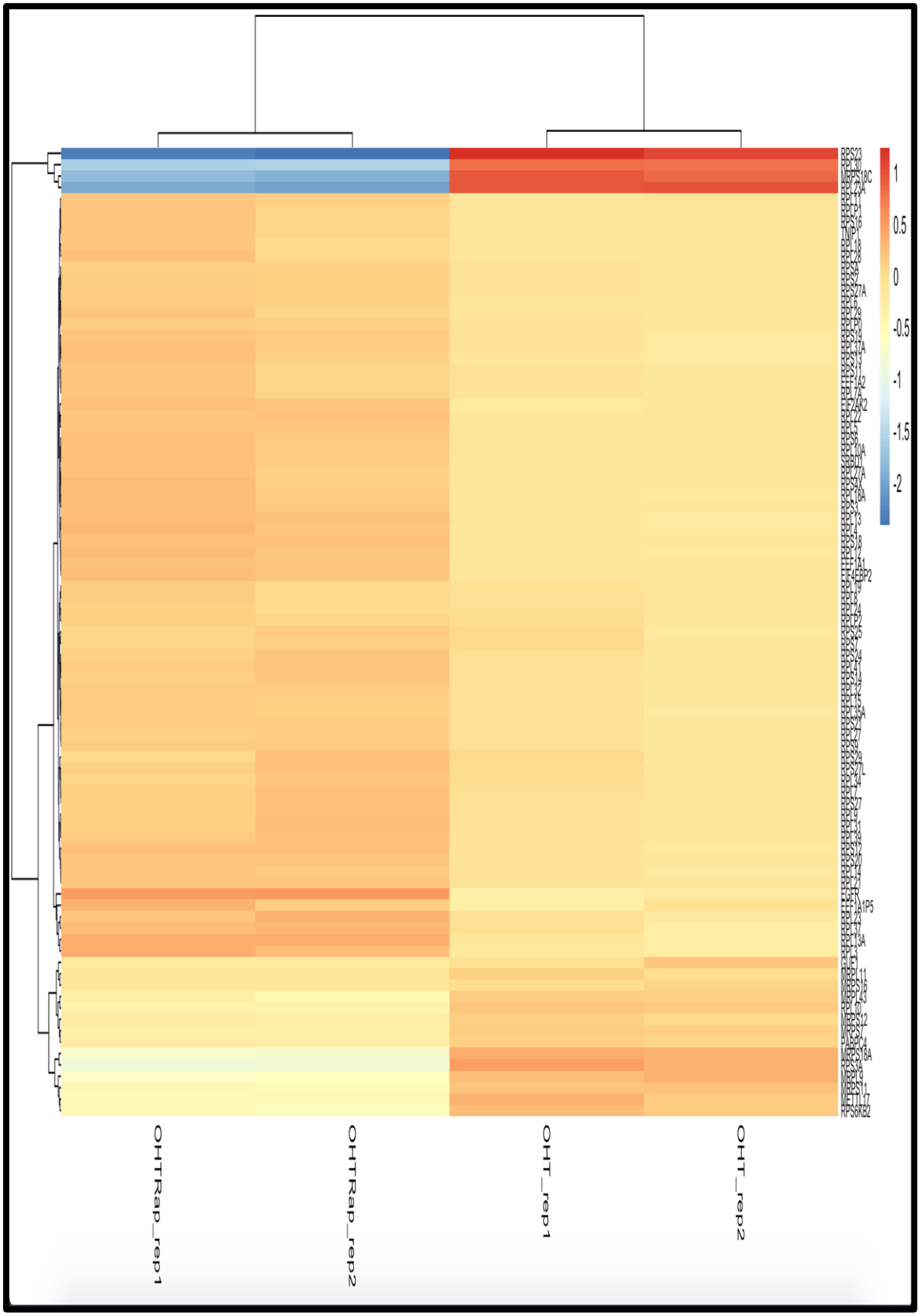

Figure 4.41 Heatmaps of DEG's associated with different GO Terms from Ribosomal Biogenesis. The heatmap shows different genes involved in the GO term Ribosomal Biogenesis.

Analysis from datasets of DE genes from a comparison between control U2OS vs Myc activated (by 4-OHT) and exposed to Rapamycin U2OS cells threw interesting results.

A list of upregulated DE genes was used in gProfiler to produce the top 20 Biological Process Gene Ontology Terms (Figure 4.42). The observed Gene Ontology terms are associated with the upregulated genes from Myc activated and Rapamycin incubated cells seem to be related with ribosome biogenesis and other rRNA related process.

ID	Source	Term ID	Term Name	p_{adj} (query_1)
1	GO:BP	GO:0044237	cellular metabolic process	6.094×10^{-12}
2	GO:BP	GO:0034470	ncRNA processing	2.098×10^{-10}
3	GO:BP	GO:0042254	ribosome biogenesis	2.744×10^{-9}
4	GO:BP	GO:0008152	metabolic process	2.780×10^{-9}
5	GO:BP	GO:0034660	ncRNA metabolic process	5.987×10^{-9}
6	GO:BP	GO:0044281	small molecule metabolic process	1.131×10^{-8}
7	GO:BP	GO:0044238	primary metabolic process	1.418×10^{-8}
8	GO:BP	GO:0071704	organic substance metabolic process	1.858×10^{-8}
9	GO:BP	GO:0022613	ribonucleoprotein complex biogenesis	2.675×10^{-8}
10	GO:BP	GO:0007005	mitochondrion organization	1.038×10^{-7}
11	GO:BP	GO:0044283	small molecule biosynthetic process	4.864×10^{-7}
12	GO:BP	GO:0006364	rRNA processing	8.557×10^{-7}
13	GO:BP	GO:0006807	nitrogen compound metabolic process	2.236×10^{-6}
14	GO:BP	GO:0016072	rRNA metabolic process	3.106×10^{-6}
15	GO:BP	GO:0071840	cellular component organization or biogenesis	3.996×10^{-6}
16	GO:BP	GO:1901566	organonitrogen compound biosynthetic process	1.526×10^{-5}
17	GO:BP	GO:1901564	organonitrogen compound metabolic process	2.968×10^{-5}
18	GO:BP	GO:0019693	ribose phosphate metabolic process	4.674×10^{-5}
19	GO:BP	GO:0034641	cellular nitrogen compound metabolic process	8.152×10^{-5}
20	GO:BP	GO:0043436	oxoacid metabolic process	1.670×10^{-4}

Figure 4.42 Top 20 Biological Process Gene Ontology Terms. A list of the DE upregulated genes from control vs 4-OHT + Rapamycin U2OS cells was used to produce Gene Ontology Terms. The Top GO terms are related to Ribosome biogenesis.

Using a list of DE downregulated genes from the same experiment the top 20 Gene Ontology terms were produced in gProfiler (Figure 4.43). We can observe that several Gene Ontology terms relate with cytoskeletal terms, along with other structural-related terms.

ID	Source	Term ID	Term Name	p_{adj} (query_1)
1	GO:BP	GO:0016043	cellular component organization	8.315×10^{-9}
2	GO:BP	GO:0071840	cellular component organization or biogenesis	3.660×10^{-8}
3	GO:BP	GO:0030198	extracellular matrix organization	4.855×10^{-7}
4	GO:BP	GO:0043062	extracellular structure organization	5.404×10^{-7}
5	GO:BP	GO:0045229	external encapsulating structure organization	6.684×10^{-7}
6	GO:BP	GO:0007010	cytoskeleton organization	2.927×10^{-5}
7	GO:BP	GO:0006996	organelle organization	5.555×10^{-5}
8	GO:BP	GO:1990778	protein localization to cell periphery	5.787×10^{-5}
9	GO:BP	GO:1904375	regulation of protein localization to cell periphe...	3.692×10^{-4}
10	GO:BP	GO:0031589	cell-substrate adhesion	2.176×10^{-3}
11	GO:BP	GO:0097435	supramolecular fiber organization	2.866×10^{-3}
12	GO:BP	GO:0009653	anatomical structure morphogenesis	2.976×10^{-3}
13	GO:BP	GO:0051128	regulation of cellular component organization	4.127×10^{-3}
14	GO:BP	GO:0018057	peptidyl-lysine oxidation	5.385×10^{-3}
15	GO:BP	GO:0072659	protein localization to plasma membrane	1.626×10^{-2}
16	GO:BP	GO:0007017	microtubule-based process	2.341×10^{-2}
17	GO:BP	GO:0006928	movement of cell or subcellular component	2.630×10^{-2}
18	GO:BP	GO:0030199	collagen fibril organization	3.087×10^{-2}
19	GO:BP	GO:0000226	microtubule cytoskeleton organization	3.525×10^{-2}
20	GO:BP	GO:0030029	actin filament-based process	4.811×10^{-2}

Figure 4.43 Top 20 Biological Component terms from DE Downregulated Genes. A list of DE downregulated genes from Myc activated + Rapamycin exposure U2OS was used to obtain the top Gene Ontology terms associated to these genes. The top Gene Ontology terms relate to cytoskeletal organization.

4.3 Discussion

To understand the effects of Myc in the cell size regulation, a Myc-GFP expression plasmid was transfected in HeLa cells however, the effect observed on the cells was the opposite of what was expected. When analysed by flow cytometry, it was noted that cells expressing a GFP signal (and therefore Myc) were smaller than un-transfected cells. When the cells were analysed by their DNA content (cell cycle distribution), it was noted that only the cells in G1 phase expressed Myc, which could in part explain why only smaller cells showed a Myc-GFP signal. To properly understand this phenomenon, a GFP-only plasmid control should have been added to the experiment. If the GFP plasmid was transfected and again only smaller (and G1 phase) showed the signal, this would probably mean that the plasmid itself could be toxic for the cells and causing a cell cycle arrest, which would show that it wasn't a

direct effect of Myc's expression. Nonetheless, if the GFP-expressing cells are of normal size, then Myc's expression would perhaps be responsible for a cell cycle arrest in HeLa cells. More experiments would be required to elucidate this phenomenon.

After an unsuccessful result with the transfection of the Myc-GFP plasmid, it was decided to proceed with the more stable MycER system. The U2OS cell line containing the MycER construct on its genome was kindly gifted by Dr Stefano Campaner from the *Instituto Italiano di Tecnologia.*

This cell line continuously expresses the Myc protein fused to the oestrogen receptor (MycER) which is inactivated unless the cells are induced with 4-hydroxy tamoxifen (4-OHT).

4-Hydroxitamoxifen is known to be a less than a friendly molecule for cells, as it is normally used to inhibit proliferation of Oestrogen receptor^{+} (ER^{+}) breast cancer cells. It has also been shown to induce a dose-dependent transient increase in cell proliferation in the mammary epithelium of mouse cells (Shehata et al., 2014). For these reasons it is important to consider other alternatives and controls for 4-OHT treatments. If possible, we could have a non-transformed (no MycER) U2OS cells and exposed them to 4-OHT to visualize if any side effect from the 4-OHT would arise. Another alternative could be the use of a T-REx™ system where a potent CMV promoter can drive a strong expression of a cloned Myc gene that can be repressed upon addition of Tetracycline (https://www.thermofisher.com/order/catalog/product/K103001#/K103001).

In order to demonstrate the presence of the MycER construct in the U2OS cells, we proceeded to perform total protein extraction on these and on Raji cells as they are derived from a Burkitt's lymphoma and known to express high levels of Myc **(**Nishikura et al., 1985). As observed by others, a band of ~ 97 kDa was detected only for U2OS cells bearing the MycER construct (Gandarillas and Watt, 1997, Littlewood et al., 1995).

A strong induction of Myc was forced on U2OS cells upon incubation with 1 μM 4-OHT which then were analysed by both Moxi Z and Flow cytometry to analyse the changes in their cell size. Myc overexpression was shown to increase ~11 % of the size by flow cytometry along with an increment of 10% diameter and ~22 % volume. This is in line with the idea that Myc is an evolutionarily conserved growth control master regulator (Grifoni and Bellosta, 2015, Young et al., 2011, Gallant, 2013). In *Drosophila,* dMyc expression levels correlate with cell size, where dMyc mutants generate smaller flies and, on the other hand, increased expression of dMyc in *Drosophila* imaginal disc cells increased their size (Arabi et al., 2005, Gallant et al., 1996, Johnston et al., 1999).

In mammalian cells, loss and gain of Myc function has been associated with diminished and enhanced cell growth, respectively (Sansom et al., 2007). The Murine model of lymphomagenesis (Eμ-myc mice) which features the expression of a Myc transgene under control of the Ig heavy chain enhancer (Eμ) has been used to show how this malignancy with enhanced Myc expression produces larger B cells than normal cells (Iritani and Eisenman, 1999, Sabo et al., 2014). The same can be observed with the P493-6 cell line, which possesses conditional Myc expression and increases its size upon Myc induction (Schuhmacher et al., 1999). Myc has also been shown to increase cell size of chicken embryo limb cells when analysed through flow cytometry (Piedra et al., 2002) and a high expression of Myc in liver cells in vivo also resulted in significant cell size increment (Kim et al., 2010). This overall shows the importance of Myc as a positive regulator of growth in cells. Our results are in line with what has been observed before, with U2OS cells induced to overexpress Myc increasing their size significantly.

Nonetheless, cells that were induced with 4-OHT but serum starved were able to maintain the same size as the uninduced and non-starved U2OS cells, a similar behaviour as that observed in 493-6 cells overexpressing Myc yet not incubated with foetal calf serum (Schuhmacher et al., 1999).

As cell size is tightly related to cell cycle, we analysed the cell cycle distribution of U2OS cells upon Myc induction by 4-OHT. Our results showed that the proportion of cells in G1 reduced whilst that of S phase and G2 increased. This is similar to what was observed by Eilers et al, where rat fibroblast expressing the MycER construct

increased their S phase population upon 24 hours of induction (Eilers et al., 1989). In P493-6 cell lines it has been shown that reduction of Myc expression can lead cells into a G0/G1 cell cycle arrest and upon its re-expression cells start cycling again (Pajic et al., 2000). It is known that Myc can induce DNA replication through the activation and induction of Cyclin E/CDK2 and therefore transit from G1 to S phase (Baluchamy et al., 2003, Santoni-Rugiu et al., 2000) as well as trigger rapid hyperphosphorylation of the Rb protein which further allows activation of both cyclinD1 and cyclin E-associated kinase activities (Steiner et al., 1995, Riley et al., 1994).

As expected, Myc induction produced larger cells independently of the cell cycle distribution; this mass accumulation could be driven by the transcription factor's capacity to enhance total cellular RNA content (Sabo et al., 2014) of which 80% is rRNA. Ribosome biogenesis represents the most expensive, complex, finely tuned, multi-step process that the cell must carry-out; therefore, it happens to be one of the most intricately regulated and controlled (Pelletier et al., 2018).

Arabi et al noticed that, by inhibiting the proteasome, Myc accumulated within the nucleoli, which indicated that Myc has nucleolar functions (Arabi et al., 2003). Myc and Max interact in nucleoli associating with ribosomal DNA after recruitment of the Myc cofactor TRRAP, which subsequently recruits RNA Polymerase I (Pol I), starting rDNA transcription (Arabi et al., 2005). In both D. *melanogaster* and mammalian cells, Myc positively regulates the synthesis of rRNA by Pol I and may do so by direct or indirect mechanisms (Grandori et al., 2005, Arabi et al., 2005, Wall et al., 2008, Poortinga et al., 2004). Based on this, U2OS cells were stained with Pyronin Y to measure the levels of rRNA by flow cytometry. As expected, Myc induced cells had twice as much rRNA than the control cells, which agrees with the notion that net RNA synthesis is markedly decreased in Myc null cells (Mateyak et al., 1997). As Myc is an important regulator of cell growth as well as of RNA synthesis, and ribosomal RNA constitutes the bulk of cellular RNA, it makes sense that this is a driver of the mass accumulation in the cell.

Along with the increased synthesis of rRNA in the U2OS cells, we observed that global protein synthesis was doubled in those cells induced with 4-OHT. This is consistent with what has been observed by several groups in different cell lines; COS7 cells

carrying the MycER chimera increased their translation rate by 50% upon addition of oestradiol (Eilers et al., 1989). An obvious increase in total protein synthesis was recorded in MycER NIH3T3 cells upon 4-OHT addition (De Benedetti and Graff, 2004) and mouse promyelocyte cells expressing MycER exhibited high levels of ^{35}S methionine incorporation (Wall et al., 2008). This boost of protein synthesis could be explained by the fact that Myc regulates several aspects of protein synthesis such as increasing ribosome biogenesis, tRNA levels and key factors involved in translation initiation elongation.

To detect changes in translation we opted to use the SUnSET technique because it would allow us to have a single cell resolution by analysing with flow cytometry however, a big caveat of this technique is the price. Using SUnSET for flow cytometry requires a lot of optimizations for the antibody's right concentration, nowadays most people use SUnSET in combination with western blot which makes it cheaper but sacrifices the single cell resolution. Alternative techniques can be used to analyse the translation of the cells, such as ^{35}S metabolic labelling, although very reliable it comes with the caveats of sacrificing the single cell resolution and the requirement of a specific radiation handling facility (Schmidt et al., 2009). This could be avoided by using non-radioactive alternatives now on the market. Another approach is to use polysome profiling which would give us a snapshot of the translation status of the cells, those under Rapamycin treatments would probably show a higher abundance of monosomes rather than polysomes (McGlincy and Ingolia, 2017). This can also be scaled up to ribosome profiling which would allow us to calculate translation efficiency by comparing the abundance of mRNA to the abundance of ribosomes that translate this mRNA allowing us to learn which transcripts translate better than others (Spealman et al., 2016).

mRNA translation can be separated into three distinct stages: initiation, elongation and termination. The translational initiation phase begins with recruitment of a 43S ribosomal complex to the 5'-methylguanosine-cap of the mRNA, then it scans along the mRNA until it encounters the first start codon and ends with joining of 60S large ribosomal subunit. The cap-dependent ribosomal binding step is thought to be rate-

limiting. This step is stimulated by eukaryotic initiation factor (eIF) 4F, a complex consisting of three subunits: eIF4E, the least abundant of all initiation factors (Duncan et al., 1987) which binds directly to the mRNA cap structure; eIF4A an RNA helicase that prepares the mRNA template for ribosome loading; and eIF4G, a large molecular scaffold that bridges the 43 ribosome preinitiation complex to the mRNA.

All three members of eIF4F as well as other initiation factors, including eIF2 and eIF3 subunits are under Myc regulation.

eIF4AI, eIF3E and eIF4G1 are *bona fide* Myc targets, suggesting that the way Myc stimulates translation may be through its ability to up-regulate the rate-limiting step of translation initiation (Lin et al., 2008) (Schlosser et al., 2003, Cole and Cowling, 2009). A coordinated increase in all three subunits of eIF4F has been observed when Myc activity is stimulated (Lin et al., 2009). Hence, Myc potentiates the whole protein biosynthetic apparatus underlying its potent ability to drive cell growth (Kress et al., 2015).

Furthermore, by analysing the Gene Ontology enrichment from the DEG's of cells overexpressing Myc, we can observe a trend towards the biosynthesis of constituent macromolecules, and assembly, or disassembly of cellular components, which is clearly associated to the different processes involved in the regulation of cell growth.
As cells grow, Myc induces processes that enable synthesis of new cellular components such as ribosomes, nucleotides, and lipids. These components are used to produce numerous cellular organelles including mitochondria**,** which are essential for high levels of ATP production in support of a growing cell. In addition to respiration, mitochondria mediate many biosynthetic pathways (Wallace, 2012). Myc has been shown to induce mitochondrial biogenesis apparently through the direct activation of genes involved in mitochondrial biogenesis(Graves et al., 2012, Liu et al., 2008, Morrish and Hockenbery, 2014), specifically PGC-1B (Morrish and Hockenbery, 2014) as well as by increasing the iron transporter, the transferrin receptor (TRFC), which is essential for mitochondrial biogenesis(O'Donnell et al., 2006).

We can observe that lipid biosynthesis is amongst the GO terms enriched in the Myc overexpressing cells. This could be another process by which size is controlled, as a

growing cell needs to synthesize the different lipids that constitute the cell membrane and that of different organelles. Myc has been observed to induce fatty acid synthesis partially by using glucose carbons and turning them into phosphoglycerate that is then used as the backbone for lipid synthesis (Morrish et al., 2010, Cantor and Sabatini, 2012). Myc also regulates acetyl-CoA carboxylase (ACACA), fatty acid synthetase (FASN) and stearoyl-CoA (SCD), all key enzymes in lipid metabolism (Zeller et al., 2003).

Overall, cells overexpressing Myc are larger and have greater amounts of rRNA and protein than normal U2OS cells. Interestingly, we must consider the possibility that if done in a different order would this be the same case. Would Myc activation rescue cells previously incubated with Rapamycin? Based on the results observed in this work, we can see that Rapamycin tends to downregulate genes involve in ribosomal biogenesis and consequently a reduction of cell size, if Rapamycin is washed away and Myc is activated (via 4-OHT), we could perhaps observe that cells could return to a size similar to the control cells, as Myc could increase the ribosome biogenesis previously hampered by Rapamycin. If, however, Rapamycin continues to be exposed, it is possible that the toxic effects of the drug would eventually end up triggering cell death. More experiments would be required to further understand the effects of this possible phenomenon.

The Myc pathway seems to function along the PI3K/mTOR pathway by regulating many of the important aspects of cell growth and metabolism (Ersching et al., 2017). It is important to study the crosstalk between these pathways, as many maladies are driven by mutations, translocations or other problematic changes that alter the fine balance that exists between the two, one example being Burkitt lymphoma cells; these are Myc-driven lymphomas that can show a high dependence on the PI3K activity at the point that apoptosis is induced by LY294002 incubation (Spender and Inman, 2014). At the same time, Myc is known to downregulate the mTOR-negative regulator TSC2 (Ravitz et al., 2007). Interestingly, mTOR inhibition diminished tumorigenesis in the Eμ-myc transgenic mouse lymphoma model (Wall et al., 2013).

Rapamycin exposed U2OS cells showed a behaviour like that previously discussed in HeLa cells. The HeLa dataset was produced by incubating cells with 1 μM Rapamycin

like the U2OS cells, but only for 10 hours, unlike our experiment for 24 hours. Nevertheless, when comparing both datasets DE downregulated genes, we can observe that they share genes involved in ribosomal biogenesis, proving the importance of mTOR in the regulation of cell growth through ribosomal biogenesis. Amongst the DE upregulated genes, we can observe an increase in genes associated with autophagy, an effect caused by Rapamycin (Liao et al., 2019).

Remarkably, U2OS cells that had previously activated Myc and then exposed to Rapamycin, did not have the major increment of cell size seen with 4-OHT induced cells, nor were they affected the same way as Rapamycin exposure only. Rather, these cells were able to maintain a size similar to untreated U2OS cells. Nevertheless, their rRNA and protein content was higher than control cells', yet less than that of Myc overexpressing cells.

The Gene Ontology enrichment from these cells pointed towards cellular metabolic processes and component biogenesis. As mentioned before, Myc controls different metabolic processes which can be subsequently affected by Rapamycin treatment.

Enhanced metabolic capacity of a growing cell is essential for biomass accumulation and the ability of Myc to induce glycolysis and glutaminolysis supports the cell's need for ATP and building blocks (Osthus et al., 2000, Hu et al., 2011, Dang, 2013). In addition to its ability to stimulate glucose uptake and glycolysis, Myc also stimulates glutamine consumption and metabolism by intervening at transcriptional and posttranscriptional levels (Gao et al., 2009). It does so by inducing the expression of glutamine transporters SLC1A5 and SLC7A5 (DeBerardinis and Cheng, 2010, Le et al., 2012), increasing glutaminolysis by four-fold, and thus repurposing glutamine to convert it to proline (Liu et al., 2012). Amongst the downregulated genes found in the Myc induced U2OS cells exposed to Rapamycin, we can find the sodium-dependent glucose co-transporter SLC5A2, the amino acid transporters SLC3A1 and SLC1A5, and SHMT2, an enzyme that converts serine to glycine required for both nucleotide and amino acid biosynthesis. It is important to point out that glucose deprivation could cause an imbalanced synthesis of rRNA and ribosomal proteins, resulting in the activation of p53 and growth arrest (Drygin et al., 2010, Lippman and Broach, 2009)

Not only do glucose and glutamine contribute to the synthesis of glycoproteins and complex carbohydrates of a growing cell, but they are also involved in the production of lipids for membrane production (Cantor and Sabatini, 2012).

This could in part explain why Myc overexpressing cells exposed to Rapamycin did not have the same phenotype as those solely expressing Myc. Rapamycin could have affected multiple metabolic effectors and translational regulators that ultimately lead to a slight reduction of the cell size.

Perhaps the ER stress caused by the accumulation of unfolded proteins via Myc overexpression could also be triggering a quality control pathway that involves the Signal recognition particle (SRP), which correlates with the GO enrichment term related to proteins targeting the ER. If mutant proteins do not fold properly or fail to be delivered to the appropriate cellular compartment, they can be degraded by the proteasome. However, this mechanism doesn't prevent continued production of the mutant gene product. Karamyshev et al. propose that when mutant signal sequences fail to bind to the signal recognition particle (SRP) at the ribosome exit site, the nascent chain instead contacts Argonaute 2 (Ago2), and the mutant mRNAs are specifically degraded.

Perhaps this mechanism could protect the cell for stress induced by protein accumulation driven by Myc overexpression. As mentioned before this could be a mechanism that would aid transforming cells in their survival. However, more experimental evidence is required to confirm this.

Interestingly, when analysing the GO terms from upregulated genes from Myc activated and Rapamycin exposed cells compared to control cells, we can see that the terms related mostly to ribosomal biogenesis and other rRNA processing terms. Which helps us to think that perhaps there's an alternative mechanism driving ribosomal biogenesis if mTOR is being downregulated by Rapamycin. Perhaps this maintenance of ribosomal biogenesis could be aiding the cells exposed to rapamycin to keep a cell size similar to those untreated control cells.

Overall, we have observed that U2OS cells' growth control can be manipulated depending on which node of the pathways is altered; Rapamycin incubation produced smaller cells by hampering mTOR's function, downgrading translation, ribosomal synthesis, and different anabolic processes which ended up affecting mass accumulation. On the other hand, Myc overexpression contributed to an enlarged phenotype, by increasing the metabolic activity of the cell, increasing synthesis of macromolecules necessary for the assembly of different organelles, increasing rRNA synthesis to build up more ribosomes and directly and indirectly affecting translation rates. The interplay between both pathways interestingly showed that, even though Rapamycin hampered metabolic effectors, the continuous expression of Myc kept the cell size like controls.

Both Myc and mTOR pathways seem to interconnect and cooperate to supply downstream effectors to alleviate disruptions in the cell's homeostasis. It is important to further dissect how both pathways might interact with each other in order to comprehend how cell growth is regulated.

Chapter 5: Inhibiting ribosomal synthesis impacts the Rapamycin resistance effect of Myc activation.

5.1 Introduction

5.1.1 Ribosomal biosynthesis drives cell size

As it was observed in the last chapter, U2OS cells that were only exposed to Rapamycin shrank. However, those that were previously allowed to accumulate Myc by 4-OHT induction and then were exposed to Rapamycin, were able to maintain a size similar to non-treated cells. Given the fact that Myc's capacity to regulate growth is heavily based on its ability to stimulate ribosomal biosynthesis, it was decided to explore this possibility. Analysing sequencing results from these cells, we noted that ribosomal proteins were slightly more upregulated in Myc induced U2OS cells exposed to Rapamycin than those only induced with 4-OHT, which fuels this supposition.

Induction of ribosome biogenesis is thought to be an evolutionarily conserved function of Myc (Brown et al., 2008). In mammalian cells, the 5.8S, 18S, and 28S rRNAs are encoded by genes activated by Myc. These genes are arranged in repeats that cluster in the nucleolus, which are enriched for E-box motifs to which Myc eventually binds,

aiding in their transcription. (Arabi et al., 2005, Grandori et al., 2005, Lin et al., 2012, Schlosser et al., 2003).

UBF (upstream binding factor) binds to rDNA on multiple sites allowing the preinitiation complex assembly and remodelling of rDNA chromatin. Selectivity factor 1 (SL1/TIF-1B) interacts with UBF, binding to rDNA promoter sequences. Rrn3 (also known as TIF-1A) interacts with the UBF/SL1 complex and recruits Pol I, initiation transcription (Russell and Zomerdijk, 2005).

Myc can regulate Pol I activity by increasing UBF's abundance, allowing rRNA transcription (Poortinga et al., 2004, Poortinga et al., 2011).

In *Drosophila*, dMyc increases the expression of Pol I subunits and cofactors, which increase rDNA transcription and ribosome biogenesis. On the other hand, decreased dMyc expression in larvae downregulated rDNA transcription and decreased nucleolar size, which evidences decreased ribosome production (Grewal et al., 2005).

The transactivation domain of Myc is required for increased rDNA transcription and the carboxy-terminal regions including the basic region at residues 355-368 are important for nucleolar localization (Campbell and White, 2014).

In order to drive expression of its target genes, RNA Pol III recruits the RNA Pol-III-specific transcription factors TFIIIC and TFIIIB. TFIIIC does not have high affinity to the 5S rRNA promoter. For this reason, TFIIIA must be bound first to recruit TFIIIC. Once TFIIIC is bound, TFIIIB recognises its binding site upstream of the transcription start site. TFIIIB recruits RNA Pol III and transcription can start (Schramm and Hernandez, 2002).

The level of RNA Pol III products such as B2 RNA and tRNAs are decreased in fibroblasts deficient for Myc, but rapidly up-regulated on MycER induction (Gomez-Roman et al., 2003), a similar behaviour observed in B cells, cardiomyocytes and hepatocytes (Lin et al., 2012, Goodfellow et al., 2006, Shukla and Kumar, 2012).

Induction of tRNA synthesis was also seen in vivo when MycER was activated in transgenic mice (Goodfellow and White, 2007). Conversely, depletion of Myc by RNAi led to decreased expression of RNA Pol III products (Felton-Edkins et al., 2003, Owen et al., 2010). dMyc overexpression stimulated RNA Pol III transcription, whereas knockdown had the opposite effect (Steiger et al., 2008).

Myc has been detected at tRNA, 5S rRNA and other RNA Pol III-transcribed genes in numerous cell types (Felton-Edkins et al., 2003, Gomez-Roman et al., 2006, Lin et al., 2012).

Increased protein synthesis and activity of RNA Pol I and RNA Pol III are found in cardiomyocyte hypertrophy, a phenomenon associated with cardiac pathologies. It has been observed that these cells require increased RNA Pol I transcription to grow and Myc expression was sufficient for growth whilst chemical inhibition of Myc/Max prevented it (Goodfellow et al., 2006). The level of the TFIIIB subunit Brf1 is rate-limiting for RNA Pol III transcription in these cells and hypertrophy also induced Brf1 expression (Ernens et al., 2006).

5.1.2 Cell size and p38 MAPK signalling

The mammalian p38 MAPK pathway participates in numerous biological processes, including the regulation of cell cycle checkpoints. In response to DNA damage or oxidative stress, p38 is activated and induces a cell cycle arrest (Thornton and Rincon, 2009, Ambrosino and Nebreda, 2001).

The first member of the p38 MAPK family was independently identified as a 38 kDa protein (p38) (Han et al., 1994). Additional p38 MAPK family members, which are approximately 60% identical in their amino acid sequences, were named P38β (MAPK11), p38γ (ERK6 or MAPK12 and p38δ (MAPK13) (Jiang et al., 1996, Lechner et al., 1996, Mertens et al., 1996, Goedert et al., 1997, Jiang et al., 1997, Enslen et al., 1998). P38α is ubiquitously expressed at significant levels in most cell types.

The activation of MAPK requires phosphorylation on a flexible loop termed the phosphorylation lip or activation loop. These phosphorylations induce conformational reorganizations that relieve steric blocking and stabilize the activation loop in an open and extended conformation, facilitating substrate binding.

P38 MAPKs are activated by dual phosphorylation in the activation loop sequence Thr-Gly-Tyr. In response to appropriate stimuli, threonine and tyrosine residues can be phosphorylated by three dual specificity MKKs/MAP2K (MAPK kinases). MKK6 can phosphorylate the four p38 MAPK family members, whereas MKK3 activates P38α, p38γ and p38δ but not P38β. Both MKK3 and MKK6 are highly specific for p38 MAPKs (Jiang et al., 1997, Alonso et al., 2000). In addition, P38α can also be phosphorylated by MKK4, an activator of the JNK pathway (Doza et al., 1995, Matsuzawa et al., 2008). Upregulation of the p38 MAPK pathway can lead to increased cell size (Clerk et al., 1998, Kudoh et al., 1998, Molnar et al., 1997, Lopez-Aviles et al., 2005, Cully et al., 2010).

It has been shown that p38 is activated by hyperosmotic conditions that shrink cell volume (Han et al., 1994, Moriguchi et al., 1996, New and Han, 1998). Defects in cell size and growth were previously implicated with perturbations of p38 in mammalian tissues such as liver, bone and heart (Tormos et al., 2013, Thouverey and Caverzasio, 2015, Gonzalez-Teran et al., 2016). Mice lacking p38γ and/or p38δ have higher levels of the mTOR inhibitor DEPTOR, resulting in lower mTOR activity (Nishida et al., 2004). Liu et al observed a decrease in size following p38 inhibition. However, this reduction in size was not attributed to mTOR inhibition, as this would slow down cellular growth rates. Instead, it is proposed that p38 inhibition reduces cell size by shortening the duration of growth G1 (Liu et al., 2018).

5.2 Results

In order to determine if ribosomal synthesis was the reason that Myc overexpressing cells managed to maintain a size similar to controls, U2OS cells were allowed Myc accumulation by inducing cells with 4-OHT for 24 hours and then were incubated with

both Rapamycin and Actinomycin D, a known RNA Pol I inhibitor at very low concentrations.

Incubation with 100 ng of Actinomycin D only reduced the size of control cells. However, in Myc overexpressing cells, it had a slight effect that was not deemed significant (Figure 5.1).

Remarkably, the combination of Rapamycin and Actinomycin D reduced the size of cells with acivated Myc. (Figure 5.1).

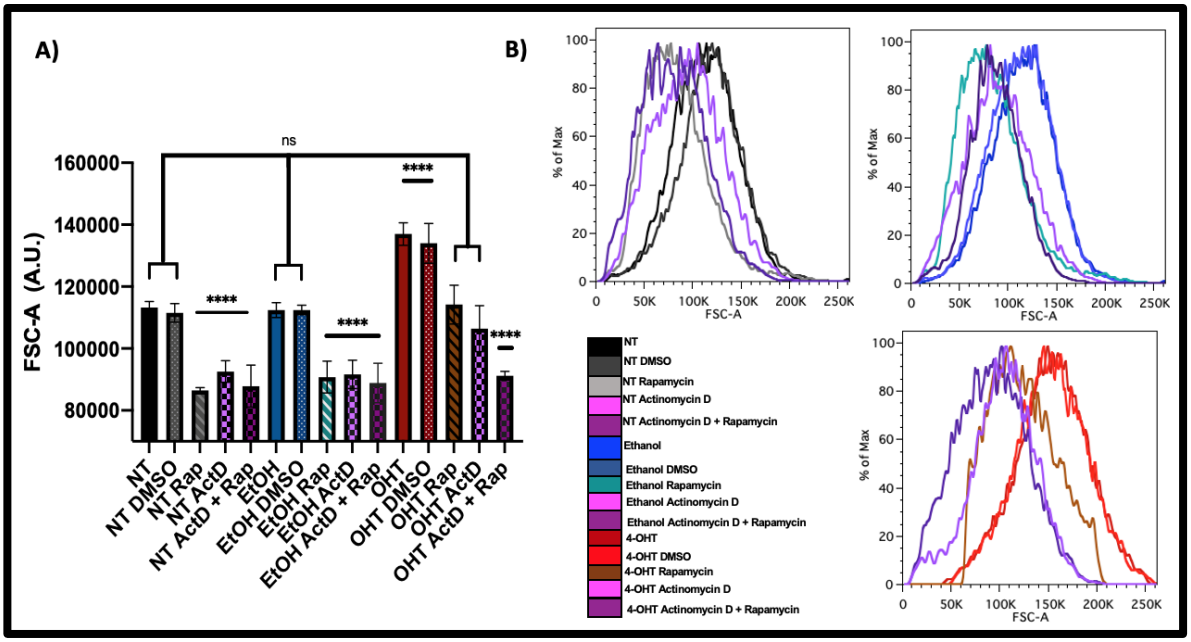

Figure 5.1 Myc Overexpression inhibitor resistance is abolished by combination of Rapamycin with a RNA Pol I inhibitor. MycER U2OS cells exposed to Actinomycin D have a reduce size when analysed by flow cytometry. A) Bar plots from U2OS cells exposed to Rapamycin, 4-OHT or both. Myc overexpressing cells exposed to both Rapamycin and Actinomycin D had a reduced size. B) Representative histogram from flow cytometry data of treatments. Arbitrary Units (A.U.). Data shown are mean values ± standard deviations (N = 3 independent biological replicates). Statistical significance was assessed by ANOVA with Tukey's test, Asterisks represent the p-value: * $p < 0.05$, ** $p < 0.01$, *** $p < 0.001$, ****$p < 0.0001$.

Since Actinomycin D in combination with Rapamycin was able to produce a cell size reduction in cells overexpressing Myc, it was then proceeded to analyse the rRNA content of the cells by staining with Pyronin Y.

As expected, all the cells treated with the RNA Pol I inhibitor had a reduced signal from Pyronin Y staining (Figure 5.2), pointing to the possibility that rRNA biosynthesis could contribute to the cell size control in Myc overexpressing cells.

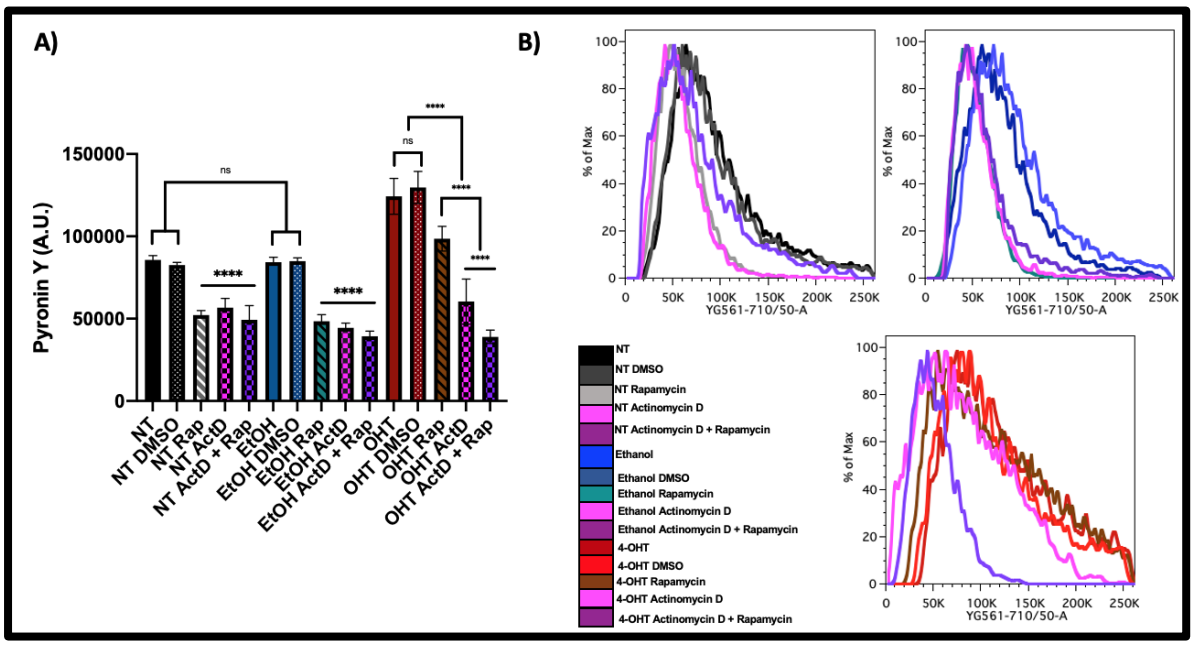

Figure 5.2 Ribosomal RNA signal was reduced by a RNA Pol I inhibitor. MycER U2OS cells exposed to Actinomycin D and 4-OHT show different levels of Pyronin Y signal determined by flow cytometry. A) Bar plots from U2OS cells exposed to Rapamycin, 4-OHT, Actinomycin D or a combination. Actinomycin D reduced Pyronin Y signal whilst Myc overexpression increased it. A combination of Rapamycin and Actinomycin D strongly reduced the Pyronin Y signal from U2OS cells overexpressing Myc. B) Representative histogram from flow cytometry data of treatments. Arbitrary Units (A.U.). Data shown are mean values ± standard deviations (N = 3 independent biological replicates). Statistical significance was assessed by ANOVA with Tukey's test, Asterisks represent the p-value: * $p < 0.05$, ** $p < 0.01$, *** $p < 0.001$, ****$p < 0.0001$.

Given the fact that Myc overexpressing cells were able to maintain a size similar to controls when the mTOR pathway was downregulated, it was hypothesized that ribosomal synthesis was the driving force that allowed cells to hamper the effects of Rapamycin exposure.

After observing that a combination of Rapamycin and Actinomycin D was able to break the growth control, it was interesting to think of a possible alternative route that could keep the ribosomal synthesis active.

Given the fact that p38 MAPK has been observed to be associated with size control, we explored the possibility of p38 aiding the ribosomal synthesis or the growth control in U2OS cells.

We incubated Myc overexpressing U2OS cells with both Rapamycin and the p38 MAPK inhibitor SB203580 to analyse if this combination was able to reduce their size. Exposure to SB203580 produced a size reduction in control cells and in 4-OHT induced cells. A combination of both Rapamycin and SB203580 reduced the size of cells overexpressing Myc (Figure 5.3).

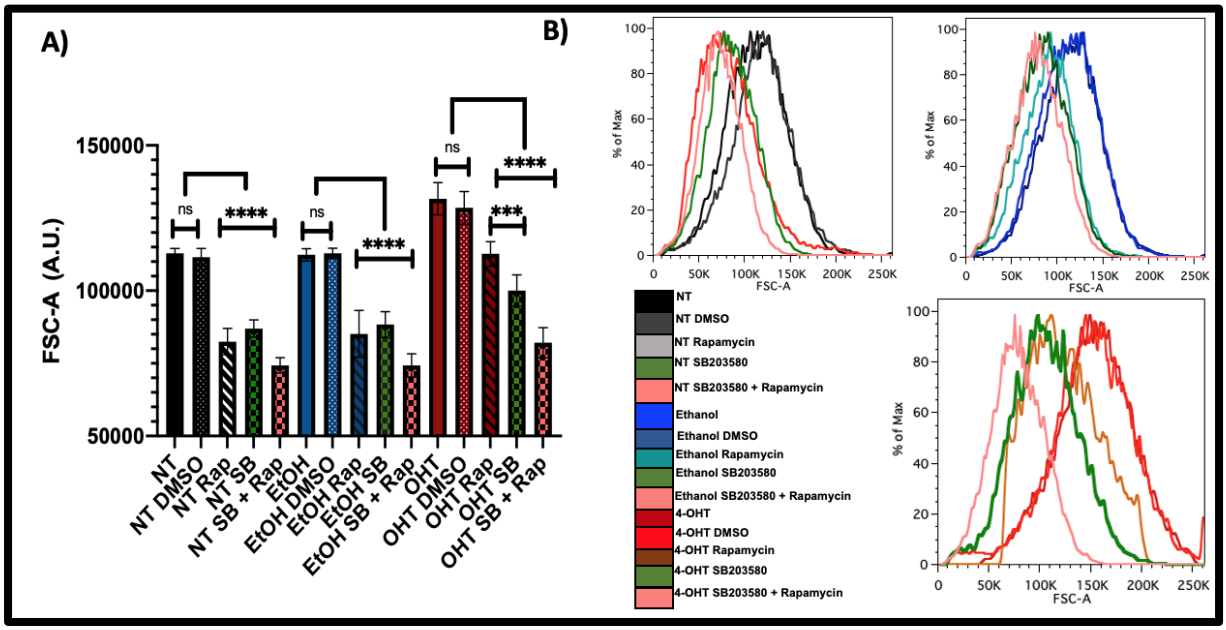

Figure 5.3 Incubation with a p38 MAPK inhibitor reduces cell size. MycER U2OS cells exposed to SB203580 have a reduce size when analysed by flow cytometry. A) Bar plots from

U2OS cells exposed to Rapamycin, 4-OHT, SB203580 or a combination. Myc overexpressing cells exposed to both Rapamycin and the p38 inhibitor had a reduced size. B) Representative histogram from flow cytometry data of treatments. Arbitrary Units (A.U.). Data shown are mean values ± standard deviations (N = 3 independent biological replicates). Statistical significance was assessed by ANOVA with Tukey's test, Asterisks represent the p-value: * p < 0.05, ** p < 0.01, *** p < 0.001, ****p < 0.0001.

After observing that the p38 inhibitor was able to reduce cell size, it was interesting to observe if this effect was related to rRNA reduction as well. For this reason, cells were again treated with the chemical inhibitors, stained with Pyronin Y and analysed by flow cytometry (Figure 5.4).

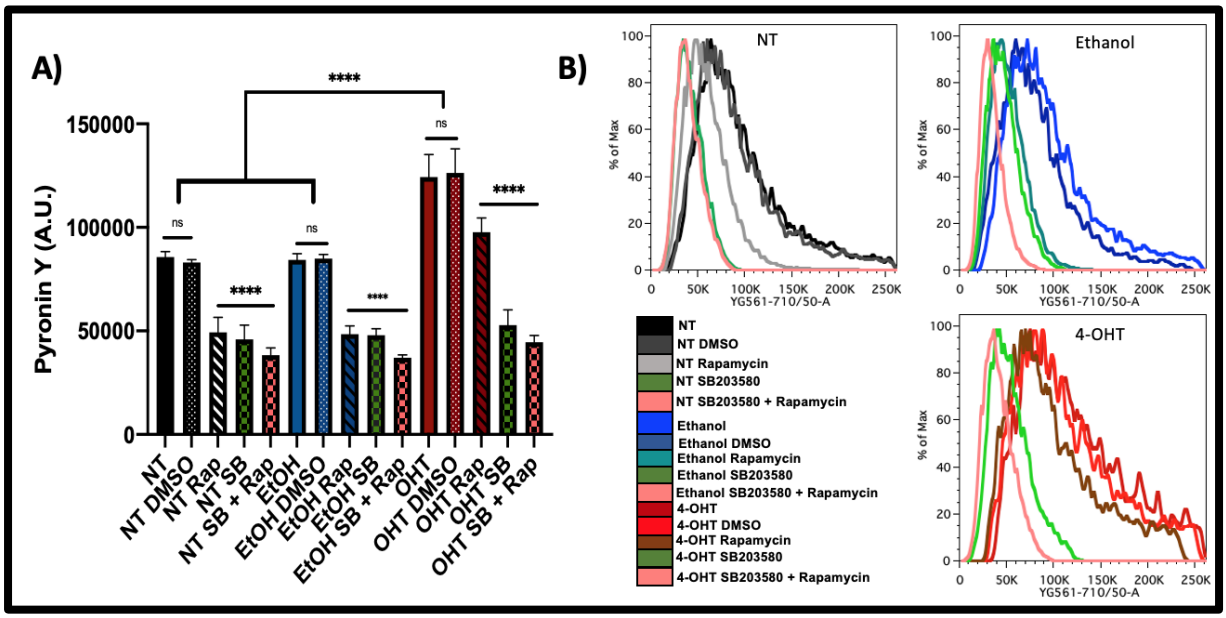

Figure 5.4 Incubation with a p38 MAPK inhibitor reduced ribosomal RNA signal. MycER U2OS cells exposed to SB203580 and 4-OHT show different levels of Pyronin Y signal determined by flow cytometry. A) Bar plots from U2OS cells exposed to Rapamycin, 4-OHT, SB203580 or a combination. The p38 MAPK inhibitor reduced Pyronin Y signal whilst Myc overexpression increased it. A combination of Rapamycin and SB203580 strongly reduced the Pyronin Y signal from U2OS cells overexpressing Myc. B) Representative histogram from flow cytometry data of treatments. Arbitrary Units (A.U.). Data shown are mean values ± standard deviations (N = 3 independent biological replicates). Statistical significance was assessed by ANOVA with Tukey's test, Asterisks represent the p-value: * p < 0.05, ** p < 0.01, *** p < 0.001, ****p < 0.0001.

Surprisingly, cells incubated with SB203580 had a lower signal from Pyronin Y. This could serve as evidence of the p38 MAPK pathway's involvement in an alternative Ribosomal biogenesis route to be analysed.

5.3 Discussion

Over the last chapters we have observed that ablation of the PI3K/AKT/mTOR pathway directly impacts the cells' growth in a negative manner, producing smaller cells in return. On the other hand, we can observe that those cells that overexpress Myc are larger in diameter and volume and possess higher amounts of rRNA and proteins.

Since Myc is a positive regulator of growth, like the mTOR pathway, it was interesting to observe that upon Rapamycin incubation, cells overexpressing Myc did not maintain the enlarged phenotype but nonetheless were not completely shrunk as those not overexpressing Myc but exposed to the mTOR inhibitor.

Given the fact that both mTOR and Myc cooperate in controlling growth through ribosomal synthesis(Ersching et al., 2017), we hypothesise that ribosomal biogenesis is the driving force for biomass accumulation. Cells not expressing Myc have a markedly decreased rRNA synthesis (Mateyak et al., 1997). This can be observed in terminal granulocyte differentiation, where cells are observed to exhibit a significant loss in cellular mass (Poortinga et al., 2004, Wall et al., 2008) which is guided by reduction of RNA Pol I on rDNA and subsequent diminished levels of rRNA synthesis, all guided by downregulation of Myc (Poortinga et al., 2011).

This highlights the important relationship between Myc and rRNA synthesis, and how this is highly associated with cell size control. At the same time this could explain why inhibition of RNA Pol I by Actinomycin D reduced the size of U2OS cells and specially of those incubated with both Rapamycin and Actinomycin D.

It is important to note that Actimonycin D was used in a concentration that is known to only affect RNA polymerase I however, given the fact that the incubation period was that of 24 hours, stress events and even cell death must be consider when analysing these results. It would be necessary to use an Annexin V conjugate to detect death cells and analyse if the results are affected by this. Perhaps this issue could be overcome by incubating cells for a shorter time, to reduce cell death.

Another issue arises if we consider that the prolonged exposure to Actinomycin D might affect total mRNA synthesis and not only rRNA. Considering that the exposure is of 24 hours, there will be a point in which ribosomal content will be depleted and this could affect the translation of other mRNAs. Another problem would be that Actinomycin D could affect RNA pol II as well, even at lower concentrations, if this was the case, we could possibly detect this by incubating cells with the modified nucleotide ethynyl uridine (EU), which can be used to detect recently synthesised RNA by flow cytometry. If Pol II is affected by Actinomycin D's lower concentration we should see that the EU signal from treated cells is far lower than non-treated controls. Another simpler option could be the use of RT-PCR to detect whether Actinomycin D treatment is downregulating specific mRNAs or just rRNA.

Myc over expressing cells exposed to Rapamycin were able to maintain a similar size to control cells. Upon disruption of rRNA synthesis we observed that these cells reduced their size more than when only incubated with Rapamycin. For this reason, it was in our interest to find an mTOR-independent route that could control cell size through ribosome biogenesis.

Since irregularities with the p38 MAPK have previously been linked to growth defects in multiple mammalian tissues (Tormos et al., 2013, Thouverey and Caverzasio, 2015, Gonzalez-Teran et al., 2016), and its upregulation has been observed to lead to increased cell size (Clerk et al., 1998, Kudoh et al., 1998, Molnar et al., 1997, Lopez-Aviles et al., 2005, Cully et al., 2010), we decided to explore the possibility that chemical inhibition of p38 along with that of mTOR would affect ribosome biogenesis and cell size.

Incubation with SB203580 produced a reduction of size in U2OS cells, and interestingly, incubation with the p38 inhibitor and Rapamycin was able to reduce the growth from U2OS cells overexpressing Myc.

There is evidence from other systems of p38 mediated translational regulation acting via direct phosphorylation of MAPK-interacting Kinases (MNKs), which then leads to phosphorylation of eIF4E and initiation of 5'-7-methylguanosine cap-dependent translation (Yamagiwa et al., 2003).

Notably, p38 has been shown to be activated when cells shrink (Han et al., 1994, Moriguchi et al., 1996, New and Han, 1998). Liu et al found as well that small cells display higher levels of p38 activity, and that these cells also remained in G1 for longer periods of time. Inhibition of p38 led to loss of the compensatory G1 length extension in small cells, resulting in faster proliferation, smaller cell size and increased heterogeneity in size. This suggests a model where the p38 MAPK pathway functions downstream of a cell size sensing process and feeds information about cell size to regulators of the cell cycle (Liu et al., 2018).

It would be interesting to test in future experiments if the model by Liu et al., proposing that p38 delays G1 for compensatory mechanisms after cells shrank, could be related to ribosomal synthesis, as co-incubation of both Rapamycin and SB203580 produced smaller cells, and reduced rRNA synthesis.

SB203580 has also been observed to decrease the levels of cell glucose (Antonescu et al., 2005) which, as we have mentioned before, can also be associated with downregulation of ribosomal synthesis through the PI3K/AKT/mTOR pathway.

Remarkably, Bora et al in an investigation yet to be published (currently found in the bioRxiv under doi: /10.1101/2020.11.30.403931) found significant p38-MAPK mediated regulation of protein translation and rRNA processing. The p38 inhibition was associated with profound changes in the proteome and the transcriptome of translation related genes, including overall reduced levels of translation, transcription and rRNA processing.

Insights from other cell culture-based studies implicate MYBBP1A in transcriptional repression of rRNA gene expression and as a facilitator of pre-rRNA transcript processing, with depletion of MYBBP1A resulting in the accumulation of unprocessed rRNA precursors (Hochstatter et al., 2012). Bora et al suggest MYBBP1A (under regulation of p38) may act as a checkpoint agent enabling switching from a homeostatic balance in cellular protein synthesis and the coordination of a functionally important translational response to externally provided differentiation cues (via posttranscriptional regulation of rRNAs levels available for functional ribosome biogenesis). This hypothesis is strengthened by reports, in other models, describing MYBBP1A specific functions related to rRNA expression and processing during the cellular stress response (Kumazawa et al., 2015, Ono et al., 2014).

MYBBP1A is a predominantly nucleolar protein with reported roles in the negative regulation of RNA polymerase I dependent rRNA gene transcription, co-transcriptional rRNA processing and ribosome biogenesis (Hochstatter et al., 2012, Tan et al., 2012), p53 tetramerization, cell senescence and apoptosis (Kumazawa et al., 2015, Ono et al., 2014).

The accumulation of ribosomal protein transcripts observed in our RNAseq analysis of Myc overexpressing U2OS cells exposed to Rapamycin does not necessarily reflect the status of the ribosomal protein levels in the cell. Bora et al., observed that RP transcripts were upregulated, but at the same time these ribosomal proteins were down regulated at the translation level, suggesting that their accumulation was probably due to overall impaired levels of translation.

Disturbances in ribosome biogenesis, as a result of altered signalling or stress, arrest the pre-rRNA maturation process resulting in an increased pool of ribosomal proteins. This accumulation results in the inhibition of protein synthesis and cell cycle arrest through the activation of p53 (Bibikova et al., 2014, Danilova and Gazda, 2015).

This observed accumulation of RPs in U2OS cells was perhaps because of the stress caused by treatment with Rapamycin or even by the continuous expression of Myc, which could have caused stress in the balance of ribosomal protein synthesis.

RPL5 and RPL11 have been found to be extremely important in sensing ribosomal stress. RPL11 has been shown not only to induce p53 transactivation, but also to bind Myc within the Myc box II domain and inhibit its association with TRRAP, thereby reducing histone acetylation and Myc-dependent transcription. Thus, the Myc-RPL11 circuit functions in a negative-feedback mode ((Dai et al., 2007, van Riggelen and Felsher, 2010).

An interesting observation is that many tumours rely on Myc's enhanced protein and ribosome synthesis capacities; studies in Eμ-Myc mice have shown that when these mice are crossbred with mice containing haploinsufficiencies of the genes coding RPL24 or RPL38, the rate of lymphomagenesis was reduced, which indicates that a reduction in protein synthesis, due to reduced expression of necessary RPs, was enough to counteract Myc induced transformation (Barna et al., 2008).

We have observed that Myc's increased capacity to upregulate ribosomal synthesis was driving the cells' mechanism to regulate growth even under Rapamycin treatment. Once a RNA Pol I inhibitor was incubated along with the mTOR inhibitor, Myc was not able to maintain a size similar to control cells, given that rRNA synthesis was strongly reduced.

At the same time, an alternative mechanism for cell size control is suggested by proposing that p38 plays a role in mass accumulation, probably as suggested by delaying G1 in smaller cells and at the same time interacting with the rRNA synthesis machinery and translation.

To conclude we have produced diagrams that summarise the biological phenomenon observed in this study. The first diagram shows how the mTOR pathway regulates cell size through ribosome biogenesis (Figure 5.5) and how Rapamycin blocks this, producing smaller cells in the process. The second diagrams shows the balance between Myc and the mTOR pathway in promoting cell growth, and how Rapamycin in conjunction with Actinomycin D or SB203580 block Myc's capacity to maintain a "normal" size (Figure 5.6).

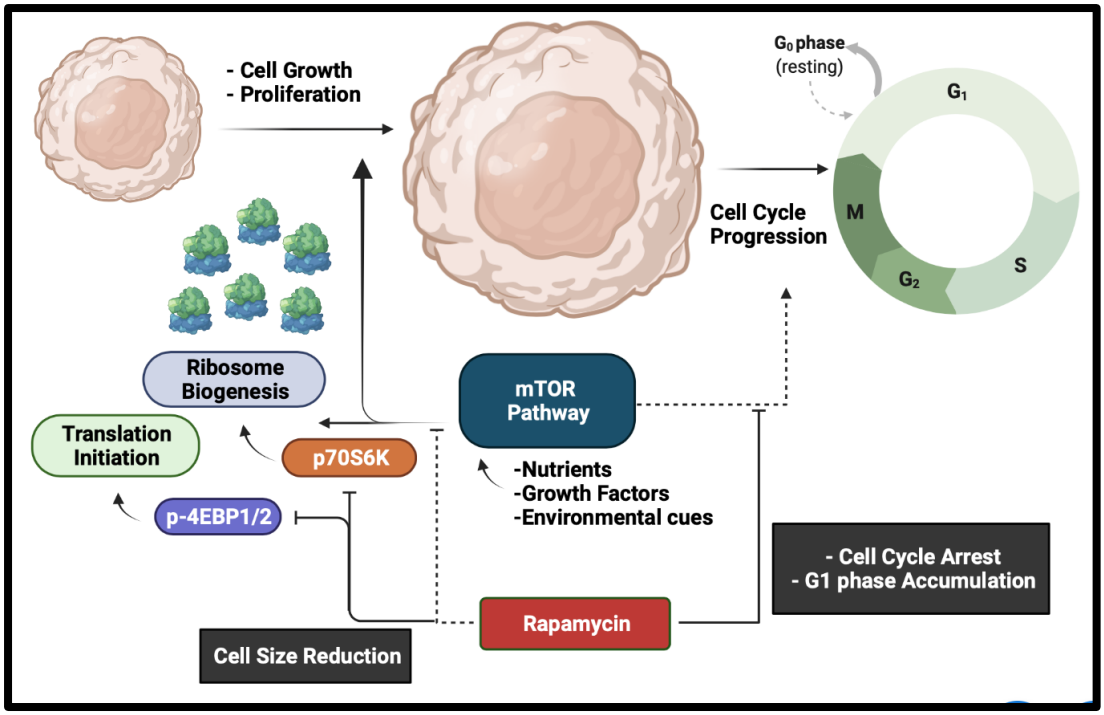

Figure 5.5 The mTOR pathway – Rapamycin relationship. The diagrams shows the way the mTOR pathway promotes cell growth and proliferation. At the same time, the capacity of Rapamycin to block these effects.

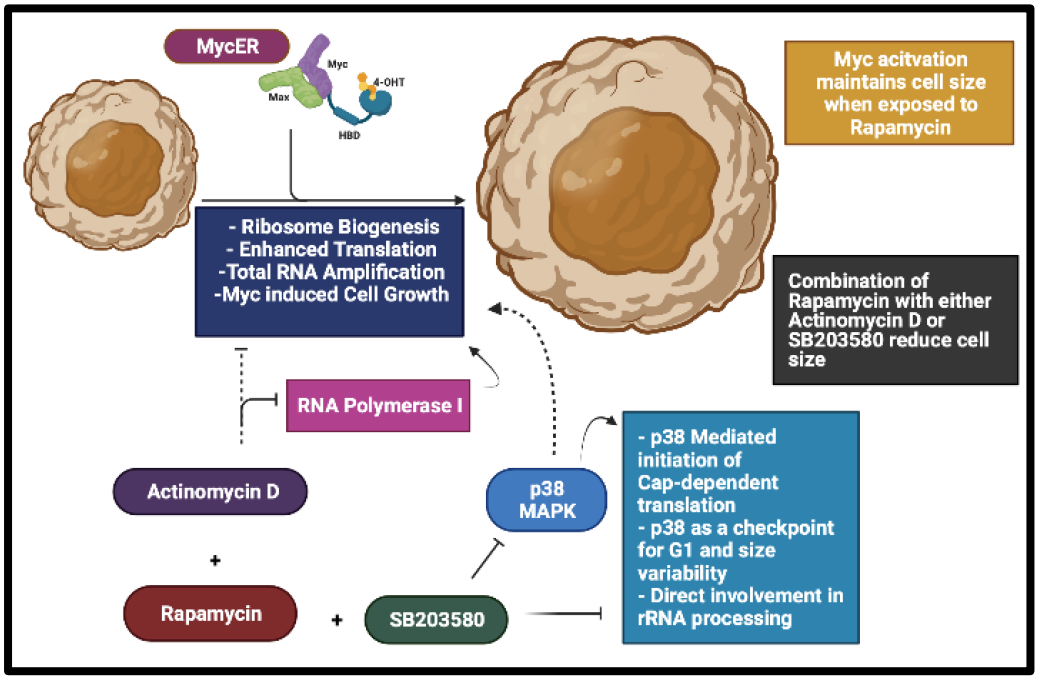

Figure 5.6 Myc induced-ribosome biogenesis drives cell size regulation. The diagram shows the interaction between different drugs that hamper ribosome biogenesis and the effects on cell size. It is proposed that p38 could be driving ribosome biogenesis alternatively of mTOR.

Chapter 6 Conclusions.

The control of cell size is a very important matter. Cells that are too small tend to be more sensitive towards apoptosis, have limited biosynthetic capacities and spend more energy maintaining ionic gradients, whereas too large cells have a reduced surface area for nutrient exchange, spend more energy on transcription of cytoskeletal genes to maintain the structural challenges of an enlarged size, and there is a cytoplasm dilution (Neurohr et al., 2019). Disease can arise from dysregulation of the pathways controlling cell size (Jiang and Liu, 2008, Ruggero, 2009).

Cell size is also known to be a source of extrinsic noise; as transcripts scale with size, understanding growth mechanisms is important to design more reliable gene circuits. It is for this reason that it is important to further dissect the interactions that occur between these pathways.

We have observed that suppression of an individual member of the PI3K/AKT/mTOR pathway is enough to produce a smaller mammalian cell phenotype and alter its proliferation. Furthermore, dissecting the gene expression of cells challenged with Rapamycin, it was observed that the main events affected were those related to protein accumulation through the translation machinery and ribosome biogenesis. An interesting fact is that increased protein synthesis and cell growth are critical for tumorigenesis (Montanaro et al., 2008, White, 2008).

Tumour cells are generally larger than normal cells and contain more and bigger nucleoli, a phenotype indicative of increased ribosome synthesis (Busch et al., 1963, Pahuja et al., 2003, Arora et al., 2003). The key mechanism observed to be dysregulated in many maladies is Myc, which has been traditionally associated with growth and proliferation.

We analysed the effects of overexpressing Myc on U2OS cells and observed that upon its induction, the cells showed an increased size when analysed by flow cytometry,

which was further corroborated by measurements of their volume and diameter. The cells' cell cycle distribution was also affected.

In tumour cells Myc-dependent increases in protein synthesis augment cell growth and this effect is coupled to increased cell cycle progression and cell survival. This mass accumulation is also achieved by its ability to promote ribosome biogenesis (Ruggero and Pandolfi, 2003, Barna et al., 2008, Poortinga et al., 2004, Grandori et al., 2005). When analysing the gene response to overexpressing Myc, we observe that cellular component biogenesis, arrangements in the cytoskeleton and different biosynthetic processes were altered. These are biological processes that play important roles in cell size regulation.

To analyse how these pathways interact with each other, cells were allowed to accumulate Myc and then were challenged with Rapamycin, which led to cells maintaining a "normal size", similar to the non-treated cells. This interesting behaviour was further analysed by measuring their ribosomal RNA and protein content with flow cytometry. Surprisingly, we could observe that the levels of both protein and rRNA were slightly higher than those of non-treated cells, yet lower than Myc overexpressing cells. This biomass "leftover" accumulation led us to think that the mechanism underlying the shrinkage resistance was driven by ribosomal synthesis.

It is interesting to notice that when gene expression of Myc overexpressing cells exposed to Rapamycin was analysed, there was evidence of altered metabolic processes, which could be associated with the response to Rapamycin treatment.
Myc over expressing cells incubated with both Rapamycin and Actinomycin D had a smaller size than those only exposed to Rapamycin. This demonstrates that rRNA synthesis was involved in the size control.

Considering that an alternative route could be driving this mechanism, we consulted the literature and found that p38 MAPK has been associated with cell size control and does not tend to be directly involved with Myc. For this reason, we tried a similar strategy by combining Rapamycin treatment with SB203580, an inhibitor of p38 MAPK. This reduced both the cell size and the rRNA content of the cells, further showing an interaction of p38 with ribosomal synthesis.

Interestingly, Liu et al suggest that p38 MAPK functions as a growth control mechanism by sensing cell size and delaying the G1/S transition (Liu et al., 2018). The G1 phase is the decisive moment where the cell accumulates most of its biomass in order to go through replication of DNA. It would be interesting to test in future experiments if p38 could interact with other molecules that could sense the ribosomal content (and with it, cell size) and regulate the G1/S transition.

We therefore consider that regulation of cell size comes with an interaction between different pathways that ultimately leads to maintaining the levels of ribosomal biogenesis. Understanding the mechanisms behind cell size control is very important as this process is involved in multiple issues, like disease, or transcriptional noise.

In the case of disease, multiple cancers are dependent on Myc over expression, which leads to larger nucleoli, increased ribosome biogenesis, increased protein synthesis (Montanaro et al., 2008, White, 2008, Busch et al., 1963) and consequentially larger tumour cells than their healthier counterparts. For this reason, different pharmacological strategies targeting the growth control mechanisms are being developed and a deeper knowledge of cell size regulation is necessary.

At the end, we consider that if cell size and its variability are to be understood and controlled, we must first dissect the molecular sensors regulating growth control, which we propose to interact with ribosomal synthesis.

Our original goal was to manipulate cell size to reduce transcriptional noise, however, given multiple circumstances including the 2019 SARS CoV2 pandemic, many of our planned experiments were forced to be suspended and the project had to adapt and take a different path.

References

ABBAS, A. K., LICHTMAN, A. H., PILLAI, S., BAKER, D. L. & BAKER, A. 2018. *Cellular and molecular immunology,* Philadelphia, PA, Elsevier.

ADDIE, M., BALLARD, P., BUTTAR, D., CRAFTER, C., CURRIE, G., DAVIES, B. R., DEBRECZENI, J., DRY, H., DUDLEY, P., GREENWOOD, R., JOHNSON, P. D., KETTLE, J. G., LANE, C., LAMONT, G., LEACH, A., LUKE, R. W., MORRIS, J., OGILVIE, D., PAGE, K., PASS, M., PEARSON, S. & RUSTON, L. 2013. Discovery of 4-amino-N-[(1S)-1-(4-chlorophenyl)-3-hydroxypropyl]-1-(7H-pyrrolo[2,3-d]pyrimidin -4-yl)piperidine-4-carboxamide (AZD5363), an orally bioavailable, potent inhibitor of Akt kinases. *J Med Chem,* 56**,** 2059-73.

ADHIKARY, S. & EILERS, M. 2005. Transcriptional regulation and transformation by Myc proteins. *Nat Rev Mol Cell Biol,* 6**,** 635-45.

ALBERTS, B. 1998. *Essential cell biology : an introduction to the molecular biology of the cell,* New York, Garland Pub.

ALONSO, G., AMBROSINO, C., JONES, M. & NEBREDA, A. R. 2000. Differential activation of p38 mitogen-activated protein kinase isoforms depending on signal strength. *J Biol Chem,* 275**,** 40641-8.

AMBROSINO, C. & NEBREDA, A. R. 2001. Cell cycle regulation by p38 MAP kinases. *Biol Cell,* 93**,** 47-51.

ANDREWS, L. M., JONES, M. R., DIGMAN, M. A. & GRATTON, E. 2013. Detecting Pyronin Y labeled RNA transcripts in live cell microenvironments by phasor-FLIM analysis. *Methods Appl Fluoresc,* 1**,** 015001.

ANTONESCU, C. N., HUANG, C., NIU, W., LIU, Z., EYERS, P. A., HEIDENREICH, K. A., BILAN, P. J. & KLIP, A. 2005. Reduction of insulin-stimulated glucose uptake in L6 myotubes by the protein kinase inhibitor SB203580 is independent of p38MAPK activity. *Endocrinology,* 146**,** 3773-81.

ARABI, A., RUSTUM, C., HALLBERG, E. & WRIGHT, A. P. 2003. Accumulation of c-Myc and proteasomes at the nucleoli of cells containing elevated c-Myc protein levels. *J Cell Sci,* 116**,** 1707-17.

ARABI, A., WU, S., RIDDERSTRALE, K., BIERHOFF, H., SHIUE, C., FATYOL, K., FAHLEN, S., HYDBRING, P., SODERBERG, O., GRUMMT, I., LARSSON, L. G. & WRIGHT, A. P. 2005. c-Myc associates with ribosomal DNA and activates RNA polymerase I transcription. *Nat Cell Biol,* 7**,** 303-10.

ARORA, B., JINDAL, K., KUMAR, S., REKHI, B., ARORA, H. & ARORA, D. R. 2003. Quantitative evaluation of AgNORs in bone tumours. *Pathology,* 35**,** 106-8.

AVRUCH, J., HARA, K., LIN, Y., LIU, M., LONG, X., ORTIZ-VEGA, S. & YONEZAWA, K. 2006. Insulin and amino-acid regulation of mTOR signaling and kinase activity through the Rheb GTPase. *Oncogene,* 25**,** 6361-72.

BALUCHAMY, S., RAJABI, H. N., THIMMAPAYA, R., NAVARAJ, A. & THIMMAPAYA, B. 2003. Repression of c-Myc and inhibition of G1 exit in cells conditionally overexpressing p300 that is not dependent on its histone acetyltransferase activity. *Proc Natl Acad Sci U S A,* 100**,** 9524-9.

BARNA, M., PUSIC, A., ZOLLO, O., COSTA, M., KONDRASHOV, N., REGO, E., RAO, P. H. & RUGGERO, D. 2008. Suppression of Myc oncogenic activity by ribosomal protein haploinsufficiency. *Nature,* 456**,** 971-5.

BAYANI, J., ZIELENSKA, M., PANDITA, A., AL-ROMAIH, K., KARASKOVA, J., HARRISON, K., BRIDGE, J. A., SORENSEN, P., THORNER, P. & SQUIRE, J. A. 2003. Spectral karyotyping identifies recurrent complex rearrangements of chromosomes 8, 17, and 20 in osteosarcomas. *Genes Chromosomes Cancer,* 36**,** 7-16.

BENSAUDE, O. 2011. Inhibiting eukaryotic transcription: Which compound to choose? How to evaluate its activity? *Transcription,* 2**,** 103-108.

BERETTA, L., GINGRAS, A. C., SVITKIN, Y. V., HALL, M. N. & SONENBERG, N. 1996. Rapamycin blocks the phosphorylation of 4E-BP1 and inhibits cap-dependent initiation of translation. *EMBO J,* 15**,** 658-64.

BERNAL-MIZRACHI, E., WEN, W., STAHLHUT, S., WELLING, C. M. & PERMUTT, M. A. 2001. Islet beta cell expression of constitutively active Akt1/PKB alpha induces striking hypertrophy, hyperplasia, and hyperinsulinemia. *J Clin Invest,* 108**,** 1631-8.

BIANCONI, E., PIOVESAN, A., FACCHIN, F., BERAUDI, A., CASADEI, R., FRABETTI, F., VITALE, L., PELLERI, M. C., TASSANI, S., PIVA, F., PEREZ-AMODIO, S., STRIPPOLI, P. & CANAIDER, S. 2013. An estimation of the number of cells in the human body. *Ann Hum Biol,* 40**,** 463-71.

BIBIKOVA, E., YOUN, M. Y., DANILOVA, N., ONO-URUGA, Y., KONTO-GHIORGHI, Y., OCHOA, R., NARLA, A., GLADER, B., LIN, S. & SAKAMOTO, K. M. 2014. TNF-mediated inflammation represses GATA1 and activates p38 MAP kinase in RPS19-deficient hematopoietic progenitors. *Blood,* 124**,** 3791-8.

BOEHLKE, C., KOTSIS, F., PATEL, V., BRAEG, S., VOELKER, H., BREDT, S., BEYER, T., JANUSCH, H., HAMANN, C., GODEL, M., MULLER, K., HERBST, M., HORNUNG, M., DOERKEN, M., KOTTGEN, M., NITSCHKE, R., IGARASHI, P., WALZ, G. & KUEHN, E. W. 2010. Primary cilia regulate mTORC1 activity and cell size through Lkb1. *Nat Cell Biol,* 12**,** 1115-22.

BRAZIL, D. P. & HEMMINGS, B. A. 2001. Ten years of protein kinase B signalling: a hard Akt to follow. *Trends Biochem Sci,* 26**,** 657-64.

BROWN, S. J., COLE, M. D. & ERIVES, A. J. 2008. Evolution of the holozoan ribosome biogenesis regulon. *BMC Genomics,* 9**,** 442.

BRUNN, G. J., WILLIAMS, J., SABERS, C., WIEDERRECHT, G., LAWRENCE, J. C., JR. & ABRAHAM, R. T. 1996. Direct inhibition of the signaling functions of the mammalian target of rapamycin by the phosphoinositide 3-kinase inhibitors, wortmannin and LY294002. *EMBO J,* 15**,** 5256-67.

BUSCH, H., BYVOET, P. & SMETANA, K. 1963. The nucleolus of the cancer cell: a review. *Cancer Res,* 23**,** 313-39.

CAMPBELL, K. J. & WHITE, R. J. 2014. MYC regulation of cell growth through control of transcription by RNA polymerases I and III. *Cold Spring Harb Perspect Med,* 4.

CANCRO, M. P. 2004. Peripheral B-cell maturation: the intersection of selection and homeostasis. *Immunol Rev,* 197**,** 89-101.

CANTOR, J. R. & SABATINI, D. M. 2012. Cancer cell metabolism: one hallmark, many faces. *Cancer Discov,* 2**,** 881-98.

CARABET, L. A., RENNIE, P. S. & CHERKASOV, A. 2018. Therapeutic Inhibition of Myc in Cancer. Structural Bases and Computer-Aided Drug Discovery Approaches. *Int J Mol Sci,* 20.

CASPERSSON, T., FOLEY, G. E., KILLANDER, D. & LOMAKKA, G. 1963. Cytochemical Differences between Mammalian Cell Lines of Normal and Neoplastic Origins. Correlation with Heterotransplant- Ability in Syrian Hamsters. *Exp Cell Res,* 32**,** 553-65.

CHAUVIN, C., KOKA, V., NOUSCHI, A., MIEULET, V., HOAREAU-AVEILLA, C., DREAZEN, A., CAGNARD, N., CARPENTIER, W., KISS, T., MEYUHAS, O. & PENDE, M. 2014. Ribosomal protein S6 kinase activity controls the ribosome biogenesis transcriptional program. *Oncogene,* 33**,** 474-83.

CHEN, M. & JIANG, P. 2004. Altered subcellular distribution of nucleolar protein fibrillarin by actinomycin D in HEp-2 cells. *Acta Pharmacol Sin,* 25**,** 902-6.

CHOI, A. R., KIM, J. H., WOO, Y. H., CHEON, J. H., KIM, H. S. & YOON, S. 2016. Co-treatment of LY294002 or MK-2206 with AZD5363 Attenuates AZD5363-induced Increase in the Level of Phosphorylated AKT. *Anticancer Res,* 36**,** 5849-5858.

CHOI, A. R., KIM, J. H. & YOON, S. 2014. Sensitization of cancer cells through reduction of total Akt and downregulation of salinomycin-induced pAkt, pGSk3beta, pTSC2, and p4EBP1 by cotreatment with MK-2206. *Biomed Res Int,* 2014**,** 295760.

CLERK, A., MICHAEL, A. & SUGDEN, P. H. 1998. Stimulation of the p38 mitogen-activated protein kinase pathway in neonatal rat ventricular myocytes by the G protein-coupled receptor agonists, endothelin-1 and phenylephrine: a role in cardiac myocyte hypertrophy? *J Cell Biol,* 142**,** 523-35.

COLE, M. D. & COWLING, V. H. 2009. Specific regulation of mRNA cap methylation by the c-Myc and E2F1 transcription factors. *Oncogene,* 28**,** 1169-75.

CONACCI-SORRELL, M., MCFERRIN, L. & EISENMAN, R. N. 2014. An overview of MYC and its interactome. *Cold Spring Harb Perspect Med,* 4**,** a014357.

CONLON, I. & RAFF, M. 1999. Size control in animal development. *Cell,* 96**,** 235-44.

CONLON, I. & RAFF, M. 2003. Differences in the way a mammalian cell and yeast cells coordinate cell growth and cell-cycle progression. *J Biol,* 2**,** 7.

CONLON, I. J., DUNN, G. A., MUDGE, A. W. & RAFF, M. C. 2001. Extracellular control of cell size. *Nat Cell Biol,* 3**,** 918-21.

COOPER, K. L., OH, S., SUNG, Y., DASARI, R. R., KIRSCHNER, M. W. & TABIN, C. J. 2013. Multiple phases of chondrocyte enlargement underlie differences in skeletal proportions. *Nature,* 495**,** 375-8.

CORTES, C. L., VEIGA, S. R., ALMACELLAS, E., HERNANDEZ-LOSA, J., FERRERES, J. C., KOZMA, S. C., AMBROSIO, S., THOMAS, G. & TAULER, A. 2016. Effect of low doses of actinomycin D on neuroblastoma cell lines. *Mol Cancer,* 15**,** 1.

CUENDA, A., ROUSE, J., DOZA, Y. N., MEIER, R., COHEN, P., GALLAGHER, T. F., YOUNG, P. R. & LEE, J. C. 1995. SB 203580 is a specific inhibitor of a MAP kinase homologue which is stimulated by cellular stresses and interleukin-1. *FEBS Lett,* 364**,** 229-33.

CULLY, M., GENEVET, A., WARNE, P., TREINS, C., LIU, T., BASTIEN, J., BAUM, B., TAPON, N., LEEVERS, S. J. & DOWNWARD, J. 2010. A role for p38 stress-activated protein kinase in regulation of cell growth via TORC1. *Mol Cell Biol,* 30**,** 481-95.

DAI, M. S., ARNOLD, H., SUN, X. X., SEARS, R. & LU, H. 2007. Inhibition of c-Myc activity by ribosomal protein L11. *EMBO J,* 26**,** 3332-45.

DANG, C. V. 2013. MYC, metabolism, cell growth, and tumorigenesis. *Cold Spring Harb Perspect Med,* 3.

DANG, C. V., O'DONNELL, K. A., ZELLER, K. I., NGUYEN, T., OSTHUS, R. C. & LI, F. 2006. The c-Myc target gene network. *Semin Cancer Biol,* 16**,** 253-64.

DANIELIAN, P. S., WHITE, R., HOARE, S. A., FAWELL, S. E. & PARKER, M. G. 1993. Identification of residues in the estrogen receptor that confer differential sensitivity to estrogen and hydroxytamoxifen. *Mol Endocrinol,* 7**,** 232-40.

DANILOVA, N. & GAZDA, H. T. 2015. Ribosomopathies: how a common root can cause a tree of pathologies. *Dis Model Mech,* 8**,** 1013-26.

DARZYNKIEWICZ, Z. & HUANG, X. 2004. Analysis of cellular DNA content by flow cytometry. *Curr Protoc Immunol,* Chapter 5**,** Unit 5 7.

DARZYNKIEWICZ, Z., HUANG, X. & ZHAO, H. 2017. Analysis of Cellular DNA Content by Flow Cytometry. *Curr Protoc Immunol,* 119**,** 5 7 1-5 7 20.

DARZYNKIEWICZ, Z., KAPUSCINSKI, J., TRAGANOS, F. & CRISSMAN, H. A. 1987. Application of pyronin Y(G) in cytochemistry of nucleic acids. *Cytometry,* 8**,** 138-45.

DAVIES, B. R., GREENWOOD, H., DUDLEY, P., CRAFTER, C., YU, D. H., ZHANG, J., LI, J., GAO, B., JI, Q., MAYNARD, J., RICKETTS, S. A., CROSS, D., COSULICH, S., CHRESTA, C. C., PAGE, K., YATES, J., LANE, C., WATSON, R., LUKE, R., OGILVIE, D. & PASS, M. 2012. Preclinical pharmacology of AZD5363, an inhibitor of AKT: pharmacodynamics, antitumor activity, and correlation of monotherapy activity with genetic background. *Mol Cancer Ther,* 11**,** 873-87.

DE BENEDETTI, A. & GRAFF, J. R. 2004. eIF-4E expression and its role in malignancies and metastases. *Oncogene,* 23**,** 3189-99.

DEBERARDINIS, R. J. & CHENG, T. 2010. Q's next: the diverse functions of glutamine in metabolism, cell biology and cancer. *Oncogene,* 29**,** 313-24.

DELIU, L. P., GHOSH, A. & GREWAL, S. S. 2017. Investigation of protein synthesis in Drosophila larvae using puromycin labelling. *Biol Open,* 6**,** 1229-1234.

DENNIS TU, J. L., TAYLAN OZDERE, TAE JUN LEE AND LINGCHONG YOU 2006. Engineering Gene Circuits: Foundations and Applications. *Nanotechnology in Biology and Medicine*.

DHAWAN, S., GEORGIA, S. & BHUSHAN, A. 2007. Formation and regeneration of the endocrine pancreas. *Curr Opin Cell Biol,* 19**,** 634-45.

DOWLING, R. J., TOPISIROVIC, I., ALAIN, T., BIDINOSTI, M., FONSECA, B. D., PETROULAKIS, E., WANG, X., LARSSON, O., SELVARAJ, A., LIU, Y., KOZMA, S. C., THOMAS, G. & SONENBERG, N. 2010a. mTORC1-mediated cell proliferation, but not cell growth, controlled by the 4E-BPs. *Science,* 328**,** 1172-6.

DOWLING, R. J., TOPISIROVIC, I., FONSECA, B. D. & SONENBERG, N. 2010b. Dissecting the role of mTOR: lessons from mTOR inhibitors. *Biochim Biophys Acta,* 1804**,** 433-9.

DOZA, Y. N., CUENDA, A., THOMAS, G. M., COHEN, P. & NEBREDA, A. R. 1995. Activation of the MAP kinase homologue RK requires the phosphorylation of Thr-180 and Tyr-182 and both residues are phosphorylated in chemically stressed KB cells. *FEBS Lett,* 364**,** 223-8.

DRYGIN, D., RICE, W. G. & GRUMMT, I. 2010. The RNA polymerase I transcription machinery: an emerging target for the treatment of cancer. *Annu Rev Pharmacol Toxicol,* 50**,** 131-56.

DUNCAN, R., MILBURN, S. C. & HERSHEY, J. W. 1987. Regulated phosphorylation and low abundance of HeLa cell initiation factor eIF-4F suggest a role in translational control. Heat shock effects on eIF-4F. *J Biol Chem,* 262**,** 380-8.

EILERS, M., PICARD, D., YAMAMOTO, K. R. & BISHOP, J. M. 1989. Chimaeras of myc oncoprotein and steroid receptors cause hormone-dependent transformation of cells. *Nature,* 340**,** 66-8.

EL-NAGGAR, A. K. 2004. Concurrent flow cytometric analysis of DNA and RNA. *Methods Mol Biol,* 263**,** 371-84.
ELOWITZ, M. B. & LEIBLER, S. 2000. A synthetic oscillatory network of transcriptional regulators. *Nature,* 403**,** 335-8.
ELOWITZ, M. B., LEVINE, A. J., SIGGIA, E. D. & SWAIN, P. S. 2002. Stochastic gene expression in a single cell. *Science,* 297**,** 1183-6.
ENGELMAN, J. A., LUO, J. & CANTLEY, L. C. 2006. The evolution of phosphatidylinositol 3-kinases as regulators of growth and metabolism. *Nat Rev Genet,* 7**,** 606-19.
ENSLEN, H., RAINGEAUD, J. & DAVIS, R. J. 1998. Selective activation of p38 mitogen-activated protein (MAP) kinase isoforms by the MAP kinase kinases MKK3 and MKK6. *J Biol Chem,* 273**,** 1741-8.
ENTREVAN, M. 2013. Biological Mechanisms of Noise in Gene Expression. *Biosciences Master Reviews***,** 8.
ERNENS, I., GOODFELLOW, S. J., INNES, F., KENNETH, N. S., DERBLAY, L. E., WHITE, R. J. & SCOTT, P. H. 2006. Hypoxic stress suppresses RNA polymerase III recruitment and tRNA gene transcription in cardiomyocytes. *Nucleic Acids Res,* 34**,** 286-94.
ERSCHING, J., EFEYAN, A., MESIN, L., JACOBSEN, J. T., PASQUAL, G., GRABINER, B. C., DOMINGUEZ-SOLA, D., SABATINI, D. M. & VICTORA, G. D. 2017. Germinal Center Selection and Affinity Maturation Require Dynamic Regulation of mTORC1 Kinase. *Immunity,* 46**,** 1045-1058 e6.
FABIAN, M. C., LAKEY, J. R., RAJOTTE, R. V. & KNETEMAN, N. M. 1993. The efficacy and toxicity of rapamycin in murine islet transplantation. In vitro and in vivo studies. *Transplantation,* 56**,** 1137-42.
FARNIER, C., KRIEF, S., BLACHE, M., DIOT-DUPUY, F., MORY, G., FERRE, P. & BAZIN, R. 2002. The signaling pathway for beta1-integrin/ERKs is involved in the adaptation of adipocyte functions to cell size. *Ann N Y Acad Sci,* 973**,** 594-7.
FARNIER, C., KRIEF, S., BLACHE, M., DIOT-DUPUY, F., MORY, G., FERRE, P. & BAZIN, R. 2003. Adipocyte functions are modulated by cell size change: potential involvement of an integrin/ERK signalling pathway. *Int J Obes Relat Metab Disord,* 27**,** 1178-86.
FELTON-EDKINS, Z. A., KENNETH, N. S., BROWN, T. R., DALY, N. L., GOMEZ-ROMAN, N., GRANDORI, C., EISENMAN, R. N. & WHITE, R. J. 2003. Direct regulation of RNA polymerase III transcription by RB, p53 and c-Myc. *Cell Cycle,* 2**,** 181-4.
FERNANDEZ, P. C., FRANK, S. R., WANG, L., SCHROEDER, M., LIU, S., GREENE, J., COCITO, A. & AMATI, B. 2003. Genomic targets of the human c-Myc protein. *Genes Dev,* 17**,** 1115-29.
FINGAR, D. C., SALAMA, S., TSOU, C., HARLOW, E. & BLENIS, J. 2002. Mammalian cell size is controlled by mTOR and its downstream targets S6K1 and 4EBP1/eIF4E. *Genes Dev,* 16**,** 1472-87.
FOSTER, K. G. & FINGAR, D. C. 2010. Mammalian target of rapamycin (mTOR): conducting the cellular signaling symphony. *J Biol Chem,* 285**,** 14071-7.
FUKASAWA, K., WIENER, F., VANDE WOUDE, G. F. & MAI, S. 1997. Genomic instability and apoptosis are frequent in p53 deficient young mice. *Oncogene,* 15**,** 1295-302.
GALLANT, P. 2013. Myc function in Drosophila. *Cold Spring Harb Perspect Med,* 3**,** a014324.
GALLANT, P., SHIIO, Y., CHENG, P. F., PARKHURST, S. M. & EISENMAN, R. N. 1996. Myc and Max homologs in Drosophila. *Science,* 274**,** 1523-7.
GANDARILLAS, A. & WATT, F. M. 1997. c-Myc promotes differentiation of human epidermal stem cells. *Genes Dev,* 11**,** 2869-82.

GAO, P., TCHERNYSHYOV, I., CHANG, T. C., LEE, Y. S., KITA, K., OCHI, T., ZELLER, K. I., DE MARZO, A. M., VAN EYK, J. E., MENDELL, J. T. & DANG, C. V. 2009. c-Myc suppression of miR-23a/b enhances mitochondrial glutaminase expression and glutamine metabolism. *Nature,* 458**,** 762-5.

GAO, X., LI, N. & ZHANG, J. 2019. SB203580, a p38MAPK inhibitor, attenuates olfactory dysfunction by inhibiting OSN apoptosis in AR mice (activation and involvement of the p38 mitogen-activated protein kinase in olfactory sensory neuronal apoptosis of OVA-induced allergic rhinitis). *Brain Behav,* 9**,** e01295.

GHARBI, S. I., ZVELEBIL, M. J., SHUTTLEWORTH, S. J., HANCOX, T., SAGHIR, N., TIMMS, J. F. & WATERFIELD, M. D. 2007. Exploring the specificity of the PI3K family inhibitor LY294002. *Biochem J,* 404**,** 15-21.

GIORDANO, E., CIRULLI, V., BOSCO, D., ROUILLER, D., HALBAN, P. & MEDA, P. 1993. B-cell size influences glucose-stimulated insulin secretion. *Am J Physiol,* 265**,** C358-64.

GOEDERT, M., CUENDA, A., CRAXTON, M., JAKES, R. & COHEN, P. 1997. Activation of the novel stress-activated protein kinase SAPK4 by cytokines and cellular stresses is mediated by SKK3 (MKK6); comparison of its substrate specificity with that of other SAP kinases. *EMBO J,* 16**,** 3563-71.

GOMEZ-ROMAN, N., FELTON-EDKINS, Z. A., KENNETH, N. S., GOODFELLOW, S. J., ATHINEOS, D., ZHANG, J., RAMSBOTTOM, B. A., INNES, F., KANTIDAKIS, T., KERR, E. R., BRODIE, J., GRANDORI, C. & WHITE, R. J. 2006. Activation by c-Myc of transcription by RNA polymerases I, II and III. *Biochem Soc Symp***,** 141-54.

GOMEZ-ROMAN, N., GRANDORI, C., EISENMAN, R. N. & WHITE, R. J. 2003. Direct activation of RNA polymerase III transcription by c-Myc. *Nature,* 421**,** 290-4.

GONZALEZ-TERAN, B., LOPEZ, J. A., RODRIGUEZ, E., LEIVA, L., MARTINEZ-MARTINEZ, S., BERNAL, J. A., JIMENEZ-BORREGUERO, L. J., REDONDO, J. M., VAZQUEZ, J. & SABIO, G. 2016. p38gamma and delta promote heart hypertrophy by targeting the mTOR-inhibitory protein DEPTOR for degradation. *Nat Commun,* 7**,** 10477.

GOODFELLOW, S. J., INNES, F., DERBLAY, L. E., MACLELLAN, W. R., SCOTT, P. H. & WHITE, R. J. 2006. Regulation of RNA polymerase III transcription during hypertrophic growth. *EMBO J,* 25**,** 1522-33.

GOODFELLOW, S. J. & WHITE, R. J. 2007. Regulation of RNA polymerase III transcription during mammalian cell growth. *Cell Cycle,* 6**,** 2323-6.

GOODMAN, C. A. & HORNBERGER, T. A. 2013. Measuring protein synthesis with SUnSET: a valid alternative to traditional techniques? *Exerc Sport Sci Rev,* 41**,** 107-15.

GRAFF, J. R., KONICEK, B. W., VINCENT, T. M., LYNCH, R. L., MONTEITH, D., WEIR, S. N., SCHWIER, P., CAPEN, A., GOODE, R. L., DOWLESS, M. S., CHEN, Y., ZHANG, H., SISSONS, S., COX, K., MCNULTY, A. M., PARSONS, S. H., WANG, T., SAMS, L., GEEGANAGE, S., DOUGLASS, L. E., NEUBAUER, B. L., DEAN, N. M., BLANCHARD, K., SHOU, J., STANCATO, L. F., CARTER, J. H. & MARCUSSON, E. G. 2007. Therapeutic suppression of translation initiation factor eIF4E expression reduces tumor growth without toxicity. *J Clin Invest,* 117**,** 2638-48.

GRAHAM, F. L., SMILEY, J., RUSSELL, W. C. & NAIRN, R. 1977. Characteristics of a human cell line transformed by DNA from human adenovirus type 5. *J Gen Virol,* 36**,** 59-74.

GRAHAM, M. D. 2013. The Coulter principle: Imaginary origins. *Cytometry A,* 83**,** 1057-61.

GRANDORI, C., GOMEZ-ROMAN, N., FELTON-EDKINS, Z. A., NGOUENET, C., GALLOWAY, D. A., EISENMAN, R. N. & WHITE, R. J. 2005. c-Myc binds to human ribosomal DNA and stimulates transcription of rRNA genes by RNA polymerase I. *Nat Cell Biol,* 7**,** 311-8.

GRAVES, J. A., WANG, Y., SIMS-LUCAS, S., CHEROK, E., ROTHERMUND, K., BRANCA, M. F., ELSTER, J., BEER-STOLZ, D., VAN HOUTEN, B., VOCKLEY, J. & PROCHOWNIK, E. V. 2012. Mitochondrial structure, function and dynamics are temporally controlled by c-Myc. *PLoS One,* 7**,** e37699.

GREGORY, T. R. 2002. A bird's-eye view of the C-value enigma: genome size, cell size, and metabolic rate in the class aves. *Evolution,* 56**,** 121-30.

GREWAL, S. S., LI, L., ORIAN, A., EISENMAN, R. N. & EDGAR, B. A. 2005. Myc-dependent regulation of ribosomal RNA synthesis during Drosophila development. *Nat Cell Biol,* 7**,** 295-302.

GRIFONI, D. & BELLOSTA, P. 2015. Drosophila Myc: A master regulator of cellular performance. *Biochim Biophys Acta,* 1849**,** 570-81.

GUILHERME, A., VIRBASIUS, J. V., PURI, V. & CZECH, M. P. 2008. Adipocyte dysfunctions linking obesity to insulin resistance and type 2 diabetes. *Nat Rev Mol Cell Biol,* 9**,** 367-77.

GUO, Y., NIU, C., BRESLIN, P., TANG, M., ZHANG, S., WEI, W., KINI, A. R., PANER, G. P., ALKAN, S., MORRIS, S. W., DIAZ, M., STIFF, P. J. & ZHANG, J. 2009. c-Myc-mediated control of cell fate in megakaryocyte-erythrocyte progenitors. *Blood,* 114**,** 2097-106.

HAN, J., LEE, J. D., BIBBS, L. & ULEVITCH, R. J. 1994. A MAP kinase targeted by endotoxin and hyperosmolarity in mammalian cells. *Science,* 265**,** 808-11.

HARTL, M., MITTERSTILLER, A. M., VALOVKA, T., BREUKER, K., HOBMAYER, B. & BISTER, K. 2010. Stem cell-specific activation of an ancestral myc protooncogene with conserved basic functions in the early metazoan Hydra. *Proc Natl Acad Sci U S A,* 107**,** 4051-6.

HEITMAN, J., MOVVA, N. R. & HALL, M. N. 1991. Targets for cell cycle arrest by the immunosuppressant rapamycin in yeast. *Science,* 253**,** 905-9.

HENG, H. H. 2013. Genomics: HeLa genome versus donor's genome. *Nature,* 501**,** 167.

HENNESSY, B. T., SMITH, D. L., RAM, P. T., LU, Y. & MILLS, G. B. 2005. Exploiting the PI3K/AKT pathway for cancer drug discovery. *Nat Rev Drug Discov,* 4**,** 988-1004.

HOCHSTATTER, J., HOLZEL, M., ROHRMOSER, M., SCHERMELLEH, L., LEONHARDT, H., KEOUGH, R., GONDA, T. J., IMHOF, A., EICK, D., LANGST, G. & NEMETH, A. 2012. Myb-binding protein 1a (Mybbp1a) regulates levels and processing of pre-ribosomal RNA. *J Biol Chem,* 287**,** 24365-77.

HONGYAN, L., CHUNYAN, W. & YUE'E, Y. 2017. LY294002, a PI3K inhibitor, attenuates Tourette syndrome in rats. *Metab Brain Dis,* 32**,** 1619-1625.

HOU, G., ZHAO, Q., ZHANG, M., FAN, T., LIU, M., SHI, X., REN, Y., WANG, Y., ZHOU, J. & LU, Z. 2018. Down-regulation of Rictor enhances cell sensitivity to PI3K inhibitor LY294002 by blocking mTORC2-medicated phosphorylation of Akt/PRAS40 in esophageal squamous cell carcinoma. *Biomed Pharmacother,* 106**,** 1348-1356.

HSIEH, A. C., LIU, Y., EDLIND, M. P., INGOLIA, N. T., JANES, M. R., SHER, A., SHI, E. Y., STUMPF, C. R., CHRISTENSEN, C., BONHAM, M. J., WANG, S., REN, P., MARTIN, M., JESSEN, K., FELDMAN, M. E., WEISSMAN, J. S., SHOKAT, K. M., ROMMEL, C. & RUGGERO, D. 2012. The translational landscape of mTOR signalling steers cancer initiation and metastasis. *Nature,* 485**,** 55-61.

HU, S., BALAKRISHNAN, A., BOK, R. A., ANDERTON, B., LARSON, P. E., NELSON, S. J., KURHANEWICZ, J., VIGNERON, D. B. & GOGA, A. 2011. 13C-pyruvate imaging reveals alterations in glycolysis that precede c-Myc-induced tumor formation and regression. *Cell Metab,* 14**,** 131-42.

HUO, Y., IADEVAIA, V. & PROUD, C. G. 2011. Differing effects of rapamycin and mTOR kinase inhibitors on protein synthesis. *Biochem Soc Trans,* 39**,** 446-50.

IHLE, N. T. & POWIS, G. 2010. Inhibitors of phosphatidylinositol-3-kinase in cancer therapy. *Mol Aspects Med,* 31**,** 135-44.

INOKI, K., LI, Y., ZHU, T., WU, J. & GUAN, K. L. 2002. TSC2 is phosphorylated and inhibited by Akt and suppresses mTOR signalling. *Nat Cell Biol,* 4**,** 648-57.

IRITANI, B. M. & EISENMAN, R. N. 1999. c-Myc enhances protein synthesis and cell size during B lymphocyte development. *Proc Natl Acad Sci U S A,* 96**,** 13180-5.

ISFORT, R. J., CODY, D. B., LOVELL, G. & DOERSEN, C. J. 1995. Analysis of oncogenes, tumor suppressor genes, autocrine growth-factor production, and differentiation state of human osteosarcoma cell lines. *Mol Carcinog,* 14**,** 170-8.

JEFFERIES, H. B., FUMAGALLI, S., DENNIS, P. B., REINHARD, C., PEARSON, R. B. & THOMAS, G. 1997. Rapamycin suppresses 5'TOP mRNA translation through inhibition of p70s6k. *EMBO J,* 16**,** 3693-704.

JIANG, B. H. & LIU, L. Z. 2008. PI3K/PTEN signaling in tumorigenesis and angiogenesis. *Biochim Biophys Acta,* 1784**,** 150-8.

JIANG, Y., CHEN, C., LI, Z., GUO, W., GEGNER, J. A., LIN, S. & HAN, J. 1996. Characterization of the structure and function of a new mitogen-activated protein kinase (p38beta). *J Biol Chem,* 271**,** 17920-6.

JIANG, Y., GRAM, H., ZHAO, M., NEW, L., GU, J., FENG, L., DI PADOVA, F., ULEVITCH, R. J. & HAN, J. 1997. Characterization of the structure and function of the fourth member of p38 group mitogen-activated protein kinases, p38delta. *J Biol Chem,* 272**,** 30122-8.

JOHNSTON, L. A., PROBER, D. A., EDGAR, B. A., EISENMAN, R. N. & GALLANT, P. 1999. Drosophila myc regulates cellular growth during development. *Cell,* 98**,** 779-90.

KAPUSCINSKI, J. & DARZYNKIEWICZ, Z. 1987. Interactions of acridine orange with double stranded nucleic acids. Spectral and affinity studies. *J Biomol Struct Dyn,* 5**,** 127-43.

KIM, J., WOO, A. J., CHU, J., SNOW, J. W., FUJIWARA, Y., KIM, C. G., CANTOR, A. B. & ORKIN, S. H. 2010. A Myc network accounts for similarities between embryonic stem and cancer cell transcription programs. *Cell,* 143**,** 313-24.

KIM, K. H. & SEDERSTROM, J. M. 2015. Assaying Cell Cycle Status Using Flow Cytometry. *Curr Protoc Mol Biol,* 111**,** 28 6 1-28 6 11.

KRESS, T. R., SABO, A. & AMATI, B. 2015. MYC: connecting selective transcriptional control to global RNA production. *Nat Rev Cancer,* 15**,** 593-607.

KUDOH, S., KOMURO, I., HIROI, Y., ZOU, Y., HARADA, K., SUGAYA, T., TAKEKOSHI, N., MURAKAMI, K., KADOWAKI, T. & YAZAKI, Y. 1998. Mechanical stretch induces hypertrophic responses in cardiac myocytes of angiotensin II type 1a receptor knockout mice. *J Biol Chem,* 273**,** 24037-43.

KUFE, D. W., HOLLAND, J. F., FREI, E. & AMERICAN CANCER SOCIETY. 2003. *Cancer medicine 6,* Hamilton, Ont. ; Lewiston, NY, BC Decker.

KULESHOV, M. V., JONES, M. R., ROUILLARD, A. D., FERNANDEZ, N. F., DUAN, Q., WANG, Z., KOPLEV, S., JENKINS, S. L., JAGODNIK, K. M., LACHMANN, A., MCDERMOTT, M. G., MONTEIRO, C. D., GUNDERSEN, G. W. & MA'AYAN, A. 2016. Enrichr: a comprehensive gene set enrichment analysis web server 2016 update. *Nucleic Acids Res,* 44**,** W90-7.

KUMAR, S., BOEHM, J. & LEE, J. C. 2003. p38 MAP kinases: key signalling molecules as therapeutic targets for inflammatory diseases. *Nat Rev Drug Discov,* 2**,** 717-26.

KUMAZAWA, T., NISHIMURA, K., KATAGIRI, N., HASHIMOTO, S., HAYASHI, Y. & KIMURA, K. 2015. Gradual reduction in rRNA transcription triggers p53 acetylation and apoptosis via MYBBP1A. *Sci Rep,* 5**,** 10854.

KURNICK, N. B. 1955a. Cytochemical changes during normal growth and compensatory hypertrophy of the rat kidney. *J Histochem Cytochem,* 3**,** 290-4.

KURNICK, N. B. 1955b. Pyronin Y in the methyl-green-pyronin histological stain. *Stain Technol,* 30**,** 213-30.

LALI, F. V., HUNT, A. E., TURNER, S. J. & FOXWELL, B. M. 2000. The pyridinyl imidazole inhibitor SB203580 blocks phosphoinositide-dependent protein kinase activity, protein kinase B phosphorylation, and retinoblastoma hyperphosphorylation in interleukin-2-stimulated T cells independently of p38 mitogen-activated protein kinase. *J Biol Chem,* 275**,** 7395-402.

LAMOUREUX, F., THOMAS, C., CRAFTER, C., KUMANO, M., ZHANG, F., DAVIES, B. R., GLEAVE, M. E. & ZOUBEIDI, A. 2013. Blocked autophagy using lysosomotropic agents sensitizes resistant prostate tumor cells to the novel Akt inhibitor AZD5363. *Clin Cancer Res,* 19**,** 833-44.

LAMOUREUX, F. & ZOUBEIDI, A. 2013. Dual inhibition of autophagy and the AKT pathway in prostate cancer. *Autophagy,* 9**,** 1119-20.

LAPLANTE, M. & SABATINI, D. M. 2012. mTOR signaling in growth control and disease. *Cell,* 149**,** 274-93.

LE, A., LANE, A. N., HAMAKER, M., BOSE, S., GOUW, A., BARBI, J., TSUKAMOTO, T., ROJAS, C. J., SLUSHER, B. S., ZHANG, H., ZIMMERMAN, L. J., LIEBLER, D. C., SLEBOS, R. J., LORKIEWICZ, P. K., HIGASHI, R. M., FAN, T. W. & DANG, C. V. 2012. Glucose-independent glutamine metabolism via TCA cycling for proliferation and survival in B cells. *Cell Metab,* 15**,** 110-21.

LECHNER, C., ZAHALKA, M. A., GIOT, J. F., MOLLER, N. P. & ULLRICH, A. 1996. ERK6, a mitogen-activated protein kinase involved in C2C12 myoblast differentiation. *Proc Natl Acad Sci U S A,* 93**,** 4355-9.

LESLIE, N. R. & DOWNES, C. P. 2002. PTEN: The down side of PI 3-kinase signalling. *Cell Signal,* 14**,** 285-95.

LI, J., KIM, S. G. & BLENIS, J. 2014. Rapamycin: one drug, many effects. *Cell Metab,* 19**,** 373-9.

LI, Z., VAN CALCAR, S., QU, C., CAVENEE, W. K., ZHANG, M. Q. & REN, B. 2003. A global transcriptional regulatory role for c-Myc in Burkitt's lymphoma cells. *Proc Natl Acad Sci U S A,* 100**,** 8164-9.

LIAO, Y., DUAN, B., ZHANG, Y., ZHANG, X. & XIA, B. 2019. Excessive ER-phagy mediated by the autophagy receptor FAM134B results in ER stress, the unfolded protein response, and cell death in HeLa cells. *J Biol Chem,* 294**,** 20009-20023.

LIN, C. J., CENCIC, R., MILLS, J. R., ROBERT, F. & PELLETIER, J. 2008. c-Myc and eIF4F are components of a feedforward loop that links transcription and translation. *Cancer Res,* 68**,** 5326-34.

LIN, C. J., MALINA, A. & PELLETIER, J. 2009. c-Myc and eIF4F constitute a feedforward loop that regulates cell growth: implications for anticancer therapy. *Cancer Res,* 69**,** 7491-4.

LIN, C. Y., LOVEN, J., RAHL, P. B., PARANAL, R. M., BURGE, C. B., BRADNER, J. E., LEE, T. I. & YOUNG, R. A. 2012. Transcriptional amplification in tumor cells with elevated c-Myc. *Cell,* 151**,** 56-67.

LIN, Y. C., BOONE, M., MEURIS, L., LEMMENS, I., VAN ROY, N., SOETE, A., REUMERS, J., MOISSE, M., PLAISANCE, S., DRMANAC, R., CHEN, J., SPELEMAN, F., LAMBRECHTS, D., VAN DE PEER, Y., TAVERNIER, J. & CALLEWAERT, N. 2014. Genome dynamics of the human embryonic kidney 293 lineage in response to cell biology manipulations. *Nat Commun,* 5**,** 4767.

LIPPMAN, S. I. & BROACH, J. R. 2009. Protein kinase A and TORC1 activate genes for ribosomal biogenesis by inactivating repressors encoded by Dot6 and its homolog Tod6. *Proc Natl Acad Sci U S A,* 106**,** 19928-33.

LITTLEWOOD, T. D., HANCOCK, D. C., DANIELIAN, P. S., PARKER, M. G. & EVAN, G. I. 1995. A modified oestrogen receptor ligand-binding domain as an improved switch for the regulation of heterologous proteins. *Nucleic Acids Res,* 23**,** 1686-90.

LIU, H. S., ZHANG, J., GUO, J. L., LIN, C. Y. & WANG, Z. W. 2016a. Phosphoinositide 3-kinase inhibitor LY294002 ameliorates the severity of myosin-induced myocarditis in mice. *Curr Res Transl Med,* 64**,** 21-7.

LIU, J., FU, X. Q., ZHOU, W., YU, H. G., YU, J. P. & LUO, H. S. 2011. LY294002 potentiates the anti-cancer effect of oxaliplatin for gastric cancer via death receptor pathway. *World J Gastroenterol,* 17**,** 181-90.

LIU, S., GINZBERG, M. B., PATEL, N., HILD, M., LEUNG, B., LI, Z., CHEN, Y. C., CHANG, N., WANG, Y., TAN, C., DIENA, S., TRIMBLE, W., WASSERMAN, L., JENKINS, J. L., KIRSCHNER, M. W. & KAFRI, R. 2018. Size uniformity of animal cells is actively maintained by a p38 MAPK-dependent regulation of G1-length. *Elife,* 7.

LIU, W., LE, A., HANCOCK, C., LANE, A. N., DANG, C. V., FAN, T. W. & PHANG, J. M. 2012. Reprogramming of proline and glutamine metabolism contributes to the proliferative and metabolic responses regulated by oncogenic transcription factor c-MYC. *Proc Natl Acad Sci U S A,* 109**,** 8983-8.

LIU, X. F., XIANG, L., ZHOU, Q., CARRALOT, J. P., PRUNOTTO, M., NIEDERFELLNER, G. & PASTAN, I. 2016b. Actinomycin D enhances killing of cancer cells by immunotoxin RG7787 through activation of the extrinsic pathway of apoptosis. *Proc Natl Acad Sci U S A,* 113**,** 10666-71.

LIU, Y. C., LI, F., HANDLER, J., HUANG, C. R., XIANG, Y., NERETTI, N., SEDIVY, J. M., ZELLER, K. I. & DANG, C. V. 2008. Global regulation of nucleotide biosynthetic genes by c-Myc. *PLoS One,* 3**,** e2722.

LLOYD, A. C. 2013. The regulation of cell size. *Cell,* 154**,** 1194-205.

LOPEZ-AVILES, S., GRANDE, M., GONZALEZ, M., HELGESEN, A. L., ALEMANY, V., SANCHEZ-PIRIS, M., BACHS, O., MILLAR, J. B. & ALIGUE, R. 2005. Inactivation of the Cdc25 phosphatase by the stress-activated Srk1 kinase in fission yeast. *Mol Cell,* 17**,** 49-59.

LU, D. F., WANG, Y. S., LI, C., WEI, G. J., CHEN, R., DONG, D. M. & YAO, M. 2015. Actinomycin D inhibits cell proliferations and promotes apoptosis in osteosarcoma cells. *Int J Clin Exp Med,* 8**,** 1904-11.

MACVILLE, M., SCHROCK, E., PADILLA-NASH, H., KECK, C., GHADIMI, B. M., ZIMONJIC, D., POPESCU, N. & RIED, T. 1999. Comprehensive and definitive molecular cytogenetic characterization of HeLa cells by spectral karyotyping. *Cancer Res,* 59**,** 141-50.

MAJNO, G. & JORIS, I. 2004. *Cells, tissues, and disease : principles of general pathology,* New York, Oxford University Press.

MALUMBRES, M. & BARBACID, M. 2009. Cell cycle, CDKs and cancer: a changing paradigm. *Nat Rev Cancer,* 9**,** 153-66.

MARGUERAT, S. & BAHLER, J. 2012. Coordinating genome expression with cell size. *Trends Genet,* 28**,** 560-5.
MASTERS, J. R. 2002. HeLa cells 50 years on: the good, the bad and the ugly. *Nat Rev Cancer,* 2**,** 315-9.
MATEYAK, M. K., OBAYA, A. J., ADACHI, S. & SEDIVY, J. M. 1997. Phenotypes of c-Myc-deficient rat fibroblasts isolated by targeted homologous recombination. *Cell Growth Differ,* 8**,** 1039-48.
MATSUZAWA, A., TSENG, P. H., VALLABHAPURAPU, S., LUO, J. L., ZHANG, W., WANG, H., VIGNALI, D. A., GALLAGHER, E. & KARIN, M. 2008. Essential cytoplasmic translocation of a cytokine receptor-assembled signaling complex. *Science,* 321**,** 663-8.
MAYER, C., ZHAO, J., YUAN, X. & GRUMMT, I. 2004. mTOR-dependent activation of the transcription factor TIF-IA links rRNA synthesis to nutrient availability. *Genes Dev,* 18**,** 423-34.
MAYNARD, J., RICKETTS, S. A., GENDRIN, C., DUDLEY, P. & DAVIES, B. R. 2013. 2-Deoxy-2-[18F]fluoro-D-glucose positron emission tomography demonstrates target inhibition with the potential to predict anti-tumour activity following treatment with the AKT inhibitor AZD5363. *Mol Imaging Biol,* 15**,** 476-85.
MAZZINI, G. & DANOVA, M. 2017. Fluorochromes for DNA Staining and Quantitation. *Methods Mol Biol,* 1560**,** 239-259.
MCGLINCY, N. J. & INGOLIA, N. T. 2017. Transcriptome-wide measurement of translation by ribosome profiling. *Methods,* 126**,** 112-129.
MEJA, K., STENGEL, C., SELLAR, R., HUSZAR, D., DAVIES, B. R., GALE, R. E., LINCH, D. C. & KHWAJA, A. 2014. PIM and AKT kinase inhibitors show synergistic cytotoxicity in acute myeloid leukaemia that is associated with convergence on mTOR and MCL1 pathways. *Br J Haematol,* 167**,** 69-79.
MERTENS, S., CRAXTON, M. & GOEDERT, M. 1996. SAP kinase-3, a new member of the family of mammalian stress-activated protein kinases. *FEBS Lett,* 383**,** 273-6.
MIETTINEN, T. P., PESSA, H. K., CALDEZ, M. J., FUHRER, T., DIRIL, M. K., SAUER, U., KALDIS, P. & BJORKLUND, M. 2014. Identification of transcriptional and metabolic programs related to mammalian cell size. *Curr Biol,* 24**,** 598-608.
MOLNAR, A., THEODORAS, A. M., ZON, L. I. & KYRIAKIS, J. M. 1997. Cdc42Hs, but not Rac1, inhibits serum-stimulated cell cycle progression at G1/S through a mechanism requiring p38/RK. *J Biol Chem,* 272**,** 13229-35.
MONTANARO, L., TRERE, D. & DERENZINI, M. 2008. Nucleolus, ribosomes, and cancer. *Am J Pathol,* 173**,** 301-10.
MORIGUCHI, T., TOYOSHIMA, F., GOTOH, Y., IWAMATSU, A., IRIE, K., MORI, E., KUROYANAGI, N., HAGIWARA, M., MATSUMOTO, K. & NISHIDA, E. 1996. Purification and identification of a major activator for p38 from osmotically shocked cells. Activation of mitogen-activated protein kinase kinase 6 by osmotic shock, tumor necrosis factor-alpha, and H2O2. *J Biol Chem,* 271**,** 26981-8.
MORRISH, F. & HOCKENBERY, D. 2014. MYC and mitochondrial biogenesis. *Cold Spring Harb Perspect Med,* 4.
MORRISH, F., NOONAN, J., PEREZ-OLSEN, C., GAFKEN, P. R., FITZGIBBON, M., KELLEHER, J., VANGILST, M. & HOCKENBERY, D. 2010. Myc-dependent mitochondrial generation of acetyl-CoA contributes to fatty acid biosynthesis and histone acetylation during cell cycle entry. *J Biol Chem,* 285**,** 36267-74.

MUNSKY, B., NEUERT, G. & VAN OUDENAARDEN, A. 2012. Using gene expression noise to understand gene regulation. *Science,* 336**,** 183-7.
MURPHY, D. J., JUNTTILA, M. R., POUYET, L., KARNEZIS, A., SHCHORS, K., BUI, D. A., BROWN-SWIGART, L., JOHNSON, L. & EVAN, G. I. 2008. Distinct thresholds govern Myc's biological output in vivo. *Cancer Cell,* 14**,** 447-57.
NESBIT, C. E., GROVE, L. E., YIN, X. & PROCHOWNIK, E. V. 1998. Differential apoptotic behaviors of c-myc, N-myc, and L-myc oncoproteins. *Cell Growth Differ,* 9**,** 731-41.
NESTEL, P. J., AUSTIN, W. & FOXMAN, C. 1969. Lipoprotn lipase content and triglyceride fatty acid uptake in adipose tissue of rats of differing body weights. *J Lipid Res,* 10**,** 383-7.
NEUROHR, G. E., TERRY, R. L., LENGEFELD, J., BONNEY, M., BRITTINGHAM, G. P., MORETTO, F., MIETTINEN, T. P., VAITES, L. P., SOARES, L. M., PAULO, J. A., HARPER, J. W., BURATOWSKI, S., MANALIS, S., VAN WERVEN, F. J., HOLT, L. J. & AMON, A. 2019. Excessive Cell Growth Causes Cytoplasm Dilution And Contributes to Senescence. *Cell,* 176**,** 1083-1097 e18.
NEW, L. & HAN, J. 1998. The p38 MAP kinase pathway and its biological function. *Trends Cardiovasc Med,* 8**,** 220-8.
NIE, Z., HU, G., WEI, G., CUI, K., YAMANE, A., RESCH, W., WANG, R., GREEN, D. R., TESSAROLLO, L., CASELLAS, R., ZHAO, K. & LEVENS, D. 2012. c-Myc is a universal amplifier of expressed genes in lymphocytes and embryonic stem cells. *Cell,* 151**,** 68-79.
NIFOROU, K. M., ANAGNOSTOPOULOS, A. K., VOUGAS, K., KITTAS, C., GORGOULIS, V. G. & TSANGARIS, G. T. 2008. The proteome profile of the human osteosarcoma U2OS cell line. *Cancer Genomics Proteomics,* 5**,** 63-78.
NISHIDA, K., YAMAGUCHI, O., HIROTANI, S., HIKOSO, S., HIGUCHI, Y., WATANABE, T., TAKEDA, T., OSUKA, S., MORITA, T., KONDOH, G., UNO, Y., KASHIWASE, K., TANIIKE, M., NAKAI, A., MATSUMURA, Y., MIYAZAKI, J., SUDO, T., HONGO, K., KUSAKARI, Y., KURIHARA, S., CHIEN, K. R., TAKEDA, J., HORI, M. & OTSU, K. 2004. p38alpha mitogen-activated protein kinase plays a critical role in cardiomyocyte survival but not in cardiac hypertrophic growth in response to pressure overload. *Mol Cell Biol,* 24**,** 10611-20.
NISHIKURA, K., ERIKSON, J., AR-RUSHDI, A., HUEBNER, K. & CROCE, C. M. 1985. The translocated c-myc oncogene of Raji Burkitt lymphoma cells is not expressed in human lymphoblastoid cells. *Proc Natl Acad Sci U S A,* 82**,** 2900-4.
NOOROLYAI, S., SHAJARI, N., BAGHBANI, E., SADREDDINI, S. & BARADARAN, B. 2019. The relation between PI3K/AKT signalling pathway and cancer. *Gene,* 698**,** 120-128.
O'DONNELL, K. A., YU, D., ZELLER, K. I., KIM, J. W., RACKE, F., THOMAS-TIKHONENKO, A. & DANG, C. V. 2006. Activation of transferrin receptor 1 by c-Myc enhances cellular proliferation and tumorigenesis. *Mol Cell Biol,* 26**,** 2373-86.
OHANNA, M., SOBERING, A. K., LAPOINTE, T., LORENZO, L., PRAUD, C., PETROULAKIS, E., SONENBERG, N., KELLY, P. A., SOTIROPOULOS, A. & PENDE, M. 2005. Atrophy of S6K1(-/-) skeletal muscle cells reveals distinct mTOR effectors for cell cycle and size control. *Nat Cell Biol,* 7**,** 286-94.
ONO, W., HAYASHI, Y., YOKOYAMA, W., KURODA, T., KISHIMOTO, H., ITO, I., KIMURA, K., AKAOGI, K., WAKU, T. & YANAGISAWA, J. 2014. The nucleolar protein Myb-binding protein 1A (MYBBP1A) enhances p53 tetramerization and acetylation in response to nucleolar disruption. *J Biol Chem,* 289**,** 4928-40.

OSTHUS, R. C., SHIM, H., KIM, S., LI, Q., REDDY, R., MUKHERJEE, M., XU, Y., WONSEY, D., LEE, L. A. & DANG, C. V. 2000. Deregulation of glucose transporter 1 and glycolytic gene expression by c-Myc. *J Biol Chem,* 275**,** 21797-800.

OWEN, T. J., O'NEIL, J. D., DAWSON, C. W., HU, C., CHEN, X., YAO, Y., WOOD, V. H., MITCHELL, L. E., WHITE, R. J., YOUNG, L. S. & ARRAND, J. R. 2010. Epstein-Barr virus-encoded EBNA1 enhances RNA polymerase III-dependent EBER expression through induction of EBER-associated cellular transcription factors. *Mol Cancer,* 9**,** 241.

PADOVAN-MERHAR, O., NAIR, G. P., BIAESCH, A. G., MAYER, A., SCARFONE, S., FOLEY, S. W., WU, A. R., CHURCHMAN, L. S., SINGH, A. & RAJ, A. 2015. Single mammalian cells compensate for differences in cellular volume and DNA copy number through independent global transcriptional mechanisms. *Mol Cell,* 58**,** 339-52.

PAHUJA, S., CHOUDHURY, M. & GUPTA, U. 2003. Proliferative activity in squamous intraepithelial and invasive lesions of cervix: analysis by AgNOR staining. *Indian J Pathol Microbiol,* 46**,** 573-5.

PAJIC, A., SPITKOVSKY, D., CHRISTOPH, B., KEMPKES, B., SCHUHMACHER, M., STAEGE, M. S., BRIELMEIER, M., ELLWART, J., KOHLHUBER, F., BORNKAMM, G. W., POLACK, A. & EICK, D. 2000. Cell cycle activation by c-myc in a burkitt lymphoma model cell line. *Int J Cancer,* 87**,** 787-93.

PELENGARIS, S., KHAN, M. & EVAN, G. 2002. c-MYC: more than just a matter of life and death. *Nat Rev Cancer,* 2**,** 764-76.

PELLETIER, J., THOMAS, G. & VOLAREVIC, S. 2018. Ribosome biogenesis in cancer: new players and therapeutic avenues. *Nat Rev Cancer,* 18**,** 51-63.

PENDE, M., KOZMA, S. C., JAQUET, M., OORSCHOT, V., BURCELIN, R., LE MARCHAND-BRUSTEL, Y., KLUMPERMAN, J., THORENS, B. & THOMAS, G. 2000. Hypoinsulinaemia, glucose intolerance and diminished beta-cell size in S6K1-deficient mice. *Nature,* 408**,** 994-7.

PERRY, R. P. & KELLEY, D. E. 1970. Inhibition of RNA synthesis by actinomycin D: characteristic dose-response of different RNA species. *J Cell Physiol,* 76**,** 127-39.

PICARD, D. 1993. Steroid-binding domains for regulating the functions of heterologous proteins in cis. *Trends Cell Biol,* 3**,** 278-80.

PIEDRA, M. E., DELGADO, M. D., ROS, M. A. & LEON, J. 2002. c-Myc overexpression increases cell size and impairs cartilage differentiation during chick limb development. *Cell Growth Differ,* 13**,** 185-93.

PIRKMAJER, S. & CHIBALIN, A. V. 2011. Serum starvation: caveat emptor. *Am J Physiol Cell Physiol,* 301**,** C272-9.

PJURA, P. E., GRZESKOWIAK, K. & DICKERSON, R. E. 1987. Binding of Hoechst 33258 to the minor groove of B-DNA. *J Mol Biol,* 197**,** 257-71.

PONTEN, J. & SAKSELA, E. 1967. Two established in vitro cell lines from human mesenchymal tumours. *Int J Cancer,* 2**,** 434-47.

POORTINGA, G., HANNAN, K. M., SNELLING, H., WALKLEY, C. R., JENKINS, A., SHARKEY, K., WALL, M., BRANDENBURGER, Y., PALATSIDES, M., PEARSON, R. B., MCARTHUR, G. A. & HANNAN, R. D. 2004. MAD1 and c-MYC regulate UBF and rDNA transcription during granulocyte differentiation. *EMBO J,* 23**,** 3325-35.

POORTINGA, G., WALL, M., SANIJ, E., SIWICKI, K., ELLUL, J., BROWN, D., HOLLOWAY, T. P., HANNAN, R. D. & MCARTHUR, G. A. 2011. c-MYC coordinately regulates ribosomal gene chromatin remodeling and Pol I availability during granulocyte differentiation. *Nucleic Acids Res,* 39**,** 3267-81.

PROUD, C. G. 2009. mTORC1 signalling and mRNA translation. *Biochem Soc Trans,* 37**,** 227-31.
RAHL, P. B., LIN, C. Y., SEILA, A. C., FLYNN, R. A., MCCUINE, S., BURGE, C. B., SHARP, P. A. & YOUNG, R. A. 2010. c-Myc regulates transcriptional pause release. *Cell,* 141**,** 432-45.
RAJ, A. & VAN OUDENAARDEN, A. 2008. Nature, nurture, or chance: stochastic gene expression and its consequences. *Cell,* 135**,** 216-26.
RAMEH, L. E. & CANTLEY, L. C. 1999. The role of phosphoinositide 3-kinase lipid products in cell function. *J Biol Chem,* 274**,** 8347-50.
RASER, J. M. & O'SHEA, E. K. 2004. Control of stochasticity in eukaryotic gene expression. *Science,* 304**,** 1811-4.
RATHMELL, J. C., VANDER HEIDEN, M. G., HARRIS, M. H., FRAUWIRTH, K. A. & THOMPSON, C. B. 2000. In the absence of extrinsic signals, nutrient utilization by lymphocytes is insufficient to maintain either cell size or viability. *Mol Cell,* 6**,** 683-92.
RAUGHT, B., PEIRETTI, F., GINGRAS, A. C., LIVINGSTONE, M., SHAHBAZIAN, D., MAYEUR, G. L., POLAKIEWICZ, R. D., SONENBERG, N. & HERSHEY, J. W. 2004. Phosphorylation of eucaryotic translation initiation factor 4B Ser422 is modulated by S6 kinases. *EMBO J,* 23**,** 1761-9.
RAVI, V., JAIN, A., AHAMED, F., FATHMA, N., DESINGU, P. A. & SUNDARESAN, N. R. 2018. Systematic evaluation of the adaptability of the non-radioactive SUnSET assay to measure cardiac protein synthesis. *Sci Rep,* 8**,** 4587.
RAVITZ, M. J., CHEN, L., LYNCH, M. & SCHMIDT, E. V. 2007. c-myc Repression of TSC2 contributes to control of translation initiation and Myc-induced transformation. *Cancer Res,* 67**,** 11209-17.
REIMAND, J., ARAK, T., ADLER, P., KOLBERG, L., REISBERG, S., PETERSON, H. & VILO, J. 2016. g:Profiler-a web server for functional interpretation of gene lists (2016 update). *Nucleic Acids Res,* 44**,** W83-9.
RIBAS, R., PANCHOLI, S., GUEST, S. K., MARANGONI, E., GAO, Q., THULEAU, A., SIMIGDALA, N., POLANSKA, U. M., CAMPBELL, H., RANI, A., LICCARDI, G., JOHNSTON, S., DAVIES, B. R., DOWSETT, M. & MARTIN, L. A. 2015. AKT Antagonist AZD5363 Influences Estrogen Receptor Function in Endocrine-Resistant Breast Cancer and Synergizes with Fulvestrant (ICI182780) In Vivo. *Mol Cancer Ther,* 14**,** 2035-48.
RICHARDSON, C. J., BROENSTRUP, M., FINGAR, D. C., JULICH, K., BALLIF, B. A., GYGI, S. & BLENIS, J. 2004. SKAR is a specific target of S6 kinase 1 in cell growth control. *Curr Biol,* 14**,** 1540-9.
RILEY, D. J., LEE, E. Y. & LEE, W. H. 1994. The retinoblastoma protein: more than a tumor suppressor. *Annu Rev Cell Biol,* 10**,** 1-29.
ROHBAN, S., CERUTTI, A., MORELLI, M. J., D'ADDA DI FAGAGNA, F. & CAMPANER, S. 2017. The cohesin complex prevents Myc-induced replication stress. *Cell Death Dis,* 8**,** e2956.
RUGGERO, D. 2009. The role of Myc-induced protein synthesis in cancer. *Cancer Res,* 69**,** 8839-43.
RUGGERO, D. & PANDOLFI, P. P. 2003. Does the ribosome translate cancer? *Nat Rev Cancer,* 3**,** 179-92.
RUSSELL, J. & ZOMERDIJK, J. C. 2005. RNA-polymerase-I-directed rDNA transcription, life and works. *Trends Biochem Sci,* 30**,** 87-96.
SABO, A., KRESS, T. R., PELIZZOLA, M., DE PRETIS, S., GORSKI, M. M., TESI, A., MORELLI, M. J., BORA, P., DONI, M., VERRECCHIA, A., TONELLI, C., FAGA, G., BIANCHI, V., RONCHI, A.,

LOW, D., MULLER, H., GUCCIONE, E., CAMPANER, S. & AMATI, B. 2014. Selective transcriptional regulation by Myc in cellular growth control and lymphomagenesis. *Nature,* 511**,** 488-492.

SALANS, L. B., KNITTLE, J. L. & HIRSCH, J. 1968. The role of adipose cell size and adipose tissue insulin sensitivity in the carbohydrate intolerance of human obesity. *J Clin Invest,* 47**,** 153-65.

SANSOM, O. J., MENIEL, V. S., MUNCAN, V., PHESSE, T. J., WILKINS, J. A., REED, K. R., VASS, J. K., ATHINEOS, D., CLEVERS, H. & CLARKE, A. R. 2007. Myc deletion rescues Apc deficiency in the small intestine. *Nature,* 446**,** 676-9.

SANTONI-RUGIU, E., FALCK, J., MAILAND, N., BARTEK, J. & LUKAS, J. 2000. Involvement of Myc activity in a G(1)/S-promoting mechanism parallel to the pRb/E2F pathway. *Mol Cell Biol,* 20**,** 3497-509.

SCARNATI, M. S., KATARIA, R., BISWAS, M. & PARADISO, K. G. 2018. Active presynaptic ribosomes in the mammalian brain, and altered transmitter release after protein synthesis inhibition. *Elife,* 7.

SCHALM, S. S., FINGAR, D. C., SABATINI, D. M. & BLENIS, J. 2003. TOS motif-mediated raptor binding regulates 4E-BP1 multisite phosphorylation and function. *Curr Biol,* 13**,** 797-806.

SCHEPERS, G. W. 1992. Re: "Changing attitudes and opinions: asbestos and cancer 1934-1965". *Am J Ind Med,* 22**,** 461-6.

SCHLOSSER, I., HOLZEL, M., MURNSEER, M., BURTSCHER, H., WEIDLE, U. H. & EICK, D. 2003. A role for c-Myc in the regulation of ribosomal RNA processing. *Nucleic Acids Res,* 31**,** 6148-56.

SCHMIDT, E. E. & SCHIBLER, U. 1995. Cell size regulation, a mechanism that controls cellular RNA accumulation: consequences on regulation of the ubiquitous transcription factors Oct1 and NF-Y and the liver-enriched transcription factor DBP. *J Cell Biol,* 128**,** 467-83.

SCHMIDT, E. K., CLAVARINO, G., CEPPI, M. & PIERRE, P. 2009. SUnSET, a nonradioactive method to monitor protein synthesis. *Nat Methods,* 6**,** 275-7.

SCHRAMM, L. & HERNANDEZ, N. 2002. Recruitment of RNA polymerase III to its target promoters. *Genes Dev,* 16**,** 2593-620.

SCHUHMACHER, M., STAEGE, M. S., PAJIC, A., POLACK, A., WEIDLE, U. H., BORNKAMM, G. W., EICK, D. & KOHLHUBER, F. 1999. Control of cell growth by c-Myc in the absence of cell division. *Curr Biol,* 9**,** 1255-8.

SEHGAL, S. N. 2003. Sirolimus: its discovery, biological properties, and mechanism of action. *Transplant Proc,* 35**,** 7S-14S.

SEHGAL, S. N., BAKER, H. & VEZINA, C. 1975. Rapamycin (AY-22,989), a new antifungal antibiotic. II. Fermentation, isolation and characterization. *J Antibiot (Tokyo),* 28**,** 727-32.

SFEIR, A. & DE LANGE, T. 2012. Removal of shelterin reveals the telomere end-protection problem. *Science,* 336**,** 593-7.

SHAHBAZIAN, D., ROUX, P. P., MIEULET, V., COHEN, M. S., RAUGHT, B., TAUNTON, J., HERSHEY, J. W., BLENIS, J., PENDE, M. & SONENBERG, N. 2006. The mTOR/PI3K and MAPK pathways converge on eIF4B to control its phosphorylation and activity. *EMBO J,* 25**,** 2781-91.

SHAHREZAEI, V. & SWAIN, P. S. 2008. The stochastic nature of biochemical networks. *Curr Opin Biotechnol,* 19**,** 369-74.

SHAPIRO, H. M. 1981. Flow cytometric estimation of DNA and RNA content in intact cells stained with Hoechst 33342 and pyronin Y. *Cytometry,* 2**,** 143-50.
SHAPIRO, H. M. 2003. *Practical flow cytometry,* New York, Wiley-Liss.
SHAW, G., MORSE, S., ARARAT, M. & GRAHAM, F. L. 2002. Preferential transformation of human neuronal cells by human adenoviruses and the origin of HEK 293 cells. *FASEB J,* 16**,** 869-71.
SHEHATA, M., VAN AMERONGEN, R., ZEEMAN, A. L., GIRADDI, R. R. & STINGL, J. 2014. The influence of tamoxifen on normal mouse mammary gland homeostasis. *Breast Cancer Res,* 16**,** 411.
SHIMA, H., PENDE, M., CHEN, Y., FUMAGALLI, S., THOMAS, G. & KOZMA, S. C. 1998. Disruption of the p70(s6k)/p85(s6k) gene reveals a small mouse phenotype and a new functional S6 kinase. *EMBO J,* 17**,** 6649-59.
SHUKLA, S. K. & KUMAR, V. 2012. Hepatitis B virus X protein and c-Myc cooperate in the upregulation of ribosome biogenesis and in cellular transformation. *FEBS J,* 279**,** 3859-71.
SIDDIQUI, N. & SONENBERG, N. 2015. Signalling to eIF4E in cancer. *Biochem Soc Trans,* 43**,** 763-72.
SMITH, U. 1971. Effect of cell size on lipid synthesis by human adipose tissue in vitro. *J Lipid Res,* 12**,** 65-70.
SMITH, U. & JACOBSSON, B. 1973. Studies of human adipose tissue in culture. II. Effects of insulin and of medium glucose on lipolysis and cell size. *Anat Rec,* 176**,** 181-3.
SOMMER, E. M., DRY, H., CROSS, D., GUICHARD, S., DAVIES, B. R. & ALESSI, D. R. 2013. Elevated SGK1 predicts resistance of breast cancer cells to Akt inhibitors. *Biochem J,* 452**,** 499-508.
SPEALMAN, P., WANG, H., MAY, G., KINGSFORD, C. & MCMANUS, C. J. 2016. Exploring Ribosome Positioning on Translating Transcripts with Ribosome Profiling. *Methods Mol Biol,* 1358**,** 71-97.
SPENDER, L. C. & INMAN, G. J. 2014. Developments in Burkitt's lymphoma: novel cooperations in oncogenic MYC signaling. *Cancer Manag Res,* 6**,** 27-38.
STEIGER, D., FURRER, M., SCHWINKENDORF, D. & GALLANT, P. 2008. Max-independent functions of Myc in Drosophila melanogaster. *Nat Genet,* 40**,** 1084-91.
STEINER, P., PHILIPP, A., LUKAS, J., GODDEN-KENT, D., PAGANO, M., MITTNACHT, S., BARTEK, J. & EILERS, M. 1995. Identification of a Myc-dependent step during the formation of active G1 cyclin-cdk complexes. *EMBO J,* 14**,** 4814-26.
STEPANENKO, A. A. & DMITRENKO, V. V. 2015. HEK293 in cell biology and cancer research: phenotype, karyotype, tumorigenicity, and stress-induced genome-phenotype evolution. *Gene,* 569**,** 182-90.
STINE, Z. E., WALTON, Z. E., ALTMAN, B. J., HSIEH, A. L. & DANG, C. V. 2015. MYC, Metabolism, and Cancer. *Cancer Discov,* 5**,** 1024-39.
TAN, B. C., YANG, C. C., HSIEH, C. L., CHOU, Y. H., ZHONG, C. Z., YUNG, B. Y. & LIU, H. 2012. Epigeneitc silencing of ribosomal RNA genes by Mybbp1a. *J Biomed Sci,* 19**,** 57.
TEE, A. R. 2018. The Target of Rapamycin and Mechanisms of Cell Growth. *Int J Mol Sci,* 19.
TERADA, N., PATEL, H. R., TAKASE, K., KOHNO, K., NAIRN, A. C. & GELFAND, E. W. 1994. Rapamycin selectively inhibits translation of mRNAs encoding elongation factors and ribosomal proteins. *Proc Natl Acad Sci U S A,* 91**,** 11477-81.
TESI, A., DE PRETIS, S., FURLAN, M., FILIPUZZI, M., MORELLI, M. J., ANDRONACHE, A., DONI, M., VERRECCHIA, A., PELIZZOLA, M., AMATI, B. & SABO, A. 2019. An early Myc-

dependent transcriptional program orchestrates cell growth during B-cell activation. *EMBO Rep,* 20**,** e47987.
THOREEN, C. C., CHANTRANUPONG, L., KEYS, H. R., WANG, T., GRAY, N. S. & SABATINI, D. M. 2012. A unifying model for mTORC1-mediated regulation of mRNA translation. *Nature,* 485**,** 109-13.
THORNTON, T. M. & RINCON, M. 2009. Non-classical p38 map kinase functions: cell cycle checkpoints and survival. *Int J Biol Sci,* 5**,** 44-51.
THOUVEREY, C. & CAVERZASIO, J. 2015. Focus on the p38 MAPK signaling pathway in bone development and maintenance. *Bonekey Rep,* 4**,** 711.
TORMOS, A. M., ARDUINI, A., TALENS-VISCONTI, R., DEL BARCO BARRANTES, I., NEBREDA, A. R. & SASTRE, J. 2013. Liver-specific p38alpha deficiency causes reduced cell growth and cytokinesis failure during chronic biliary cirrhosis in mice. *Hepatology,* 57**,** 1950-61.
VAN HOEWYK, D. 2016. Use of the non-radioactive SUnSET method to detect decreased protein synthesis in proteasome inhibited Arabidopsis roots. *Plant Methods,* 12**,** 20.
VAN RIGGELEN, J. & FELSHER, D. W. 2010. Myc and a Cdk2 senescence switch. *Nat Cell Biol,* 12**,** 7-9.
VANHAESEBROECK, B. & WATERFIELD, M. D. 1999. Signaling by distinct classes of phosphoinositide 3-kinases. *Exp Cell Res,* 253**,** 239-54.
VLAHOS, C. J., MATTER, W. F., HUI, K. Y. & BROWN, R. F. 1994. A specific inhibitor of phosphatidylinositol 3-kinase, 2-(4-morpholinyl)-8-phenyl-4H-1-benzopyran-4-one (LY294002). *J Biol Chem,* 269**,** 5241-8.
VOLFSON, D., MARCINIAK, J., BLAKE, W. J., OSTROFF, N., TSIMRING, L. S. & HASTY, J. 2006. Origins of extrinsic variability in eukaryotic gene expression. *Nature,* 439**,** 861-4.
WALL, M., POORTINGA, G., HANNAN, K. M., PEARSON, R. B., HANNAN, R. D. & MCARTHUR, G. A. 2008. Translational control of c-MYC by rapamycin promotes terminal myeloid differentiation. *Blood,* 112**,** 2305-17.
WALL, M., POORTINGA, G., STANLEY, K. L., LINDEMANN, R. K., BOTS, M., CHAN, C. J., BYWATER, M. J., KINROSS, K. M., ASTLE, M. V., WALDECK, K., HANNAN, K. M., SHORTT, J., SMYTH, M. J., LOWE, S. W., HANNAN, R. D., PEARSON, R. B., JOHNSTONE, R. W. & MCARTHUR, G. A. 2013. The mTORC1 inhibitor everolimus prevents and treats Emu-Myc lymphoma by restoring oncogene-induced senescence. *Cancer Discov,* 3**,** 82-95.
WALLACE, D. C. 2012. Mitochondria and cancer. *Nat Rev Cancer,* 12**,** 685-98.
WATSON, J. V. 2004. *Introduction to flow cytometry,* Cambridge Eng. ; New York, Cambridge University Press.
WENDEL, H. G., DE STANCHINA, E., FRIDMAN, J. S., MALINA, A., RAY, S., KOGAN, S., CORDON-CARDO, C., PELLETIER, J. & LOWE, S. W. 2004. Survival signalling by Akt and eIF4E in oncogenesis and cancer therapy. *Nature,* 428**,** 332-7.
WERSTO, R. P., CHREST, F. J., LEARY, J. F., MORRIS, C., STETLER-STEVENSON, M. A. & GABRIELSON, E. 2001. Doublet discrimination in DNA cell-cycle analysis. *Cytometry,* 46**,** 296-306.
WESIERSKA-GADEK, J. & SCHMID, G. 2005. The subcellular distribution of the p53 tumour suppressor, and organismal ageing. *Cell Mol Biol Lett,* 10**,** 439-53.
WHITE, R. J. 2008. RNA polymerases I and III, non-coding RNAs and cancer. *Trends Genet,* 24**,** 622-9.

WOLF, E., LIN, C. Y., EILERS, M. & LEVENS, D. L. 2015. Taming of the beast: shaping Myc-dependent amplification. *Trends Cell Biol,* 25**,** 241-8.

WROBLESKI, S. T. & DOWEYKO, A. M. 2005. Structural comparison of p38 inhibitor-protein complexes: a review of recent p38 inhibitors having unique binding interactions. *Curr Top Med Chem,* 5**,** 1005-16.

XIAO, G., MAO, S., BAUMGARTEN, G., SERRANO, J., JORDAN, M. C., ROOS, K. P., FISHBEIN, M. C. & MACLELLAN, W. R. 2001. Inducible activation of c-Myc in adult myocardium in vivo provokes cardiac myocyte hypertrophy and reactivation of DNA synthesis. *Circ Res,* 89**,** 1122-9.

XING, C. G., ZHU, B. S., LIU, H. H., LIN, F., YAO, H. H., LIANG, Z. Q. & QIN, Z. H. 2008. LY294002 induces p53-dependent apoptosis of SGC7901 gastric cancer cells. *Acta Pharmacol Sin,* 29**,** 489-98.

YAMAGIWA, Y., MARIENFELD, C., TADLOCK, L. & PATEL, T. 2003. Translational regulation by p38 mitogen-activated protein kinase signaling during human cholangiocarcinoma growth. *Hepatology,* 38**,** 158-66.

YAN, W., XIAOLI, L., GUOLIANG, A., ZHONGHUI, Z., DI, L., XIMENG, L., PIYE, N., LI, C. & LIN, T. 2016. SB203580 inhibits epithelial-mesenchymal transition and pulmonary fibrosis in a rat silicosis model. *Toxicol Lett,* 259**,** 28-34.

YANG, H., RUDGE, D. G., KOOS, J. D., VAIDIALINGAM, B., YANG, H. J. & PAVLETICH, N. P. 2013. mTOR kinase structure, mechanism and regulation. *Nature,* 497**,** 217-23.

YOUNG, S. L., DIOLAITI, D., CONACCI-SORRELL, M., RUIZ-TRILLO, I., EISENMAN, R. N. & KING, N. 2011. Premetazoan ancestry of the Myc-Max network. *Mol Biol Evol,* 28**,** 2961-71.

YUDUSHKIN, I. 2019. Getting the Akt Together: Guiding Intracellular Akt Activity by PI3K. *Biomolecules,* 9.

ZANET, J., PIBRE, S., JACQUET, C., RAMIREZ, A., DE ALBORAN, I. M. & GANDARILLAS, A. 2005. Endogenous Myc controls mammalian epidermal cell size, hyperproliferation, endoreplication and stem cell amplification. *J Cell Sci,* 118**,** 1693-704.

ZELLER, K. I., JEGGA, A. G., ARONOW, B. J., O'DONNELL, K. A. & DANG, C. V. 2003. An integrated database of genes responsive to the Myc oncogenic transcription factor: identification of direct genomic targets. *Genome Biol,* 4**,** R69.

ZHANG, J., SHEN, B. & LIN, A. 2007. Novel strategies for inhibition of the p38 MAPK pathway. *Trends Pharmacol Sci,* 28**,** 286-95.

ZHU, L. 2005. Tumour suppressor retinoblastoma protein Rb: a transcriptional regulator. *Eur J Cancer,* 41**,** 2415-27.